Structure and Mechanical Properties of Multiblock Copolymers:
Toward the development of enhanced mechanical response materials

A DISSERTATION
SUBMITTED TO THE FACULTY OF THE GRADUATE SCHOOL
OF THE UNIVERSITY OF MINNESOTA
BY

Intaek Lee

IN PARTIAL FULFILLMENT OF THE REQUIREMENTS
FOR THE DEGREE OF
DOCTOR OF PHILOSOPHY

Frank S. Bates

January 2014

Acknowledgements

Frist and foremost, I would like to thank my advisor, Prof. Frank S. Bates, for his invaluable guidance and support. He encouraged me to devote myself to research during my Ph.D. years. I have learned numerous scientific lessons from working with him. It would not be possible to accomplish this study without his insightful advice. I would also like to thank the faculty members in the polymer group, Prof. Marc A. Hillmyer, Prof. Timothy P. Lodge, and Prof. Christopher W. Macosko, for their valuable instructions and conversations.

I am deeply grateful to many of my colleagues and University staff. I would like to especially thank Dr. Guillaume Fleury and Tessie Panthani, who have worked with me and contributed their efforts into this project. I also want to thank Soo-Hyung Choi, Sangwoo Lee, Mike Bluemle, Adam Meuler, Ameara Mansour, David Giles, Bob Hafner, Fang Zhou, and Letitia Yao for training me on synthesis and characterization techniques. I am also appreciative to Bates group members, Sangwon Kim, Guillermo Alfonzo, Dawud Tan, Erica Redline, Brian Habersberger, Luca Martinetti, Jingwen Zhang, Whitney Kruse, Athanasios Touris, Ajay Vidyasagar, Carmelo Declet-Perez, Tim Gillard, Karen Haman, Zaifei Wang, Sam Dalsin, Jie Lu, Touqi Li, Sid Chanpuriya, John McAllister, Alex Mannion, Jeff Ting, and Yiming Zeng for thoughtful discussion and kind friendship.

I would like to thank many of my friends who made my graduate school life more enjoyable: MN 83 friends (Minseok Oh, Hyung-Keun Im, Brian Chung, Jaehee Cho, Dongwon Lee, Sangsoo Hwang, Soo Yong Choi, Sunghun Jung), Yal-gae friends

(Sangyun Kim, Hyungsuk Nam, Chi-Hoon Sung, Sunwoo Kim, Hanjae Lee), Yonsei Chemeng friends (Yoonseok Baek, Sun-Gou Ji, Taejun Kim, Hojin Yu, Donghwan Kim), MN Bros friends (Kwangwui Kim, Deukyeol Choe, Hayoung Yoo, Dongsoo Han, Simon J Choi), CEMS Korean people, KPCM people.

Finally, I would like to express my sincere gratitude to my parents and brother for their endless love and support.

To My Family

Abstract

Block polymers have attracted much scientific interest for decades, and most studies have focused on the simplest molecular architectures: linear AB diblock and ABA triblock copolymers. Multiblock copolymers containing a large number of blocks are expected to have distinct microstructures and a mechanical response which is different from that of conventional diblock and triblock copolymers. This research addresses synthesis and characterization of poly(cyclohexylethylene)-polyethylene (CECECECEC) nonablock copolymers, poly(styrene-*b*-butadiene) (PS-PB) multiblock copolymers, and poly(lactide-*b*-butadiene) (PLA-PB) multiblock copolymers. CECECECEC nonablock copolymers having a large center C block were synthesized using sequential anionic polymerization followed by catalytic hydrogenation. The CECECECEC samples exhibited different morphologies with varying size of PE blocks. As the PE block size increased, the microstructure was transformed with the sequence of disordered homogeneous phase – lamellae with mixed phase of outer CECE blocks – layer-in-layer microstructure. Moreover, the secondary phase segregation of outer CECE blocks (layer-in-layer morphology) allowed ductile and tough mechanical behavior. PS-PB multiblock copolymers with alternating and random block sequences were synthesized using a combination of living anionic polymerization and urethane based polycondensation. Molecular characterization revealed the successful synthesis of the desired multiblock products through the proposed procedure. Structural analysis demonstrated a random bicontinuous-like morphology over a wide range of compositions, $0.69 \leq f_{PS} \leq 0.85$.

Tensile tests showed yielding followed by necking and an overall ductility that translates into much greater toughness than that typically found in glassy continuous SBS triblock copolymers. PLA-PB multiblock copolymers ($0.5 \leq f_{PLA} \leq 0.9$) were synthesized in a two-step procedure: PLA-PB-PLA triblock copolymers were prepared using ring-opening polymerization, followed by chain extension with the condensation reaction. Multiblock copolymer and homologous triblock materials exhibited nearly identical and well-ordered morphologies, in sharp contrast with the findings of PS-PB multiblock polymers. These results indicate a transition from classically ordered morphologies to a state of bicontinuous disorder for multiblocks containing $\langle n \rangle \geq 10$, where $\langle n \rangle$ is the average total number of blocks. In tensile tests, most PLA-PB multiblock copolymers exhibited dramatically enhanced mechanical properties compared to the corresponding LBL triblock copolymers. These results suggest that a multiblock copolymer strategy offers new possibilities to obtain unique microstructures and physical properties from many other combinations of polymers.

Table of Contents

List of Tables x
List of Figures xi

Chapter 1 Introductory Remarks 1
1.1 Introduction 1
1.2 Block Copolymer Phase Behavior 5
1.3 Block Copolymer Mechanical Properties 18
1.4 Thesis Outline 41
1.5 References 43

Chapter 2 Block Copolymer Synthesis and Characterization 54
2.1 Synthesis of Block Copolymers 55
2.1.1 Polymer Selection 55
2.1.2 Living Anionic Polymerization 57
2.1.3 Ring-Opening Polymerization 59
2.1.4 Coupling Chemistry 61
2.1.5 Catalytic Hydrogenation 62
2.2 Characterization of Block Copolymers 64
2.2.1 Size Exclusion Chromatography 64
2.2.2 Nuclear Magnetic Resonance Spectroscopy 67
2.2.3 Differential Scanning Calorimetry 75
2.2.4 Small-Angle X-ray Scattering 76
2.2.5 Dynamic Mechanical Spectroscopy 80
2.2.6 Transmission Electron Microscopy 83
2.2.7 Tensile Testing 85
2.3 References 86

Chapter 3 Poly(cyclohexylethylene)-Polyethylene Nonablock Copolymers 90
3.1 Introduction..... 90
3.2 Experimental Section..... 94
3.2.1 Synthesis of PCHE-PE nonablock copolymers..... 94
3.2.2 Molecular Characterization..... 98
3.2.3 Differential Scanning Calorimetry (DSC)..... 100
3.2.4 Dynamic Mechanical Spectroscopy (DMS)..... 100
3.2.5 Small-Angle X-ray Scattering (SAXS)..... 101
3.2.6 Tensile Testing..... 101
3.3 Results and Discussion..... 102
3.3.1 Synthesis..... 102
3.3.2 Thermal Analysis..... 108
3.3.3 Rheological Properties..... 114
3.3.4 Structural Analysis..... 121
3.3.5 PE Block Size Effect on Morphology..... 126
3.3.6 Tensile Properties..... 130
3.4 Conclusions..... 134
3.5 References..... 135

Chapter 4 Alternating and Random Poly(styrene-*b*-butadiene) Multiblock Copolymers.....139
4.1 Introduction..... 139
4.2 Experimental Section..... 142
4.2.1 Synthesis of α,ω-Dihydroxy Homopolymers..... 142
4.2.2 Synthesis of Random (PS-ran-PB)$_n$ Multiblock Copolymers..... 143
4.2.3 Synthesis of Alternating (PS-alt-PB)$_n$ Multiblock Copolymers..... 145
4.2.4 Molecular Characterization..... 146
4.2.5 Differential Scanning Calorimetry (DSC)..... 147
4.2.6 Small-Angle X-ray Scattering (SAXS)..... 147
4.2.7 Transmission Electron Microscopy (TEM)..... 147

4.2.8 Tensile Testing 148
4.3 Results and Discussion 148
4.3.1 Synthesis 148
4.3.2 Thermal Properties 160
4.3.3 Structural Analysis 164
4.3.4 Tensile Properties 170
4.4 Conclusions 175
4.5 References 176

Chapter 5 Poly(lactide-*b*-butadiene) Multiblock Copolymers 182
5.1 Introduction 182
5.2 Experimental Section 185
5.2.1 Synthesis of Poly(lactide-*b*-butadiene-*b*-lactide) (LBL) Triblock Copolymers. 185
5.2.2 Synthesis of PLA-PB Multiblock Copolymers 186
5.2.3 Molecular Characterization 187
5.2.4 Differential Scanning Calorimetry (DSC) 188
5.2.5 Dynamic Mechanical Analysis (DMA) 189
5.2.6 Small-Angle X-ray Scattering (SAXS) 189
5.2.7 Transmission Electron Microscopy (TEM) 190
5.2.8 Tensile Testing 190
5.3 Results and Discussion 191
5.3.1 Synthesis 191
5.3.2 PLA-PB χ Parameter (Order-Disorder Transition Temperature) 198
5.3.3 Thermal Analysis 200
5.3.4 Morphological Characeristics 204
5.3.5 Mechanical Properties 214
5.3.6 Comparison with PS-PB Multiblock Polymers 221
5.4 Conclusion 222
5.5 References 224

Chapter 6 Concluding Remarks 232
6.1 Summary 232
6.2 Reference 235

Bibliography 236

List of Tables

Table 2.1 Comparison of PCHE and PS. Reproduced from Bates et al.[2] 56
Table 2.2 ^{1}H NMR chemical shifts of polymers used in this study. 70
Table 2.3 Allowed reflections for several morphologies of block copolymers. 79
Table 3.1 Molecular characteristic of CECECECEC nonablock copolymers. 105
Table 3.2 Thermal analytic results of CECECECEC. 111
Table 3.3 Characterized morphologies and domain spacings of CECECECEC block copolymers. 125
Table 3.4 Tensile properties of CECECECEC block copolymers. 132
Table 4.1 Molecular characterization data for HO-PS-OH and HO-PB-OH homopolymers 150
Table 4.2 Molecular characteristics of the $(PS\text{-}PB)_n$ multiblock copolymers. 157
Table 4.3 Glass transition temperatures and calculated weight fractions of PS-rich and PB-rich microdomains. 163
Table 4.4 Domain spacings of $(PS\text{-}PB)_n$ multiblock copolymers. 166
Table 4.5 Tensile properties of the $(PS\text{-}PB)_n$ multiblock copolymers. 172
Table 5.1 Molecular characteristics LBL triblock copolymers and PLA-PB multiblock copolymers 192
Table 5.2 Characterized morphologies and principal domain spacings of LBL triblock copolymers and PLA-PB multiblock copolymers 212
Table 5.3 Characterization results for lamellae-forming LBL triblock copolymers 213
Table 5.4 Tensile properties of LBL triblock, $(LBL\text{-}OCONH\text{-})_n$ and $(LBL\text{-}COO\text{-})_n$ multiblock copolymers 217

List of Figures

Figure 1.1 Different morphologies for AB diblock copolymers. Reproduced from Bates and Fredrickson.[6] 6

Figure 1.2 Theoretical phase diagram for diblock copolymers calculated by (a) mean-field theory (b) fluctuation theory with $\overline{N}$ = 10^4. Reproduced from Bates and Fredrickson.[18] 8

Figure 1.3 (a) Phase diagram for symmetric diblock melts calculated by SCFT. Reproduced from Matsen and Bates.[100] (b) Experimentally determined phase diagram for PI-PS diblock copolymer. Reproduced from Khandpur et al.[96] 11

Figure 1.4 SCFT phase diagrams for diblock copolymer melts with different conformational asymmetries. (a) a_A/a_B = 1.0 (b) a_A/a_B = 1.5 (c) a_A/a_B = 2.0, where a is the statistical segment length. Reproduced from Matsen and Bates.[95] 11

Figure 1.5 Triblock copolymer phase diagram (solid curves) and diblock copolymer phase diagram (dashed curves). Reproduced from Matsen and Thompson.[101] 13

Figure 1.6 ABC linear triblock copolymer morphologies. Reproduced from Bates and Fredrickson.[6] 15

Figure 1.7 Various morphologies of $V(IS)_4IV$ ((a), (b), (c)) and $V(SI)_2I$ ((d), (e), (f)). Volume fractions of the V block are (a) 0.08, (b) 0.21, (c) 0.53, (d) 0.64, (e) 0.75, (f) 0.88. Reproduced from Matsushita.[120] (g) Scheme of the composition-dependent morphological transition of $A(BC)_nBA$ and $A(BC)_nB$ terpolymers. Reproduced form Masuda et al.[118] 18

Figure 1.8 Illustration of (a) extensional strain and (b) simple shear strain. Reproduced from Ward and Sweeney.[121] 19

Figure 1.9 Stress-strain curves for a typical polymer showing deferent regions of mechanical behavior: (a) brittle fracture; (b) ductile; (c) ductile with necking; (d) elastomeric. Reproduced from Ward and Sweeney.[121] 20
Figure 1.10 Formation of craze in a glassy polymer. 22
Figure 1.11 Deformation mechanisms of the amorphous phase in semicrystalline polymers: (a) interlamellar slip, (b) interlamellar separation, (c) stack rotation of lamellae. Reproduced from Bowden.[126] 23
Figure 1.12 Stress–strain curves for SBS triblock copolymers with different morphologies at fixed molecular weight and block composition; (a) lamellar; (b) cylindrical; (c) bicontinuous morphology. Reproduced from Sakurai et al.[134] 27
Figure 1.13 Stress–strain curves for SBS triblock copolymers of various styrene contents. Reproduced from Holden et al.[133] 29
Figure 1.14 Stress-strain properties of SIS (□) and mSImS (○) triblock copolymers. Reproduced from Fetters and Morton.[137] 29
Figure 1.15 Representation of the deformation processes involved in the strain-induced plastic-to-rubber transition. Reproduced from Fujimura et al.[139] 31
Figure 1.16 Schematic representation of structural changes caused by deformation of originally oriented SBS polymer with the cylindrical microdomains: (a) SD (stretching direction) perpendicular, (b) SD parallel, and (c) SD at 45° to the original orientation of the cylindrical domains. Reproduced from Pakula et al.[143] 33
Figure 1.17 Illustration of chain architectures of lamellae-forming CE diblock, CEC triblock, CECEC pentablock copolymers. 35
Figure 1.18 Schematics showing the role of bridging PCHE chains in CECEC. Reproduced from Ryu et al.[109] 36
Figure 1.19 The effect of microdomain orientation in a cylindrical pentablock copolymer: (a) bridging (yellow circle) and looping (green circle)

PCHE chains in a cylindrical morphology, (b) copolymers with a random orientation of cylinders, (c) grains of cylinders aligned with their axes parallel to the film plane, and (d) cylinders aligned with their axes perpendicular to the film plane. Reproduce from Khanna et al.[110] 37

Figure 1.20 (a) Average fraction of middle A blocks in bridged conformation f_{br} as a function of middle block fraction f_3 for symmetric ABABA pentablock copolymers. (b) Average distance between neighboring B cylinders as a function of middle block fraction f_3 for symmetric ABABA pentablock copolymers. Reproduced from Drolet and Fredrickson.[108] 38

Figure 1.21 The failure strain as a function of ψ_E for C/E block copolymer architectures. Reproduced from Phatak et al.[32] 40

Figure 1.22 Stress-strain curves $(EP)_n$ block copolymers with n = 2, 4, 6, 8, 10, and 12. For $n \leq 8$ the materials strain soften, while for $n \geq 10$ they strain harden. Reproduced from Koo et al.[33] 41

Figure 2.1 SEC traces of HO-PB-OH (before polymerization, dashed line) and LBL triblock copolymer (after polymerization, solid line). 67

Figure 2.2 Representative ^{1}H NMR spectrum of SBSBSBSBS nonablock copolymers. The unsaturated polymer samples were measured in deuterated chloroform ($CDCl_3$) at room temperature. 71

Figure 2.3 Representative ^{1}H NMR spectrum of (a) α,ω-dihydroxyl polybutadiene (HO-PB-OH) and (b) poly(lactide-*b*-butadiene-*b*-lactide) (LBL). The proton assignments and integrated peak areas are denoted above the peaks. 74

Figure 2.4 Representative DSC trace of CECECECEC with cooling and heating rate of 10 °C/min. The glass transition, melting and crystallization temperatures are denoted by the arrows. 76

Figure 2.5 Scheme of the elastic scattering from a single scatterer. 77

Figure 2.6 Scheme of Bragg's law. (a) The incident and scattering wave vectors make an incident angle of $\theta/2$ with each plain. The interplanar distance is D. (b) The bold line indicates the additional distance of the waves scattered from the second plane. The length of each bold line is $D\sin(\theta/2)$.[14] 79

Figure 2.7 Illustration of simple shear flow between parallel plates. Reproduced from Hiemenz and Lodge.[14] 81

Figure 2.8 Illustration of low-frequency G' behaviors of disordered state and several ordered structures. Reproduced from Kossuth et al.[34] 83

Figure 3.1 Chain architecture and expected microstructure of CECECECEC nonablock copolymers. The CECECECEC block copolymers have a large center C block (f_5 = 0.4–0.7) and small CECE outer blocks with the same sizes of C and E blocks (C blocks: $f_1 = f_3 = f_7 = f_9$, E blocks: $f_2 = f_4 = f_6 = f_8$), where f_n (n = 1 to 9) indicates the volume fraction of nth block. 93

Figure 3.2 Synthesis scheme of CECECECEC nonablock copolymers. 98

Figure 3.3 Representative SEC traces of SBSBSBSBS nonablock copolymer (solid line) and corresponding aliquot of the first block (dashed line) obtained with THF as the mobile phase at room temperature. 103

Figure 3.4 SEC trace of $(SBSB)_2$S-85-70-104k block copolymer (○) as well as Gaussian fitting curves for coupled (red line) and uncoupled (blue line) chains. The coupling efficiency was calculated from the area of the fitting curves. 104

Figure 3.5 ^{1}H NMR spectra of (a) $(SBSB)_2$S-75-50-63k and (b) $(CECE)_2$C-75-50-63k nonablock copolymers. The unsaturated and saturated polymer samples were measured in deuterated chloroform ($CDCl_3$) at room temperature and deuterated toluene (C_7D_8) at 70°C, respectively. 107

Figure 3.6 DSC heating trace of $(CECE)_2$C-55-40-87k. Dashed line indicates the baseline. T_m is determined as the baseline intercept of the tangent to

the downward slope of the melting peak. ΔH_m is calculated as the integrated area of the peak above the baseline.....110
Figure 3.7 Block molecular weight effect on the glass transition temperatures of PCHE microdomains in CECECECEC nonablock copolymers.....112
Figure 3.8 Crystallinity of PCHE/PE block copolymers as a function of the number-average molecular weight of PE blocks. Circles and squares denote CE diblocks and CEC triblocks, respectively. Dashed line indicates the crystallinity of the homopolymer PE. Data points were reproduced from Weimann et al.[24] Triangles indicate CECECECEC nonablock copolymers investigated in this study. 114
Figure 3.9 Storage modulus G' during isochronal temperature sweep test for $(CECE)_2C$-65-50-51k. The T_{ODT} where a sudden discontinuity of the G' occurred is indicated by the arrow.....115
Figure 3.10 Master curves of modulus versus reduced frequency for CECECECEC nonablock copolymers. The reference temperature (T_{ref}) is 160 °C. Closed and open symbols denote the storage modulus G' and the loss modulus G'', respectively. 118
Figure 3.11 Master curves of modulus versus reduced frequency for CECECECEC nonablock copolymers. The reference temperature (T_{ref}) is 160 °C except for $(CECE)_2C$-75-70-134k, which is 180 °C. Closed and open symbols denote the storage modulus G' and the loss modulus G'', respectively.....119
Figure 3.12 Shift factors (a_T) as a function of temperatures for CECECECEC nonablock copolymers. The solid line represents a fit of Williams-Landel-Ferry (WLF) equation with parameters C_1 and C_2. The reference temperature (T_{ref}) is 160 °C.....120

Figure 3.13 Shift factors (a_T) as a function of temperatures for CECECECEC nonablock copolymers. The solid line represents a fit of Williams-Landel-Ferry (WLF) equation with parameters C_1 and C_2. The reference temperature (T_{ref}) is 160 °C except for $(CECE)_2$C-75-70-134k, which is 180 °C. 121
Figure 3.14 SAXS patterns for CECECECEC nonablock copolymers obtained at 140 °C except for $(CECE)_2$C-55-40-87k-AN, which is 25 °C. Data sets are shifted vertically for clarity. 124
Figure 3.15 Feasible microstructures of CECECECEC block copolymers: (a) homogeneous phase and small secondary crystals; (b) primary phase separation and crystallization induced secondary structure; (c) layer-in-layer structure with primary and secondary phase separation 129
Figure 3.16 Representative stress-strain curves for CECECECEC block copolymers. The inset shows the stress-strain curves at small strain region. 131
Figure 4.1 Synthetic scheme for preparing α,ω-dihydroxy homopolymers. 143
Figure 4.2 Schematic representation of the synthesis of (a) $(PS\text{-}ran\text{-}PB)_n$ and (b) $(PS\text{-}alt\text{-}PB)_n$ multiblock copolymers....144
Figure 4.3 SEC traces of HO-PS-OH polymers (a and c) and following reaction with IPDI (b, d, and e). Addition of a stoichiometric amount of IPDI at 40 °C (b) and 5 °C (d) results in large and small amounts of coupled polymer, respectively. Addition of excess IPDI at room temperature (e) suppresses polycondensation leading to the desired product, OCN-PS-NCO-4b. 152
Figure 4.4 ^{1}H NMR spectra of (a) HO-PS-OH-4 and (b) OCN-PS-NCO-4b in $CDCl_3$. The insets show the 2.6–4.5 ppm region of the spectra. 154
Figure 4.5 FTIR spectra of (a) HO-PS-OH-4 and (b) OCN-PS-NCO-4b....155
Figure 4.6 SEC traces obtained from multiblock copolymers (solid line) PS-alt-PB-4 and PS-ran-PB-4 as well as prepolymers (dashed line) HO-PS-OH-4 and HO-PB-OH-2. 158

Figure 4.7 ^{1}H NMR spectrum of PS-alt-PB-4 multiblock copolymer. 160
Figure 4.8 DSC traces of (PS-PB)$_n$ multiblock copolymers obtained while heating. Arrows indicate glass transition temperatures for the PS-rich and PB-rich microdomains. 164
Figure 4.9 SAXS patterns obtained at room temperature for (PS-PB)$_n$ mutltiblock copolymers. 167
Figure 4.10 TEM images from (PS-PB)$_n$ multiblock copolymers. Each sample was stained with OsO_4. PS and PB domains appear as light and dark region, respectively. Scale bars correspond to 50 nm. 169
Figure 4.11 Representative engineering stress versus strain curves for the (PS-PB)$_n$ multiblock copolymers. 171
Figure 4.12 Comparison of the tensile behavior of similar composition and molecular weight SBS triblock (LN1) and (PS-PB)$_n$ multiblock (PS-alt-PB-3). 174
Figure 5.1 Synthetic scheme for (a) LBL triblock copolymer, (b) (LBL-OCONH-)$_n$ multiblock copolymer, and (c) (LBL-COO-)$_n$ multiblock copolymer. 186
Figure 5.2 SEC traces of synthesized (LBL-OCONH-)$_n$ and (LBL-COO-)$_n$ multiblock copolymer series as well as starting LBL triblock copolymers and HO-PB-OH. 193
Figure 5.3 ^{1}H NMR spectra of (a) LBL60, (b) (LBL60-OCONH-)$_n$, and (c) (LBL60-COO-)$_n$ in $CDCl_3$. The insert shows the 3.8–4.5 ppm and 6.5–8.0 ppm region of spectrum. The signals between 7 and 7.5 ppm are associated with residual protons in the deuterated chloroform ($CDCl_3$). 195
Figure 5.4 ^{1}H NMR spectra of LBL60 (a) before and (b) after the reaction with trifluoroacetic anhydride (TFAA). The modification using TFAA moves the peak of methine proton next to the terminal hydroxyl group ($\delta H_{a'}$) from 4.36 ppm to higher frequency. The shifted methine proton peak ($\delta H_{a''}$) overlaps with the proton peaks of PLA and PB repeat units (4.95–5.55 ppm). 196

Figure 5.5 Isochoronal temperature ramp data on heating for LBL triblock copolymers: LBL50-2 (▽), LBL50 (△), LBL60 (◇), LBL70 (○), and LBL80 (□). The arrows indicate T_{ODT} values. 200

Figure 5.6 DSC heating curves of LBL triblock, (LBL-OCONH-)$_n$ and (LBL-COO-)$_n$ multiblock copolymers. Arrows indicates T_gs of PB and PLA domains ($T_g^{PB\text{-}domain}$ and $T_g^{PLA\text{-}domain}$). 201

Figure 5.7 PLA block molecular weight effect on the glass transition temperatures of PB and PLA microphases in multiblock copolymers ($T_g^{PB\text{-}domain}$ and $T_g^{PLA\text{-}domain}$). The dashed line is T_g of PLA homopolymer calculated from Flory–Fox equation,[68] and the dotted line is T_g of PB homopolymer (HO-PB-OH) measured by DSC.....203

Figure 5.8 SAXS patterns for LBL triblock and PLA-PB multiblock copolymers obtained at room temperature. Data sets are shifted vertically for clarity. 207

Figure 5.9 TEM images from LBL triblock and (LBL-OCONH-)$_n$ multiblock copolymers. Samples were stained with OsO_4 to enhance the contrast. The light and dark microdomains are associated with PLA and PB domains, respectively. Scale bars correspond to 100 nm and inserts are high-magnification images.....208

Figure 5.10 Actual experimental scattering data (○) and Percus–Yevick hard-sphere model (solid line) for (a) LBL90, (b) (LBL90-OCONH-)$_n$, and (c) (LBL90-COO-)$_n$. The best fit to the LBL90 scattering data was obtained with R = 5.7 nm, σ_R = 0.79 nm, R_{HS} = 9.1 nm, and η = 0.41. The best fit to (LBL90-OCONH-)$_n$ data occurs for R = 5.6 nm, σ_R = 0.81 nm, R_{HS} = 9.3 nm, and η = 0.41, whereas to (LBL90-COO-)$_n$ data, R = 5.6 nm, σ_R = 0.87 nm, R_{HS} = 9.0 nm, and η = 0.36. 209

Figure 5.11 Measured domain spacing, D, as a function of the total degree of polymerization, N. The D values fall on a straight line which slope is ca. 2/3, indicating the lamella period scales as $D \sim N^{2/3}$. 213

Figure 5.12 Representative stress versus strain curves for the LBL triblock, (LBL-OCONH-)$_n$ and (LBL-COO-)$_n$ multiblock copolymers. 215
Figure 5.13 Mechanical properties of LBL triblock, (LBL-OCONH-)$_n$ and (LBL-COO-)$_n$ multiblock copolymers: (a) elastic modulus; (b) strain at break; (c) stress at break (tensile strength); (d) toughness.....216

Chapter 1 Introductory Remarks

1.1 Introduction

Polymer materials are very close to our everyday lives and are used in many products. Polymers are not only used in commodities such as footwear, fabrics, adhesives, diapers, toys, and packaging, but are also in advanced technologies such as bullet proof vests, stealth aircraft, and resorbable sutures.[1] Many researchers have investigated synthetic procedures, molecular structures, physical properties, and applications of the polymers, resulting in tremendous progress and great achievements. The developments in the polymer science field allow the production of new materials with specific properties for a designed application.

The necessity of distinctive properties in the desired materials has led to an interest in combining the positive properties of different polymers. Scientists began to find a way to combine and control the unique properties of different polymers. At first, blending of homopolymers was considered as a method to obtain desired properties, with some of these polymer blends demonstrating successful results. For instance, high impact polystyrene (HIPS), which is a blend of glassy polystyrene and rubbery polybutadiene,

exhibits a high modulus and a good impact resistance.[2-3] General Electric Plastics (now SABIC Innovative Plastics) also commercialized another miscible blend, Noryl, which combines heat resistance, dimensional stability, and ductility of poly(*p*-phenylene oxide) with the low cost and fluidity of polystyrene.[4] However, most polymers are immiscible with one another, even when their monomers can be easily mixed. The enthalpic incompatibilities between the different polymer chains cause macrophase separation of the blends with little interface adhesion between the different polymers.[5]

The synthesis of block copolymers can be a pathway to combine the desired physical properties of polymers while avoiding the poor interfacial adhesion of immiscible blends. Since block copolymers are comprised of covalently bonded homopolymer blocks, it is possible to maintain the distinct properties of the homopolymers without macroscopic separation. Instead, block copolymers have microscopic-separated structures on a molecular scale, which can be controlled by changing the fractions of each block. Since these microphase structures have a large effect on the physical properties of the block copolymers, it is very important to control the microstructures to obtain desired materials. Numerous microphase structures of the block copolymers have been unearthed and studied with the improvement of the characterization techniques such as small-angle X-ray scattering (SAXS) and transmission electron microscopy (TEM). The typical microstructures of block copolymers are lamellae, bicontinuous gyroid, hexagonally packed cylinders, and body-centered cubic spheres.[6-7]

Studies about block copolymers were facilitated by the development of living

anionic polymerization which opened a way to produce precise control over block molecular weight and dispersity.[8-10] This technique allowed major progress in polymer synthesis as well as polymer physics. Moreover, the advent of living anionic polymerization provided possibilities for various architectures of block copolymers such as linear AB, ABA[11-12], ABC[13-15], ABCBA[15], ABCD[13-14], star copolymers[16] and so forth.[17] Well-defined polymers with precisely synthesized molecular structures using anionic polymerization provided a comprehensive investigation into morphologies.[18] Living anionic polymerization also offers facile mechanisms for functionalizing polymer chain ends, which can amplify the advantages of anionic polymerization by using well-established coupling chemistry.

An upsurge of the number of controlled synthetic pathways for block copolymers allows various chain structures and extended combinations of monomer sequences. Atom transfer radical polymerization (ATRP),[19] reversible addition-fragmentation transfer polymerization (RAFT),[20-21] stable free radical polymerization (SFRP),[22] ring-opening polymerization (ROP),[23-24] etc. have appeared as powerful tools for the synthesis of well-designed block copolymers.

Numerous block copolymers accessed using the developed synthetic techniques have attracted interest because of their unique microstructures, fascinating physical properties, and useful applications.[25] A lot of effort has been devoted to investigating the simplest molecular architectures like linear AB and ABA block copolymers, and has leaded to a comprehensive experimental and theoretical understanding of their phase behavior and physical properties.[18,26-29] However, much less research has been directed

toward multiblock copolymers which have a large number of blocks[30-38] or an increased number of block components.[39-43] Increasing the number of blocks would affect the thermodynamics of self-assembly and chain conformations. Thus, multiblock copolymers are expected to have distinct microstructures and a mechanical response which is different from that of conventional diblock and triblock copolymers.

The successful synthesis of conventional polymers from petroleum-based feedstocks ushered in the modern age of plastics. In the recent years, however, decreasing reserve of fossil fuels and growing concern for the environment have aroused great interest in bio-based and biodegradable polymers derived from non-petrochemical sources. Also, oil prices have reached an all-time high, and daily polymer prices have increased with the increase of the oil price. Hence, green chemistry and sustainability are necessary steps in the polymer field. These sustainable polymers are attractive from a renewable biomass feedstock perspective but also have benefits due to disposal options with minor environmental impact.[44-45] Polylactide (PLA) is one of the most promising renewable polymers which can be produced from plant derived resources. PLA has been vastly studied in respect of synthesis,[46-50] catalysis,[51-55] stereochemistry control,[56-59] and modification of physical properties.[60-74] Other renewable polymers consisting of monomers extracted from vegetable oils have also been widely investigated.[75-78] It is obvious that these bio-based materials will have increasing importance and expanding markets. Thus, it will be very important to reveal the structure-property relationships and degradation properties of these novel plastics.[45]

1.2 Block Copolymer Phase Behavior

The thermodynamic behavior of a polymer can be explained by the Flory–Huggins theory, which is an extension of regular solution theory. Flory–Huggins theory expresses the free energy of mixing of a two-component system, ΔG_m, according to the following equation.

$$\frac{\Delta G_m}{k_B T} = \frac{f_A}{N_A} \ln f_A + \frac{f_B}{N_B} \ln f_B + f_A f_B \chi_{AB} \tag{1.1}$$

where, k_B is the Boltzmann constant, T is the temperature, f_A and f_B are the volume fractions of A and B, N_A and N_B are the volumetric degree of polymerization of A and B, and χ_{AB} is the Flory–Huggins interaction parameter.[1] The first two terms in the above equation represent the configurational entropy, which favor the mixing between the two components (this term is negative). The last term is the enthalpic contribution which is usually positive and therefore favors separation. In most cases, the entropic contribution is very small because the polymers have a large degree of polymerization N. Hence, the enthalpic term with the χ_{AB} parameter dominates the above expression.

The Flory–Huggins interaction parameter, χ_{AB}, which describes the free-energy cost per monomer of contact between A and B monomers, is a crucial parameter to explain the phase behavior of block copolymers and is given by:

$$\chi_{AB} = \frac{z}{k_B T}\left(\varepsilon_{AB} - \frac{\varepsilon_{AA} + \varepsilon_{BB}}{2} \right) \tag{1.2}$$

where, z is the number of nearest-neighbor monomers to a copolymer configuration cell, and ε_{AB} is the interaction energy per monomer between A and B monomers.[6] Positive χ_{AB} exhibits the repulsion between A and B monomers, and negative value indicates the

tendency to mix. Additionally, χ_{AB} varies inversely with temperature. Since entropic and enthalpic contributions are proportional to N^{-1} and χ respectively, the product χN can be used for the determination of block copolymer phase behavior.[18,79] At sufficiently high temperatures, the small χ value favors mixing of both phases, resulting in a disordered state. Otherwise, a decrease of temperature and an increase of N cause an increase of the χ value and the loss of configurational energy, respectively. In this case, the microphase separation occurs (microdomains rich in A and B are formed), but the polymers cannot undergo macrophase separation because they are covalently bonded to each other. The separated microdomains are regularly arranged and form a particular ordered morphology rather than being randomly located. The typical morphologies encountered in the block copolymer field are shown in Figure 1.1; lamellae (LAM or L), hexagonally packed cylinders (HEX or C), body-centered cubic spheres (BCC or S), and bicontinuous gyroid (GYR or G), which can be controlled by changing block composition f.[7]

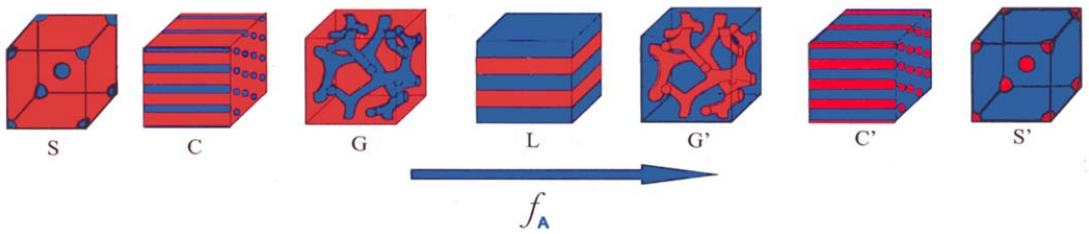

Figure 1.1 Different morphologies for AB diblock copolymers. Reproduced from Bates and Fredrickson.[6]

As mentioned above, the block copolymer phase behavior is mainly governed by two parameters: the product χN and the volume fraction of each block f. The product χN

controls the state of segregation, which can be divided into three regimes: strong segregation limit (for $\chi N >> 10$), weak segregation limit (for $\chi N \sim 10$) and intermediate segregation limit.[28]

In the strong segregation limit (SSL) regime, the theories are based on the assumption that the interface between the domains is very narrow compared to the domain sizes. Meier,[80] Leary and Williams,[81] Helfand and Wasserman[82-85] developed theories to describe the ordered microdomain structures in SSL. Helfand and Wasserman introduced self-consistent-field theory (SCFT) which allows quantitative calculations of free energies, composition profiles, and chain conformations.[83] They mentioned three major contributions to the free energy in SSL: (a) the tendency of domains to grow in order to reduce the interfacial energy per unit volume, (b) the loss of entropy due to localization of block joints at the interface, and (c) the entropy loss caused by chain stretching to keep a uniform density.[82-83] In this limit, entropy loss by stretching is large enough to ignore confinement entropy by the chain joints, which allows lager domain sizes. Helfand and Wasserman also applied this numerical method to spherical[84] and cylindrical[85] morphologies. Another SSL theory was developed by Semenov.[86] Semenov established an analytical method for estimating the free energy in the asymptotic limit $\chi N \rightarrow \infty$. This analytical approach has been further studied by Milner, Witten and Cates.[87-88]

The second limit regime is the weak segregation limit (WSL), which describes the phase behavior near the order-disorder transition temperature (T_{ODT}). In the WSL regime, which is the onset of the microphase structures from the homogeneous polymer melts, the narrow interface approximation of Helfand[82-83] cannot be used. Leibler[26] built up a theory

for the WSL. He considered a molten AB diblock copolymer which has the same volume and statistical segment length of monomers A and B. He also suggested two parameters related to the phase equilibrium: the composition f and the product χN. Leibler found a correlation function for the limit of stability of disordered molten state using the random phase approximation (RPA) introduced by de Gennes,[89] and constructed a phase diagram by comparing the free energies of the different ordered morphologies (Figure 1.2(a)).

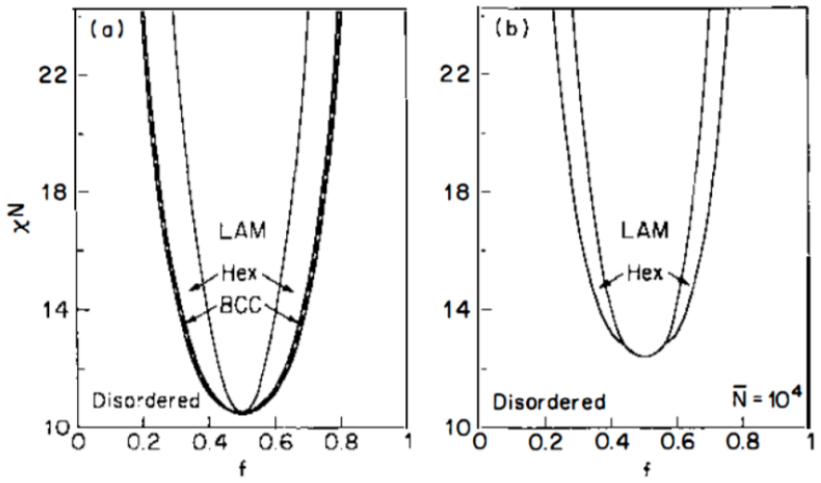

Figure 1.2 Theoretical phase diagram for diblock copolymers calculated by (a) mean-field theory (b) fluctuation theory with $\overline{N} = 10^4$. Reproduced from Bates and Fredrickson.[18]

Leibler's theory predicts a critical point at $\chi N = 10.495$ and $f = 0.5$. For compositionally symmetric diblock copolymer melt ($f = 0.5$), it is expected that the system is in the disordered phase when χN is less than the critical value. As χN increases (temperature decreases or N increases), the symmetric diblock melts undergoes a second

order phase transition to a lamellar morphology at the critical point. For an asymmetric diblock melt ($f \neq 0.5$), a first order transition to a body-centered cubic sphere morphology from the homogeneous melt is predicted by Leibler. This mean-field theory also suggests order-order transitions (OOT) between different morphologies by changing χN.[26] Later, the experimental phase diagram presented the possibility of the direct transition to lamellae from disordered melt without passing through BCC or HEX morphologies. To link this experimental result to the theory, Fredrickson and Helfand[90] investigated a fluctuation correction for Leibler's mean-field theory. Their theory, which considers the effect of the composition fluctuations, predicts a first order phase transition for symmetric diblock copolymer rather than the second order phase transition expected by Leibler. In fluctuation theory, the location of critical point is at $(\chi N)_{ODT} = 10.495 + 41.022\ \overline{N}^{1/3}$, where $\overline{N} = Na^6\rho^2$ and a, ρ are the statistical segment length and the number density of polymers, respectively.[79,90] They also theoretically proved the first order transitions to lamellae and hexagonally packed cylinder from asymmetric diblock melts, which were previously observed in experiments (Figure 1.2(b)). Moreover, they found the recovery of Leibler's theory when the block copolymers have an infinite molecular weight.

The above theories were able to predict the classical microphase structures. However, these approaches failed to approve the stability of bicontinuous gyroid phase that was experimentally identified later than the other phases.[7,91] Matsen and coworkers[92-93] theoretically examined the complex gyroid (G) morphology as well as classical ordered phases which are lamellae (L), hexagonally packed cylinders (C), body-centered cubic

spheres (S), and close-packed spheres(CPS) using SCFT in the intermediate segregation limit (ISL). They also constructed the phase diagram with two parameters: χN and f (Figure 1.3(a)). In ISL regime, as composition f changes from 0.5 to 0 or 1, the SCFT calculation predicts a sequence of order-order transitions: lamella–gyroid–cylinder–sphere–disorder. This theory suggests that the gyroid structure loses its stability above χN ~ 60 due to excessive packing frustration induced by the narrow interfaces. However, the recent work of Cochran and coworkers theoretically determined that the gyroid phase survives over a narrow compositional range into the strong segregation limit (SSL) for diblock copolymers.[94] Additionally, Matsen et al.[93,95] studied the effect of conformational asymmetry on the phase boundaries. The major result of asymmetrical conformation is that the order-disorder and order-order phase boundaries shift to compositions which are richer in the segments (Figure 1.4).[79] Khandpur and coworkers[96] mapped experimental phase diagram for polyisoprene-*b*-polystyrene (PI-PS) diblock copolymer melts. Figure 1.3(b) shows that experimental results are very similar to theoretically predicted phase diagram in Figure 1.3(a). Unlike the SCFT prediction, the experimental phase diagram shows an asymmetric shape which is attributed by the conformational asymmetry of monomers, i.e., isoprene and styrene monomers have different sizes and shapes.[6] Moreover, Khandpur's diagram has perforated layers (PL) structure, but SCFT calculation expects that PL is an unstable microphase. Later, other researchers found that the PL mesostructure is a long-lived metastable structure in the region where gyroid (G) is stable.[97-99]

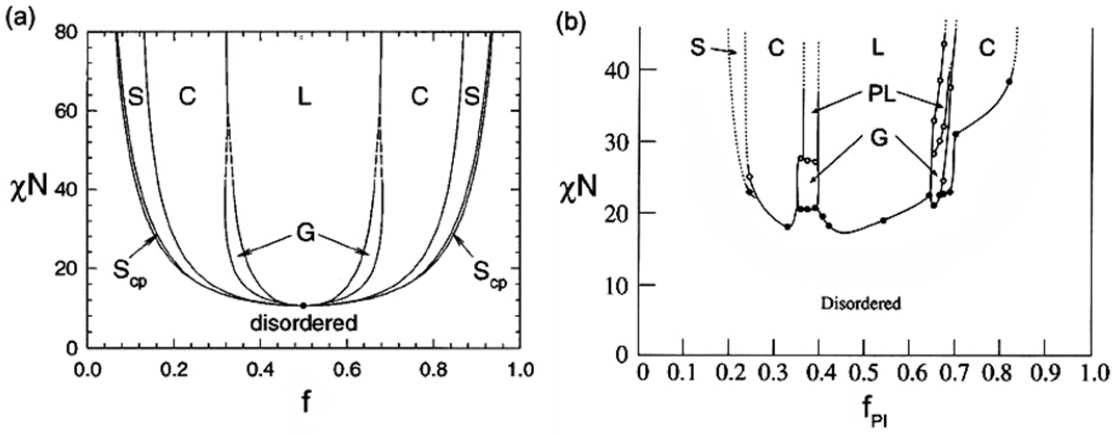

Figure 1.3 (a) Phase diagram for symmetric diblock melts calculated by SCFT. Reproduced from Matsen and Bates.[100] (b) Experimentally determined phase diagram for PI-PS diblock copolymer. Reproduced from Khandpur et al.[96]

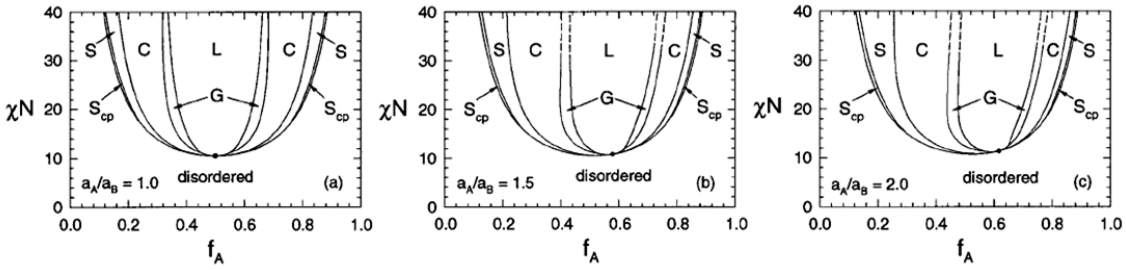

Figure 1.4 SCFT phase diagrams for diblock copolymer melts with different conformational asymmetries. (a) a_A/a_B = 1.0 (b) a_A/a_B = 1.5 (c) a_A/a_B = 2.0, where a is the statistical segment length. Reproduced from Matsen and Bates.[95]

The above research on AB diblock copolymers was extended to ABA triblock copolymers. For ordered ABA triblock copolymers, polymer chains have a tendency to

stretch to diminish the interfacial area. However, because B chains at the center of B-rich region are enclosed by other B chains, they are relatively unstretched. Thus, if all the ABA triblocks are cut to AB diblocks at this location, the cutting cannot affect the free energy of melts.[101] Helfand and Wasserman[83] predicted similar microdomain sizes for AB diblock and ABA triblock copolymers, where A blocks have the same size for AB and ABA, and B block of ABA is twice the size of B block of AB. Mayes and coworkers[27,102] also studied microphase separation of ABA triblock copolymer melts with Leibler's mean-field approach.[26] Matsen and Thompson[101] mapped the theoretical phase diagram of symmetric ABA triblock copolymers (degree of polymerization 2N) using SCFT calculation, and compared with their homologous AB diblock copolymers (degree of polymerization N). The results are shown in Figure 1.5. The phase behavior of AB and ABA copolymers are very similar to each other except for several key differences. Triblock copolymers remain ordered at lower χN (higher temperature) than their AB diblock counterparts, because the B block ends in AB diblock melts decrease the degree of segregation by easily entering into A domain.[101] They also found that triblock copolymers have microphase structures with larger domain spacing and their phase regions are shifted to smaller f_A due to the softer B domains in triblock melts. Although triblock and homologous diblock copolymer melts have very similar phase behavior, they evidently exhibit different mechanical properties due to the effect of bridging and looping induced by the triblock architecture. Bridging is the conformation when the two B ends are located on different domains, and looping is the conformation when both of B ends are at the same interface. The mechanical property section (see Section 1.3) will deal with

the details of bridging and looping.

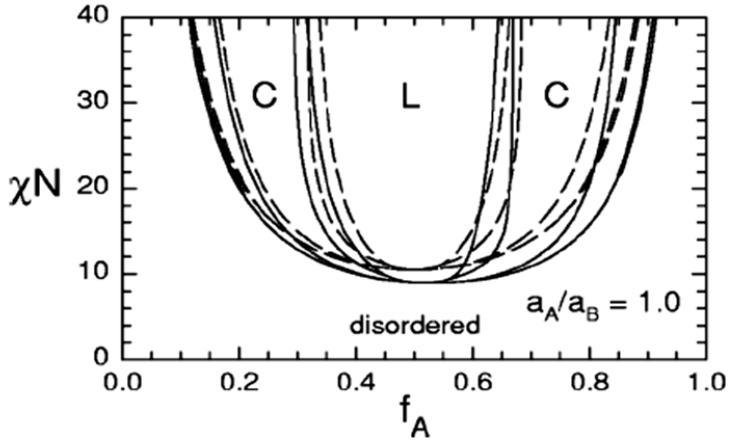

Figure 1.5 Triblock copolymer phase diagram (solid curves) and diblock copolymer phase diagram (dashed curves). Reproduced from Matsen and Thompson.[101]

After a nearly complete understanding of the thermodynamic behavior of AB diblock copolymers and their counterparts, the interest of researchers moved to ABC triblock terpolymers. In AB diblock copolymers, two parameters, χN and f_A, are enough to describe the phase behavior. However, ABC triblock systems have three different interaction parameters (χ_{AB}, χ_{BC}, χ_{AC}) and two independent composition variables (f_A and f_B).[6] Block sequence, for instance ABC, ACB, and BAC also can have dramatic effects on their behavior. This expansion of parameters brings about not only laborious experimental synthesis and characterization, but also difficult theoretical analysis. Despite these challenges, studies about ABC triblock copolymers have been accomplished and shown progressive results.[40,103-105] The complex morphologies for

linear ABC triblock copolymers theoretically proposed by Bates and Fredrickson[6] are shown in Figure 1.6.

When an ABC triblock is formed with equal block length ($f_A = f_B = f_C = 1/3$) and similar interaction parameters ($\chi_{AB} \approx \chi_{BC} \approx \chi_{AC}$), a consequent structure is three phase lamellae (Figure 1.6(a)). However, when $\chi_{AB} << \chi_{BC}$, this asymmetric interaction makes core-shell hexagonal phase (Figure 1.6(b)) to minimize BC interfacial area. Other morphologies can result when $\chi_{AB} \approx \chi_{BC} >> \chi_{AC}$ with small values of f_B. In this case, discontinuous B domains are favored to increase the AC interfacial area (Figure 1.6(c), (d), and (e)). The nearly symmetric system, where $\chi_{AB} \approx \chi_{BC} < \chi_{AC}$ and $f_A \approx f_C$, tends to minimize the contacts between A and C. For this system, as f_B increases, the resulting morphologies change with the following sequence: (a), (l), (f), and (g) in Figure 1.6.[6,39,106] Chatterjee et al. experimentally investigated various microphases of the ABC block architecture in polyisoprene-*block*-polystyrene-*block*-poly(ethylene oxide) (ISO) triblock copolymer system[42], and Qin et al. captured many of those microstructures using SCFT.[107]

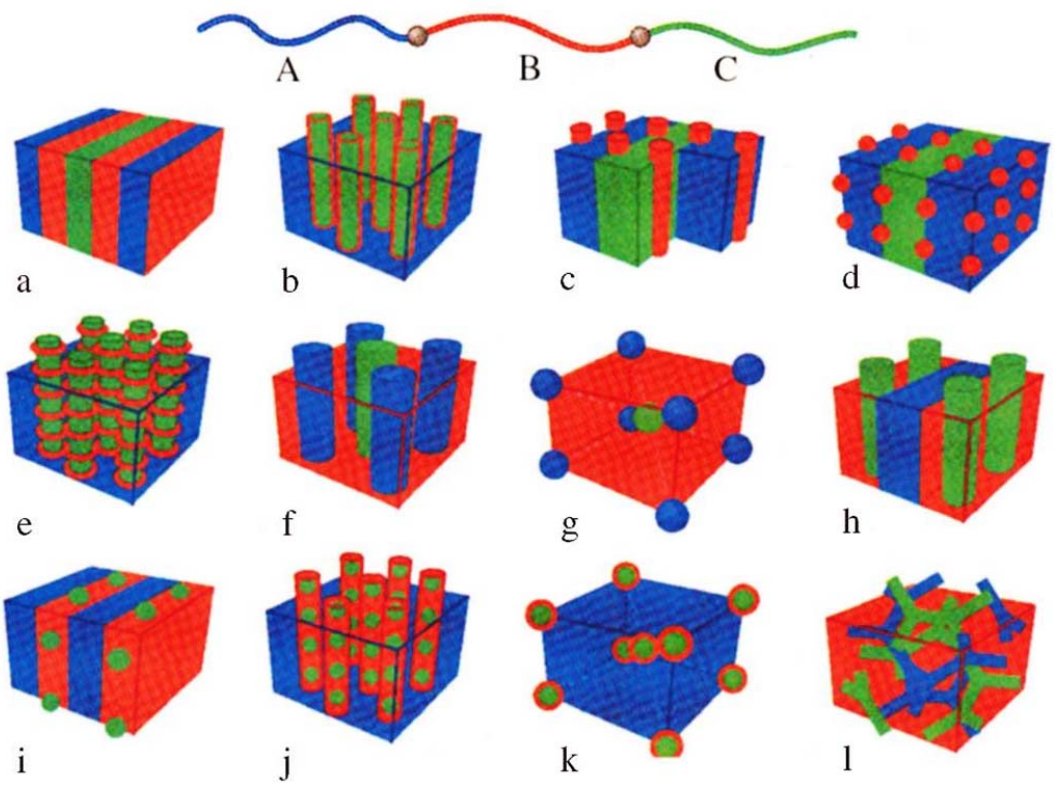

Figure 1.6 ABC linear triblock copolymer morphologies. Reproduced from Bates and Fredrickson.[6]

The classical morphologies, lamellae, hexagonally packed cylinders, body-centered cubic spheres, and bicontinuous gyroid are theoretically and experimentally well-established for the low-level structures. Relatively less effort has been devoted to the phase behavior of high-level structures (i.e., the multiblock copolymers). It is worthwhile to study multiblock copolymers having more blocks or block elements because they could have unique microstructures and physical properties.

Several researchers investigated the phase behavior of tetrablock and pentablock copolymers. Drolet and Fredrickson[108] studied the optimization of bridging in a

cylindrical CECEC pentablock copolymer as well as the morphologies of the ABCA tetrablock copolymers using SCFT calculations. Ryu[109] and Khanna[110] reported the deformation and fracture properties of the CECEC pentablocks with lamellae and hexagonally packed cylinder morphologies. Meuler et al.[111] probed the OSISO pentablock system, where O denotes poly(ethylene oxide), and identified two-domain lamellae $(LAM)_2$, orthorhombic Fddd network (O^{70}, "O" indicates an orthorhombic unit cell and "70" refers to the number of the space group in the crystallographic tables[112]) and three-domain lamellae (LAM_3) morphologies. Recently, Lee et al.[43] documented formation of the *σ*-phase in a low molecular weight sphere forming poly(isoprene-*b*-lactide) (IL) diblock copolymer and SISO tetrablock copolymer.

For higher-level multiblock copolymers, more complex behavior is expected due to a large expansion of associated parameters. However, less research has investigated multiblock copolymers. Benoit and Hadziioannou[113], Kavassalis and Whitmore[114], and Zielinski and Spontak[115] examined the theoretical relationship between the microphase separation and the number of blocks for linear multiblock copolymers. Wu et al.[30] reported the effect of the block number on T_{ODT} and viscoelastic behaviors for symmetric poly(styrene-*b*-isoprene) $(SI)_n$ (n = 1 – 10) multiblocks. They observed that T_{ODT} initially increases with increasing n and levels off starting with the tetrablock copolymers (n = 3), which is consistent with some random phase approximation (RPA) calculations. Recently, Matsushita's group examined some hierarchical structures exhibiting a double periodicity in multiblock terpolymers.[116-118] They reported that $S(IS)_4IS$ and $V(IS)_4IV$ undecablock copolymers (where S, I, and V denote polystyrene, polyisoprene, and poly(2-

vinylpyridine), correspondingly) have three-layered lamellae-in-lamellae and five-layered lamella-in-lamellae structures, respectively.[116-117] These hierarchical structures were further investigated with the $V(IS)_4IV$ and $V(SI)_2I$ copolymers with varying the volume fraction of V component.[118] Figure 1.7 summarizes the TEM observation results and the composition-dependent morphological transition of $A(BC)_nBA$ and $A(BC)_nB$ type terpolymers. Overall structures showed that the short I and S blocks developed alternating lamellae, while V domains were transformed with the conventional sequence of the morphological transition (sphere-cylinder-lamellae-matrix) with keeping a hierarchical nature. Moreover, Fleury and Bates[119] identified a perpendicular lamellae in parallel lamellae mesostructure with two different length scales in CECEC-P block copolymers, where P is poly(ethylene-*alt*-propylene).

Examination of the morphologies for the block copolymer is essential to understand their physical properties because the microdomain structures have a crucial effect on the behavior of the block copolymers. In this study, morphological behavior of poly(cyclohexylethylene)-polyethylene nonablock copolymers, poly(styrene-*b*-butadiene) multiblock copolymers, and poly(lactide-*b*-butadiene) multiblock copolymers will be examined with several characterization techniques (described in Section 2.2). In addition, the correlation between morphologies and physical properties will be investigated.

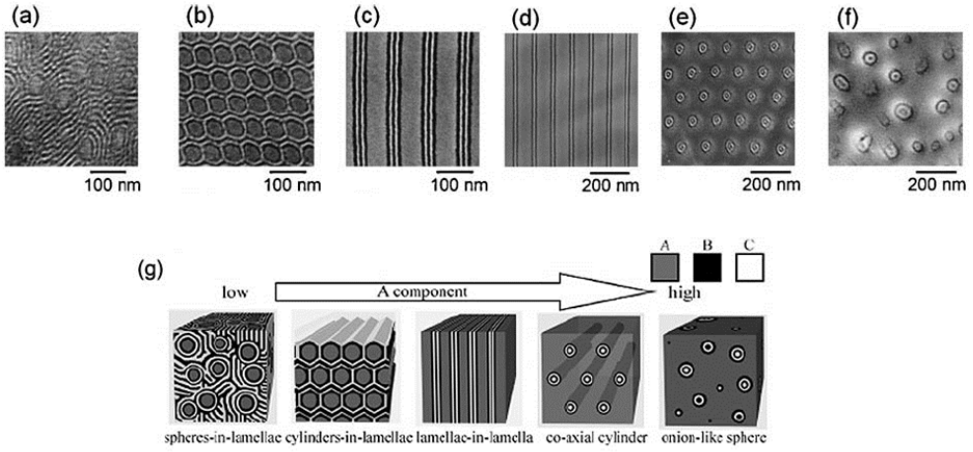

Figure 1.7 Various morphologies of $V(IS)_4IV$ ((a), (b), (c)) and $V(SI)_2I$ ((d), (e), (f)). Volume fractions of the V block are (a) 0.08, (b) 0.21, (c) 0.53, (d) 0.64, (e) 0.75, (f) 0.88. Reproduced from Matsushita.[120] (g) Scheme of the composition-dependent morphological transition of $A(BC)_nBA$ and $A(BC)_nB$ terpolymers. Reproduced form Masuda et al.[118]

1.3 Block Copolymer Mechanical Properties

Clarifying the basic terminologies related to the mechanical properties would be a good starting point to understand this field. The engineering stress, σ, is defined as the applied force per initial cross-sectional area, and the true stress is the force divided by the instantaneous cross-sectional area. The strain, ε, is the change of size or shape of materials. Usually, two types of strain are considered. One is the extensional strain which is defined as the fractional increase in length in the stretching direction. Another one is the simple shear strain defined by the displacement of parallel plates (Figure 1.8).[121]

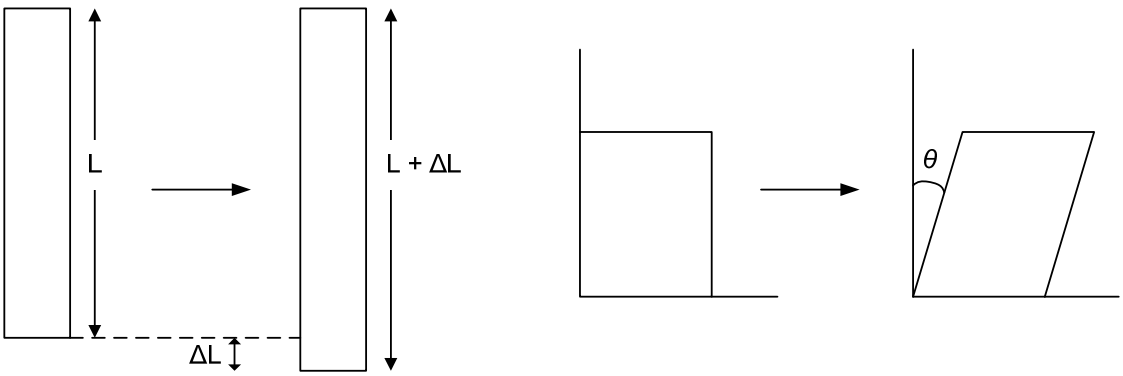

Figure 1.8 Illustration of (a) extensional strain and (b) simple shear strain. Reproduced from Ward and Sweeney.[121]

This study will use uniaxial tensile tests to analyze mechanical properties of the materials. After the testing, the results will be plotted as stress-strain curves. With this resulting plot, several significant parameters can be obtained. The Young's modulus, E, can be calculated from the slope of stress-strain curve in the linear-elastic region where the stress is proportional to the strain. This modulus is one of measures of stiffness of the material. The yield stress, σ_y, is defined as the limit of the elastic recoverable deformation or the onset of plastic irrecoverable deformation. In general, the yield stress can be identified by the maximum stress in the stress-strain curve. The stress at break (tensile strength), σ_b, is the stress where the specimen breaks. The strain at break, ε_b, is the strain at which the sample ruptures. The toughness of a material is the total energy absorbed up to failure, which is proportional to the area under the stress-strain curve.

Polymers have several types of stress-strain behavior. Figure 1.9 shows typical stress-strain curves of the polymer. Curve (a) illustrates the case when the polymer

fractures in a brittle manner. The Young's modulus is relatively higher than other cases, and the stress increases linearly with the increase of strain up to the break point. Normally, the value of the strain at failure is less than 10% in this case. Curve (b) and (c) illustrate ductile failure characteristic of the yielding process, which shows the yield point at the beginning of plastic deformation. Sometimes, ductile materials exhibit necking phenomenon shown in curve (c). Curve (d) shows rubber-like behavior which has no yield point. In this case, strains at failure are generally very large, up to 1000%, and moduli are lower by 2-3 orders of magnitude.[1]

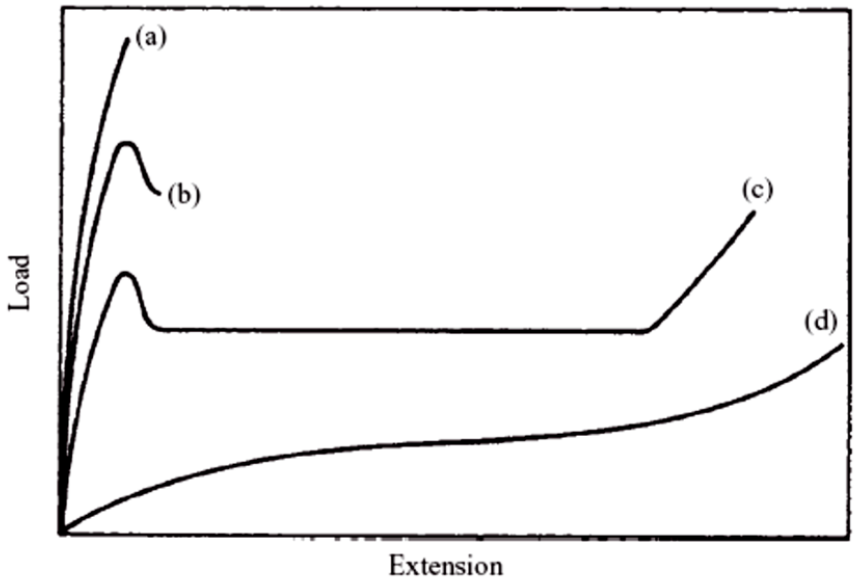

Figure 1.9 Stress-strain curves for a typical polymer showing deferent regions of mechanical behavior: (a) brittle fracture; (b) ductile; (c) ductile with necking; (d) elastomeric. Reproduced from Ward and Sweeney.[121]

More than one mechanical behavior can be seen in one kind of polymer. By varying the temperature, polyethylene and polypropylene can have brittle-to-ductile transition.[122-123] At low temperature, the molecular mobility is reduced, and polymer chains are hard to move around. Consequently, the covalent bonds are easily ruptured by a small deformation, which means brittle fracture. Otherwise, because the chains have a greater mobility at high temperatures, ductile behavior is observed. The variation of the rate of deformation can also cause this kind of transition.[1] In general, however, a single polymer shows one of the characteristic behaviors under ambient conditions.

Glassy polymers, such as polystyrene, poly(cyclohexylethylene), and poly(D,L-lactide), display brittle fracture; they exhibit high modulus and stress at break, but low strain at break and toughness (Figure 1.9(a)). In glassy polymers, the fracture occurs by crazing. Unlike metals and ceramics, the structural irregularity of the glassy polymer causes strain localization/concentration. Since cracks cannot propagate through the grain boundaries, microvoids are created in the polymer to accommodate the applied strain. This localized cavitation process causes crazes in the polymer sample.[1] Figure 1.10 illustrates craze formation in a glassy polymer. The craze structure consists of microvoids and surrounding fibrils. Because creating a new surface requires the energy, crazing can dissipate the externally supplied mechanical energy into fibrils. In this way, the craze enhances the mechanical strength of polymers.

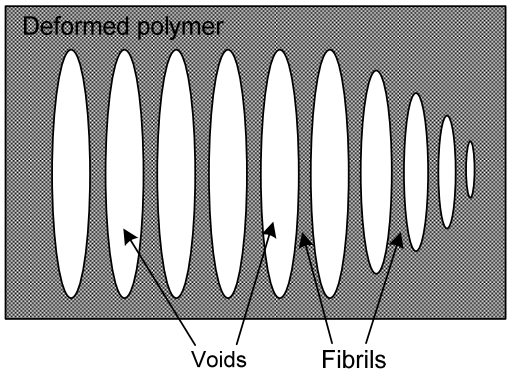

Figure 1.10 Formation of craze in a glassy polymer.

Plastic (ductile) materials, such as semicrystalline polyethylene, show a yielding deformation. In yielding, the strain is dispersed over a huge volume of the sample, and the delocalized strain prevents focusing the stress on a small region. The most dramatic consequence of the yielding is necking, where the specimen undergoes a change into a thin shape along its length. In Figure 1.9, curve (c) describes this phenomenon. Initially the stress increases almost linearly as the strain increases. When stress reaches its maximum, the specimen begins to neck, and consequently the stress falls. Then, the engineering stress achieves a minimum. In this region, the stress stays at approximately constant value as the neck propagates through the specimen. After the propagating neck covers the whole length of the sample, further strain causes the rise of the stress, which is described as a strain hardening.

There are three principal modes of deformation of the amorphous material in semicrystalline polymers: (1) interlamellar slip, (2) interlamellar separation, (3) stack rotation (Figure 1.11).[124-126] Interlamellar slip (Figure 1.11(a)) includes the shear of

lamellae parallel to each other with the amorphous phase undergoing shear. The elastic deformation of semicrystalline polymer comes from this reversible interlamellar slip. Figure 1.11(b) shows the lamellar separation mechanism induced by a component of tension or compression parallel to the lamellar surface. Because this type of deformation involves a change in volume, it is usually costly in energy. Stack rotation is described in Figure 1.11(c). The stacks of lamellae must be surrounded by amorphous region to rotate freely under the stress. The plastic deformation of polymer crystals generally occurs without destroying the crystalline order, except for large deformation accompanied with cavitation and voiding. Crystalline structure can deform physically by crystallographic slip, by twinning, and by martensitic transformation.[125]

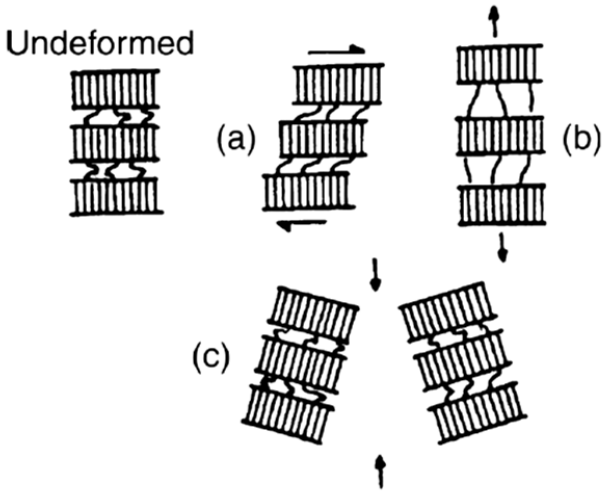

Figure 1.11 Deformation mechanisms of the amorphous phase in semicrystalline polymers: (a) interlamellar slip, (b) interlamellar separation, (c) stack rotation of lamellae. Reproduced from Bowden.[126]

Rubbery homopolymers like cross-liked polybutadiene exhibit elastic behavior described with low modulus, high extension, and strain hardening (Figure 1.9(d)). The elastomeric material is mainly characterized by large deformability and high recoverability. When the polymer chain is stretched, the entropy is reduced by fewer available chain conformations with increased ordering. Then, releasing the applied force leads the stretched chain to return to unstretched and coiled state which allows higher entropy. Thus, rubbery material can go back to original state when the external force is removed.

Different glassy, semicrystalline, and rubbery polymer blocks can be covalently bonded to produce desirable block copolymers. These block copolymers would have a wide range of mechanical properties which can be controlled by chain architecture, molecular weight, block composition and morphology.

Chain architecture of the block copolymer is a crucial factor in determining the mechanical properties. Several studies reported enhanced tensile properties of SBS and SIS block copolymers compared to SB, SI, BSB, and ISI blocks, where S, B, and I denote polystyrene, polybutadiene, and polyisoprene, respectively.[127-128] The enhanced toughness of SBS and SIS is attributed to their block chain configuration. The flexible PB and PI chains in the middle can connect the hard glassy domains, which make the rubber chains act like cross-links. In contrast, the absence of rubbery chains tying down the domains in BSB and ISI blocks results in brittle behavior.

The mechanical behavior of block copolymers is also affected by their molecular weight. In general, higher molecular weight displays better mechanical properties with

more chain entanglements. Molecular weight between entanglements, M_e is an important parameter. More entangled polymer chains have lower values of M_e and vice versa. Several researchers studied the effect of molecular weights on mechanical properties of polystyrene. Yang et al.[129] reported that a polystyrene chain shorter than 2–3 times M_e ($M_{e,PS}$ = 13,000 g/mol[130]) cannot build up tensile strength while polystyrene polymers have a molecular weight over $10M_e$ showed a constant strength.[129,131] The chain shorter than $2–3M_e$ will be easily pulled out by the external force because one of the chain ends will be smaller than M_e. On the contrary, the chains longer than $10M_e$ will be anchored by several entanglements. Many factors, such as temperature, deformation type, and deformation rate, can also have an effect on the plastic deformation. If all other things are equal, M_e would be a crucial molecular parameter.

Block composition of block copolymer is another important design parameter for the mechanical response. In glass/rubber block copolymer system, the relative amount of glassy and rubbery blocks can tune the mechanical behavior of their block copolymers. As the hard glassy block content increases, the block copolymer will vary from a flexible rubber to a tough, rigid plastic.[132] Holden et al.[133] studied the mechanical properties of SBS block copolymers having styrene contents ranging from 13 to 80% by weight along with PS and PB homopolymers. The block copolymers having a low content of PS (< 28 wt%) exhibited elastic behavior with the high elongation and low modulus. With the moderate amount of PS (30–65%), the tensile curves showed ductile and tough behavior with a yield followed by drawing. The SBS triblock copolymer containing a high content of PS (> 80%) becomes brittle.

Morphology of block copolymer also has significant effect on the mechanical properties. Sakurai et al.[134] and Qiao et al.[135] investigated the importance of morphology within SBS and SIS triblock copolymer system. They isolated the morphology effect from other factors, such as molecular weight and block composition, by using solvent casting with solvents of varying selectivity. Mechanical behavior of SBS and SIS thin films at fixed molecular weight and block composition were studied using tensile tests. Stress–strain curves and measured mechanical properties of triblock copolymers varied and depended on the morphologies; the results showed that modulus and yield stress increased with increasing glassy domain connectivity (see Figure 1.12). Dair et al.[136] investigated the stress–strain properties of isoprene–rich SIS triblock copolymers with the lamellar, cylindrical, spherical, double–gyroid morphologies. The sphere and cylinder samples exhibited a rubber-like behavior with very broad and diffuse response with no apparent yield point. The lamellar and double–gyroid samples showed a distinct yield point, but only double–gyroid microstructure exhibited stable necking and drawing.

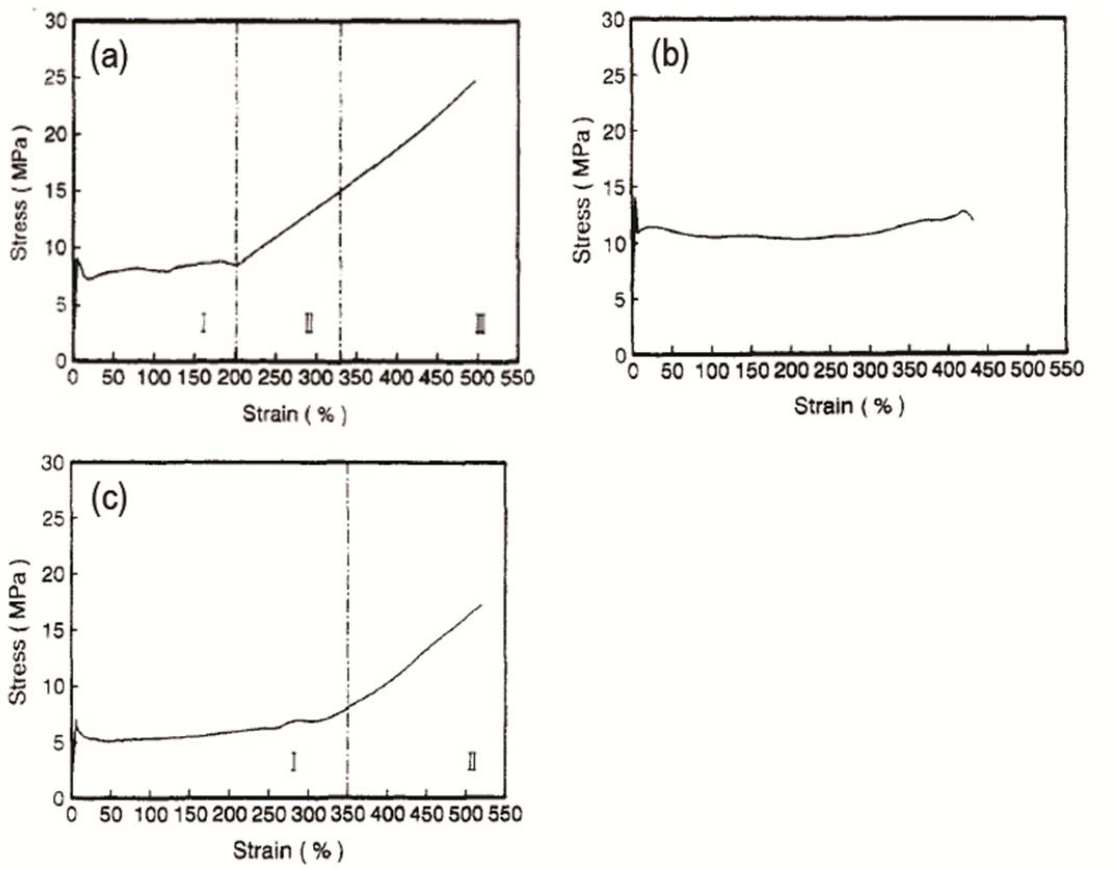

Figure 1.12 Stress–strain curves for SBS triblock copolymers with different morphologies at fixed molecular weight and block composition; (a) lamellar; (b) cylindrical; (c) bicontinuous morphology. Reproduced from Sakurai et al.[134]

Mechanical properties of glass–rubber block copolymers have been widely investigated. Matsuo et al.[128] studied stress–strain behavior affected by different chain architectures. They synthesized SB, SBS, BSB, and SBSB block copolymers and measured the mechanical properties using a tensile tester. SBS and SBSB block copolymers exhibited very tough mechanical behavior with the high elongation at break. However, SB and BSB block copolymers showed a brittle fracture even though the

rubbery PB component was incorporated. Holden et al.[133] examined SBS triblock copolymer having different glassy PS contents and their stress–strain curves are displayed in Figure 1.13. As the hard PS content increased, the SBS samples showed a transition of elastic–plastic–brittle behavior. Fetters and Morton[137] compared the mechanical behavior of SIS and mSImS triblock copolymers with virtually identical composition and molecular weight, where mS denotes poly(α-methylstyrene). In Figure 1.14, the measured tensile properties of the SIS (33% styrene) polymer exhibited tensile strength of 26 MPa and elongation of 1100 %, which are comparable to values of vulcanized natural rubber. The mSImS triblock copolymer showed substantially higher modulus and tensile strength compared to the corresponding SIS triblock copolymer, which implied that the poly(α-methylstyrene) domains are able to absorb more energy than the polystyrene. Furthermore, mSImS triblock exhibited superior mechanical strength at elevated temperature, which is attributed to the higher glass transition temperature (T_g) of mS ($T_{g,mS}$ = 165°C and $T_{g,S}$ = 105 °C).[138]

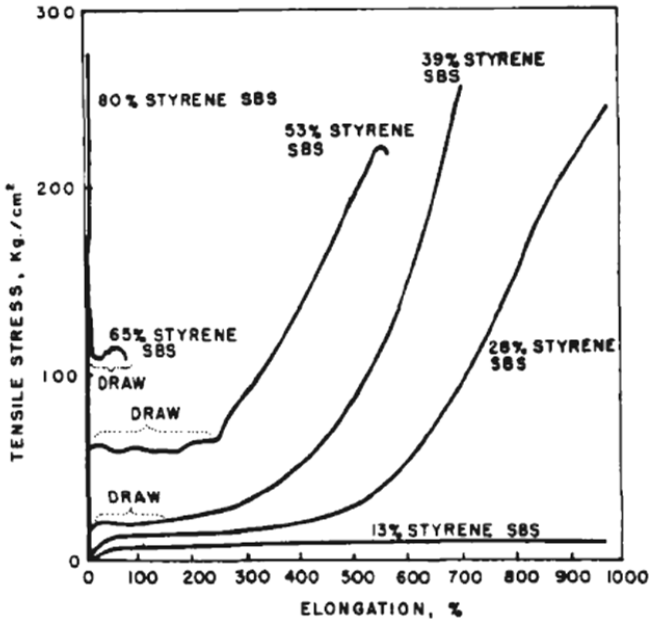

Figure 1.13 Stress–strain curves for SBS triblock copolymers of various styrene contents. Reproduced from Holden et al.[133]

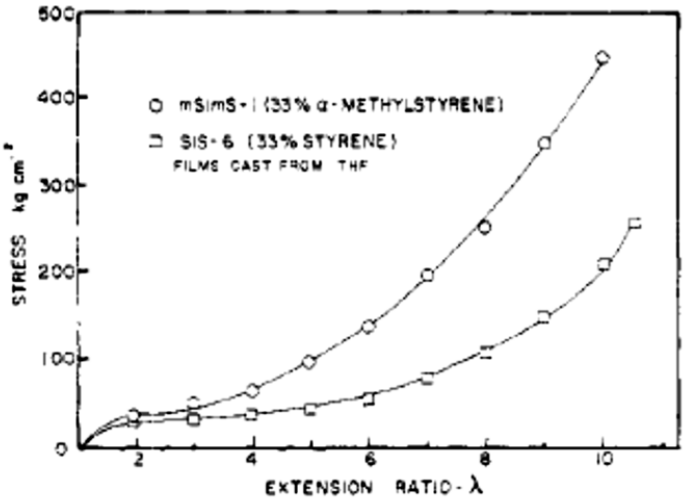

Figure 1.14 Stress-strain properties of SIS (□) and mSImS (○) triblock copolymers. Reproduced from Fetters and Morton.[137]

Fujimura et al.[127,139-140] studied SBS triblock copolymers having randomly oriented lamellar morphology, which were spin-cast from solution. They used small-angle X-ray scattering (SAXS) and transmission electron microscopy (TEM) to reveal a deformation mechanism of lamellar structure of the glass and rubber components. They concluded that the strain-induced plastic-to-rubber transition is caused by structural change from lamellar domains to fragmented PS domains dispersed in a PB matrix. This structural change is schematically summarized in Figure 1.15. The changes in structure from (a) to (b) illustrate the initial stage of deformation with the expansion of the lamellar spacing for the lamellae oriented perpendicular to the stretch direction. The changes in structure from (b) to (d) illustrate the deformation in the yielding and necking processes including kinking, shearing, destruction, and orientation of the lamellae. Upon further stretching (illustrated in (e)), polystyrene domains were fragmentized and dispersed in the rubbery matrix. The polystyrene fragments act as surface-active filler particles for the polybutadiene chains in the matrix.[140]

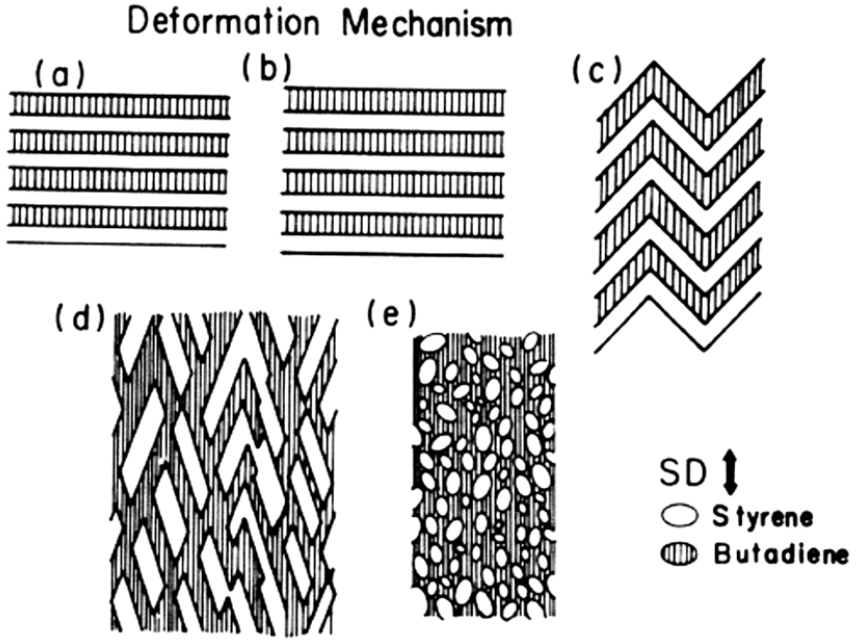

Figure 1.15 Representation of the deformation processes involved in the strain-induced plastic-to-rubber transition. Reproduced from Fujimura et al.[139]

Yamaoka and Kimura[141] investigated a lamellar SBS starblock copolymers treated by injection molding and by compression molding. Randomly oriented lamellar sample (injection molded) was deformed irregularly by predominant shear yielding to oriented and destructive lamellae, followed by fragmentation of PS domains. The oriented lamellar specimen was deformed regularly in zigzag by shear yielding, which resulted in the formation of chevron-like morphology without fragmentation. Cohen at al.[142] studied the deformation mechanism of lamellar films of the SBS triblock copolymer at different orientations of the deformation relative to the lamellar layer. Deformation parallel to the lamellae led to yielding with propagation of stable necking. The glassy PS layers broke up at yield, resulting in a plastic-to-rubber transition. Perpendicular deformation resulted

in folding of the layered structure into chevron morphology, and symmetric kink boundaries are formed at high strain. Diagonal (45°) stretching led to asymmetric kink boundaries without necking phenomena.

Morphological changes related to deformation of SBS triblock copolymer having a cylindrical microstructure (PS cylinders in a PB matrix) were also examined by Pakula et al. using SAXS and TEM.[143] They showed that the early and intermediate stages of deformation of cylindrical SBS are controlled by its morphology, while the deformation is governed by molecular orientation in the PB phase at large extensions. The deformation mechanism of oriented cylindrical SBS triblock copolymers at different stretching directions is summarized in Figure 1.16. At small deformations, cylindrical microstructure oriented perpendicular to the applied force exhibited an increase of the interdomain distance followed by fragmentation into small regions. Samples with the microstructure oriented along the stretching direction showed micronecking and breaking of PS microdomains in the early stage of deformation. The cylindrical structure oriented 45° to the drawing direction, at low-strain region, kept their cylinder morphology and underwent homogeneous reorientation of the structure by a shearing mechanism in the polybutadiene phase. At large deformations, cylinders in any direction went through the inhomogeneous reorientation of fragmented domains and developed chevron structures.

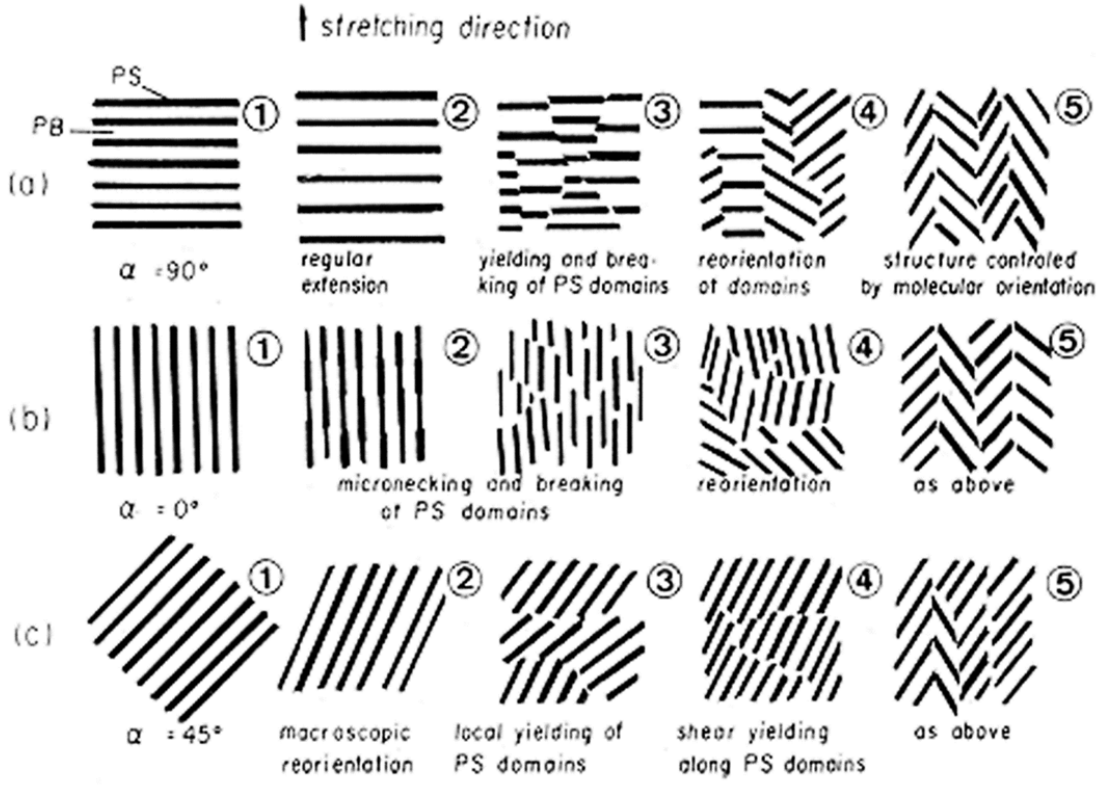

Figure 1.16 Schematic representation of structural changes caused by deformation of originally oriented SBS polymer with the cylindrical microdomains: (a) SD (stretching direction) perpendicular, (b) SD parallel, and (c) SD at 45° to the original orientation of the cylindrical domains. Reproduced from Pakula et al.[143]

Many researchers have also studied mechanical behavior of glass–semicrystalline block copolymers. Khanna et al.[110] studied the effect of chain architecture in C/E lamellar block copolymers by comparing symmetric (f_E = 0.48) CE diblock, CEC triblock, and CECEC pentablock polymer films. Because of the entropic penalty for looping and the small difference in surface energies between C and E blocks, these block copolymers

exhibited different equilibrium orientations. The triblock and pentablock lamellae align perpendicular to the film plane while the diblock lamellae show the parallel orientation.[110] They reported that CE diblock copolymer showed brittle fracture with little deformation by crazing at the beginning of the test. Adding E block cannot allow any enhanced mechanical properties compared to PCHE homopolymer.[109] This brittle behavior caused by the diblock architecture, which was also noted in SB diblock copolymer system.[128] Otherwise, CEC and CECEC exhibited ductile behavior and do not fail below the limit of the test (27% strain), and deformed by shear yielding.[110]

Hermel[144] and Lim[5] reported similar results for isotropic CEC and CECEC lamellae. The ductile behavior of the CEC and CECEC was obviously distinguished from the brittle behavior of CE. The mechanical behavior of shear-aligned CEC and CECEC lamellae was also investigated by Hermel et al.[145] and Phatak et al.[32] The triblock and pentablock lamellar samples were aligned with a perpendicular orientation under the reciprocating shear. For aligned (anisotropic) structure, triblocks and pentablocks had different mechanical behavior. When they applied strain normal to the lamellae, CEC triblock exhibited the brittle failure. However, CECEC pentablock showed ductility and enhanced toughness with a chevron structure deformation.[145]

The different mechanical behavior between diblock, triblock and pentablock can be described by understanding the concepts of bridging and looping chain conformations.[109,145-148] Various chain architectures of C/E block copolymers are shown in Figure 1.17. Since diblock copolymers lack bridging and looping, only van der Waals interactions and chain entanglements hold the domain together.[5] Hence, CE diblock

copolymers are very brittle. For CEC triblock copolymers, the middle E block can form bridges and loops which stitch other blocks together. In the isotropic CEC, brittle fracture is prevented by the plastic deformation of the semicrystalline domains. On the other hand, CECEC pentablock copolymers have enough bridging and looping configurations in all domains, which allow higher toughness and nearly orientation-independent mechanical properties.[32,145]

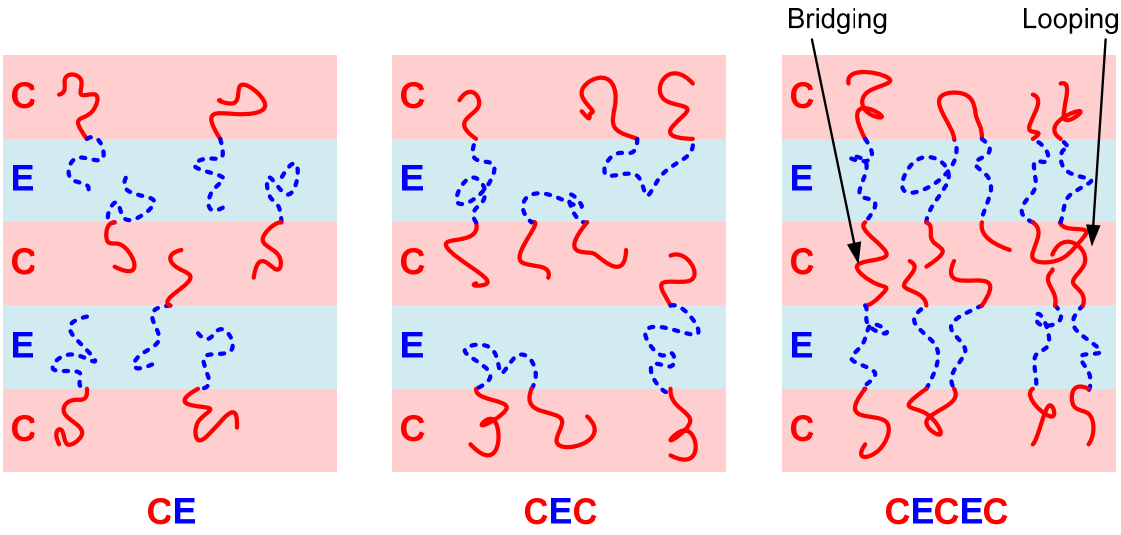

Figure 1.17 Illustration of chain architectures of lamellae-forming CE diblock, CEC triblock, CECEC pentablock copolymers.

In cylindrical morphology (E block cylinders are distributed out continuous C domain), a similar mechanical behavior was found for CEC and CECEC block copolymers. Ryu et al.[109] studied chain architecture effects on deformation and fracture in cylindrical C/E block copolymers. They found a brittle to ductile transition by changing

chain architecture from CEC to CECEC. This toughness of pentablock copolymer is attributed to the existence of middle block C connected with cylindrical E domains by bridging (see Figure 1.18).[109]

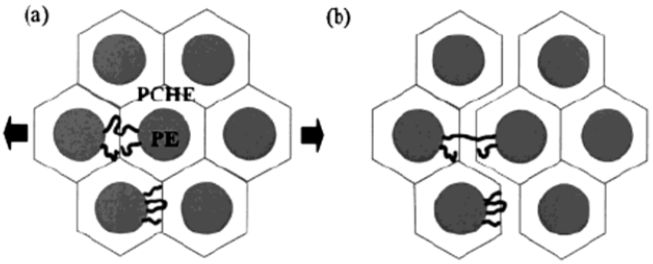

Figure 1.18 Schematics showing the role of bridging PCHE chains in CECEC. Reproduced from Ryu et al.[109]

Much research has been conducted on the mechanical properties affected by structural orientation in glass–semicrystalline block copolymer system. For lamellar structures, isotropic CEC material exhibits very different mechanical behavior from aligned lamellar CEC block copolymer.[5,32,144] The aligned lamellar CEC has brittle fracture when the strain is applied along the lamellar normal. However, the isotropic CEC material shows ductile and tough behaviors, indicating that toughness of materials also comes from the isotropic structure itself.[32] Ruokolainen et al.[149] investigated an important effect of structural orientation on the fracture behavior of CEC film with cylindrical morphology. When the cylinder orientation of the E block was random or parallel to the applied strain, a ductile behavior was observed. Otherwise, when the cylindrical axes were perpendicular to the sample film surface and hence transverse to the direction of the

strain, a brittle behavior was observed.[149] Khanna and coworkers[110] reported similar behavior for CECEC cylindrical pentablock copolymers. The Results are summarized in Figure 1.19.

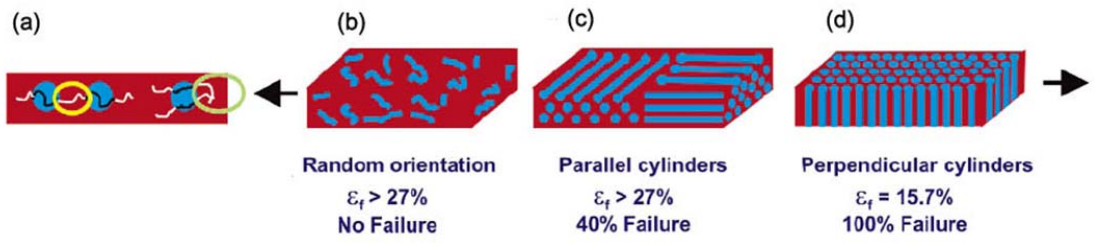

Figure 1.19 The effect of microdomain orientation in a cylindrical pentablock copolymer: (a) bridging (yellow circle) and looping (green circle) PCHE chains in a cylindrical morphology, (b) copolymers with a random orientation of cylinders, (c) grains of cylinders aligned with their axes parallel to the film plane, and (d) cylinders aligned with their axes perpendicular to the film plane. Reproduce from Khanna et al.[110]

As mentioned earlier, the presence of bridging in the middle block is a crucial factor in determining the toughness of pentablock copolymers. As described in Figure 1.17 and Figure 1.19(a), center C block chains can have two options: bridging and looping. Drolet and Fredrickson[108] studied optimization of chain bridging in ABABA pentablock copolymers with self-consistent-field theory (SCFT) calculation. They considered symmetric pentablock system; outer A(glassy, hard) blocks had equal volume fractions ($f_1 = f_5$), and inner B(soft) blocks also had the same size ($f_2 = f_4$). Overall glass content was constrained to be 70% ($f_A = f_1 + f_2 + f_3 = 0.70$) for high modulus, and the expected morphology was hexagonal B cylinders in a continuous A domain. The

calculated results are shown in Figure 1.20. The fraction of center A blocks in bridged conformation, f_{br}, increased with the increase of the center block fraction, f_3 (Figure 1.20(a)). Considering the relation between bridge fraction and toughness, this figure suggests that toughness should be optimal when the center block faction is close to 0.5.[108] Figure 1.20(b) shows the variation of the distance between cylinders, D_{cyl}, with f_3. A rapid drop of D_{cyl} was observed when $0.12 \leq f_3 \leq 0.20$; in this interval, the length of the outer A blocks controlled the spacing between cylinders. In the regime of $0.4 \leq f_3 \leq 0.54$, D_{cyl} rapidly increased, indicating intercylinder spacing is controlled by the central A block.[108]

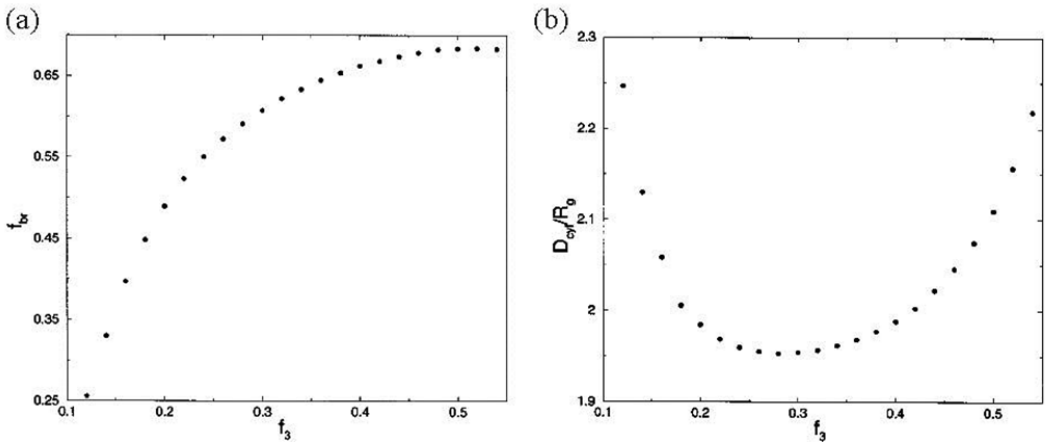

Figure 1.20 (a) Average fraction of middle A blocks in bridged conformation f_{br} as a function of middle block fraction f_3 for symmetric ABABA pentablock copolymers. (b) Average distance between neighboring B cylinders as a function of middle block fraction f_3 for symmetric ABABA pentablock copolymers. Reproduced from Drolet and Fredrickson.[108]

Phatak et al.[32] studied tensile properties of polydomain CEC, ECEC, CECEC, and ECECE block copolymers, and blends of these materials. They revealed a critical relationship between the mechanical properties and the connectivity of semicrystalline E blocks. They plotted the failure strain, ε_f (strain at break, ε_b) as a function of the weight fraction of tied down E chains, ψ_E, defined as

$$\psi_E = \begin{cases} \dfrac{n_{CEC}M_{E,CEC} + n_{ECEC}M_{E,ECEC}}{n_{CEC}M_{E,CEC} + 2n_{ECEC}M_{E,ECEC}} & \text{for CEC/ECEC blends} \\ \dfrac{n_{CEC}M_{E,CEC} + n_{ECECE}M_{E,ECECE}}{n_{CEC}M_{E,CEC} + 3n_{ECECE}M_{E,ECECE}} & \text{for CEC/ECECE blends} \end{cases} \quad (1.3)$$

where, $M_{E,X}$ is the molecular weight of a E block in copolymer X and n_x is the number fraction of chains of copolymer X in a blend. They also included the data from the literature for CE, ECE, CEC, CECEC block copolymers,[31,144] and the results are shown in Figure 1.21. Toughness of block copolymers can be achieved by more pinning down E chains (increase of ψ_E), and when $\psi_E > 0.8$, all architectures have a good mechanical behavior ($\varepsilon_f > 300\%$).[32] They also found that changing the symmetry of ECECE block copolymer can provide a way to enhance mechanical properties. Asymmetric ECECE with a middle-to-end block ratio ($N_{2,E}/N_{1,E}$) of 2.6 exhibited a notably high failure strain which is not consistent with the universal curve (the open triangle symbol in Figure 1.21).[32]

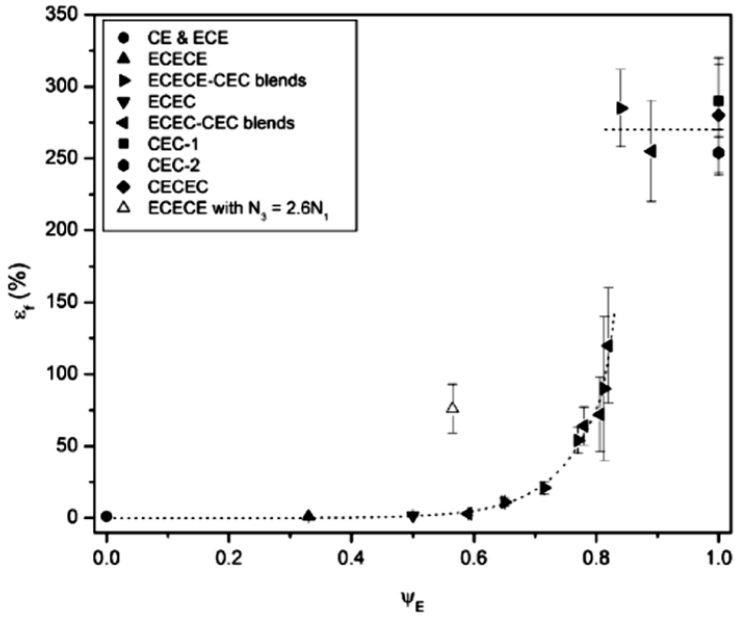

Figure 1.21 The failure strain as a function of ψ_E for C/E block copolymer architectures. Reproduced from Phatak et al.[32]

Koo et al.[33] reported the structure–property relationship in another multiblock copolymer system having more number of blocks. They investigated linear $(EP)_n$ (n = 2, 4, 6, 8, 10, and 12) multiblock copolymers containing semicrystalline polyethylene (E) and rubbery poly(ethylene-*alt*-propylene) (P) blocks with $M_w[(EP)_0] \approx 23$ kg/mol. In $(EP)_n$ multiblock copolymers, the total number of blocks was $n + 1$ and the terminal E blocks have half the molecular weight of the internal E and P blocks to ensure compositional symmetry ($f_E \approx f_P$). The measured stress–strain curves of $(EP)_n$ samples are displayed in Figure 1.22. The interesting feature of this study was the transition from strain softening ($(EP)_n$ with $n \leq 8$) to strain hardening ($(EP)_n$ with $n \geq 10$). Two categories of the tensile strength of these materials were identified: weak (σ_b < 10 MPa) and strong

(σ_b > 20 MPa) tensile strengths. High strength was exhibited by the disordered undecablock (n = 10) and tridecablock (n = 12) copolymers. Structural analysis suggested that the transition of mechanical behavior is attributed to a transition from decoupled to coupled E crystals, which implies a change in morphology.[33]

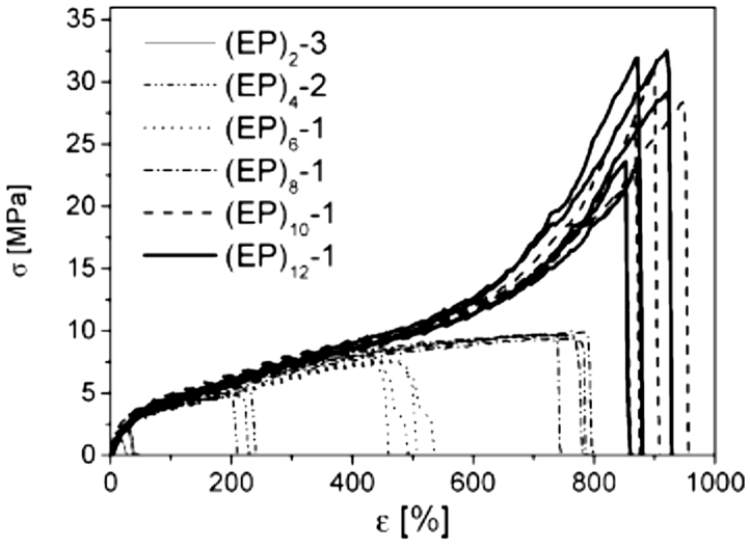

Figure 1.22 Stress-strain curves $(EP)_n$ block copolymers with n = 2, 4, 6, 8, 10, and 12. For $n \leq 8$ the materials strain soften, while for $n \geq 10$ they strain harden. Reproduced from Koo et al.[33]

1.4 Thesis Outline

This thesis describes synthesis and characterization of multiblock copolymers containing a large number of blocks to enlarge understanding of multiblock copolymer system. In this project, poly(cyclohexylethylene)-polyethylene (CECECECEC)

nonablock copolymers, poly(styrene-*b*-butadiene) (PS-PB) multiblock copolymers, and poly(lactide-*b*-butadiene) (PLA-PB) multiblock copolymers were investigated to acquire more knowledge about phase behavior and structure–property relationships of multiblock copolymers. This chapter reviewed the literature concerning the structural and mechanical properties of block copolymers that can provide background information related to this study. Multiblock copolymers were prepared using living anionic polymerization, ring-opening polymerization, coupling chemistry, and catalytic hydrogenation. Then, the synthesized block copolymers were characterized though size exclusion chromatography (SEC), nuclear magnetic resonance (NMR) spectroscopy, differential scanning calorimetry (DSC), small-angle X-ray scattering (SAXS), dynamic mechanical spectroscopy (DMS), transmission electron microscopy (TEM), and tensile testing. Descriptions of these synthetic and analytic methods are given in Chapter 2. Microstructures and mechanical responses of CECECECEC nonablock copolymers consisting of a large center C block are presented in Chapter 3. CECECECEC exhibited three different possible microstructures with varying size of the PE blocks, which also affected their mechanical properties. Synthesis and characterization of alternating and random PS-PB multiblock copolymers are described in Chapter 4. The investigated PS-PB multiblock samples showed random bicontinuous-like morphology irrespective of their compositions and block sequences. The multiblock copolymers also exhibited enhanced mechanical properties compared to the conventional SBS triblock copolymers. Chapter 5 includes sustainable multiblock copolymers of polylactide and polybutadiene. PLA-PB multiblock copolymers displayed different ordered microstructures with varying

volume fraction of PLA, and measured mechanical properties of PLA-PB multiblock samples were superior to the corresponding triblock copolymers. Lastly, Chapter 6 contains a summary of our findings from Chapter 3–5.

1.5 References

[1] Hiemenz, P. C.; Lodge, T. P. *Polymer Chemistry*, 2nd ed.; Taylor & Francis Group: New York, 2007.

[2] Cigna, G.; Matarrese, S.; Biglione, G. F. *J. Appl. Polym. Sci.* **1976,** *20*, 2285-2295.

[3] Anzaldi, S.; Bonifaci, L.; Malaguti, E.; Vighi, M.; Ravanetti, G. P. *J. Mater. Sci. Lett.* **1994,** *13*, 1555-1557.

[4] Ruzette, A.-V.; Leibler, L. *Nat Mater* **2005,** *4*, 19-31.

[5] Lim, L. S. *Effects fo Glassy, Rubbery, and Semicrystalline Blocks on the Mechanical Response of Polyolefin Block Copolymers*. Ph.D. Dissertation, University of Minnesota, 2005.

[6] Bates, F. S.; Fredrickson, G. H. *Physics Today* **1999,** *52*, 32.

[7] Hajduk, D. A.; Harper, P. E.; Gruner, S. M.; Honeker, C. C.; Kim, G.; Thomas, E. L.; Fetters, L. J. *Macromolecules* **1994,** *27*, 4063-4075.

[8] Szwarc, M. *Adv. Polym. Sci.* **1983,** *49*, 1-177.

[9] Morton, M. *Anionic Polymerization : Principles and Practice*; Academic Press New York, 1983.

[10] Hsieh, H. L.; Quirk, R. P. *Anionic Polymerization: Principles and Practical Applications*; Marcel Dekker: New York, 1996.

[11] Szwarc, M.; Levy, M.; Milkovich, R. *J. Am. Chem. Soc.* **1956,** *78*, 2656-2657.

[12] Miyamoto, T.; Kodama, K.; Shibayama, K. *Journal of Polymer Science Part A-2: Polymer Physics* **1970,** *8*, 2095-2103.

[13] Pan, J.; Chen, M.; Warner, W.; He, M.; Dalton, L.; Hogen-Esch, T. E. *Macromolecules* **2000,** *33*, 4673-4681.

[14] Watkins, D. M.; Fox, M. A. *Macromolecules* **1995,** *28*, 4939-4950.

[15] Mateva, R.; Filyanova, R.; Velichkova, R.; Gancheva, V. *J. Polym. Sci., Part A: Polym. Chem.* **2003,** *41*, 487-496.

[16] Iatrou, H.; Hadjichristidis, N. *Macromolecules* **1992,** *25*, 4649-4651.

[17] Schlick, S.; Levy, M. *The Journal of Physical Chemistry* **1960,** *64*, 883-886.

[18] Bates, F. S.; Fredrickson, G. H. *Annu. Rev. Phys. Chem.* **1990,** *41*, 525-557.

[19] Kamigaito, M.; Ando, T.; Sawamoto, M. *Chem. Rev.* **2001,** *101*, 3689-3746.

[20] Chiefari, J.; Chong, Y. K.; Ercole, F.; Krstina, J.; Jeffery, J.; Le, T. P. T.; Mayadunne, R. T. A.; Meijs, G. F.; Moad, C. L.; Moad, G.; Rizzardo, E.; Thang, S. H. *Macromolecules* **1998,** *31*, 5559-5562.

[21] Moad, G.; Rizzardo, E.; Thang, S. H. *Aust. J. Chem.* **2005,** *58*, 379-410.

[22] Georges, M. K.; Veregin, R. P. N.; Kazmaier, P. M.; Hamer, G. K. *Macromolecules* **1993,** *26*, 2987-2988.

[23] Penczek, S.; Kubisa, P.; Matyjaszewski, K. *Cationic ring-opening polymerization of heterocyclic monomers*; Springer-Verlag: New York, 1980.

[24] Penczek, S.; Cypryk, M.; Duda, A.; Kubisa, P.; Słomkowski, S. *Prog. Polym. Sci.* **2007,** *32*, 247-282.

[25] Bates, F. S.; Hillmyer, M. A.; Lodge, T. P.; Bates, C. M.; Delaney, K. T.; Fredrickson, G. H. *Science* **2012,** *336*, 434-440.

[26] Leibler, L. *Macromolecules* **1980,** *13*, 1602-1617.

[27] Mayes, A. M.; de la Cruz, M. O. *The Journal of Chemical Physics* **1989,** *91*, 7228-7235.

[28] Fredrickson, G. H.; Bates, F. S. *Annu. Rev. Mater. Sci.* **1996,** *26*, 501-550.

[29] Holden, G.; Kricheldorf, H. R.; Quirk, R. P. *Thermoplastic Elastomers*, 3rd ed.; Hanser Gardner Publications: Cincinnati, 2004.

[30] Wu, L.; Cochran, E. W.; Lodge, T. P.; Bates, F. S. *Macromolecules* **2004,** *37*, 3360-3368.

[31] Lim, L. S.; Harada, T.; Hillmyer, M. A.; Bates, F. S. *Macromolecules* **2004,** *37*, 5847-5850.

[32] Phatak, A.; Lim, L. S.; Reaves, C. K.; Bates, F. S. *Macromolecules* **2006,** *39*, 6221-6228.

[33] Koo, C. M.; Hillmyer, M. A.; Bates, F. S. *Macromolecules* **2006,** *39*, 667-677.

[34] Arriola, D. J.; Carnahan, E. M.; Hustad, P. D.; Kuhlman, R. L.; Wenzel, T. T. *Science* **2006,** *312*, 714-719.

[35] Watanabe, H.; Matsumiya, Y.; Sawada, T.; Iwamoto, T. *Macromolecules* **2007,** *40*, 6885-6897.

[36] Khariwala, D. U.; Taha, A.; Chum, S. P.; Hiltner, A.; Baer, E. *Polymer* **2008,** *49*, 1365-1375.

[37] Fleury, G.; Bates, F. S. *Macromolecules* **2009,** *42*, 3598-3610.

[38] Matsumiya, Y.; Watanabe, H.; Takano, A.; Takahashi, Y. *Macromolecules* **2013,** *46*, 2681-2695.

[39] Mogi, Y.; Nomura, M.; Kotsuji, H.; Ohnishi, K.; Matsushita, Y.; Noda, I. *Macromolecules* **1994,** *27*, 6755-6760.

[40] Stadler, R.; Auschra, C.; Beckmann, J.; Krappe, U.; Voight-Martin, I.; Leibler, L. *Macromolecules* **1995,** *28*, 3080-3097.

[41] Hadjichristidis, N.; Iatrou, H.; Pitsikalis, M.; Pispas, S.; Avgeropoulos, A. *Prog. Polym. Sci.* **2005,** *30*, 725-782.

[42] Chatterjee, J.; Jain, S.; Bates, F. S. *Macromolecules* **2007,** *40*, 2882-2896.

[43] Lee, S.; Bluemle, M. J.; Bates, F. S. *Science* **2010,** *330*, 349-353.

[44] Avérous, L.; Pollet, E. *Environmental Silicate Nano-biocomposites*; Springer: 2012.

[45] Williams, C. K.; Hillmyer, M. A. *Polymer Reviews* **2008,** *48*, 1-10.

[46] Benninga, H. *A history of lactic acid making*; Kluwer Academic Publishing: Boston, London, Dordrecht, 1990.

[47] Datta, R.; Tsai, S.-P.; Bonsignore, P.; Moon, S.-H.; Frank, J. R. *FEMS Microbiology Reviews* **1995,** *16*, 221-231.

[48] Kricheldorf, H. R.; Sumbél, M. *Eur. Polym. J.* **1989,** *25*, 585-591.

[49] Kricheldorf, H. R.; Kreiser, I. *Die Makromolekulare Chemie* **1987,** *188*, 1861-1873.

[50] Inata, H.; Matsumura, S. *J. Appl. Polym. Sci.* **1985,** *30*, 3325-3337.

[51] O'Keefe, B. J.; Hillmyer, M. A.; Tolman, W. B. *J. Chem. Soc., Dalton Trans.* **2001**, 2215-2224.

[52] Bourissou, D.; Moebs-Sanchez, S.; Martín-Vaca, B. *Comptes Rendus Chimie* **2007,**

10, 775-794.

[53] Cheng, M.; Attygalle, A. B.; Lobkovsky, E. B.; Coates, G. W. *J. Am. Chem. Soc.* **1999,** *121*, 11583-11584.

[54] Williams, C. K.; Breyfogle, L. E.; Choi, S. K.; Nam, W.; Young, V. G.; Hillmyer, M. A.; Tolman, W. B. *J. Am. Chem. Soc.* **2003,** *125*, 11350-11359.

[55] Stevels, W. M.; Ankoné, M. J. K.; Dijkstra, P. J.; Feijen, J. *Macromolecules* **1996,** *29*, 3332-3333.

[56] Spassky, N.; Wisniewski, M.; Pluta, C.; Le Borgne, A. *Macromol. Chem. Phys.* **1996,** *197*, 2627-2637.

[57] Ovitt, T. M.; Coates, G. W. *J. Am. Chem. Soc.* **1999,** *121*, 4072-4073.

[58] Hormnirun, P.; Marshall, E. L.; Gibson, V. C.; White, A. J. P.; Williams, D. J. *J. Am. Chem. Soc.* **2004,** *126*, 2688-2689.

[59] Ma, H.; Spaniol, T. P.; Okuda, J. *Angew. Chem. Int. Ed.* **2006,** *45*, 7818-7821.

[60] Perego, G.; Cella, G. D.; Bastioli, C. *J. Appl. Polym. Sci.* **1996,** *59*, 37-43.

[61] Bigg, D. M. *Adv. Polym. Tech.* **2005,** *24*, 69-82.

[62] Labrecque, L. V.; Kumar, R. A.; Davé, V.; Gross, R. A.; McCarthy, S. P. *J. Appl. Polym. Sci.* **1997,** *66*, 1507-1513.

[63] Jacobsen, S.; Fritz, H. G. *Polymer Engineering & Science* **1999,** *39*, 1303-1310.

[64] Baiardo, M.; Frisoni, G.; Scandola, M.; Rimelen, M.; Lips, D.; Ruffieux, K.; Wintermantel, E. *J. Appl. Polym. Sci.* **2003,** *90*, 1731-1738.

[65] Kulinski, Z.; Piorkowska, E. *Polymer* **2005,** *46*, 10290-10300.

[66] Wang, L.; Ma, W.; Gross, R. A.; McCarthy, S. P. *Polym. Degrad. Stab.* **1998,** *59*,

161-168.

[67] Broz, M. E.; VanderHart, D. L.; Washburn, N. R. *Biomaterials* **2003,** *24*, 4181-4190.

[68] Anderson, K. S.; Lim, S. H.; Hillmyer, M. A. *J. Appl. Polym. Sci.* **2003,** *89*, 3757-3768.

[69] Jiang, L.; Wolcott, M. P.; Zhang, J. *Biomacromolecules* **2005,** *7*, 199-207.

[70] Hashima, K.; Nishitsuji, S.; Inoue, T. *Polymer* **2010,** *51*, 3934-3939.

[71] Feng, F.; Ye, L. *J. Appl. Polym. Sci.* **2011,** *119*, 2778-2783.

[72] Kowalczyk, M.; Piorkowska, E. *J. Appl. Polym. Sci.* **2012,** *124*, 4579-4589.

[73] Zhu, K. J.; Xiangzhou, L.; Shilin, Y. *J. Appl. Polym. Sci.* **1990,** *39*, 1-9.

[74] Frick, E. M.; Zalusky, A. S.; Hillmyer, M. A. *Biomacromolecules* **2003,** *4*, 216-223.

[75] Lligadas, G.; Ronda, J. C.; Galià, M.; Cádiz, V. *Biomacromolecules* **2010,** *11*, 2825-2835.

[76] Meier, M. A. R.; Metzger, J. O.; Schubert, U. S. *Chem. Soc. Rev.* **2007,** *36*, 1788-1802.

[77] Güner, F. S.; Yağcı, Y.; Tuncer Erciyes, A. *Prog. Polym. Sci.* **2006,** *31*, 633-670.

[78] Belgacem, M. N.; Gandini, A. *Monomers, Polymers and Composites from Renewable Resources*; Elsevier: Amsterdam, 2008.

[79] Hadjichristidis, N.; Pispas, S.; Floudas, G. *Block Copolymers: Synthetic Strategies, Physical Properties, and Applications.*; Wiley-Intescience: Hoboken, 2003.

[80] Meier, D. J. *J. Polym. Sci., Part B: Polym. Phys.* **1996,** *34*, 1821-1838.

[81] Leary, D. F.; Williams, M. C. *Journal of polymer Science Part B: Polymer Letters* **1970,** *8*, 335-340.

[82] Helfand, E. *Macromolecules* **1975,** *8*, 552-556.

[83] Helfand, E.; Wasserman, Z. R. *Macromolecules* **1976,** *9*, 879-888.

[84] Helfand, E.; Wasserman, Z. R. *Macromolecules* **1978,** *11*, 960-966.

[85] Helfand, E.; Wasserman, Z. *Macromolecules* **1980,** *13*, 994-998.

[86] Semenov, A. N. *Soviet Physics JETP* **1985,** *61*, 733-742.

[87] Milner, S. T.; Witten, T. A.; Cates, M. E. *EPL (Europhysics Letters)* **1988,** *5*, 413-418.

[88] Milner, S. T.; Witten, T. A.; Cates, M. E. *Macromolecules* **1988,** *21*, 2610-2619.

[89] de Gennes, P. G. *Scaling concepts in polymer physics*; Cornell University Press: Ithaca, 1979.

[90] Fredrickson, G. H.; Helfand, E. *The Journal of Chemical Physics* **1987,** *87*, 697-705.

[91] Schulz, M. F.; Bates, F. S.; Almdal, K.; Mortensen, K. *Phys. Rev. Lett.* **1994,** *73*, 86.

[92] Matsen, M. W.; Bates, F. S. *Macromolecules* **1996,** *29*, 1091-1098.

[93] Matsen, M. W.; Schick, M. *Macromolecules* **1994,** *27*, 7157-7163.

[94] Cochran, E. W.; Garcia-Cervera, C. J.; Fredrickson, G. H. *Macromolecules* **2006,** *39*, 2449-2451.

[95] Matsen, M. W.; Bates, F. S. *J. Polym. Sci., Part B: Polym. Phys.* **1997,** *35*, 945-952.

[96] Khandpur, A. K.; Foerster, S.; Bates, F. S.; Hamley, I. W.; Ryan, A. J.; Bras, W.; Almdal, K.; Mortensen, K. *Macromolecules* **1995,** *28*, 8796-8806.

[97] Hajduk, D. A.; Takenouchi, H.; Hillmyer, M. A.; Bates, F. S.; Vigild, M. E.; Almdal, K. *Macromolecules* **1997,** *30*, 3788-3795.

[98] Qi, S.; Wang, Z.-G. *Physical Review E* **1997,** *55*, 1682.

[99] Vigild, M. E.; Almdal, K.; Mortensen, K.; Hamley, I. W.; Fairclough, J. P. A.; Ryan, A. J. *Macromolecules* **1998,** *31*, 5702-5716.

[100] Matsen, M. W.; Bates, F. S. *The Journal of Chemical Physics* **1997,** *106*, 2436-2448.

[101] Matsen, M. W.; Thompson, R. B. *The Journal of Chemical Physics* **1999,** *111*, 7139-7146.

[102] Mayes, A. M.; de la Cruz, M. O. *The Journal of Chemical Physics* **1991,** *95*, 4670-4677.

[103] Cochran, E. W.; Bates, F. S. *Phys. Rev. Lett.* **2004,** *93*, 087802.

[104] Cochran, E. W.; Morse, D. C.; Bates, F. S. *Macromolecules* **2003,** *36*, 782-792.

[105] Zheng, W.; Wang, Z.-G. *Macromolecules* **1995,** *28*, 7215-7223.

[106] Matsushita, Y.; Suzuki, J.; Seki, M. *Physica B: Condensed Matter* **1998,** *248*, 238-242.

[107] Qin, J.; Bates, F. S.; Morse, D. C. *Macromolecules* **2010,** *43*, 5128-5136.

[108] Drolet, F.; Fredrickson, G. H. *Macromolecules* **2001,** *34*, 5317-5324.

[109] Ryu, C. Y.; Ruokolainen, J.; Fredrickson, G. H.; Kramer, E. J.; Hahn, S. F. *Macromolecules* **2002,** *35*, 2157-2166.

[110] Khanna, V.; Ruokolainen, J.; Kramer, E. J.; Hahn, S. F. *Macromolecules* **2006,** *39*, 4480-4492.

[111] Meuler, A. J.; Fleury, G.; Hillmyer, M. A.; Bates, F. S. *Macromolecules* **2008,** *41*, 5809-5817.

[112] Hahn, T. *International Tables of Crystallography*, 4 ed.; Kluwer: London 1995;

Vol. A.

[113] Benoit, H.; Hadziioannou, G. *Macromolecules* **1988,** *21*, 1449-1464.

[114] Kavassalis, T. A.; Whitmore, M. D. *Macromolecules* **1991,** *24*, 5340-5345.

[115] Zielinski, J. M.; Spontak, R. J. *Macromolecules* **1992,** *25*, 653-662.

[116] Nagata, Y.; Masuda, J.; Noro, A.; Cho, D.; Takano, A.; Matsushita, Y. *Macromolecules* **2005,** *38*, 10220-10225.

[117] Masuda, J.; Takano, A.; Nagata, Y.; Noro, A.; Matsushita, Y. *Phys. Rev. Lett.* **2006,** *97*, 098301-4.

[118] Masuda, J.; Takano, A.; Suzuki, J.; Nagata, Y.; Noro, A.; Hayashida, K.; Matsushita, Y. *Macromolecules* **2007,** *40*, 4023-4027.

[119] Fleury, G.; Bates, F. S. *Macromolecules* **2009,** *42*, 1691-1694

[120] Matsushita, Y. *Polym. J.* **2008,** *40*, 177-183.

[121] Ward, I. M.; Sweeney, J. *An introduction to The Mechanical Properties of Solid Polymers*, 2nd ed.; Wiley: New York, 1983.

[122] Mandelkern, L.; Smith, F. L.; Failla, M.; Kennedy, M. A.; Peacock, A. J. *Journal of Polymer Science Part B-Polymer Physics* **1993,** *31*, 491-493.

[123] Pang, Y. Y.; Dong, X.; Liu, K. P.; Han, C. C.; Chen, E. Q.; Wang, D. J. *Polymer* **2008,** *49*, 4259-4270.

[124] Pope, D. P.; Keller, A. *Journal of Polymer Science: Polymer Physics Edition* **1975,** *13*, 533-566.

[125] Galeski, A. *Prog. Polym. Sci.* **2003,** *28*, 1643-1699.

[126] Bowden, P. B.; Young, R. J. *Journal of Materials Science* **1974,** *9*, 2034-2051.

[127] Kawai, H.; Hashimoto, T.; Miyoshi, K.; Uno, H.; Fujimura, M. *Journal of Macromolecular Science* **1980,** *B17*, 427-472.

[128] Matsuo, M.; Ueno, T.; Horino, H.; Chujyo, S.; Asai, H. *Polymer* **1968,** *9*, 425-436.

[129] Yang, A. C. M.; Kramer, E. J.; Kuo, C. C.; Phoenix, S. L. *Macromolecules* **1986,** *19*, 2010-2019.

[130] Fetters, L. J.; Lohse, D. J.; Richter, D.; Witten, T. A.; Zirkel, A. *Macromolecules* **1994,** *27*, 4639-4647.

[131] McCormick, H. W.; Brower, F. M.; Kin, L. *Journal of Polymer Science* **1959,** *39*, 87-100.

[132] Mark, J. E.; Erman, B.; Eirich, F. R. *Science and technology of rubber*; Academic Press: Burlington, 2011.

[133] Holden, G.; Bishop, E. T.; Legge, N. R. *Journal of Polymer Science Part C: Polymer Symposia* **1969,** *26*, 37-57.

[134] Sakurai, S.; Sakamoto, J.; Shibayama, M.; Nomura, S. *Macromolecules* **1993,** *26*, 3351-3356.

[135] Qiao, L.; Leibig, C.; Hahn, S. F.; Winey, K. I. *Industrial & Engineering Chemistry Research* **2006,** *45*, 5598-5602.

[136] Dair, B. J.; Honeker, C. C.; Alward, D. B.; Avgeropoulos, A.; Hadjichristidis, N.; Fetters, L. J.; Capel, M.; Thomas, E. L. *Macromolecules* **1999,** *32*, 8145-8152.

[137] Fetters, L. J.; Morton, M. *Macromolecules* **1969,** *2*, 453-458.

[138] Holden, G.; Legge, N. R.; Quirk, R. P.; Schroeder, H. E. *Thermoplastic Elastomers*, 2nd ed.; Hanser Publishers: New York, 1996.

[139] Fujimura, M.; Hashimoto, T.; Kawai, H. *Rubber Chem. Technol.* **1978,** *51*, 215-224.

[140] Hashimoto, T.; Fujimura, M.; Saijo, K.; Kawai, H.; Diamant, J.; Shen, M. Strain-Induced Plastic-to-Rubber Transition of a SBS Block Copolymer and Its Blend with PS. In *Multiphase Polymers*, AMERICAN CHEMICAL SOCIETY: 1979; Vol. 176, pp 257-275.

[141] Yamaoka, I.; Kimura, M. *Polymer* **1993,** *34*, 4399-4409.

[142] Cohen, Y.; Albalak, R. J.; Dair, B. J.; Capel, M. S.; Thomas, E. L. *Macromolecules* **2000,** *33*, 6502-6516.

[143] Pakula, T.; Saijo, K.; Kawai, H.; Hashimoto, T. *Macromolecules* **1985,** *18*, 1294-1302.

[144] Hermel, T. J. *Effects of Chain architecture on the Mechanical Response of Glassy/Semicrystalline Block Copolymers: CEC versus CECEC Lamellae*. Ph.D. Dissertation, University of Minnesota, 2003.

[145] Hermel, T. J.; Hahn, S. F.; Chaffin, K. A.; Gerberich, W. W.; Bates, F. S. *Macromolecules* **2003,** *36*, 2190-2193.

[146] Mori, Y.; Lim, L. S.; Bates, F. S. *Macromolecules* **2003,** *36*, 9879-9888.

[147] Wu, L.; Lodge, T. P.; Bates, F. S. *J. Rheol.* **2005,** *49*, 1231-1252.

[148] Wu, L.; Lodge, T. P.; Bates, F. S. *Macromolecules* **2006,** *39*, 294-299.

[149] Ruokolainen, J.; Fredrickson, G. H.; Kramer, E. J.; Ryu, C. Y.; Hahn, S. F.; Magonov, S. N. *Macromolecules* **2002,** *35*, 9391-9402.

Chapter 2 Block Copolymer Synthesis and Characterization

The careful synthesis and characterization of block copolymers are important to understand chemical structure-physical property relationships in polymers. In this study, block copolymers with the various molecular structures were synthesized via a combination of different techniques including anionic polymerization, ring-opening polymerization, coupling chemistry, and catalytic hydrogenation. To obtain the desired properties, several different block copolymers were prepared using polystyrene (PS or S), polybutadiene (PB or B), polycyclohexylethylene (PCHE or C, hydrogenated PS), polyethylene (PE or E, hydrogenated PB), and polylactide (PLA or L). The block copolymers were characterized with size exclusion chromatography (SEC), proton nuclear magnetic resonance spectroscopy (^{1}H NMR), differential scanning calorimetry (DSC), dynamic mechanical spectroscopy (DMS), small-angle X-ray scattering (SAXS), transmission electron microscopy (TEM), and tensile testing. In this chapter, these synthesis and characterization techniques will be discussed.

2.1 Synthesis of Block Copolymers

2.1.1 Polymer Selection

This section describes each polymer component that has been selected for this study. To enhance the mechanical properties of the multiblock copolymers, a combination of glassy, semicrystalline, and/or rubbery blocks have been considered as targeted systems. First, polystyrene (PS or S) and polybutadiene (PB or B) were used as glassy and rubbery components, respectively. Poly(styrene-*b*-butadiene-*b*-styrene) (SBS) triblock copolymer was the first successfully commercialized block copolymer.[1] In SBS block copolymer system, the glassy PS blocks pin down the rubbery PB chains, resulting in tough and elastic behavior. This study investigated PS-PB multiblock copolymers that have more complicated molecular architectures with a large number of blocks. These multiblock copolymers have more bridging and looping chain confirmations between microdomains with increasing numbers of blocks, which results in improved mechanical properties.

Polycyclohexylethylene (PCHE or C), resulting from the hydrogenation of polystyrene, was also used as the glassy block. The elimination of the reactive functionalities during the hydrogenation process leads to a polymer with enhanced properties compared to PS, including higher glass transition temperature T_g, greater thermal, oxidative, and UV stability.[2] Particularly, the increase of the T_g is an important improvement because of a higher upper use temperature. A comparison of the physical properties of the PCHE and the PS is shown in Table 2.1. Despite these attractive properties, PCHE has a limitation in applications due to its brittleness. Because of a large entanglement molecular weight (M_e), very high molecular weight chains are necessary to

obtain adequate toughness in PCHE homopolymers.

Table 2.1 Comparison of PCHE and PS. Reproduced from Bates et al.[2]

Property	PCHE	PS
T_g (°C)	147	106
M_e (g/mol)	40,000	13,309[3]
Density (g/cc)	0.947	1.06
Heat Capacity, 25 °C (J/g·K)	2.0	1.2
Total Transmittance (%)	91	91
Flexural Modulus (GPa)	2.8	3.1
% Water Absorption, 23 °C, 24 h	0.025	0.06

In order to make tough block copolymers, polyethylene (PE or E) was copolymerized with PCHE. The PE is a semicrystalline polymer, which exhibits a ductile behavior during tensile testing.[4] The PCHE-PE multiblock copolymers exhibit a relatively large value of the Flory–Huggins interaction parameter (χ = 0.06 at 100 °C[5]), leading to microphase separation of the different blocks at modest molecular weights. PE was synthesized by the hydrogenation of poly(1,4-butadiene) ($PB_{1,4}$ or $B_{1,4}$).

Polylactide (PLA) is a commercially-produced thermoplastic synthesized from renewable resources, which can be semicrystalline or totally amorphous depending on the stereopurity.[6-7] Today's emphasis on green chemistry and concern for the environment

have aroused interest in sustainable polymer materials. PLA is one of the most promising biopolymers and has been widely used in biomedical, packaging, and textile applications due to its biodegradability and biocompatibility.[8-11] In situations where a high-level of toughness is required, however, the use of PLA is limited because of the brittleness of the homopolymer. To overcome this drawback and broaden its application, extensive effort has been put into improving the mechanical properties of PLA. In this study, PLA-PB multiblock copolymers were synthesized and characterized to develop mechanically enhanced PLA-based sustainable polymers.

2.1.2 Living Anionic Polymerization

Living anionic polymerization is a powerful tool for the preparation of well-defined block copolymers. Using this method, it is possible to synthesize macromolecules with control of molecular weight, molecular weight distribution, block composition and microstructure.[12-14] A living polymerization is a chain polymerization that proceeds without irreversible termination or transfer reaction.[15-16] Thus, the desired block copolymers with various structures can be prepared by adding different monomers sequentially in living polymerization systems. This technique also offers facile mechanisms for functionalizing chain termini and coupling polymer chains, which provides a capability for more complex molecular architectures.

For the living polymerization, the rate of initiation, R_i, is defined as

$$R_i = k_i[I][M] \tag{2.1}$$

where k_i is the initiation rate constant, [I] and [M] are the concentrations of initiator and

unreacted monomer, respectively. In a similar way, the rate of polymerization, R_p, in nonterminating system can be depicted by the rate of propagation

$$R_P = k_p[M^-][M] \tag{2.2}$$

where k_p is the rate constant of propagation and $[M^-]$ is the total concentration of the anionic propagating centers. Under the assumption of an instantaneous initiation ($k_i \gg k_p$) and no termination or transfer reactions, the total concentration of propagating chain $[M^-]$ is equal to initial concentration of initiator $[I]_0$. Thus, the rate of polymerization can be rewritten as:

$$R_p = k_p[I]_0[M] \tag{2.3}$$

The synthesized polymer chains are characterized by two molecular properties: average molecular weight (M) and polydispersity index (PDI). Two different average molecular weights, number-average molecular weight (M_n) and weight-average molecular weight (M_w), are normally used and described by,

$$M_n = \frac{\sum_i n_i M_i}{\sum_i n_i} \tag{2.4}$$

$$M_w = \frac{\sum_i n_i M_i^2}{\sum_i n_i M_i} \tag{2.5}$$

where n_i is the number of molecules with molecular weight M_i. Qualitatively, M_n is the characteristic average molecular weight when the number of molecules is the important factor, whereas M_w is the characteristic molecular weight when the size of each molecule is a significant feature.[14]

In living anionic polymerization, the number-average degree of polymerization, N_n,

is simply expressed by the ratio of the initial concentration of monomer $[M]_0$ to the initial concentration of mono-functional initiator $[I]_0$,

$$N_n = \frac{[M]_0}{[I]_0}. \tag{2.6}$$

The polydispersity index (PDI), provides information about the breadth of the molecular distribution. For an ideal controlled polymerization,[14,17]

$$\text{PDI} = \frac{M_w}{M_n} = \frac{N_w}{N_n} \approx 1 + \frac{1}{N_n} \tag{2.7}$$

where N_n and N_w are the number-average degree of polymerization and the weight-average degree of polymerization, respectively. Narrow molecular weight distributions are feasible for large polymers, although non-ideal conditions such as finite R_i broaden the PDI in practice.

In this study, the following block copolymers were synthesized using the anionic polymerization technique: PS-PB nonablock copolymer (SBSBSBSBS), α,ω-dihydroxy polystyrene (HO-PS-OH) and α,ω-dihydroxy polybutadiene (HO-PB-OH). The detailed procedures of synthesis are described below.

2.1.3 Ring-Opening Polymerization

Ring-opening polymerization (ROP) is a significant polymerization technique for synthesis of various polymers, and it has been widely studied in industrial and academic fields.[18-20] A range of aliphatic cyclic monomers, such as cyclic ester, amines, sulfides, and olefins, have been successfully polymerized via ring-opening polymerization, where

a particular bond in the cycle is cleaved, and then reformed between different monomers in a linear sequence.[14]

The ability of a cyclic monomer to polymerize via ring-opening mechanism is determined by two important factors: thermodynamic and kinetic features.[21] Thermodynamically, the primary driving force for ring-opening is ring strain of the cyclic monomer. The amount of ring strain is strongly related to the number of atoms in the ring. The three- and four-membered rings are highly strained, and have a large exothermic enthalpy of polymerization that shift the equilibrium to macromolecule side. On the contrary, the five- and six-membered rings are the least strained and exhibit smaller enthalpy changes of polymerization. In this case, polymerization is less favorable and some of cyclic compounds are unable to go through ring-opening polymerization. In kinetic terms, the appropriate polymerization mechanism, that can convert the monomers into the polymer chain in the operable time, should exist. A number of mechanisms, such as anionic, cationic, metathesis, radical and enzymatic, are available for ring-opening polymerization depending on the monomer, catalytic/initiating system, and the nature of the active species.[21]

Synthesis of polylactide (PLA) via ring-opening polymerization of lactide monomer has attracted interest over the past few years. PLA has been widely used in biomedical, food packaging, and textile industries due to its biodegradability and biocompatibility.[8-11] PLA also can be prepared by polycondensation of lactic acid monomer. However, ring-opening polymerization of lactide allows for better control of polymerization in terms of molecular weight, polydispersity, polymer chain-ends and

tacticity.[21]

In this study, ring-opening polymerization of D,L-lactide was used to synthesize poly(lactide-*b*-butadiene-*b*-lactide) (LBL) triblock copolymers. The detailed synthetic procedures are explained below.

2.1.4 Coupling Chemistry

Coupling Reaction in Living Anionic Polymerization

Living anionic polymer chains can be linked by using a proper coupling agent. In living anionic polymerization, coupling reaction is the effective way to overcome some limits of sequential monomer addition. Difunctional coupling agents offer a synthetic way of block crossover which may not be available with the sequential addition. With the coupling method, for instance, the center B block of ABA triblock copolymer can be linked to the A end blocks under circumstances where sequential addition is not feasible due to the relative reactivity of the living chain and monomers.[13] The coupling procedure is also able to reduce the number of monomer addition steps for the block copolymer synthesis, which can decrease the polymerization time and the possibility of termination by impurities. Coupling reactions can provide star polymers by using multifunctional coupling agents. With a high-functional coupling agent, more complex structures, such as comb and brush polymers, can be obtained. In the coupling chemistry, the steric factor plays a significant role in achieving high conversion. If the coupling sites are near to each other or the living polymer is too bulky, it can be challenging to get a complete coupling.

In this research, *α*,*α*′-dibromo-*p*-xylene was used as a coupling agent to make

SBSBSBSBS nonablock copolymers by linking two living SBSBS pentablock chains.

Polycondensation of α,ω-Dihydroxyl functionalized polymers

Polycondensation is another useful way to prepare long chain polymers, where bi-functional monomers react with each other resulting in the formation of characteristic linkages such as urethane, ester, or amide bonds. Polyurethanes are typical polymers which utilize a polycondensation mechanism. Polyurethanes containing a large number of blocks have unique morphological structure with segregated hard and soft segments as well as tough mechanical properties.[22-24] Unlike living anionic polymerization, polycondensation can be used for various combinations of monomers regardless of monomer reactivity, but it is more affected by the functionality of the end groups. Additionally, it is difficult to control the block length, and the resulting polymers generally have a broad molecular weight distribution.

In this work, well-defined *α*,*ω*-dihydroxyl functionalized polymers were synthesized using living anionic or ring-opening polymerization; then, the presynthesized dihydroxyl polymers were coupled via polycondensation reaction with diisocyanate or diacid chloride.

2.1.5 Catalytic Hydrogenation

The hydrogenation of polydienes is one of the most effective ways to improve the physical and mechanical properties of polymers, such as the thermal and oxidative stabilities. The first hydrogenation of natural rubber was completed in 1869.[25] Since that time, numerous studies dealing with polymer hydrogenation have been accomplished.

Early research on polymer hydrogenation reported a large amount of chain scission, indicating a destructive hydrogenation. In the 1950s, the impressive work of non-destructive hydrogenation using the nickel-on-kieselguhr catalyst was achieved,[26] which provided the foundation of the current polymer hydrogenation chemistry.

There are two types of hydrogenation in the polymer field: homogeneous and heterogeneous catalytic hydrogenations. Various homogeneous hydrogenation catalysts were discovered in the 1960s. An important characteristic of homogenous catalyst is the selectivity of hydrogenation for alkenes and alkynes. These catalysts can saturate alkene and alkyne carbon chains while preserving other unsaturated groups such as aromatic, carbonyl, and cyano groups.[27] Heterogeneous catalysts can hydrogenate both alkenes and aromatics. The heterogeneous hydrogenation catalysts are composed of a metal (Pt, Pd, or Ni) deposited on an inert support such as silica or activated carbon.[28] The advantage of the heterogeneous catalyst is that the used catalysts can be easily separated from the saturated product after the hydrogenation process and reused. The Dow Chemical Company reported a unique wide-pore silica support catalyst when loaded with small Pt or Pt/Re particles, which showed dramatically improved efficiency at 170 °C under modest hydrogen pressure (ca. 500 psi).[29] This new catalyst leads to > 98% saturation of polystyrene and polydienes in about 2 hours. In addition, the ratio of catalyst to polymer was drastically reduced down to a level of 0.01 to 0.1; previous studies reported an order of magnitude greater in catalyst loadings to achieve complete saturation.[29-31] Choosing the appropriate hydrogenation techniques based on the reaction conditions and desired selectivity is an important consideration.

In this research, the Pt/Re catalyst supported on porous SiO_2 (Dow Chemical Co.) was used as a heterogeneous catalyst to obtain saturated CECECECEC block copolymers by the hydrogenation of SBSBSBSBS polymers. About 5 grams of the precursor polymer was dissolved into 500 mL cyclohexane, and added to a 1 L high-pressure reactor with about 1.5 gram of the Pt/Re catalyst. The reactor was sealed and purged with argon for several minutes to remove any oxygen. Then the reactor was pressurized to 500 psig with hydrogen and heated up to 170 °C. The hydrogenation was conducted for about 12 hours, and then the reactor was cooled down to room temperature. The resultant polymer solution was filtered at 70 °C using a 0.22 μm Millipore Durapore® membrane filter to remove the catalyst. Then the hydrogenated polymer was recovered by precipitation into a 3:1 mixture of methanol and isopropanol, and dried in a vacuum oven until constant weight. After the hydrogenation, the samples were characterized with ^{1}H NMR to confirm the complete saturation.

2.2 Characterization of Block Copolymers

2.2.1 Size Exclusion Chromatography

Size exclusion chromatography (SEC) is a versatile method for determining the molecular weight and the molecular weight distribution of polymer samples. It is also commonly called gel permeation chromatography (GPC) which emphasizes the column packing material (the gel) rather than the separation mechanism (size exclusion).[14] The SEC is composed of a column packed with porous particles (stationary phase). When the

polymer solution (mobile phase) goes through the column, the molecules of different sizes are separated based on their hydrodynamic volume, V_h. While the solution passes through the porous materials, the polymer chains can reach the pores that have similar or larger size compared to their hydrodynamic volume. Thus, small chains have a longer path length and longer elution time compared to larger chains. The eluted particles are detected using an UV absorbance, refractive index, or light scattering detector. The concentration of the eluting solution is recorded as a function of retention volume, V_R, which is the volume of the solvent that passes through the column before the specific polymer particle is eluted.

The measured elution volumes are generally calibrated with two calibration methods. The first calibration strategy is using a series of polymer standards of known molecular weights. This is a simple way to calculate the molecular weight averages and the molecular weight distribution. However, this method has limitations: achievable accuracy is limited by the accuracy in the molecular weight of standards, and appropriate polymer standards may not be available. The second method is using the universal calibration. The universal calibration assumes that the retention volume, V_R, of the polymer depends only on the hydrodynamic volume, V_h, which is proportional to the product $[\eta]M$, where $[\eta]$ is the intrinsic viscosity. From the relationship between $[\eta]$ and V_h

$$[\eta] \sim \frac{V_h}{M} \sim \frac{V_R}{M} \tag{2.8}$$

the Mark–Houwink equation can be generated,

$$[\eta] M = kM^{1+a}. \tag{2.9}$$

If the Mark–Houwink coefficients (k and a) of the sample and the reference (standard sample) are known, the molecular weight of the sample can be calculated as:

$$M_{\mathrm{s}} = \left(\frac{\left(k_{\mathrm{r}} M_{\mathrm{r}}^{1+a_{\mathrm{r}}} \right)}{k_{\mathrm{s}}} \right)^{1/1+a_{\mathrm{r}}} \tag{2.10}$$

where the subscripts 's' and 'r' stand for the sample and the reference polymers, respectively.

For block copolymers, the molecular weights were determined by a combination of size exclusion chromatography (SEC) and ^{1}H nuclear magnetic resonance (NMR). The molecular weight of an aliquot of the first homopolymer block was measured using SEC, and the SEC results were combined with the ^{1}H NMR spectra to decide the molecular weights and block mole fractions.

For most of the block copolymer samples employed in this research, size exclusion chromatography (SEC) was performed on a Thermo Separation Products (TSP) Spectra Systems AS1000 autosampler equipped with three 5 mm Phenomenex Phenogel columns, a Waters 515 pump and a Waters 2410 differential refractive index detector to analyze the number-average molecular weight (M_{n}), weight-average molecular weight (M_{w}) and molecular weight distribution ($M_{\mathrm{w}}/M_{\mathrm{n}}$). The polymer samples were run at room temperature in THF at a flow rate of 1.0 mL/min, and the instrument was calibrated using 10 polystyrene standards (M_n = 580 to 377,400 g/mol, Polymer Laboratories). Figure 2.1 shows SEC traces of HO-PB-OH macroinitiator and LBL triblock copolymers synthesized by ring-opening polymerization. When comparing the SEC traces before and after polymerization, triblock copolymer exhibited higher molecular weight (lower

elution volume) with reasonably narrow molecular weight distribution.

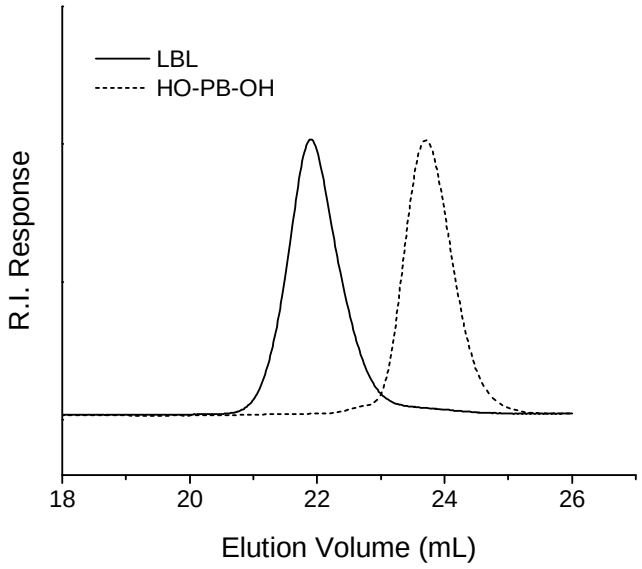

Figure 2.1 SEC traces of HO-PB-OH (before polymerization, dashed line) and LBL triblock copolymer (after polymerization, solid line).

2.2.2 Nuclear Magnetic Resonance Spectroscopy

Nuclear magnetic resonance (NMR) spectroscopy was used to determine the molecular structure, the block composition, and the extent of hydrogenation of the block copolymers. In NMR spectroscopy, a pulse of radiofrequency energy is used to excite all nuclei in the sample, and then the excited nuclei return to their ground state by releasing the absorbed energy. A detector collects this radiating energy and obtains a free induction decay (FID) in the time domain. The spectrum in the frequency domain can be achieved by converting the FID using a Fourier transform (FT). The nuclei ^{1}H, ^{13}C, ^{19}F, and ^{31}P,

which have a quantum spin number of 1/2, are usually used for NMR spectroscopy.

In proton NMR spectroscopy, the different kinds of protons feel different strength of the energy, even though all protons are simultaneously excited by the same pulse of radiofrequency energy. The effective field strength that each proton feels depends on their electronic surroundings. Here, the chemical shift, δ, in ppm is given by:

$$\delta(\text{ppm}) = \frac{\text{observed frequency - operating frequency}}{\text{operating frequency}} \times 10^6 \qquad (2.11)$$

Since different kinds of protons show characteristic chemical shifts, the chemical shift can be used to identify the molecular structure. Moreover, the integration of the peak area is proportional to the relative number of protons, which is very useful in order to calculate the composition of the multiblock copolymer. ^{1}H NMR chemical shifts of the polymers used in this study are shown in Table 2.2.

For room temperature NMR spectroscopy, Varian Unity 300 MHz and Varian Inova 500 spectrometers were used to characterize the block copolymers with deuterated chloroform ($CDCl_3$) as a solvent. For the high-temperature NMR spectroscopy of the polymers containing semicrystalline blocks, a Varian Inova 300 MHz (VXR-300) spectrometer was utilized with deuterated toluene (C_7D_8) as a solvent.

The block composition and the total molecular weight of SBSBSBSBS nonablock copolymers were determined using ^{1}H NMR analysis and the SEC results of the first block (aliquot). A representative ^{1}H NMR spectrum of SBSBSBSBS is shown in Figure 2.2 with the protons corresponding to each peak identified. By integrating the peak areas of the SBSBSBSBS spectrum, the mole fraction of polystyrene, poly(1,4-butadiene) and poly(1,2-butadiene) can be calculated. The mole fraction of polystyrene in the

SBSBSBSBS, x_{PS}, is defined as:

$$x_{PS} = \frac{(I_a + I_b)/5}{(I_a + I_b)/5 + (I_c + I_e + I_d/2)/2} \tag{2.12}$$

where I denotes the integrated peak area, and subscripts of a–e represent the specific proton assigned in Figure 2.2. The mole fractions of poly(1,4-butadiene) and poly(1,2-butadiene) can also be expressed as follows:

$$x_{PB_{1,4}} = \frac{(I_c + I_e - I_d/2)/2}{(I_a + I_b)/5 + (I_c + I_e + I_d/2)/2} \tag{2.13}$$

$$x_{PB_{1,2}} = \frac{I_d/2}{(I_a + I_b)/5 + (I_c + I_e + I_d/2)/2} \tag{2.14}$$

The corresponding volume fractions can be calculated using the density ρ and the molecular weight M_0 of each monomer.

$$f_{PS} = \frac{x_{PS}M_{0,S}/\rho_{PS}}{x_{PS}M_{0,S}/\rho_{PS} + x_{PB_{1,4}}M_{0,B}/\rho_{PB_{1,4}} + x_{PB_{1,2}}M_{0,B}/\rho_{PB_{1,2}}} \tag{2.15}$$

$$f_{PB_{1,4}} = \frac{x_{PB_{1,4}}M_{0,B}/\rho_{PB_{1,4}}}{x_{PS}M_{0,S}/\rho_{PS} + x_{PB_{1,4}}M_{0,B}/\rho_{PB_{1,4}} + x_{PB_{1,2}}M_{0,B}/\rho_{PB_{1,2}}} \tag{2.16}$$

$$f_{PB_{1,2}} = \frac{x_{PB_{1,2}}M_{0,B}/\rho_{PB_{1,2}}}{x_{PS}M_{0,S}/\rho_{PS} + x_{PB_{1,4}}M_{0,B}/\rho_{PB_{1,4}} + x_{PB_{1,2}}M_{0,B}/\rho_{PB_{1,2}}} \tag{2.17}$$

where the densities of PS, $PB_{1,4}$ and $PB_{1,2}$ are 0.969 g/cm^3, 0.826 g/cm^3,and 0.889 g/cm^3, respectively.[3]

Table 2.2 ^{1}H NMR chemical shifts of polymers used in this study.

Chemical Structure	Chemical Shift, δ (ppm)
Polystyrene	
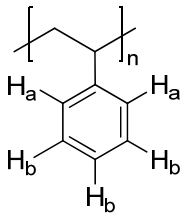	H_a: m, 6.3–6.8 H_b: m, 6.8–7.2
Poly(1,4-butadiene)	
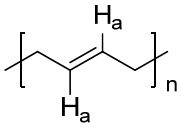	H_a: m, 5.4
Poly(1,2-butadiene)	
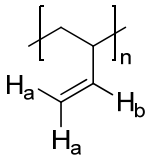	H_a: m, 4.8–5.0 H_b: m, 5.4
Poly(D,L-lactide)	
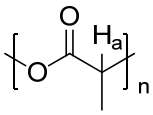	H_a: m, 5.2–5.4

SBSBSBSBS

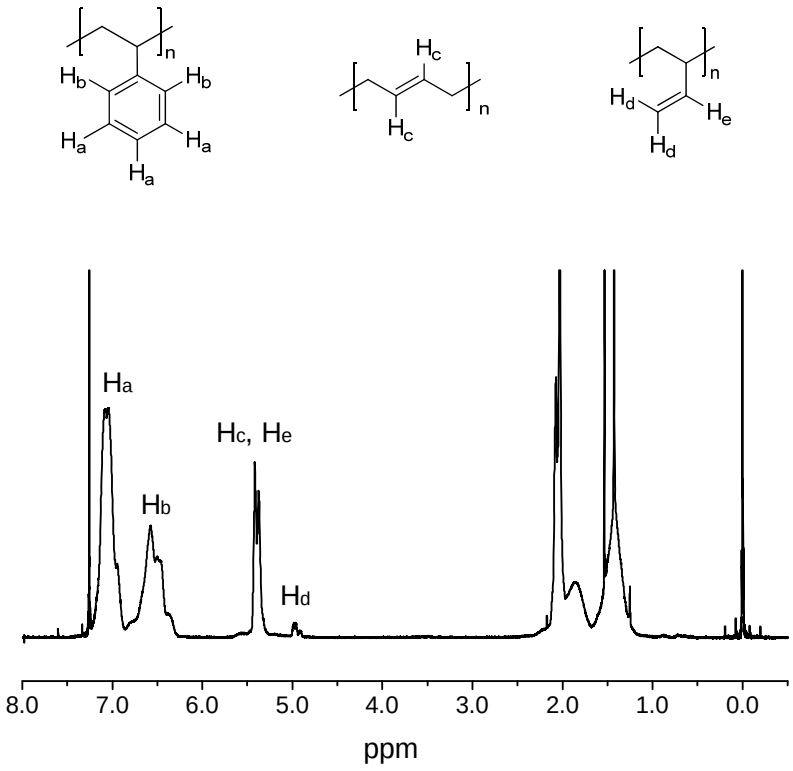

Figure 2.2 Representative ^{1}H NMR spectrum of SBSBSBSBS nonablock copolymers. The unsaturated polymer samples were measured in deuterated chloroform ($CDCl_3$) at room temperature.

The end-group analysis of ^{1}H NMR spectrum was used to calculate the molecular weight, M_n, of α,ω-dihydroxyl functionalized polymers and LBL triblock copolymers. The ^{1}H NMR spectrum of α,ω-dihydroxyl polybutadiene (HO-PB-OH) is shown in Figure 2.3 (a) as an example. The proton assignments and the integrated areas are also shown above the peaks. Because the integrated peak area (I) is proportional to the

number of hydrogen atoms, the M_n of HO-PB-OH can be calculates as:

$$M_{n,PB} = \frac{\left(I_{a+c} - I_b/2\right)/2 + I_b/2}{I_d/4} M_{0,B} = \frac{\left(82 - 77/2\right)/2 + 77/2}{4/4} 54 = 3254 \text{ g/mol} \tag{2.18}$$

LBL triblock copolymers were synthesized via ring-opening polymerization of lactide monomers with HO-PB-OH as a macroinitiator. Figure 2.3 (b) shows the ^{1}H NMR spectrum of LBL triblock copolymer that was synthesized from HO-PB-OH (Figure 2.3 (a)). After the ring-opening polymerization, the new peaks belonging to the protons in PLA were recorded. Using the end-group analysis with the integrated peak area (I) and monomer unit mass (M_0), the M_n of LBL triblock copolymer can be calculated as:

$$M_n = \frac{\left(I_{a+c+e} - I_{a+c} + I_{e'}\right)/1}{I_{d'}/4} M_{0,L} + \frac{\left(I_{a+c} - I_b/2\right)/2 + I_b/2}{I_{d'}/4} M_{0,B} = \frac{\left(175 - 82 + 2\right)/1}{4/4} 72 + \frac{\left(82 - 77/2\right)/2 + 77/2}{4/4} 54 = 10094 \text{ g/mol} \tag{2.19}$$

The mole fraction of each block of prepared LBL triblock copolymers can be described as follows:

$$x_{PLA} = \frac{\left(I_{a+c+e} - I_{a+c} + I_{e'}\right)/1}{\left(I_{a+c+e} - I_{a+c} + I_{e'}\right)/1 + \left(I_{a+c} - I_b/2\right)/2 + I_b/2} \tag{2.20}$$

$$x_{PB_{1,4}} = \frac{\left(I_{a+c} - I_b/2\right)/2}{\left(I_{a+c+e} - I_{a+c} + I_{e'}\right)/1 + \left(I_{a+c} - I_b/2\right)/2 + I_b/2} \tag{2.21}$$

$$x_{PB_{1,2}} = \frac{I_b/2}{\left(I_{a+c+e} - I_{a+c} + I_{e'}\right)/1 + \left(I_{a+c} - I_b/2\right)/2 + I_b/2} \tag{2.22}$$

where x_{PLA} , $x_{PB_{1,4}}$, and $x_{PB_{1,2}}$ are the mole fractions of polylactide, poly(1,4-butadiene),

and poly(1,2-butadiene), respectively. These mole fractions can be converted to the corresponding volume fractions using the density and the molecular weight of each monomer.

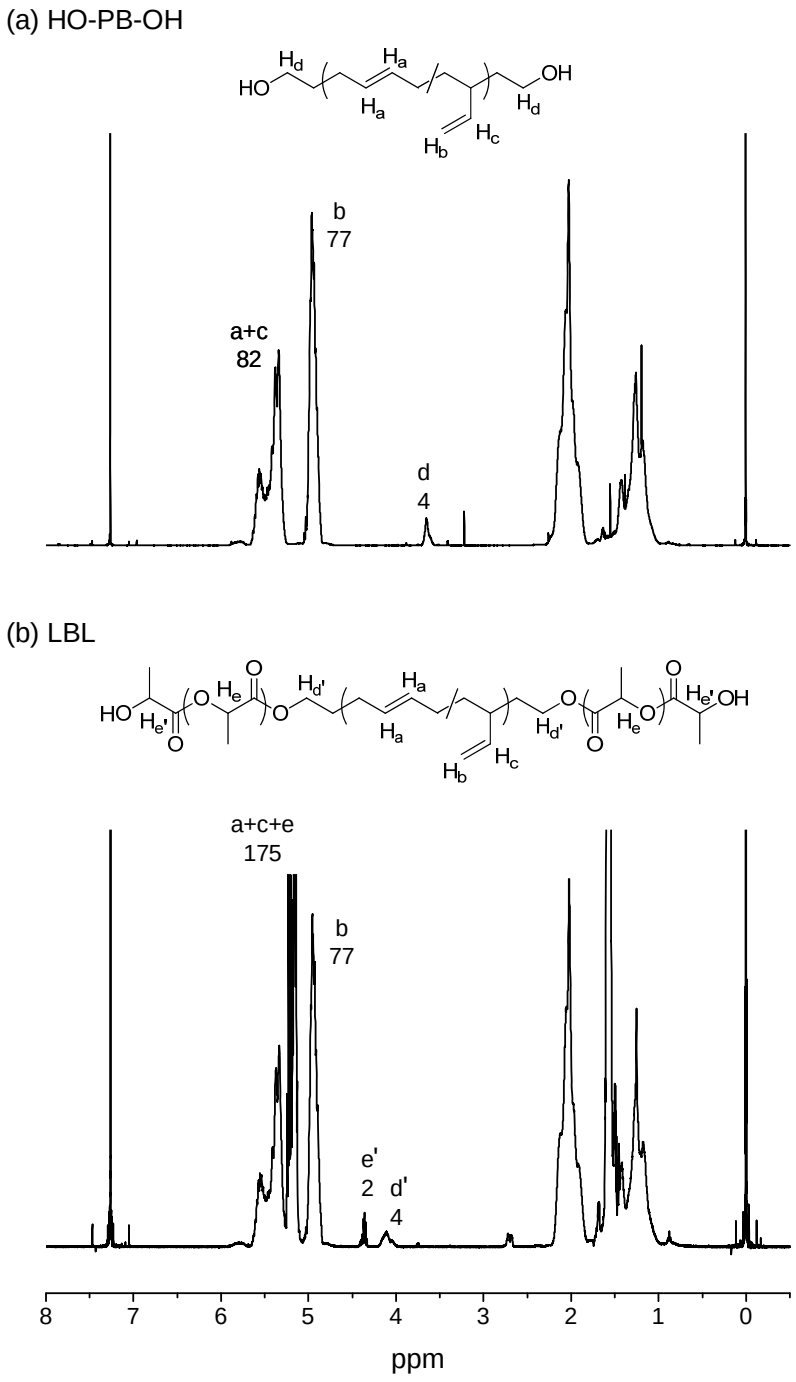

Figure 2.3 Representative ^{1}H NMR spectrum of (a) *α*,*ω*-dihydroxyl polybutadiene (HO-PB-OH) and (b) poly(lactide-*b*-butadiene-*b*-lactide) (LBL). The proton assignments and integrated peak areas are denoted above the peaks.

2.2.3 Differential Scanning Calorimetry

Differential scanning calorimetry (DSC) is a common instrument for characterizing thermal properties. In DSC, a pan containing a small amount of sample and a reference pan (usually empty) with a known heat capacity are heated simultaneously by a resistive heating element. DSC measures the heat flow to the sample which is adjusted to keep the temperatures of the two pans equal. The slope of the resulting plot is equal to the heat capacity of the sample, and any thermal transition of the material is verified by the change of the slope during the heating or cooling. In this study, the glass transition temperature (T_g), the melting temperature (T_m), the crystallization temperature (T_c), and the percent crystallinity (X_c) of the block copolymers were determined using DSC. Figure 2.4 illustrates the representative DSC trace of the CECECECEC nonablock copolymer. T_g is denoted by the inflection of the DSC curve, indicating a change in the heat capacity of the material. A peak above the curve indicates an endothermic melting process at T_m. A peak below the curve denotes the crystallization of the sample at T_c, which is an exothermic process. Moreover, the peak areas at T_m and T_c indicate the latent heat of melting and crystallization, which is useful to calculate the percent crystallinity, X_c, of a semicrystalline polymer.

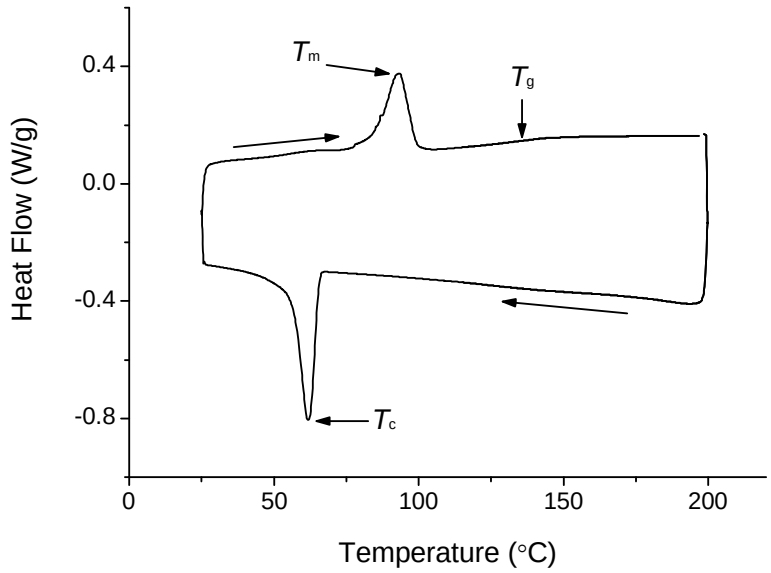

Figure 2.4 Representative DSC trace of CECECECEC with cooling and heating rate of 10 °C/min. The glass transition, melting and crystallization temperatures are denoted by the arrows.

2.2.4 Small-Angle X-ray Scattering

Small-angle X-ray scattering (SAXS) was used as a primary technique to characterize the morphological structures of the block copolymers. In SAXS, the low scattering angle (typically 0.1–10°) allows the collection of information on the nanometer length scale, such as the characteristic dimension of ordered materials. This X-ray diffraction technique is based on elastic scattering, where the energy of the incident wave is conserved through the process of diffraction. The scheme of the elastic scattering is show in Figure 2.5. The incident wave vector, $\vec{k}_i$, and the scattering wave vector, $\vec{k}_s$,

have the same magnitude of $2\pi/\lambda$ (λ is the wavelength in the material) for the elastic scattering. The scattering vector, $\vec{q}$, is defined by the difference between the incident and scattered wave vectors:

$$\vec{q} = \vec{k}_i - \vec{k}_s \tag{2.23}$$

With some trigonometry, the magnitude of $\vec{q}$ is defined as

$$\left|\vec{q}\right| = \frac{4\pi}{\lambda}\sin\left(\frac{\theta}{2}\right) \tag{2.24}$$

where θ is the scattering angle defined by the experimental equipment.

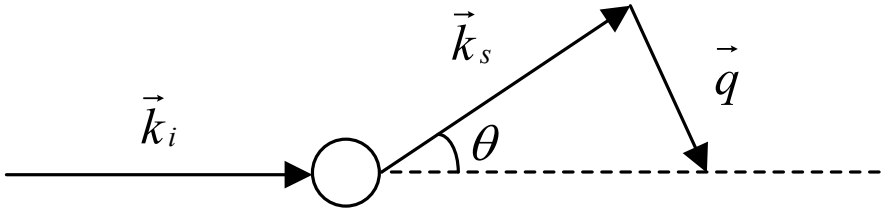

Figure 2.5 Scheme of the elastic scattering from a single scatterer.

With SAXS, morphologies of the block copolymers can be identified by a scattering pattern. The Bragg's law is the fundamental concept for the understanding of the scattering pattern. Figure 2.6 shows a scheme describing the Bragg's law. Consider the parallel planes of scatterers separated by the interplanar distance *D*. The incident wave vector, $\vec{k}_i$, and the scattering wave vector, $\vec{k}_s$, make an incident angle of $\theta/2$ with these planes. The distance the wave passes from the source to the detector is the same for all atoms in the first plane. However, the wave scattered from the second plane will travel

an additional distance of $2D\sin(\theta/2)$ (Figure 2.6 (b)). When the path difference of $2D\sin(\theta/2)$ is equal to $m\lambda$ (m is an integer), the waves scattered from one and the next plane will be in phase and show constructive interferences at the detector. Here, Bragg's law can be expressed as

$$m\lambda = 2D\sin\left(\frac{\theta}{2}\right) \tag{2.25}$$

Combining Bragg's equation with the magnitude of the scattering vector gives

$$\left|\vec{q}\right| = \frac{2\pi m}{D_{hkl}} \tag{2.26}$$

where hkl is the Miller index of the plane for a given symmetry.[32] The morphologies of block copolymers can be determined by comparing the experimental reflections with the allowed reflections for a space group using the ratio of q/q^*, where q^* is the primary scattering peak. The reflection conditions of the 230 space groups are listed in the International Tables for Crystallography.[33] The several allowed q/q^* values for common morphologies are shown in Table 2.3.

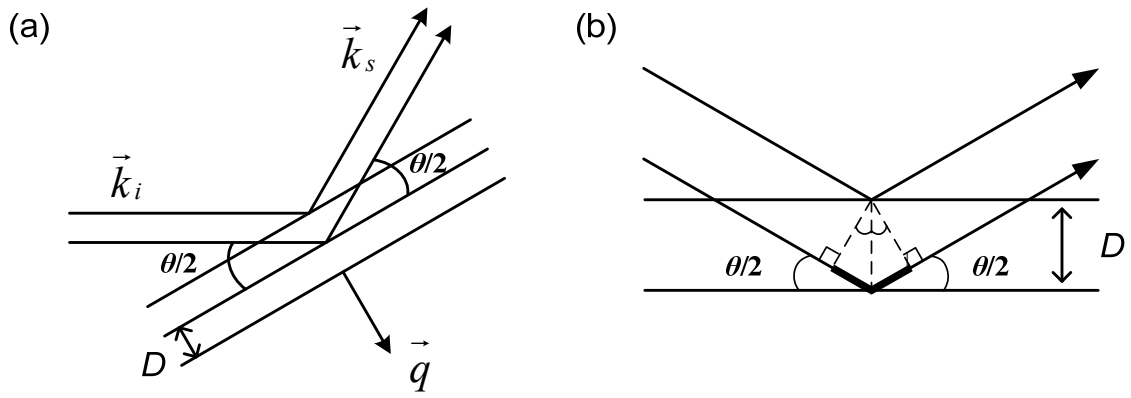

Figure 2.6 Scheme of Bragg's law. (a) The incident and scattering wave vectors make an incident angle of $\theta/2$ with each plain. The interplanar distance is D. (b) The bold line indicates the additional distance of the waves scattered from the second plane. The length of each bold line is $D\sin(\theta/2)$.[14]

Table 2.3 Allowed reflections for several morphologies of block copolymers.

Morphology	q/q^*
Lamellae	$1, 2, 3, 4, 5, 6, \cdots$
BCC spheres	$\sqrt{1}, \sqrt{2}, \sqrt{3}, \sqrt{4}, \sqrt{5}, \sqrt{6}, \cdots$
Hexagonal cylinders	$\sqrt{1}, \sqrt{3}, \sqrt{4}, \sqrt{7}, \sqrt{9}, \sqrt{12}, \cdots$
Gyroid (*Ia*3*d*)	$\sqrt{3}, \sqrt{4}, \sqrt{7}, \sqrt{8}, \sqrt{10}, \sqrt{11}, \cdots$

In this study, SAXS measurements were carried out in the College of Science and Engineering Characterization Facility at the University of Minnesota. A Riganku RU-200VBH rotating-anode x-ray machine generated Cu Kα x-rays (λ = 1.54 Å). The 2D

diffraction pattern was detected by a Siemens area detector (HI-STAR™ Siemens Analytical X-ray Instruments). Synchrotron SAXS measurements were also performed at the 5ID-D DuPont-Northwestern-Dow (DND-CAT) beamline of the Synchrotron Research Center at the Advanced Photon Source, Argonne National Laboratory. The X-ray wave length was around 0.7–0.8 Å and a sample-to-detector distance of around 4 m was employed. The collected two-dimensional scattering data were azimuthally integrated and are presented as intensity (I) vs scattering wave vector (q).

2.2.5 Dynamic Mechanical Spectroscopy

One of the most distinctive characteristics of a polymer is the viscoelastic behavior, which is the intermediate behavior between elastic solids and viscous liquids. Dynamic mechanical spectroscopy (DMS) or dynamic mechanical analysis (DMA) is used to explore the viscoelastic response of the polymer using an oscillating sinusoidal strain. An example of simple shear geometry is illustrated in Figure 2.7. The stress σ is defined by the force per area ($\sigma = F/\mathrm{A}$), and the strain is given by $\gamma = \mathrm{d}x/\mathrm{d}y$. The strain rate is described by $\dot{\gamma} = \mathrm{d}v_x/\mathrm{d}t = \mathrm{d}\left(\mathrm{d}x/\mathrm{d}y\right)/\mathrm{d}t$.

The two limits of viscoelasticity can be described by the Newton's and Hooke's laws. The liquid-like viscous behavior is described by Newton's law, which defines a viscosity η as the ratio of the stress σ to the strain rate $\dot{\gamma}$:

$$\sigma = \eta\dot{\gamma} \tag{2.27}$$

For Newtonian fluids, the viscosity, which is related to the energy dissipation by friction, is independent of the shear rate. For the solid-like elastic behavior, a modulus G is

defined as the ratio of the stress σ to the strain γ with Hooke's law:

$$\sigma = G\gamma \tag{2.28}$$

Here, the modulus is similar to a spring constant which is related to the storage of energy.

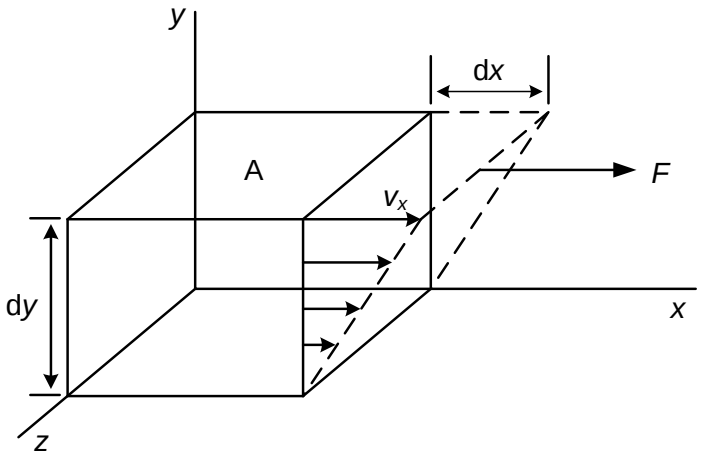

Figure 2.7 Illustration of simple shear flow between parallel plates. Reproduced from Hiemenz and Lodge.[14]

When we apply an sinusoidal strain $\gamma^* = \gamma_0 \exp(\mathrm{i}\omega t)$ to polymer melts, where γ_0 is the amplitude of the strain, ω is the frequency, and t is the time, the viscoelastic responses can be in-phase (elastic component) and 90° out-of-phase (viscous component) with the applied sinusoidal strain. These responses can be described by the complex dynamic modulus G^*,

$$G^*(\omega) = G' + \mathrm{i}G'' \tag{2.29}$$

where

$$G' = \frac{\sigma_0}{\gamma_0}\cos\delta \tag{2.30}$$

$$G'' = \frac{\sigma_0}{\gamma_0}\sin\delta\,. \tag{2.31}$$

The complex modulus is also described by the phase angle δ or the loss tangent ($\tan\delta = G''/G'$). Thus, when material has liquid-like behavior, $\tan\delta \gg 1$, and when it has solid-like behavior, $\tan\delta \ll 1$.[14]

For the rheological tests, two types of DMS measurements were performed for the block copolymers. The isothermal frequency sweep test measures G' and G'' while varying the frequency at a fixed temperature. The measured frequency sweep data at different temperatures can be superimposed using a shift factor (a_T) to create a master curves of $G'(\omega)$ and $G''(\omega)$. This procedure is called time-temperature superposition (TTS). The TTS-treated curves can be used to determine the state of order of block copolymers. In the disordered state, the low-frequency behavior shows $G' \sim \omega^2$ and $G'' \sim \omega$. Conversely, ordered microstructures exhibit different dependences of G' and G''.[34] Figure 2.8 describes the low-frequency behavior of G' for different ordered structures. Even though the behavior of the terminal regime brings some insight to the block copolymer morphology, the exact morphology should always be determined by the combination with other characterization results such as small-angle X-ray scattering and transmission electron microscopy. The second type of DMS measurement is the isochronal temperature ramping test. In this test, G' and G'' were measured while increasing or decreasing the temperature at a fixed frequency and strain amplitude. The phase transition temperatures of the block copolymers, such as order-disorder transition

temperature (T_{ODT}) and order-order transition temperature (T_{OOT}), can be assigned by sharp changes in G' during heating or cooling.

In this study, a Rheometric Scientific ARES rheometer equipped with 25 or 8 mm diameter parallel plates was used for the rheological tests. The experiments were conducted at a strain of 1.0 or 0.5 %, which was determined to be in the linear viscoelastic regime. G' and G'' moduli were monitored at a constant frequency (ω = 0.1 or 1 rad/s) while heating samples at a constant rate.

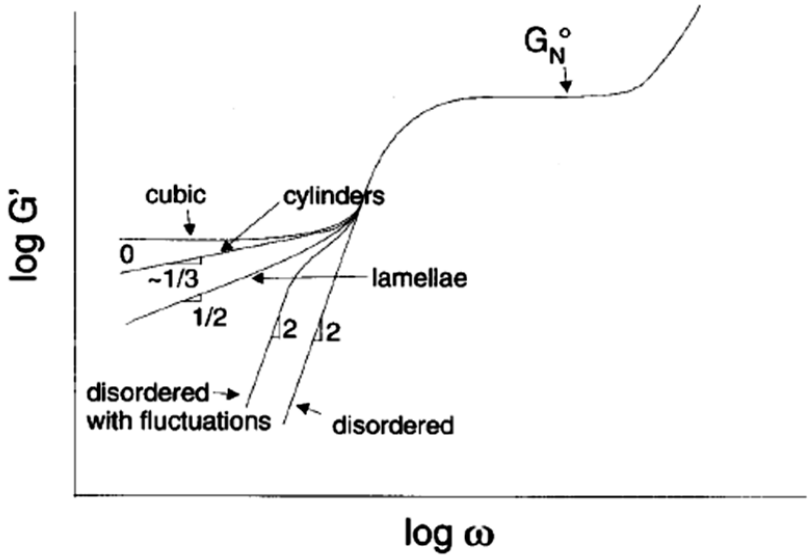

Figure 2.8 Illustration of low-frequency G' behaviors of disordered state and several ordered structures. Reproduced from Kossuth et al.[34]

2.2.6 Transmission Electron Microscopy

Transmission electron microscopy (TEM) is a useful tool to obtain real space

images of the block copolymer structures. The TEM images are produced from the interaction of the electrons with the atoms of a thin specimen. Because the electron beam in TEM mainly interacts with nuclei of the material, materials with high atomic number Z produce more scattering. Thus, the contrast will be formed with different atoms of the sample, and the regions containing higher Z elements will appear darker in the TEM images.

In preparation of TEM samples, the most important point is the sample thickness. The sample should be thin enough to get any information using the transmitted electrons. The thick region of the sample cannot transmit sufficient electrons, which results in a dark area in the image.[35] Hence, the preparation of evenly thin (typically < 100 nm) samples is very significant to obtain the correct contrast from the materials. In block copolymer systems which mostly consist of carbon, hydrogen, and oxygen, the different block domains with similar low Z atoms show little contrast naturally. In this case, staining the specific blocks with high Z atom oxides, such as osmium tetroxide (OsO_4), can provide enhanced contrast to the image. In PS/PB and PLA/PB systems, the carbon-carbon double bonds in unsaturated PB favorably react with OsO_4. Then, rubbery PB phase absorbing the high Z oxides results in a darker region compared to the unstained glassy PS or PLA phase.

In this study, TEM data were obtained using a Tecnai T12 electron microscope at the College of Science and Engineering Characterization Facility at the University of Minnesota. The polymer samples were cut into thin slices (80–100 nm thickness) by cryo-microtoming at −80 °C. Staining was performed with vapor from an aqueous

solution of OsO_4, which allowed enhanced contrast in the TEM images

2.2.7 Tensile Testing

The mechanical properties of block copolymers were characterized with uniaxial tensile testing experiments. The results are plotted as engineering stress σ versus nominal strain ε, which are given by

$$\sigma = \frac{F}{A_0} \tag{2.32}$$

$$\varepsilon = \frac{l - l_0}{l_0} = \frac{\Delta l}{l_0} \tag{2.33}$$

where F is the applied force, A_0 is the initial cross sectional area, and Δl is the sample displacement calculated from initial length l_0 and final length l of the sample. At low strain portion of the stress–strain curve, the slope of the curve in the linear elastic regime is defined as the Young's modulus E, denoted by

$$\sigma = E\varepsilon \tag{2.34}$$

The yield stress σ_y, the stress needed to introduce plastic deformation in the specimen, is chosen from the maximum in the curve, which is followed by necking. Also, the stress at break σ_b and strain at break ε_b are obtained from the point where the sample fails. The area under the curve is an indication of fracture toughness, or the total energy absorbed up to failure.[36]

In this study, uniaxial tensile tests were conducted with a Minimat (Rheometrics Scientific, Inc.) and a RSA-G2 Solids Analyzer (TA Instruments) to measure the

mechanical properties of block copolymers. For the Mininmat, specimens were molded and cut into rectangular tensile bars. For RSA-G2, the samples were prepared as the hot-pressed film, and dog-bone specimens for tensile test were made from the films using a punch and arbor press. Then the specimens were drawn until failure at a constant rate. The specific parameters for tensile tests will be given later. The results reported here represent averages taken from at least five specimens for each sample.

2.3 References

[1] Holden, G.; Milkovich, R. Rubberlike block copolymers. 627652, 1963.

[2] Bates, F. S.; Fredrickson, G. H.; Hucul, D.; Stephen F. Hahn *AlChE J.* **2001,** *47*, 762-765.

[3] Fetters, L. J.; Lohse, D. J.; Richter, D.; Witten, T. A.; Zirkel, A. *Macromolecules* **1994,** *27*, 4639-4647.

[4] Ryu, C. Y.; Ruokolainen, J.; Fredrickson, G. H.; Kramer, E. J.; Hahn, S. F. *Macromolecules* **2002,** *35*, 2157-2166.

[5] Cochran, E. W.; Bates, F. S. *Macromolecules* **2002,** *35*, 7368-7374.

[6] David, H.; Patrick, G.; Jim, L.; Jed, R. Polylactic Acid Technology. In *Natural Fibers, Biopolymers, and Biocomposites*, CRC Press: 2005.

[7] Anderson, K. S.; Schreck, K. M.; Hillmyer, M. A. *Polymer Reviews* **2008,** *48*, 85-108.

[8] Garlotta, D. *J. Polym. Environ.* **2001,** *9*, 63-84.

[9] Vink, E. T. H.; Rábago, K. R.; Glassner, D. A.; Springs, B.; O'Connor, R. P.; Kolstad, J.; Gruber, P. R. *Macromolecular Bioscience* **2004,** *4*, 551-564.

[10] Auras, R.; Harte, B.; Selke, S. *Macromolecular Bioscience* **2004,** *4*, 835-864.

[11] Belgacem, M. N.; Gandini, A. *Monomers, Polymers and Composites from Renewable Resources*; Elsevier: Amsterdam, 2008.

[12] Szwarc, M. *Adv. Polym. Sci.* **1983,** *49*, 1-177.

[13] Hsieh, H. L.; Quirk, R. P. *Anionic Polymerization: Principles and Practical Applications*; Marcel Dekker: New York, 1996.

[14] Hiemenz, P. C.; Lodge, T. P. *Polymer Chemistry*, 2nd ed.; Taylor & Francis Group: New York, 2007.

[15] Szwarc, M. *Nature* **1956,** *178*, 1168-1169.

[16] Szwarc, M.; Levy, M.; Milkovich, R. *J. Am. Chem. Soc.* **1956,** *78*, 2656-2657.

[17] Odian, G. *Principles of Polymerization*, 4th ed.; Wiley-Intescience: Hoboken, 2004.

[18] Saegusa, T.; Goethals, E. *Ring-Opening Polymerization*; American Chemical Society: Washington, D.C., 1977.

[19] McGrath, J. E. *Ring-Opening Polymerization: Kinetics, Mechanisms, and Synthesis*; American Chemical Society: Washington, D.C., 1985.

[20] Brunelle, D. J. *Ring-opening polymerization: Mechanisms, catalysis, structure, utility*; Hanser Publisher: Munich, 1993.

[21] Dubois, P.; Coulembier, O.; Raquez, J.-M. *Handbook of Ring-Opening Polymerization*; Wiley-VCH Verlag GmbH & Co. KGaA: Weinheim, 2009.

[22] Randall, D.; Lee, S. *The polyurethanes book*; John Wiley & Sons: New York, 2002.

[23] Hepburn, C. *Polyurethane Elastomers*; Applied Science: New York, 1982; p 248.

[24] Wirpsza, Z. *Polyurethanes : chemistry, technology, and applications*; Ellis Horwood:

New York, 1994.

[25] Berthelot, M. P. E. *Bull. Soc. Chim.* **1869,** *11*, 278.

[26] Jones, R. V.; Moberly, C. W.; Reynolds, W. B. *Industrial & Engineering Chemistry* **1953,** *45*, 1117-1122.

[27] Gehlsen, M. D. *Catalytic Hydrogenation of Polymers: Synthesis and Characterization of Model Polyolefins*. Ph.D. Dissertation, University of Minnesota, 1993.

[28] Lim, L. S. *Effects fo Glassy, Rubbery, and Semicrystalline Blocks on the Mechanical Response of Polyolefin Block Copolymers*. Ph.D. Dissertation, University of Minnesota, 2005.

[29] Hucul, D. A.; Hahn, S. F. *Adv. Mater.* **2000,** *12*, 1855-1858.

[30] Elias, H. G.; Etter, O. J. *J. Macromol. Sci.* **1967,** *A1-5*, 943.

[31] Gehlsen, M. D.; Weimann, P. A.; Bates, F. S.; Harville, S.; Mays, J. W.; Wignall, G. D. *J. Polym. Sci., Part B: Polym. Phys.* **1995,** *33*, 1527-1536.

[32] Guinier, A. *X-ray diffraction: in crystals, imperfect crystals, and amorphous bodies*; Dover Publications: 1994.

[33] Wilson, A. J. C. *International Tables for Crystallography: Mathematical, physical, and chemical tables*; Published for the International Union of Crystallography by Kluwer Academic Publishers: 1992; Vol. 3.

[34] Kossuth, M. B.; Morse, D. C.; Bates, F. S. *J. Rheol.* **1999,** *43*, 167-196.

[35] Williams, D. B.; Carter, C. B. *Transmission Electron Microscopy: A Textbook for Materials Science*, 2nd ed.; Springer: New York, 2009.

[36] Ward, I. M.; Sweeney, J. *An introduction to The Mechanical Properties of Solid Polymers*, 2nd ed.; Wiley: New York, 1983.

Chapter 3 Poly(cyclohexylethylene)-Polyethylene Nonablock Copolymers*

3.1 Introduction

Block copolymers have attracted lots of interest for decades because of their fascinating microstructures and unique physical properties. Various synthetic methods for block copolymers have been developed, which allows access to numerous different block copolymer systems. Among those block copolymers, poly(styrene-*b*-butadiene-*b*-styrene) (SBS) and poly(styrene-*b*-isoprene-*b*-styrene) (SIS) triblock copolymers were the first commercially successful thermoplastic elastomers.[1] In these triblock copolymers, glassy styrene blocks pin down the rubbery chains, resulting in a tough and elastic behavior. However, they have some limitations in their applications due to the relatively low glass transition temperature ($T_g \approx 100$ °C)[2] of polystyrene and the low thermal and oxidative stability of polybutadiene or polyisoprene. The low T_g of polystyrene limits the upper use temperature of the styrenic block copolymers to 60–70 °C.[1-3] Hydrogenation is an

* Part of this work was carried out in collaboration with Dr. Guillaume Fleury

effective method to enhance the physical properties of those unsaturated block copolymers. Poly(cyclohexylethylene) (PCHE or C, hydrogenated polystyrene) has a higher glass transition temperature ($T_g \approx 145$ °C)[2] than polystyrene, allowing a higher upper use temperature. Moreover, the saturation of the unsaturated polymers gives enhanced chemical, thermal, and UV stability by elimination of reactive functionalities in the backbone chain.[4] In spite of such enhanced properties, the application of the PCHE is restricted by its brittleness caused by the high molecular weight between entanglements (M_e = 40,000 g/mol)[2]. Recent research examined the way to improve the mechanical properties of PCHE by copolymerization with semicrystalline or rubbery polymers.

Combination of PCHE with semicrystalline polyethylene (PE or E, hydrogenated poly(1,4-butadiene)) can be a good strategy to overcome the liability of PCHE. Many researchers have studied the structural and mechanical behavior of the C/E block copolymer system. The macroscopic shear alignment of the C/E block copolymers was investigated by Vigild et al.[5] and Hermel et al.[6] They investigated different shear-induced lamellar orientations of CEC and CECEC produced with various shearing conditions. Hermel[7-8] and Lim[9] studied the effect of chain architecture on the mechanical properties for CEC and CECEC lamellae. In their research, CECEC pentablock copolymer showed much tougher mechanical behavior compared to CEC triblock copolymer. Khanna et al.[10] also reported similar results for C/E lamellar block copolymer films. The mechanical property tests for the aligned samples were performed by Phatak et al.[11] They compared mechanical failure of aligned CEC and CECEC lamellae. When strained along the lamellae normal, anisotropic CEC showed the brittle fracture, but anisotropic CECEC

exhibited ductility. For cylindrical morphologies, Ryu et al.[12] and Ruokolainen et al.[13] found a brittle to ductile transition by changing chain architecture from CEC to CECEC. The described mechanical properties for these block copolymer systems can be mainly explained by the effect of bridging and looping chain conformations. In general, more bridging and looping in all domains produce tougher mechanical behavior.

Most of the previous research about the mechanical behavior of the C/E copolymers has focused on low-level structures. Relatively little research has conducted on the phase behavior and physical properties of high-level multiblock copolymers. The block sequence from tetrablocks to decablocks is worth examining not only because of a sufficient molecular mobility to access equilibrium morphologies, but because of the enhanced mechanical properties induced by increasing bridging and looping with the number of blocks.[14] Moreover, Drolet and Fredrickson theoretically calculated average bridging fractions of internal blocks for ABABA pentablock copolymers; the results showed an increase in the fraction of center A blocks in bridged conformations (f_{br}) as the center block fraction is increased.[15] This study will focus on the phase and mechanical behavior of CECECECEC nonablock copolymer to find an effective method to make tough materials. Figure 3.1 shows chain architecture and expected microstructure of aimed CECECECEC nonablock copolymers. The prepared CECECECEC would have a large center C block (f_5 = 0.4–0.7) and small CECE outer blocks with the same sizes of C and E blocks (C blocks: $f_1 = f_3 = f_7 = f_9$, E blocks: $f_2 = f_4 = f_6 = f_8$), where f_n (n = 1 to 9) indicates the volume fraction of nth block. In CECECECEC block copolymers, more bridging chain conformations from the large center C block and crystalline microdomains

from the outer E blocks are expected to allow much enhanced mechanical properties.

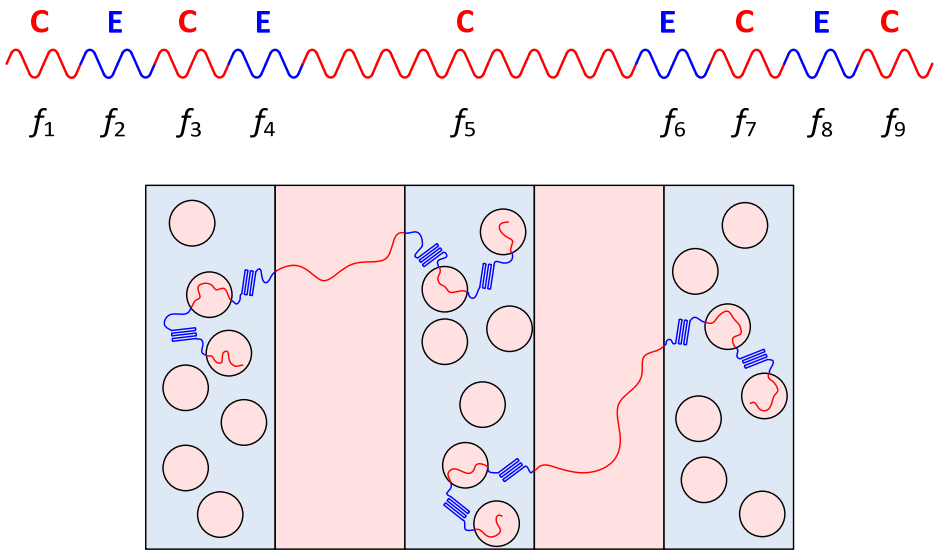

Figure 3.1 Chain architecture and expected microstructure of CECECECEC nonablock copolymers. The CECECECEC block copolymers have a large center C block (f_5 = 0.4–0.7) and small CECE outer blocks with the same sizes of C and E blocks (C blocks: $f_1 = f_3 = f_7 = f_9$, E blocks: $f_2 = f_4 = f_6 = f_8$), where f_n (n = 1 to 9) indicates the volume fraction of nth block.

In this work, poly(cyclohexylethylene)-polyethylene nonablock copolymers (CECECECEC) were prepared using sequential anionic polymerization followed by catalytic hydrogenation. The unsaturated SBSBSBSBS nonablock copolymers were synthesized by coupling of the living SBSBS pentablock chains with α,α'-dibromo-p-xylene. Then, hydrogenation with a Pt/Re catalyst produced the saturated CECECECEC block copolymers. We explored the morphological and thermal behavior of

CECECECEC samples by differential scanning calorimetry (DSC), dynamic mechanical spectroscopy (DMS), and small angle X-ray scattering (SAXS). The mechanical properties were characterized by uniaxial tensile tests.

This work was supported by the National Science Foundation. SAXS was performed at the DuPont-Northwestern-Dow Collaborative Access Team (DND-CAT) located at Sector 5 of the Advanced Photon Source (APS). DND-CAT is supported by E. I. du Pont de Nemours & Co., The Dow Chemical Company, and Northwestern University. Use of the APS, an Office of Science User Facility operated for the U.S. Department of Energy (DOE) Office of Science by Argonne National Laboratory, was supported by the U.S. DOE under Contract DE–AC02–06CH11357. Parts of this work were carried out in the Characterization Facility, University of Minnesota, which receives partial support from the NSF through the MRSEC program.

3.2 Experimental Section

3.2.1 Synthesis of PCHE-PE nonablock copolymers

The preparation of PCHE-PE nonablock copolymers (CECECECEC) starts from the anionic polymerization of SBSBSBSBS nonablock copolymers. In a living anionic polymerization, the purity of the materials and the cleanliness of the glassware are extremely important to obtain well-defined block copolymers with low PDI. Because the propagating living anions are easily killed by impurities, the purification of monomers is a mandatory step for anionic polymerization to remove any impurities present such as

inhibitor, water, oxygen and carbon dioxide. The purification agent should be selected very carefully with consideration of the agent's activity. The use of the improper purification agent can cause undesirable polymerization of the monomer during the purification step. In this study, di-*n*-butylmagnesium and *n*-butyllithium were used as purification agents for styrene and butadiene, respectively.

For the styrene monomer, the sequence of freezing–vacuum pumping–thawing was carried out three times to remove gaseous impurities. The styrene was transferred via vacuum distillation to another flask which contains the purification agent, di-*n*-butylmagnesium dried from a 1.0 M solution in heptane. The mixture of the monomer and purification agent was stirred at 40 °C for an hour. Then the styrene monomer was transferred to the second flask containing the same purification agent, and stirred for an hour again. The butadiene monomer was purified in a similar way, but *n*-butyllithium was used as the purification agent at below 0 °C using an ice bath with a salt. At the end of the purification, a designated amount of monomers were transferred to flame-treated burettes.

Cyclohexane solvent was purified by passing through two sequential purification columns. Polar contaminants are removed with activated alumina, and copper-alumina redox catalyst is used to remove oxygen.[16] The purified cyclohexane was transferred to a flame-treated flask and connected to a glass reactor. Tetrahydrofuran (THF) solvent was used to dissolve the coupling agent, *α*,*α*′-dibromo-*p*-xylene. The THF was purified using the two purification columns in a similar way, and transferred to another flask containing dried *n*-butyllithium for an additional purification step. The solution was stirred for an

hour at 20 ° C and collected in another flask to prepare the coupling agent solution.

The polymerization reaction was conducted with a multi-port glass reactor and argon-vacuum manifolds. The prepared monomer and the solvent flask were connected to the reactor. After checking for any leaks, the reactor was flamed with a torch, and argon–dynamic vacuum cycles were repeated at least six times to remove any moisture and other gaseous impurities. Then the solvent was added to the reactor and the temperature was set to 40 °C using a water bath and a heating coil. After the solvent reached thermal equilibrium, the initiator, *sec*-butyllithium, was injected to the reactor and agitated for about 10 minutes. Then the first monomer, styrene, was added and polymerized with stirring; the polymerization of the styrene block can be identified by the orange color of polystyryl anions. After at least 8 hours, an aliquot was taken with a cannula or a syringe, and injected into a degassed methanol solution. This aliquot was further characterized by size exclusion chromatography (SEC) to determine the molecular weight and PDI of the first block. The polymerization was continued with the sequential addition of monomers: butadiene–styrene–butadiene–styrene. For each block, at least 8 hours were allotted for the polymerization. Moreover, the addition of the butadiene monomer was carefully carried out by checking the pressure of the reactor which should not exceed 7–8 psi.

For the termination step, the living SBSBS pentablock chains were coupled using *α*,*α*′-dibromo-*p*-xylene to synthesize SBSBSBSBS nonablock copolymer. An excess amount of the coupling agent solution (0.25M) was injected to the reactor dropwise using a syringe to achieve complete coupling. After the termination, the SBSBSBSBS block copolymer was recovered by precipitation in a methanol/isopropanol mixture and dried

under vacuum until constant weight.

The CECECECEC block copolymer was prepared from the hydrogenation of SBSBSBSBS block copolymer using the Pt/Re catalyst supported on porous SiO_2 (Dow Chemical Co.). About 5 grams of the polymer and 1.5 grams of the catalyst were dissolved in 500 mL cyclohexane and added into 1 L stainless steel reactor. The hydrogenation reaction was performed under 500 psig hydrogen and 170 °C for about 12 hours. The saturated CECECECEC block copolymer was filtered at 70 °C and precipitated into a methanol/isopropanol mixture. The overall procedure of this synthesis is summarized in Figure 3.2.

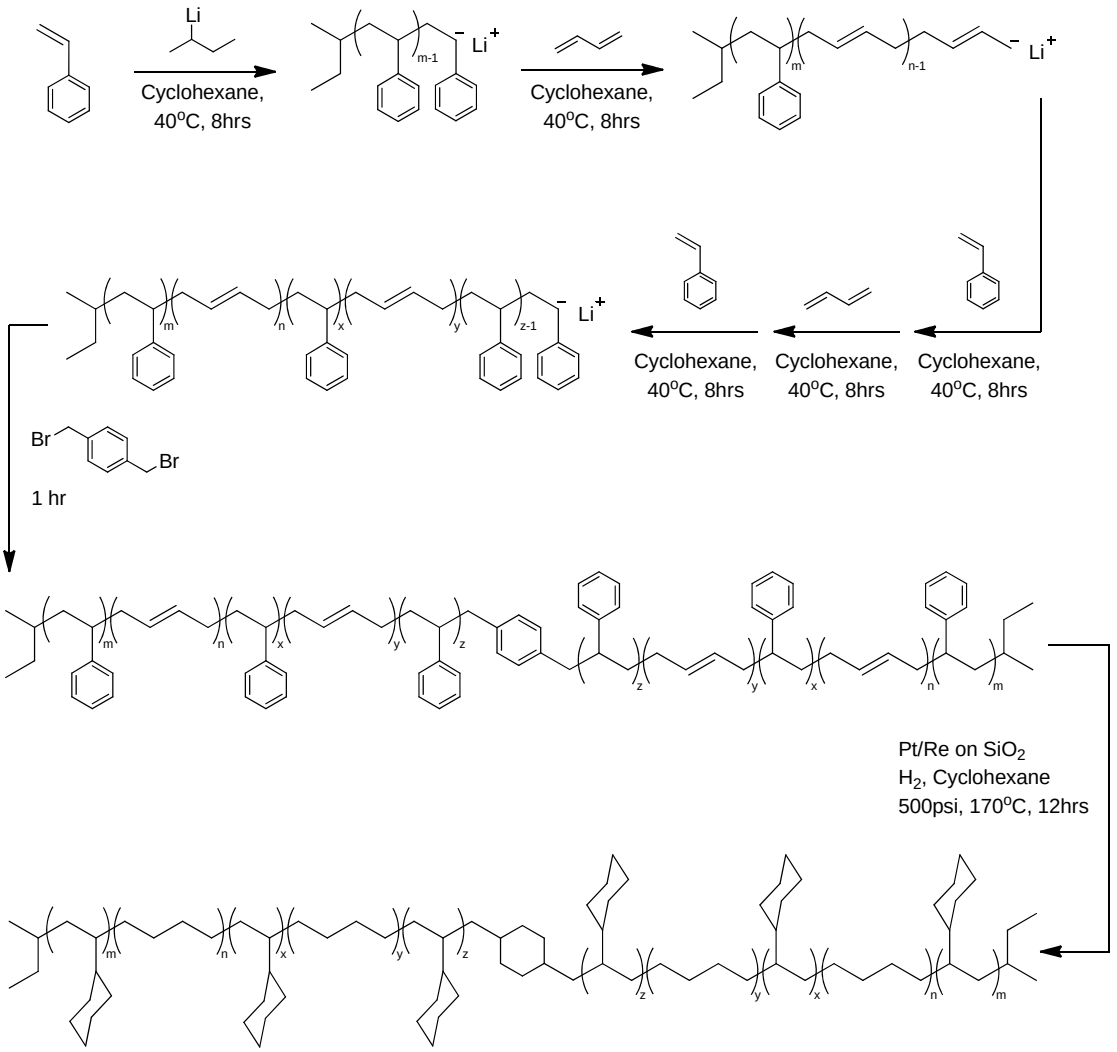

Figure 3.2 Synthesis scheme of CECECECEC nonablock copolymers.

3.2.2 Molecular Characterization

The molecular weight of an aliquot of the first styrene block was measured using size exclusion chromatography (SEC). The SEC results were combined with the ^{1}H nuclear magnetic resonance (NMR) spectra to determine the molecular weights and mole fractions of the unsaturated SBSBSBSBS nonablock copolymers. The volume fractions

were converted from mole fractions using the published homopolymer densities (ρ_{PS} = 0.969, $\rho_{1,4\text{-PB}}$ = 0.826, $\rho_{1,2\text{-PB}}$ = 0.889 g/cm^3).[17] The SEC was also used to obtain the polydispersity index (PDI = M_w/M_n) and the ratio of the coupled to uncoupled chains for the block copolymer samples. The coupling efficiency (% coupling) was calculated from the areas of Guassian fitting curves for coupled and uncoupled chains. The SEC analyses of the unsaturated block copolymer were performed on three 5 mm Phenomenex Phenogel columns with a Waters 717 plus autosampler, Waters 590 programable HPLC pump, and a Waters 410 differential refractometer. THF was used as the mobile phase at room temperature, and Ten EasiCal PS-2 polystyrene standards from Polymer Laboratories were used for calibration. ^{1}H NMR characterizations of the unsaturated polymers were acquired using Varian VAC-300 spectrometer with deuterated chloroform ($CDCl_3$) as a solvent at room temperature. For the saturated CECECECEC block copolymers, high-temperature ^{1}H NMR and high-temperature SEC were performed to determine the degree of saturation and the absence of bond breaking after the hydrogenation procedure. For high-temperature ^{1}H NMR analysis, the saturated polymer samples were dissolved in deuterated toluene (toluene-d_8) and measured with Varian Inova 300 spectrometer at 70 °C. High-temperature SEC was performed on a PL-GPC 220 system operated at 135 °C with 1,2,4-trichlorobenzene. After confirming the absence of proton peaks of unsaturated blocks, the total molecular weights and block compositions of the CECECECEC block copolymers were calculated from the results of the SBSBSBSBS with the assumption of a complete hydrogenation.

3.2.3 Differential Scanning Calorimetry (DSC)

Thermal analysis data for saturated CECECECEC block copolymer were obtained using a Thermal Analysis Q1000 DSC. Polymer samples were loaded into aluminum hermetically-sealed DSC pans and heated from 25 °C to 200 °C at a rate of 10 °C/min to erase the thermal history. Then, samples were cooled to 25 °C and reheated to 200 °C at a rate of 10 °C/min. The glass transition temperature (T_g), melting temperature (T_m), crystallization temperature (T_c), and percent crystallinity (X_c) were determined from the first cooling and the second heating data.

3.2.4 Dynamic Mechanical Spectroscopy (DMS)

The rheological analysis was performed on Rheometrics Scientific strain-controlled ARES rheometer fitted with 25 mm parallel plates. The samples were compression-molded between two Teflon-covered plates into flat discs (25 mm diameter, ~ 800 μm) at 170 °C. The disc-type sample was heated up to above the T_{ODT} (when possible) and cooled down to 160 °C (or 140 °C) to remove any thermal history. The isochronal temperature ramping test was conducted at a frequency of 0.1 rad/s and a strain of 1 % or 0.5 %. The sample was heated from 160 °C (or 140 °C) to 300 °C and cooled to the initial temperature with a rate of 0.5 °C/min. The T_{ODT} is identified by a sharp drop of G' during heating. The isothermal frequency sweep test was performed by dynamic frequency sweeps of 100 to 0.1 rad/s with the strain of 1% or 0.5% over the temperature range of 160 to 300 °C. The master curves of G' and G'' were created using time-temperature superposition (TTS) procedure.

3.2.5 Small-Angle X-ray Scattering (SAXS)

Synchrotron source SAXS were carried out at Argonne National Laboratory (Argonne, IL) with a beam wave length of λ = 0.729 Å and a sample-to-detector distance of 3.97 m. The CECECECEC polymers were heated above the order-disorder temperature T_{ODT} (when possible) and cooled down to room temperature. Then, the synchrotron SAXS measurements for the samples were performed at 140 °C. For annealing, block copolymers were annealed slightly below the T_{ODT} for 8 h, followed by slow cooling to room temperature over about 10 h. The synchrotron SAXS measurements for the annealed samples were performed at room temperature. The one-dimensional SAXS patterns were obtained by integrating the two-dimensional data, and are presented as intensity, I, versus scattering wave vector, $q = (4\pi\lambda)\sin(\theta/2)$, where θ is the scattering angle.

3.2.6 Tensile Testing

A Rheometrics Scientific Minimat equipped with a 200 N load cell was used for uniaxial tensile testing to measure the mechanical properties of block copolymer samples. Samples were compression-molded at 170 °C and cut into rectangular specimens having the dimensions of 9 mm gauge length, 3 mm gauge width, and about 1.3 mm thickness. The uniaxial deformation was operated at a crosshead speed of 5 mm/min and at room temperature. The tensile data was plotted with the engineering stress ($\sigma = F/A_0$) and the nominal strain ($\varepsilon = (l - l_0)/l_0$), where F is the force, l is the gauge length of the sample, and A_0 and l_0 are the initial cross-sectional area and length of the sample. The Young's

modulus (*E*) is calculated from the slope of the initial, linear region of the stress–strain curve, and fracture toughness is determined from the area under the curve. At least 5 specimens for each sample were measured for the average values.

3.3 Results and Discussion

3.3.1 Synthesis

The CECECECEC nonablock copolymers were synthesized via a combination of anionic polymerization, coupling chemistry, and catalytic hydrogenation. The molecular characteristics of CECECECEC are summarized in Table 3.1. The unsaturated SBSBSBSBS nonablock copolymers were prepared by anionic polymerization using *α*,*α′*-dibromo-*p*-xylene as a coupling agent. The synthesis results of the unsaturated polymers were analyzed with size exclusion chromatography (SEC) and ^{1}H nuclear magnetic resonance (NMR) techniques. Figure 3.3 shows representative SEC traces of the SBSBSBSBS nonablock copolymer and the corresponding aliquot of the first block. The peak of the SBSBSBSBS appeared at a lower elution volume, indicating the increase in molecular weight of unsaturated nonablock copolymer via the proposed synthetic procedure. All the synthesized nonablock copolymers exhibited a narrow distribution of molecular weights below 1.16 (see Table 3.1). The SEC curves of most coupled SBSBSBSBS chains showed a narrow single peak, revealing the coupling reaction using *α*,*α′*-dibromo-*p*-xylene was very efficient: above 95% coupling of the SBSBS living chains was achieved. One sample, $(SBSB)_2$S-85-70-104k, showed a bimodal SEC curve

after the coupling reaction. Figure 3.4 shows the SEC result of $(SBSB)_2S$-85-70-104k as well as Gaussian fitting curves for coupled and uncoupled chains; about 72 % of coupling efficiency was obtained from the area of the fitting curves. One possible reason for the lower coupling efficiency could be the presence of impurities in the THF used as a solvent for the coupling agent. Only for $(SBSB)_2S$-85-70-104k, the THF collected from the two purification columns was used for the synthesis without further purification. However, all other polymers were prepared from THF with the additional purification using *n*-butyllithium and exhibited better coupling efficiency (> 95% coupling).

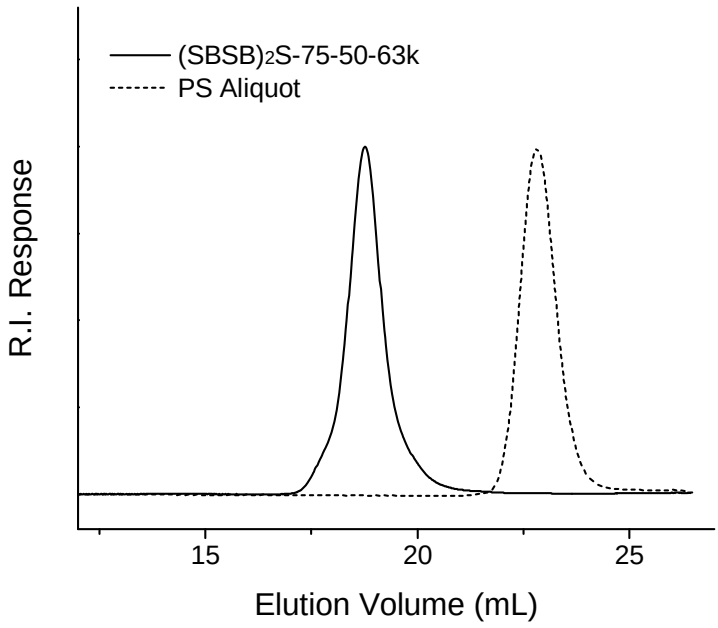

Figure 3.3 Representative SEC traces of SBSBSBSBS nonablock copolymer (solid line) and corresponding aliquot of the first block (dashed line) obtained with THF as the mobile phase at room temperature.

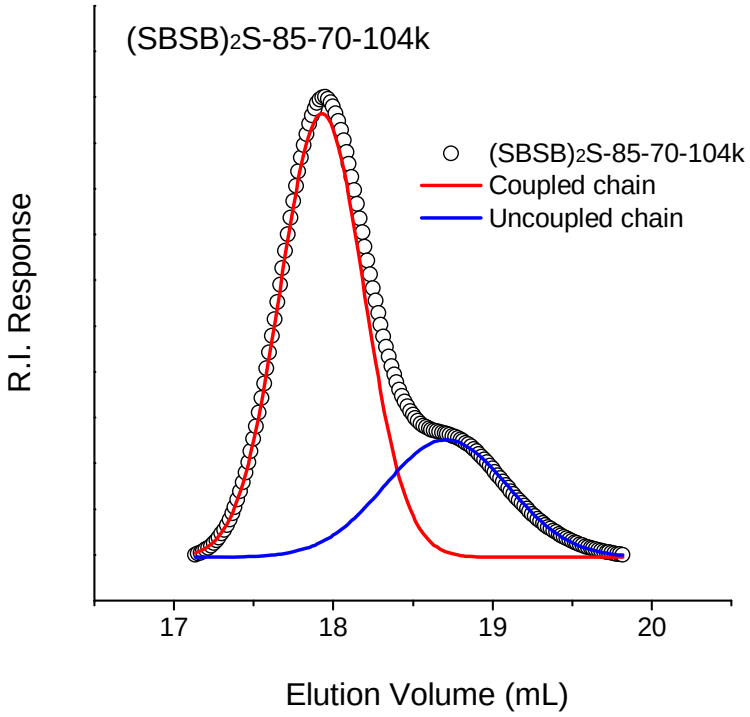

Figure 3.4 SEC trace of $(SBSB)_2S$-85-70-104k block copolymer (○) as well as Gaussian fitting curves for coupled (red line) and uncoupled (blue line) chains. The coupling efficiency was calculated from the area of the fitting curves.

Table 3.1 Molecular characteristic of CECECECEC nonablock copolymers.

Sample	M_n (g/mol) [a]	M_w/M_n [b]	f_C [c]	f_5 [d]	f_5/f_C
$(CECE)_2C$-75-50-46k	46200	1.16	0.75	0.5	0.67
$(CECE)_2C$-65-50-51k	50700	1.16	0.65	0.5	0.77
$(CECE)_2C$-75-50-63k	62700	1.13	0.75	0.5	0.67
$(CECE)_2C$-75-60-68k	67600	1.12	0.75	0.6	0.8
$(CECE)_2C$-70-40-70k	69800	1.14	0.70	0.4	0.57
$(CECE)_2C$-65-50-70k	70400	1.10	0.65	0.5	0.77
$(CECE)_2C$-55-40-87k	86900	1.11	0.55	0.4	0.73
$(CECE)_2C$-85-70-104k	103800 [e]	1.10	0.85	0.7	0.82
$(CECE)_2C$-75-70-134k	134300	1.09	0.75	0.7	0.93

[a] Molecular weight calculated from SEC results of the first PS block and ^{1}H NMR results of the SBSBSBSBS block copolymers with the assumption of a complete hydrogenation. [b] Polydispersity index measured by SEC. [c] Total volume fractions of PCHE ($f_C = f_1 + f_3 + f_5 + f_7 + f_9$). [d] Volume fraction of the center C block (f_5) [e] An effective value of the total molecular weight has been calculated by averaging the molecular weights of coupled nonablock and uncoupled pentablock copolymers, based on the coupling ratio.

Figure 3.5 shows the ^{1}H NMR spectra of unsaturated $(SBSB)_2S$-75-50-63k and saturated $(CECE)_2C$-75-50-63k nonablock copolymers. The NMR spectra of unsaturated and saturated polymer samples were obtained with deuterated chloroform ($CDCl_3$) at

room temperature and deuterated toluene (C_7D_8) at 70°C, respectively. For the unsaturated polymers (see Figure 3.5(a)), the protons of benzene rings in polystyrene occurred at 6.3–7.2 ppm (δH_a and δH_b). The proton peaks of −CH=CH− groups in poly(1,4-buatdiene) (δH_c) and −CH= groups in poly(1,2-butadiene) (δH_e) were observed at 5.3–5.5 ppm. The peaks of $=CH_2$ groups in poly(1,2-butadiene) (δH_d) also appeared at 4.8–5.0 ppm. The total molecular weight of SBSBSBSBS block copolymers were calculated from SEC results of the first PS block and ^{1}H NMR results, and the volume fractions were converted from mole fractions using published homopolymer densities.[17] ^{1}H NMR analysis also revealed that the anionic polymerization of 1,3-butadiene produced polybutadiene having a microstructure with 92% 1,4 units and 8% 1,2 units. The degree of saturation of hydrogenated polymers was determined by the high-temperature ^{1}H NMR spectroscopy. Figure 3.5(b) shows the representative ^{1}H NMR spectrum of the CECECECEC block copolymer. After the hydrogenation, the peaks for the olefin and aromatic protons ($\delta \approx 5.0$–7.5 ppm) of the SBSBSBSBS disappeared. This absence of the peaks of unsaturated PS and PB blocks indicates that the polymers are fully saturated with the proposed hydrogenation procedure. Then, the total molecular weight and volume fractions of the CECECECEC block copolymer were estimated from the results of the SBSBSBSBS with the assumption of a complete hydrogenation and are summarized in Table 3.1.

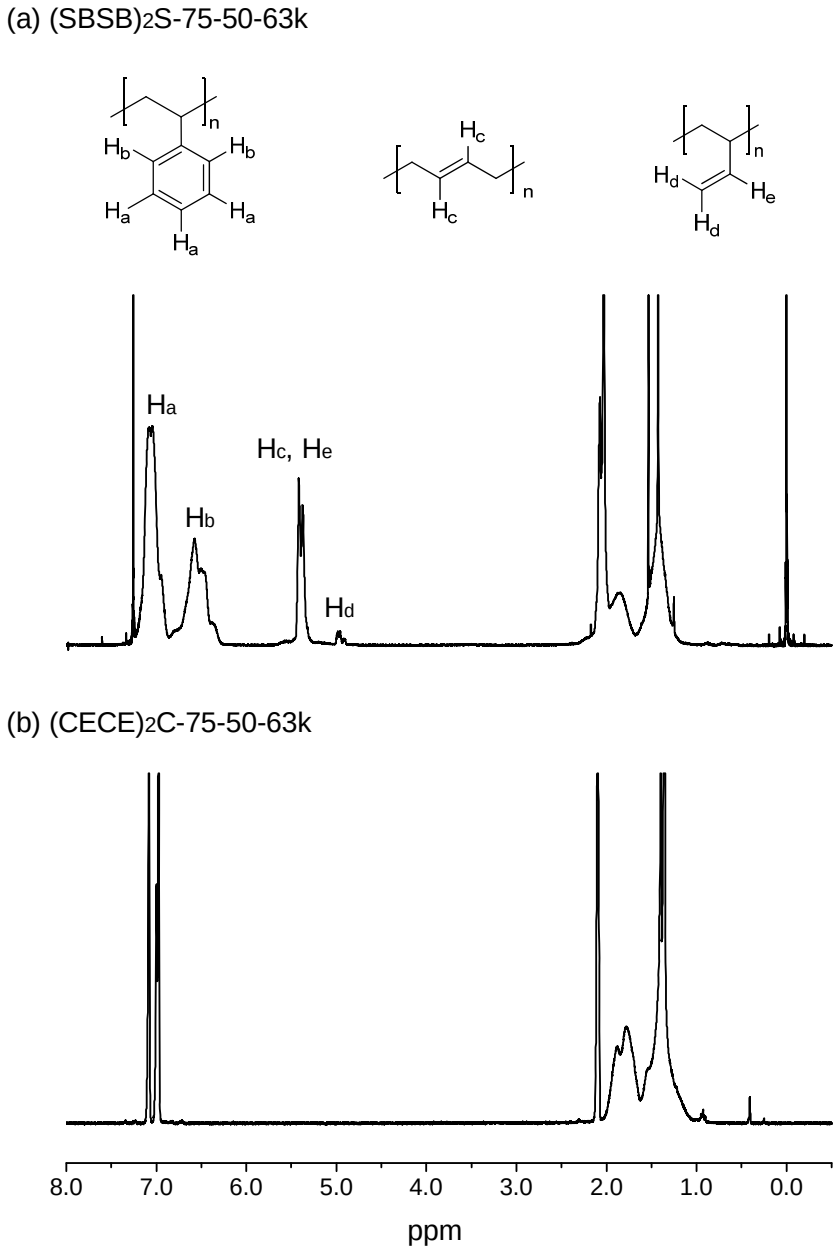

Figure 3.5 ^{1}H NMR spectra of (a) $(SBSB)_2S$-75-50-63k and (b) $(CECE)_2C$-75-50-63k nonablock copolymers. The unsaturated and saturated polymer samples were measured in deuterated chloroform ($CDCl_3$) at room temperature and deuterated toluene (C_7D_8) at 70°C, respectively.

In this study, symmetric CECECECEC nonablock copolymers consisting of a large center C block (f_5 = 0.4–0.7) have been synthesized; the outer four C blocks have the same volume fraction ($f_1 = f_3 = f_7 = f_9$) and all four E blocks were prepared with the same block size ($f_2 = f_4 = f_6 = f_8$), where f_n (n = 1 to 9) denotes the volume fraction of nth block in the nonablock copolymer. The synthesized CECECECEC nonablock copolymers have different molecular weights from 50 to 130 kg/mol, and the glassy PCHE (C) is the major component with the volume fraction of $f_C = f_1 + f_3 + f_5 + f_7 + f_9$ = 0.55–0.85.

3.3.2 Thermal Analysis

For thermal analysis of CECECECEC nonablock copolymers, differential scanning calorimetry (DSC) was used to determine the glass transition temperature (T_g), the melting temperature (T_m), the crystallization temperature (T_c), and the percent crystallinity (X_c). The polybutadiene chains of unsaturated SBSBSBSBS block copolymers which were synthesized via anionic polymerization contained 92% of linear 1,4 addition and 8% of 1,2 addition microstructures (see Section 3.3.1). Then, the saturated CECECECEC block copolymers were prepared by the catalytic hydrogenation of the SBSBSBSBS. During the hydrogenation procedure, the 8% 1,2 polybutadiene units resulted in randomly placed ethyl branches on the polyethylene chain. Solid-state NMR studies revealed that only about 10% of the ethyl branches can be incorporated into crystallites.[18] Thus, the polyethylene chain is compelled to exit a crystallite when it encounters an ethyl branch; the branches restrict the size and the ordering of the crystallites.[19] In DSC heating traces, the melting of small crystallites caused by the

existence of the ethyl branches broaden the melting peak with a little shoulder at the low-temperature region. To analyze the broad melting peak, the method of Rangagjan et al.[19] was applied and the representative DSC curve is shown in Figure 3.6. The high-temperature baseline was extended toward the low-temperature region, and the final T_m values determined as the baseline intercept of the tangent to the downward slope of the melting peak. The heat of melting, ΔH_m, is calculated as the integrated area of the melting peak above the baseline. After calculating ΔH_m, the percent crystallinity, X_c, was defined as

$$X_c = \left(\frac{\Delta H_m}{w_E \Delta H^\circ_{m,E}} \right) \tag{3.1}$$

where w_E is the weight fraction of polyethylene in the block copolymer, and $\Delta H^\circ_{m,E}$ is the theoretical heat of melting for perfectly crystalline polyethylene, 277 J/g.[20-21] The crystallization temperatures, T_c, were determined from the exothermic peak of the cooling curves. The glass transition temperature, T_g, of PCHE domains were defined as the intersections of the tangent through the inflection of the transition with the extrapolated baselines on heating. The measured values of T_m, T_c, X_c, and T_g for CECECECEC nonablock copolymers were summarized in Table 3.2.

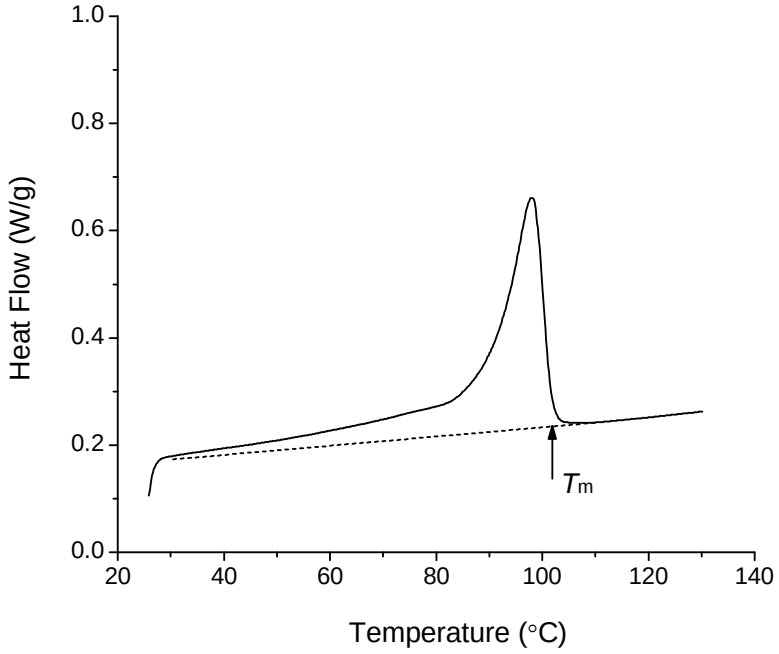

Figure 3.6 DSC heating trace of $(CECE)_2C$-55-40-87k. Dashed line indicates the baseline. T_m is determined as the baseline intercept of the tangent to the downward slope of the melting peak. ΔH_m is calculated as the integrated area of the peak above the baseline.

Table 3.2 Thermal analytic results of CECECECEC.

Sample	w_{PE} [a]	$M_{n,PE}$ [b] (kg/mol)	T_m (°C)	T_c (°C)	T_g (°C)	X_c (%)	T_{ODT} (°C)
$(CECE)_2C$-75-50-46k	0.20	2.6	97.9	49.3	118.7	7.0	–
$(CECE)_2C$-65-50-51k	0.29	4.0	100.5	59.7	126.7	20.7	190 ± 10
$(CECE)_2C$-75-50-63k	0.20	3.3	93.7	51.7	125.9	9.8	–
$(CECE)_2C$-75-60-68k	0.19	3.6	97.4	56.4	135.1	16.1	–
$(CECE)_2C$-70-40-70k	0.24	4.8	94.3	60.1	118.0	19.7	> 300
$(CECE)_2C$-65-50-70k	0.28	5.4	99.4	61.9	135.0	23.8	> 300
$(CECE)_2C$-55-40-87k	0.39	9.2	101.8	72.6	133.5	27.3	> 300
$(CECE)_2C$-85-70-104k	0.11	3.2	99.6	56.2	140.9	15.6	–
$(CECE)_2C$-75-70-134k	0.21	7.2	102.3	60.0	142.6	23.6	> 300

[a] Total weight fraction of PE in CECECECEC block copolymers. [b] Number-average molecular weight of each PE block ($M_{n,PE} = M_{n,2} = M_{n,4} = M_{n,6} = M_{n,8}$).

The glass transition temperatures of PCHE domains with the block molecular weights are displayed in Figure 3.7. The transitions of the nonablock copolymers occurred in the range from 119 to 143 °C. For the high molecular weight PCHE blocks ($M_{n,PCHE} \approx 100$ kg/mol), T_g of PCHE phases were around 141–143 °C, which is consistent with the previously reported T_gs of PCHE homopolymer.[22-23] However, the T_g of PCHE microdomain decreased as the molecular weight of PCHE block decreased. The

depression of T_g for the low molecular weight PCHE blocks can be caused by more free volume of the shorter polymer chains. The lower molecular weight blocks would have the higher fraction of the chain ends, which can drop the transition temperature by acting as an impurity. In addition, the partial phase mixing of different domains could result in the decrease in T_g. This dependence of glass transition temperature on molecular weight was observed by other studies with different systems.[24-26]

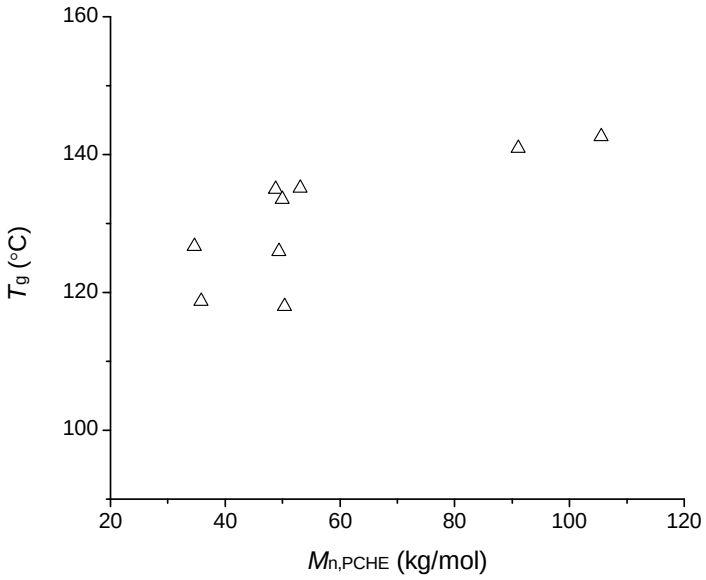

Figure 3.7 Block molecular weight effect on the glass transition temperatures of PCHE microdomains in CECECECEC nonablock copolymers.

In Figure 3.8, the percent crystallinity of CECECECEC block copolymers is plotted as a function of the molecular weight of each PE block, irrespective of morphology or overall molecular weight. The previous research data of CE diblocks and CEC triblocks[24]

are also displayed to examine the effect of the number of blocks on the crystallinity. The crystallinity for the homopolymer polyethylene is indicated by the dashed line. For the CE diblock copolymer, the molecular weight of PE has no significant effect on the crystallinity. All CE diblocks showed similar crystallinities, while their values were little less than that of the homopolymer PE. This slight decrease of the crystallinity in CE blocks comes from tethering only one end of the PE chain to the PCHE-PE interface. In CEC triblocks, the PE chains are more confined by tethering the both ends of the chain to the PCHE, resulting in the lower crystallinity for the CEC than the CE. Unlike the CE diblocks, the crystallinity of the CEC triblocks exhibited strong molecular weight dependence irrespective of the morphology. As the molecular weight of PE block increased, there was an almost linear increase in the percent crystallinity of the CEC block copolymers. In CECECECEC nonablock copolymers, samples having small PE blocks (~3 kg/mol), $(CECE)_2$C-75-50-46k and $(CECE)_2$C-75-50-63k, showed very low % crystallinity (< 10 %). The reason for the low crystallinity can be described by the phase mixing of small PE and PCHE blocks as well as topological constraints on the doubly-tethered PE chains of CECECECEC nonablock copolymers. The small blocks could be mixed because of the low driving force of phase separation, and the mixed phase would result in lowering the crystallinity. Interestingly, other CECECECEC samples containing larger PE blocks followed the almost same trend with CEC triblock copolymers. The CECECECEC block copolymers also showed lower crystallinity compared to CE diblock copolymers because of the spatial confinement and topological constraints.

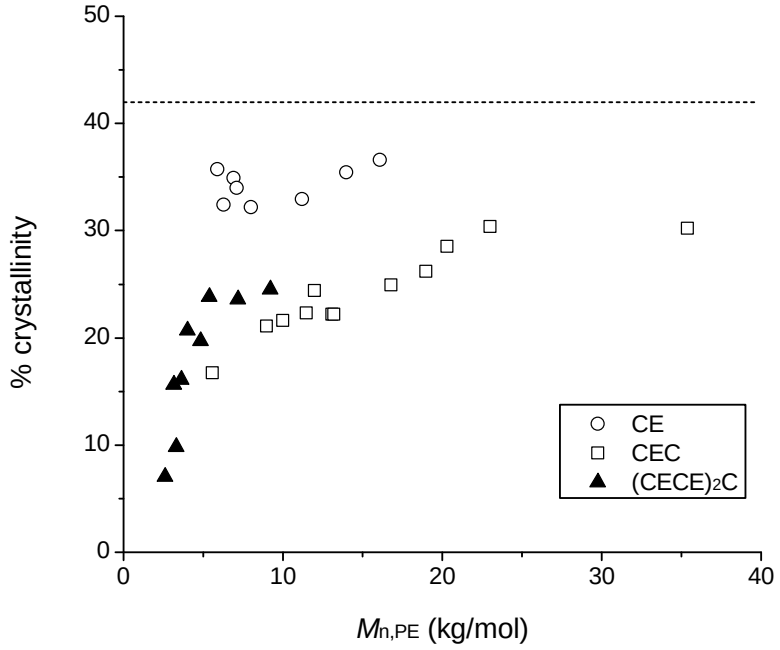

Figure 3.8 Crystallinity of PCHE/PE block copolymers as a function of the number-average molecular weight of PE blocks. Circles and squares denote CE diblocks and CEC triblocks, respectively. Dashed line indicates the crystallinity of the homopolymer PE. Data points were reproduced from Weimann et al.[24] Triangles indicate CECECECEC nonablock copolymers investigated in this study.

3.3.3 Rheological Properties

For rheological measurements of CECECECEC nonablock copolymers, dynamic mechanical spectroscopy (DMS) was performed: isochronal temperature sweep tests and dynamic frequency sweep tests were conducted to determine thermal transitions. In isochronal temperature sweep tests, the order-disorder transition temperatures (T_{ODT})

could be identified by a sudden drop of storage modulus G' during heating. In isochronal temperature ramping tests, however, most CECECECEC nonablock copolymers exhibited no order-disorder transition in the range of the investigated temperature (140–300 °C) or showed broad transitions over a wide range of temperatures, which makes hard to find out the T_{ODT} values of CECECECEC polymers. One sample, $(CECE)_2$C-65-50-51k, displayed the sharp drop of G' around 190 °C during heating, which denotes the order-disorder transition. The G' curve of $(CECE)_2$C-65-50-51k is shown in Figure 3.9, and the T_{ODT} is indicated by the arrow.

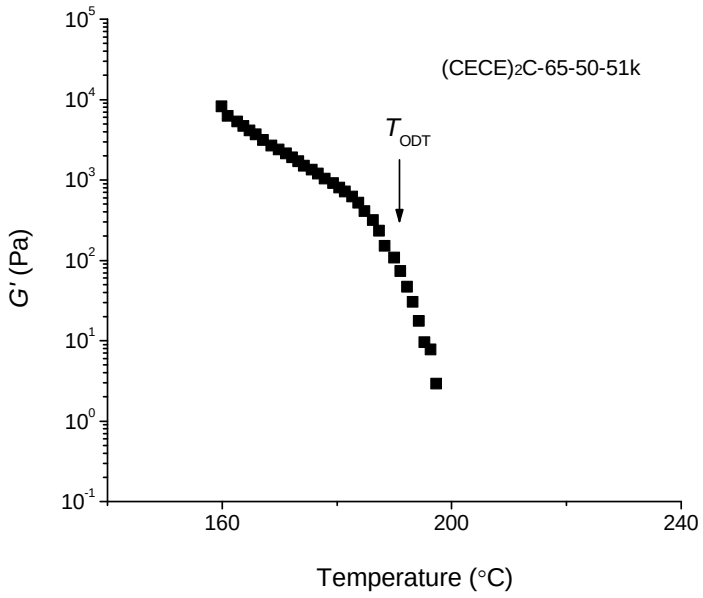

Figure 3.9 Storage modulus G' during isochronal temperature sweep test for $(CECE)_2$C-65-50-51k. The T_{ODT} where a sudden discontinuity of the G' occurred is indicated by the arrow.

The isothermal frequency sweep tests were performed to determine the frequency dependences of the storage modulus G' and the loss modulus G''. The master curves of the samples were created by using time-temperature superposition (TTS) of the isothermal frequency scans. In TTS, the measurements over a range of temperatures are reduced to one master curve at a reference temperature with the shift factor, a_T. The master curves using TTS for all polymer samples are shown in Figure 3.10 and Figure 3.11. The reference temperature (T_{ref}) is 160 °C except for $(CECE)_2$C-75-70-134k, which is 180 °C. On the graphs, the frequency dependences of G' and G'' at the low-frequency region are also denoted with $G(\omega) \sim \omega^{\alpha}$. In Figure 3.12 and Figure 3.13, shift factors (a_T) for CECECECEC nonablock copolymers are displayed as a function of temperatures. The shift factors could be approximated by the Williams-Landel-Ferry (WLF) equation with parameters C_1 and C_2,[27]

$$\log a_T = \frac{-C_1\left(T - T_{ref}\right)}{C_2 + \left(T - T_{ref}\right)} \tag{3.2}$$

and the fitted curve and constant values are also presented.

In disordered state, the low-frequency behavior would show $G' \sim \omega^2$ and $G'' \sim \omega$, consistent with liquid-like behavior. Thus, T_{ODT} could be estimated from the TTS master curves using the temperature where the exponent α of G' (the slope of G') changes close to 2. In the TTS master curve of $(CECE)_2$C-65-50-51k (see Figure 3.10), G' (closed symbols) showed two distinct branches which are $G' \sim \omega^{0.6}$ and $G' \sim \omega^2$. The gap between these two branches occurs around 190 °C which is consistent with the T_{ODT} measured by the isochronal temperature ramp test. Moreover, the exponent α can be a tool to predict the ordered state or the morphology of a block copolymer. However, the results from

dynamic mechanical spectroscopy (DMS) are not enough to identify the microstructures of the samples. To elucidate the morphologies of the CECECECEC nonablocks, SAXS measurements were performed and combined with DMS results (see Section 3.3.4).

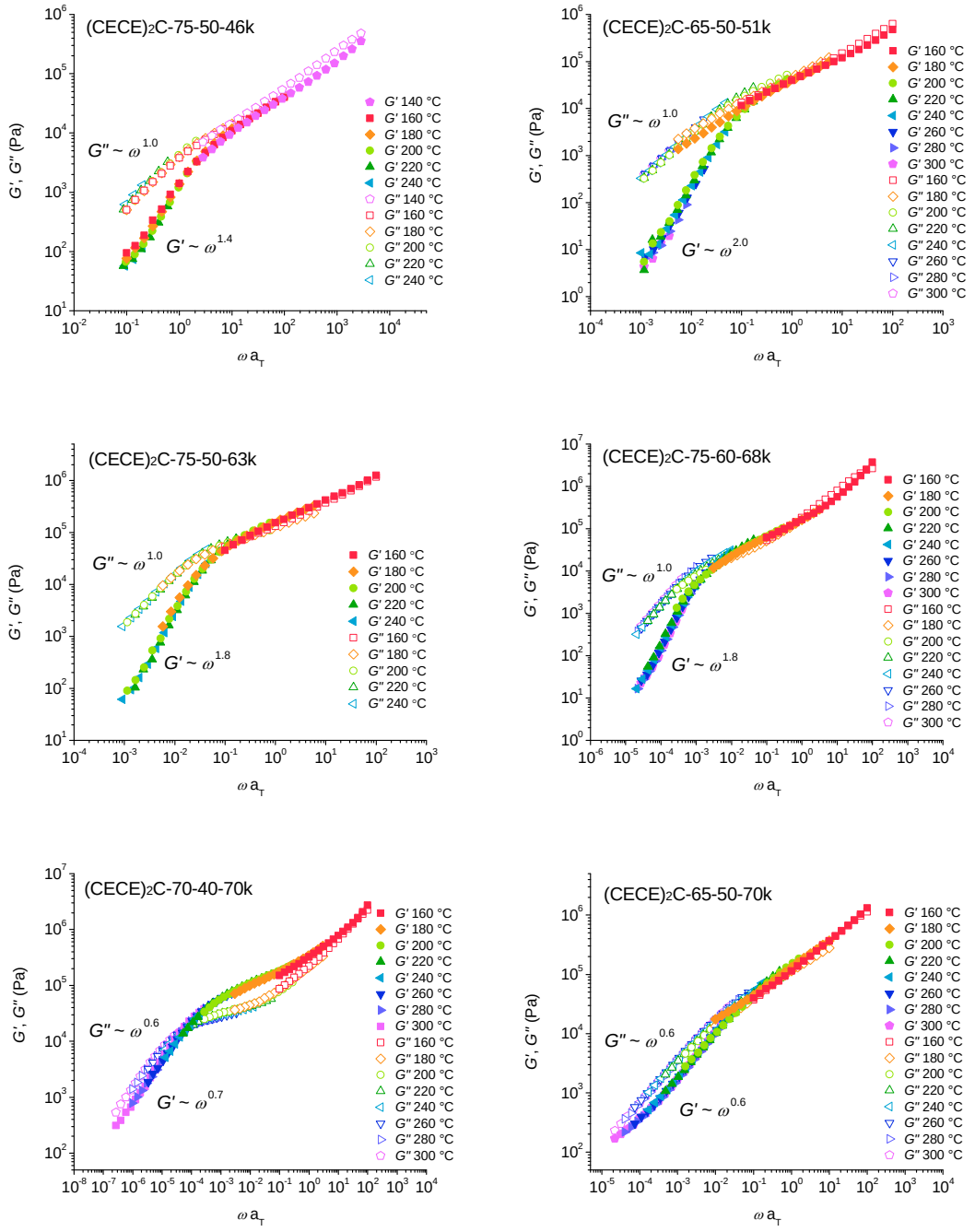

Figure 3.10 Master curves of modulus versus reduced frequency for CECECECEC nonablock copolymers. The reference temperature (T_{ref}) is 160 °C. Closed and open symbols denote the storage modulus G' and the loss modulus G'', respectively.

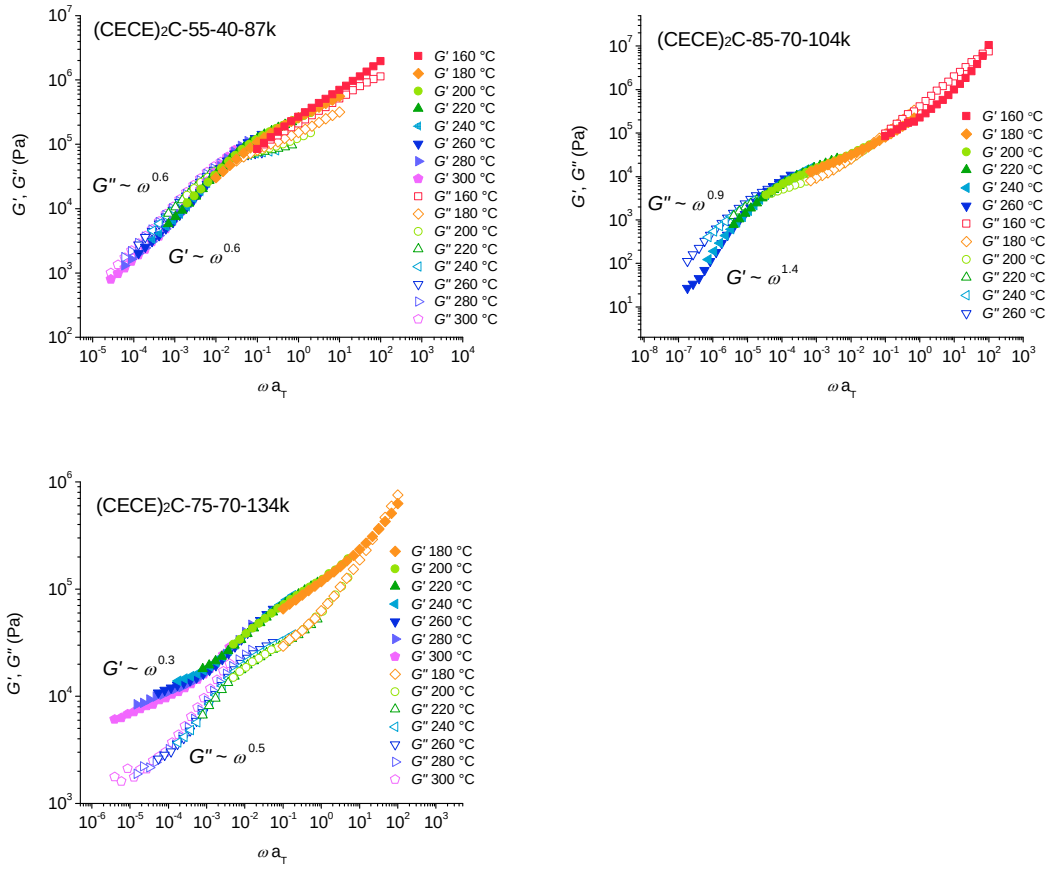

Figure 3.11 Master curves of modulus versus reduced frequency for CECECECEC nonablock copolymers. The reference temperature (T_{ref}) is 160 °C except for $(CECE)_2C$-75-70-134k, which is 180 °C. Closed and open symbols denote the storage modulus G' and the loss modulus G'', respectively.

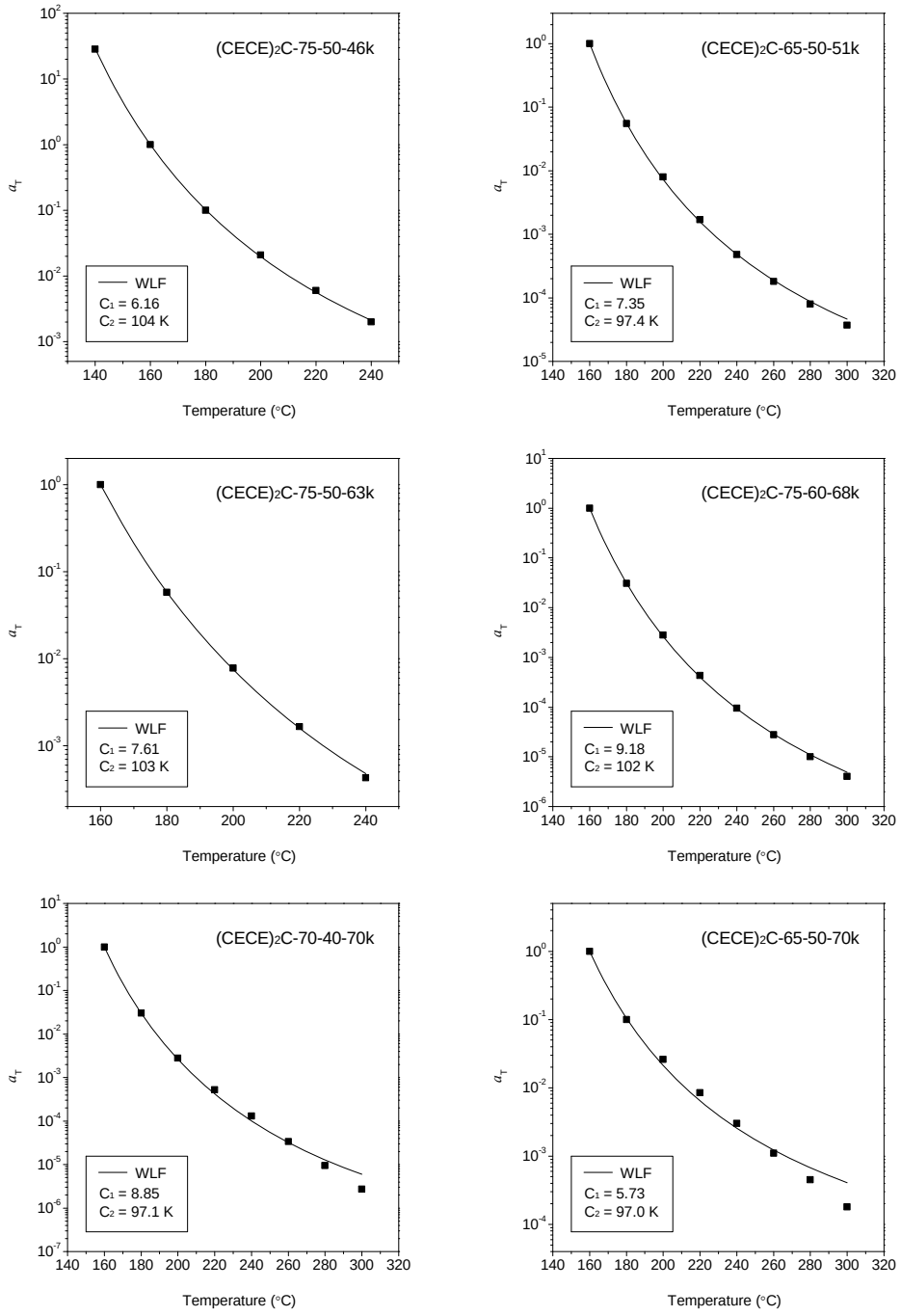

Figure 3.12 Shift factors (a_T) as a function of temperatures for CECECECEC nonablock copolymers. The solid line represents a fit of Williams-Landel-Ferry (WLF) equation with parameters C_1 and C_2. The reference temperature (T_{ref}) is 160 °C.

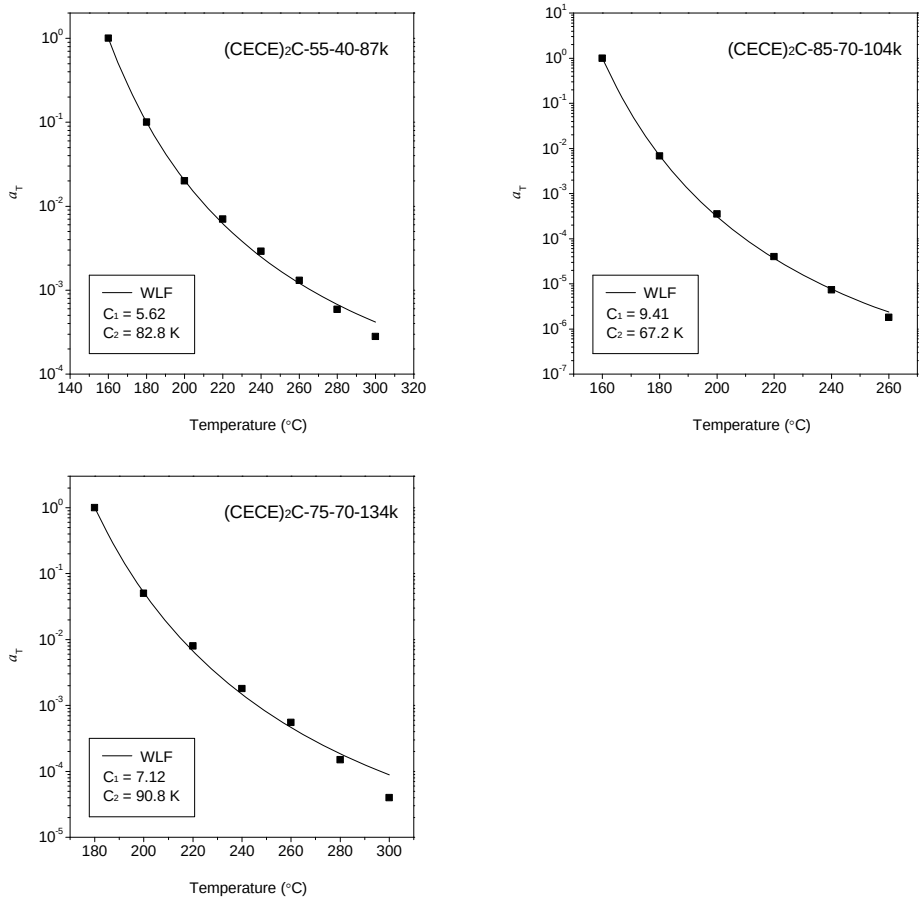

Figure 3.13 Shift factors (a_T) as a function of temperatures for CECECECEC nonablock copolymers. The solid line represents a fit of Williams-Landel-Ferry (WLF) equation with parameters C_1 and C_2. The reference temperature (T_{ref}) is 160 °C except for $(CECE)_2C$-75-70-134k, which is 180 °C.

3.3.4 Structural Analysis

The microstructures of CECECECEC block copolymers were characterized using

small-angle X-ray scattering (SAXS). The block copolymer samples were heated above the T_{ODT} (when possible) and cooled down to room temperature. The measured results were plotted as the log-scaled intensity versus the scattering vector $q = 4\pi/\lambda(\sin\theta/2)$, where λ is the wavelength of the incident X-rays and θ is the scattering angle. Figure 3.14 displays synchrotron SAXS patterns for CECECECEC nonablocks at 140 °C, except for $(CECE)_2C$-55-40-87k-AN, which is at 25 °C. The morphologies of the samples were determined using q/q^* ratio (denoted by the arrows), where q^* is the scattering vector of a first-order peak. The characterized morphologies and domain spacings of CECECECEC block copolymers are summarized in Table 3.3. The block copolymer $(CECE)_2C$-65-50-51k, $(CECE)_2C$-70-40-70k, and $(CECE)_2C$-65-50-70k showed SAXS patterns possessing ratios of $q/q^* = 1, 2, 3 \cdots$, indicating a lamellar (LAM) morphology. For the SAXS spectrum of $(CECE)_2C$-75-60-68k, a small peak at $q/q^* = 2$ could be found, while the intensity of the scattering peaks was very weak. So, it is not clear that whether this sample has a lamellar or disordered microstructure. Two nonablock copolymers containing a large volume fraction of the center C block ($f_5 = 0.7$), $(CECE)_2C$-85-70-104k and $(CECE)_2C$-75-70-134k, showed the SAXS patterns of a hexagonally packed cylinder (HEX) morphology with a sequence of reflections of $q/q^* = \sqrt{1}, \sqrt{3}, \sqrt{4}, \sqrt{7}, \sqrt{9}, \cdots$. With a careful investigation of ordered block copolymer samples, the morphologies of CECECECEC seem to be governed by the volume fraction of the center C block (f_5) rather than the total volume fraction of PCHE ($f_C = f_1 + f_3 + f_5 + f_7 + f_9$). For ordered CECECECEC block copolymers, samples with $f_5 = 0.4$–0.5 showed the lamellar structure irrespective of the total amount of PCHE ($f_C = 0.55$–0.70). The hexagonal symmetry were

found only in two samples with a large center C block, f_5 = 0.7. The microstructures controlled by f_5 also imply that the outer CECE blocks might have a mixed phase of PCHE and PE; CECE-C-ECEC nonablock copolymers can be considered as M-C-M, where M represents the C/E mixed phase. Because the center C block is much larger than the rest of the eight PCHE and PE blocks consisting of outer CECE, the outer small blocks might not have enough driving force for the microphase segregation and have the mixed phase.

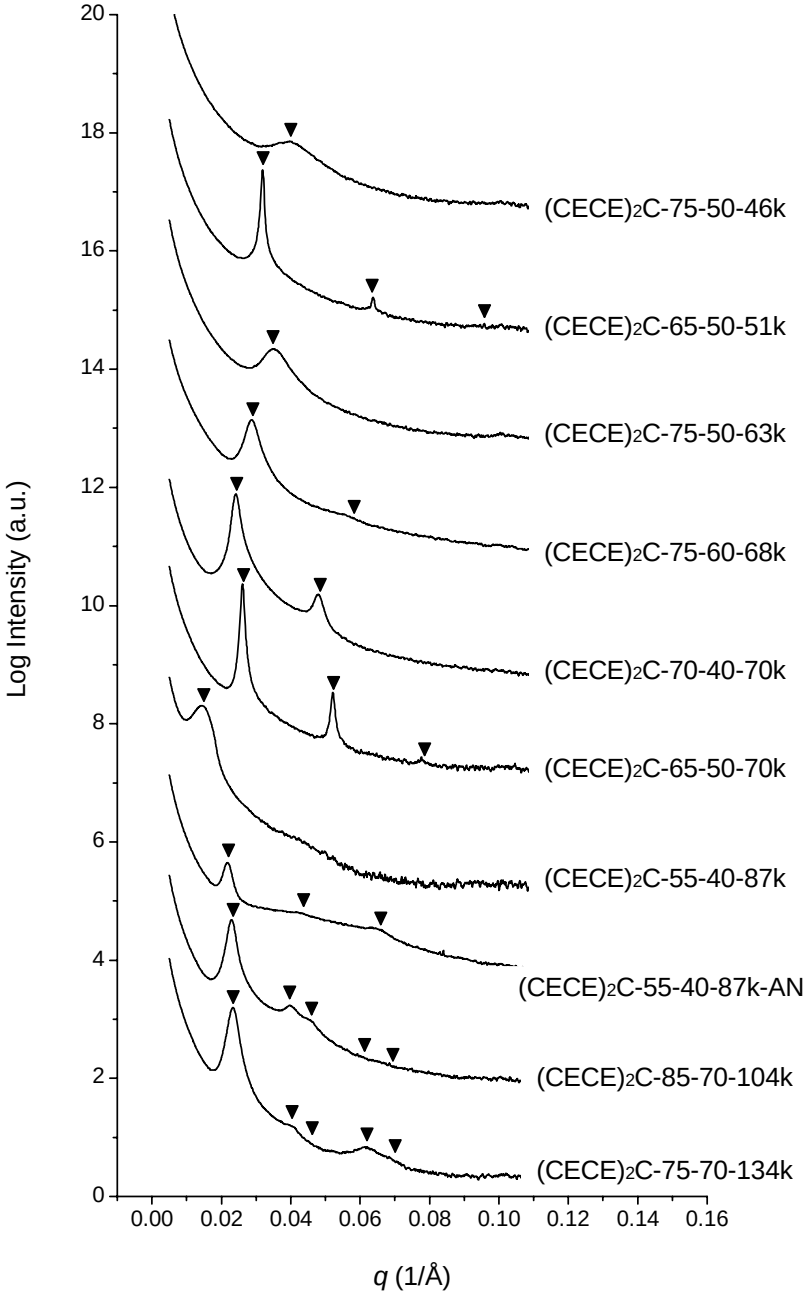

Figure 3.14 SAXS patterns for CECECECEC nonablock copolymers obtained at 140 °C except for $(CECE)_2C$-55-40-87k-AN, which is 25 °C. Data sets are shifted vertically for clarity.

Table 3.3 Characterized morphologies and domain spacings of CECECECEC block copolymers.

Sample	q^* (1/Å)	d^* (mm)	Morphology
$(CECE)_2C$-75-50-46k	0.0401	15.7	DIS
$(CECE)_2C$-65-50-51k	0.0319	19.7	LAM
$(CECE)_2C$-75-50-63k	0.0350	18.0	DIS
$(CECE)_2C$-75-60-68k	0.0287	21.9	DIS/LAM
$(CECE)_2C$-70-40-70k	0.0242	26.0	LAM
$(CECE)_2C$-65-50-70k	0.0261	24.1	LAM
$(CECE)_2C$-55-40-87k	0.0144	43.8	–
$(CECE)_2C$-55-40-87k-AN	0.0217	28.9	LAM
$(CECE)_2C$-85-70-104k	0.0229	27.4	HEX
$(CECE)_2C$-75-70-134k	0.0233	27.0	HEX

The SAXS patterns of $(CECE)_2C$-75-50-46k and $(CECE)_2C$-75-50-63k displayed a broad single scattering peak, which means there is no long-range ordered structure. This disordered microstructure (DIS) of two samples might come from their very small PE blocks which could not be strongly segregated into well-ordered microstructures. These samples did not show clear order-disorder transition temperatures in rheological tests and could have homogeneous phase with mixed PCHE and PE domains. The SAXS pattern of $(CECE)_2C$-55-40-87k also did not show distinct high order scattering peaks, indicating no ordered structure was formed; in this case, $(CECE)_2C$-55-40-87k has large PE blocks that might be large enough to have microphase separation. For further examination, the SAXS

measurements of these disordered block copolymers were performed after annealing at below the T_{ODT} for 8 h and cooling down to room temperature. In $(CECE)_2C$-75-50-46k and $(CECE)_2C$-75-50-63k samples, the annealing treatment did not affect the SAXS patterns. However, $(CECE)_2C$-55-40-87k exhibited different morphological behavior with high-temperature annealing. The annealed sample, $(CECE)_2C$-55-40-87k-AN (denoted by AN), displayed SAXS pattern of lamellar microstructure containing high order peaks at q/q^* ratios of $1, 2, 3, \cdots$(see Figure 3.14). It seems that the ordering process of $(CECE)_2C$-55-40-87k is slower than other CECECECEC multiblock copolymers. It might be correlated with additional phase separation of outer C and E blocks; among the probed samples, $(CECE)_2C$-55-40-87k has the largest outer blocks which could possibly have secondary phase segregation. However, there is no obvious explanation about this slow ordering of block copolymer chains, and further investigation is needed.

3.3.5 PE Block Size Effect on Morphology

The microstructures of investigated CECECECEC nonablock copolymers can be thought as three different states with the PE block sizes. First, CECECECEC polymers having very small PE blocks are expected to have homogeneous mixed phase with PCHE and PE chains (see Figure 3.15(a)). The small PE blocks could not have enough driving force to phase-segregate into ordered microstructures. This disordered microstructure is verified by the SAXS patterns of $(CECE)_2C$-75-50-46k and $(CECE)_2C$-75-50-63k (Figure 3.14) showing a broad single scattering peak. In the disordered homogeneous phase, small PE chains cannot crystallize well and can only have small secondary crystals; this

can explain the reason for the low % crystallinity of $(CECE)_2C$-75-50-46k and $(CECE)_2C$-75-50-63k samples (Table 3.2).

The second anticipated microstructure of CECECECEC is a lamellar (or cylindrical) morphology with mixed phase of outer CECE blocks (see Figure 3.15(b)). In these samples, the PE blocks were sufficiently large to have ordered microstructures, but not large enough to obtain the phase segregation in outer CECE blocks. The SAXS patterns of $(CECE)_2C$-65-50-51k, $(CECE)_2C$-70-40-70k, and $(CECE)_2C$-65-50-70k showed the lamellar morphology. With a larger volume fraction of center C block, $(CECE)_2C$-85-70-104k and $(CECE)_2C$-75-70-134k displayed the SAXS patterns of a hexagonally packed cylinder morphology. These assigned morphologies imply that the CECECECEC block copolymers could have a microphase separation into PCHE domain of the center block and mixed phase of the outer CECE blocks, which is possibly controlled by the volume fraction of the center C block (f_5) instead of the total volume fraction of PCHE (f_C). After this primary phase separation of center PCHE and mixed phase, crystallization of PE chains in the mixed phase could cause the crystal induced secondary structures. These samples exhibited higher % crystallinities.

The last expected morphology is a layer-in-layer microstructure (see Figure 3.15(c)). If PE block size is large enough to have the phase segregation of outer CECE blocks, the CECECECEC block copolymer would have primary and secondary microphase separation. Consequently, the large center C and outer CECE could make the primary layer structure, and the secondary layer structure could be developed in CECE blocks. From the SAXS analysis with different thermal treatments (section 3.3.4),

$(CECE)_2C$-55-40-87k, containing the largest PE blocks among the studied samples, exhibited the slower ordering process compared to other CECECECEC multiblock copolymers. The slow structural ordering could be correlated with development of the secondary lamellar structure in outer CECE blocks. With the additional phase separation, $(CECE)_2C$-55-40-87k showed the highest % crystallinity and is expected to have enhanced mechanical properties.

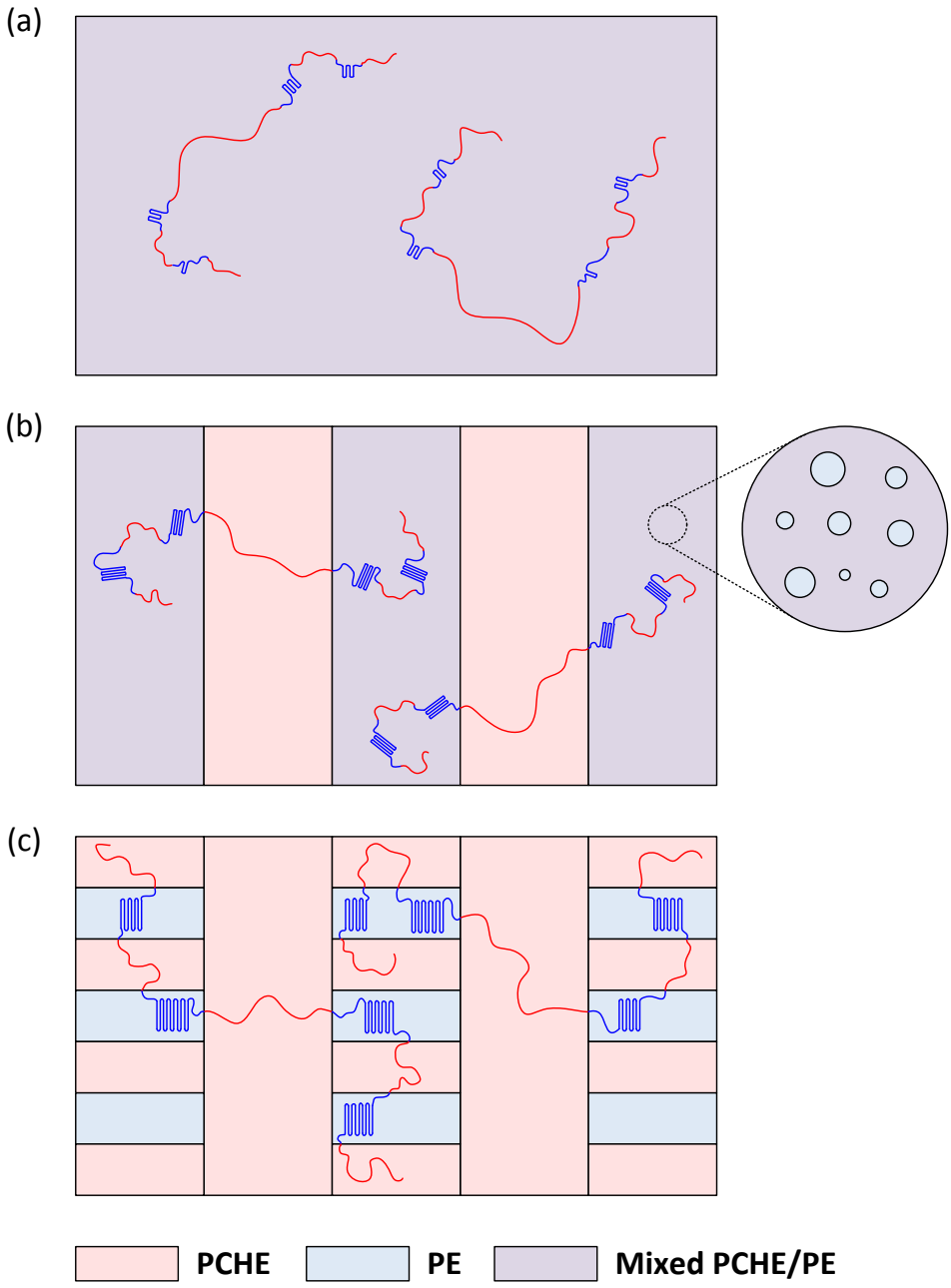

Figure 3.15 Feasible microstructures of CECECECEC block copolymers: (a) homogeneous phase and small secondary crystals; (b) primary phase separation and crystallization induced secondary structure; (c) layer-in-layer structure with primary and secondary phase separation .

3.3.6 Tensile Properties

Mechanical properties of CECECECEC block copolymers were characterized using uniaxial tensile tests. Rectangular specimens were drawn with a constant strain rate at room temperature. Figure 3.16 displays the representative stress-strain curves of CECECECEC block copolymer samples with the inset showing the small strain region. The analyzed mechanical properties for these materials, elastic modulus (E), strain at break (ε_b), stress at break (tensile strength, σ_b), yield stress (σ_y), and toughness (area under the stress-strain curve), are also summarized in Table 3.4. We note that the failure occurred near the grips for most rectangular tensile specimens; hence measured results denote conservative estimates of ε_b and σ_b.

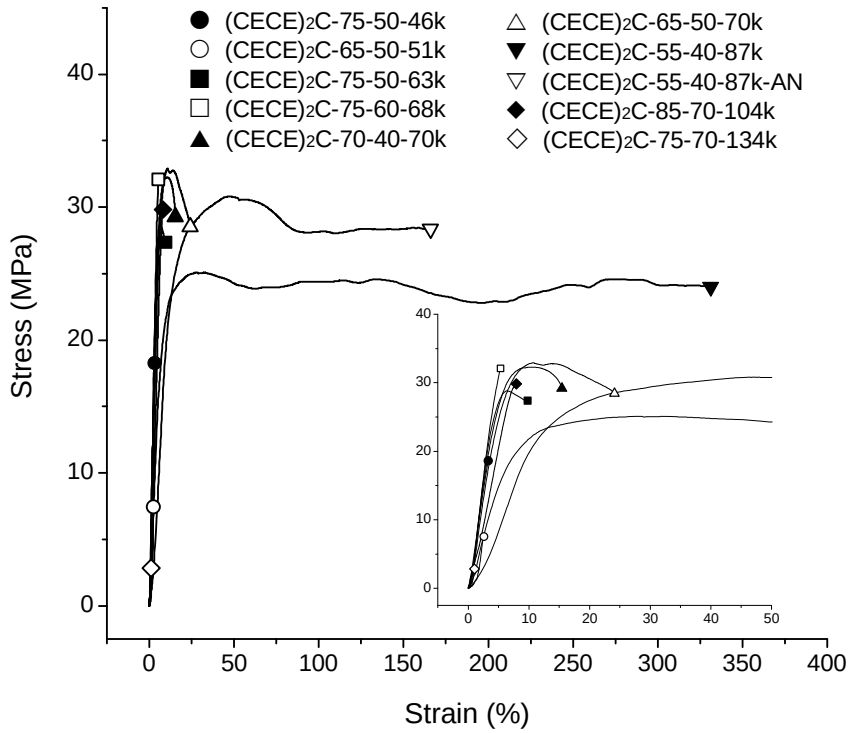

Figure 3.16 Representative stress-strain curves for CECECECEC block copolymers. The inset shows the stress-strain curves at small strain region.

Most CECECECEC block copolymer samples exhibited brittle behavior with low fracture toughness. This brittleness of nonablock copolymer samples might be attributed to the phase mixing of small PCHE and PE blocks. The structural analysis of CECECECEC suggested the possibility of a mixed phase for the outer CECE blocks. With the phase mixing, the chain architecture of CECECECEC nonablock copolymer could be thought of as MCM triblock copolymer (M represents the PCHE/PE mixed phase). In MCM triblock architecture, lack of the flexible chains to connect the brittle PCHE domains could cause the poor mechanical behavior. Also, brittleness of MCM blocks could not be prevented because the domains are connected by the rigid PCHE

chains. The poor tensile properties of triblock copolymers having a glassy center block also have been reported in different systems such as BSB and ISI, where S, B, and I denote polystyrene, polybutadiene, and polyisoprene, respectively.[11,28-30]

Table 3.4 Tensile properties of CECECECEC block copolymers.

Sample	E (Mpa)	ε_b (%)	σ_b (MPa)	σ_y (MPa)	Toughness (kJ/m^3)
$(CECE)_2C$-75-50-46k	643 ± 98	3.8 ± 0.5	19.6 ± 4.7	-	300
$(CECE)_2C$-65-50-51k	401 ± 271	3.6 ± 1.4	7.9 ± 0.6	-	60
$(CECE)_2C$-75-50-63k	681 ± 67	9.9 ± 2.3	26.3 ± 5.9	29.6 ± 1.1	2120
$(CECE)_2C$-75-60-68k	807 ± 59	5.3 ± 0.5	32.3 ± 2.1	-	890
$(CECE)_2C$-70-40-70k	652 ± 76	15.3 ± 5.6	29.7 ± 3.4	32.1 ± 0.4	3980
$(CECE)_2C$-65-50-70k	577 ± 73	25.1 ± 7.7	26.9 ± 1.8	31.7 ± 1.7	6560
$(CECE)_2C$-55-40-87k	271 ± 58	332 ± 66	22.2 ± 1.2	23.6 ± 1.1	78570
$(CECE)_2C$-55-40-87k-AN	197 ±54	166 ± 91	26.9 ± 2.0	29.6 ± 2.5	45630
$(CECE)_2C$-85-70-104k	463 ± 61	8.9 ± 2.2	31.3 ± 1.3	-	1270
$(CECE)_2C$-75-70-134k	260 ± 70	1.1 ± 0.3	2.5 ± 0.9	-	10

Comparing $(CECE)_2C$-65-50-51k and $(CECE)_2C$-65-50-70k allows some insight into the molecular weight effect on the mechanical properties of CECECECEC block copolymers. The two samples have the same block composition and morphology (i.e.,

LAM), but the different total molecular weight of the polymer. The results of the tensile tests showed that the tensile properties are improved as the molecular weight increases with the fixed block composition; the sample with higher molecular weight exhibited enhanced elastic modulus, strain at break, tensile strength, and toughness. This tendency can be explained by more chain entanglements induced by the increase of the molecular weight. The analyzed tensile results also show that the PE content of the block copolymers can control the mechanical behavior of CECECECEC. The polymer samples of $(CECE)_2C$-70-40-70k, and $(CECE)_2C$-65-50-70k have the similar total molecular weight and morphology, while the block compositions are different. When comparing these samples, increase of PE volume fraction leads to enhancement of strain at break and toughness with the compensational decrease of modulus and tensile strength. Even though an increase in the amount of the flexible PE chains allowed little ductility to CECECECEC polymers, these samples were still very brittle with the low σ_b values (5–25%).

Interestingly, one of the CECECECEC nonablock copolymers, $(CECE)_2C$-55-40-87k, exhibited the ductile behavior with much higher toughness compared to other samples. The most noticeable characteristic for this polymer is the largest PE content among the studied samples. In $(CECE)_2C$-55-40-87k, the PE blocks are large enough to have phase segregation of PCHE and PE domains in the outer CECE blocks, even though the microstructure is kinetically trapped because of its slow ordering process; the ordering becomes more difficult for the nonablock structure because chains which bridge several domains cannot arrange their conformation easily. The phase separation of outer

blocks would allow $(CECE)_2C$-55-40-87k to have CECECECEC nonablock chain architecture rather than MCM triblock structure with a mixed phase M. For the $(CECE)_2C$-55-40-87k, the flexible PE chains in the phase-segregated nonablock structure can connect other domains, and the tied PE chains would allow the ductile behavior with the plastic deformation of semicrystalline PE domains. Thus, the dramatic enhancement of toughness is further evidence of the additional secondary phase separation of $(CECE)_2C$-55-40-87k. The mechanical properties of the annealed sample of $(CECE)_2C$-55-40-87k were also characterized with the uniaxial tensile test. The annealed sample, $(CECE)_2C$-55-40-87k-AN, displayed ductile and tough mechanical behavior like the sample without annealing, $(CECE)_2C$-55-40-87k. When comparing those two samples, however, the annealed $(CECE)_2C$-55-40-87k-AN having ordered lamellar microstructure exhibited the lower fracture toughness (still much tougher compared to other samples in this study) with higher σ_y, σ_b, and lower ε_b. This mechanical difference between the same samples with the different morphologies could be attributed to the more connectivity of glassy PCHE domains in the lamellar structure compared to the disordered one.

3.4 Conclusions

Poly(cyclohexylethylene)-polyethylene nonablock copolymers (CECECECEC) consisting of a large center C block (f_5 = 0.4–0.7) were synthesized by sequential anionic polymerization of styrene and butadiene followed by coupling chemistry and catalytic hydrogenation. The molecular characterization revealed that the proposed synthetic procedure successfully prepared the desired PCHE-PE nonablock copolymers. Structural

analysis suggested three different possible microstructures for CECECECEC nonablock copolymers with varying size of PE blocks. The CECECECEC samples having very small PE blocks are expected to have the disordered homogenous phase with very low % crystallinity. With little larger PE blocks, CECECECEC exhibited the ordered morphologies with mixed phase of outer CECE blocks, which are governed by the volume fraction of the center C block (f_5). Moreover, crystallization of PE chains in the mixed phase would cause crystal induced secondary structures. In $(CECE)_2$C-55-40-87k polymer containing the largest PE blocks, the layer-in-layer structure was anticipated with the primary (center C and outer CECE) and secondary (C and E of outer blocks) phase separation. In uniaxial tensile tests, the block copolymers with the mixed end blocks exhibited the brittle fracture because the domains are only connected by the rigid PCHE chains. However, one sample $(CECE)_2$C-55-40-87k, possibly having the layer-in-layer microstructure, showed ductile behavior with much higher toughness. This enhanced toughness could be attributed to the secondary phase separation of outer CECE blocks. CECECECEC nonablock copolymers have adjustable structural and mechanical properties by controlling the block composition, which provides an opportunity for developing new materials with the desirable properties.

3.5 References

[1] Holden, G.; Milkovich, R. Rubberlike block copolymers. 627652, 1963.

[2] Bates, F. S.; Fredrickson, G. H.; Hucul, D.; Stephen F. Hahn *AlChE J.* **2001,** *47*, 762-765.

[3] Hucul, D. A.; Hahn, S. F. *Adv. Mater.* **2000,** *12*, 1855-1858.

[4] Mahanthappa, M. K.; Hillmyer, M. A.; Bates, F. S. *Macromolecules* **2008,** *41*, 1341-1351.

[5] Vigild, M. E.; Chu, C.; Sugiyama, M.; Chaffin, K. A.; Bates, F. S. *Macromolecules* **2001,** *34*, 951-964.

[6] Hermel, T. J.; Wu, L.; Hahn, S. F.; Lodge, T. P.; Bates, F. S. *Macromolecules* **2002,** *35*, 4685-4689.

[7] Hermel, T. J.; Hahn, S. F.; Chaffin, K. A.; Gerberich, W. W.; Bates, F. S. *Macromolecules* **2003,** *36*, 2190-2193.

[8] Hermel, T. J. *Effects of Chain architecture on the Mechanical Response of Glassy/Semicrystalline Block Copolymers: CEC versus CECEC Lamellae*. Ph.D. Dissertation, University of Minnesota, 2003.

[9] Lim, L. S. *Effects fo Glassy, Rubbery, and Semicrystalline Blocks on the Mechanical Response of Polyolefin Block Copolymers*. Ph.D. Dissertation, University of Minnesota, 2005.

[10] Khanna, V.; Ruokolainen, J.; Kramer, E. J.; Hahn, S. F. *Macromolecules* **2006,** *39*, 4480-4492.

[11] Phatak, A.; Lim, L. S.; Reaves, C. K.; Bates, F. S. *Macromolecules* **2006,** *39*, 6221-6228.

[12] Ryu, C. Y.; Ruokolainen, J.; Fredrickson, G. H.; Kramer, E. J.; Hahn, S. F. *Macromolecules* **2002,** *35*, 2157-2166.

[13] Ruokolainen, J.; Fredrickson, G. H.; Kramer, E. J.; Ryu, C. Y.; Hahn, S. F.;

Magonov, S. N. *Macromolecules* **2002,** *35*, 9391-9402.

[14] Wu, L.; Cochran, E. W.; Lodge, T. P.; Bates, F. S. *Macromolecules* **2004,** *37*, 3360-3368.

[15] Drolet, F.; Fredrickson, G. H. *Macromolecules* **2001,** *34*, 5317-5324.

[16] Pangborn, A. B.; Giardello, M. A.; Grubbs, R. H.; Rosen, R. K.; Timmers, F. J. *Organometallics* **1996,** *15*, 1518-1520.

[17] Fetters, L. J.; Lohse, D. J.; Richter, D.; Witten, T. A.; Zirkel, A. *Macromolecules* **1994,** *27*, 4639-4647.

[18] Hosoda, S.; Nomura, H.; Gotoh, Y.; Kihara, H. *Polymer* **1990,** *31*, 1999-2005.

[19] Rangarajan, P.; Register, R. A.; Fetters, L. J. *Macromolecules* **1993,** *26*, 4640-4645.

[20] Brandrup, J.; Immergut, E. H. *Polymer Handbook*, 3rd ed.; John Wiley & Sons: New York, 1989.

[21] Mahanthappa, M. K.; Lim, L. S.; Hillmyer, M. A.; Bates, F. S. *Macromolecules* **2007,** *40*, 1585-1593.

[22] Gehlsen, M. D.; Bates, F. S. *Macromolecules* **1993,** *26*, 4122-4127.

[23] Gehlsen, M. D.; Weimann, P. A.; Bates, F. S.; Harville, S.; Mays, J. W.; Wignall, G. D. *J. Polym. Sci., Part B: Polym. Phys.* **1995,** *33*, 1527-1536.

[24] Weimann, P. A.; Hajduk, D. A.; Chu, C.; Chaffin, K. A.; Brodil, J. C.; F. S. Bates *J. Polym. Sci., Part B: Polym. Phys.* **1999,** *37*, 2053-2068.

[25] Krause, S.; Lu, Z.; Iskandar, M. *Macromolecules* **1982,** *15*, 1076-1082.

[26] Krause, S.; Iskandar, M.; Iqbal, M. *Macromolecules* **1982,** *15*, 105-111.

[27] Ferry, J. D. *Viscoelastic properties of polymers*, 3rd ed.; Wiley: New York, 1980.

[28] Matsuo, M.; Ueno, T.; Horino, H.; Chujyo, S.; Asai, H. *Polymer* **1968,** *9*, 425-436.

[29] Kawai, H.; Hashimoto, T.; Miyoshi, K.; Uno, H.; Fujimura, M. *Journal of Macromolecular Science* **1980,** *B17*, 427-472.

[30] Lim, L. S.; Harada, T.; Hillmyer, M. A.; Bates, F. S. *Macromolecules* **2004,** *37*, 5847-5850.

Chapter 4 Alternating and Random Poly(styrene-*b*-butadiene) Multiblock Copolymers*

4.1 Introduction

Block polymers have attracted much scientific interest for decades owing to many fascinating microphase-separated morphologies, the associated physical properties, and a growing list of realized and potential applications.[1-9] Yet most studies of block copolymers have focused on the simplest molecular architectures: linear AB diblocks and ABA triblocks.[10-14] Much less research has been directed at block polymers characterized by sequences of four or more blocks[15-24] and containing more than two types of block chemistry,[1,25-29] notwithstanding a rich literature dealing with several categories of commercially important multiblock materials such polyurethanes.[30-34] Increasing the number of blocks affects the chain configurations and overall thermodynamics of self-assembly along with the kinetically mediated paths to equilibrium and nonequilibrium

* Part of this work was published in 'Lee, I.; Bates, F. S. *Macromolecules* **2013,** *46*, 4529-4539'

morphology, hence the resulting mechanical properties. Multiblock copolymers containing 10 or more blocks are expected to have distinctive microstructures, and respond differently mechanically than conventional diblocks and triblocks.

Although the past two decades have witnessed an explosion in the number of controlled synthetic approaches to preparing block polymers, living anionic polymerization still represents a versatile, and commercially the most important, method for preparing well-defined block polymers. This technique offers precise control over block molecular weight and dispersity[35-37] and provides facile mechanisms for functionalizing one or both chain termini at various stages during the development of the molecular architecture. Polycondensation of end-functionalized polymers provides a powerful way to amplify the benefits associated with anionic polymerization through the use of established coupling chemistry, including the formation of urethane, ester, or amide bonds. Unlike most controlled polymerization mechanisms, polycondensation of telechelic polymers permits the combination of monomer sequences that are otherwise inaccessible using controlled chain addition polymerization methods. Additionally, coupling relatively monodisperse preformed polymers avoids complications resulting from spurious termination during sequential multiblock polymerization, including broad distributions in the block molecular weights and poor monomer conversion.

In this chapter, a combination of living anionic polymerization and polycondensation was used to synthesize long chain poly(styrene-*b*-butadiene) $(PS\text{-}PB)_n$ multiblock copolymers containing on average $\langle n \rangle$ = 7 to 25 blocks. Well-defined α,ω-dihydroxy polystyrene (HO-PS-OH) and α,ω-dihydroxy polybutadiene (HO-PB-OH)

were synthesized using a protected initiator (3-triisopropylsilyloxy-1-propyllithium referred to as TIPSOPrLi) followed by coupling with isophorone diisocyanate (IPDI). Both random (PS-ran-PB)$_n$ and alternating (PS-alt-PB)$_n$ block architectures have been produced by controlling the sequence of addition of IPDI during the coupling reactions. The resulting multiblock copolymers have been characterized by differential scanning calorimetry (DSC), small-angle X-ray scattering (SAXS), and transmission electron microscopy (TEM) demonstrating disordered but microphase separated bicontinuous-like morphologies for compositions $0.69 \leq f_{PS} \leq 0.85$, where f_{PS} is the volume fraction of polystyrene; lamellar order was obtained with $\langle n \rangle = 7$ and $f_{PS} = 0.60$. Tensile testing reveals dramatic improvements in the toughness of these materials, which contain a majority of PS, relative to the analogous PS-PB-PS (SBS) triblock compounds.

This work was supported by the Center for Sustainable Polymers at the University of Minnesota, a National Science Foundation supported Center for Chemical Innovation (CHE–1136607) SAXS was performed at the DuPont-Northwestern-Dow Collaborative Access Team (DND-CAT) located at Sector 5 of the Advanced Photon Source (APS). DND-CAT is supported by E. I. du Pont de Nemours & Co., The Dow Chemical Company, and Northwestern University. Use of the APS, an Office of Science User Facility operated for the U.S. Department of Energy (DOE) Office of Science by Argonne National Laboratory, was supported by the U.S. DOE under Contract DE–AC02–06CH11357. Parts of this work were carried out in the Characterization Facility, University of Minnesota, which receives partial support from NSF through the MRSEC program.

4.2 Experimental Section

4.2.1 Synthesis of *α,ω*-Dihydroxy Homopolymers

α,ω-Dihydroxy polystyrene (HO-PS-OH) and *α,ω*-dihydroxy polybutadiene (HO-PB-OH) blocks were prepared by living anionic polymerization using a protected initiator approach (Figure 4.1). Styrene and butadiene were independently initiated in cyclohexane (under an argon atmosphere) with 3-triisopropylsilyloxy-1-propyllithium (TIPSOPrLi) and allowed to polymerize to near complete conversion at 40 °C, then terminated by addition of excess ethylene oxide followed by addition of degassed methanol, resulting in a single terminal alcohol group.[38-40] After drying under vacuum, the polymer was dissolved in a solution of tetrahydrofuran (THF) and excess tetra-*n*-butylammonium fluoride (TBAF) and stirred for 48 h at room temperature. The resultant HO-PS-OH and HO-PB-OH compounds were recovered by evaporation of the THF followed by dissolution in CH_2Cl_2 and extraction with water to remove residual salts.[41]

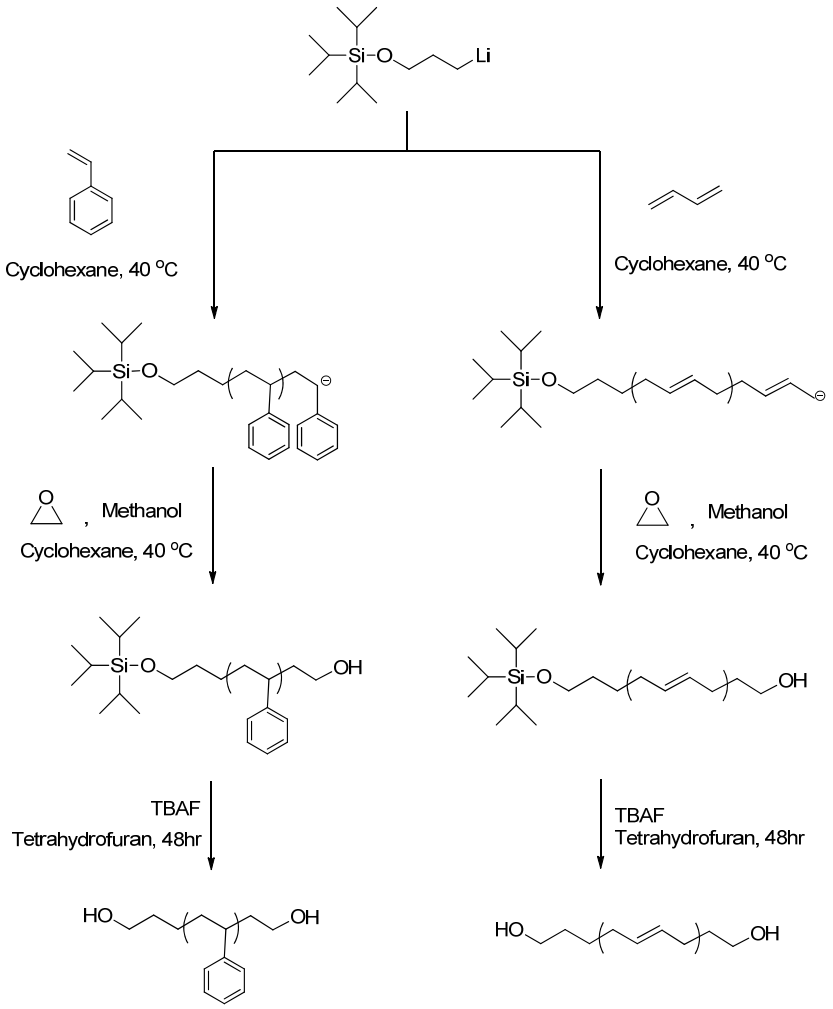

Figure 4.1 Synthetic scheme for preparing α,ω-dihydroxy homopolymers.

4.2.2 Synthesis of Random (PS-ran-PB)$_n$ Multiblock Copolymers

Random (PS-ran-PB)$_n$ multiblock copolymers were prepared by reacting isophorone diisocyanate (IPDI, Aldrich) with HO-PS-OH and HO-PB-OH in the presence of the catalyst dibutyltin dilaurate (DBTDL, Aldrich) as sketched in Figure 4.2(a). HO-PS-OH and HO-PB-OH homopolymers were added to the reactor under argon

atmosphere. The proper amount of IPDI (1 equiv of NCO to 1 equiv of OH), DBTDL (1 wt % relative to polymer), and THF as a solvent were injected into the reactor, and the solution was stirred for 150 h at 40 °C. The resulting block copolymers were recovered by precipitation into methanol followed by freeze-drying with benzene under vacuum until a constant pressure was achieved.

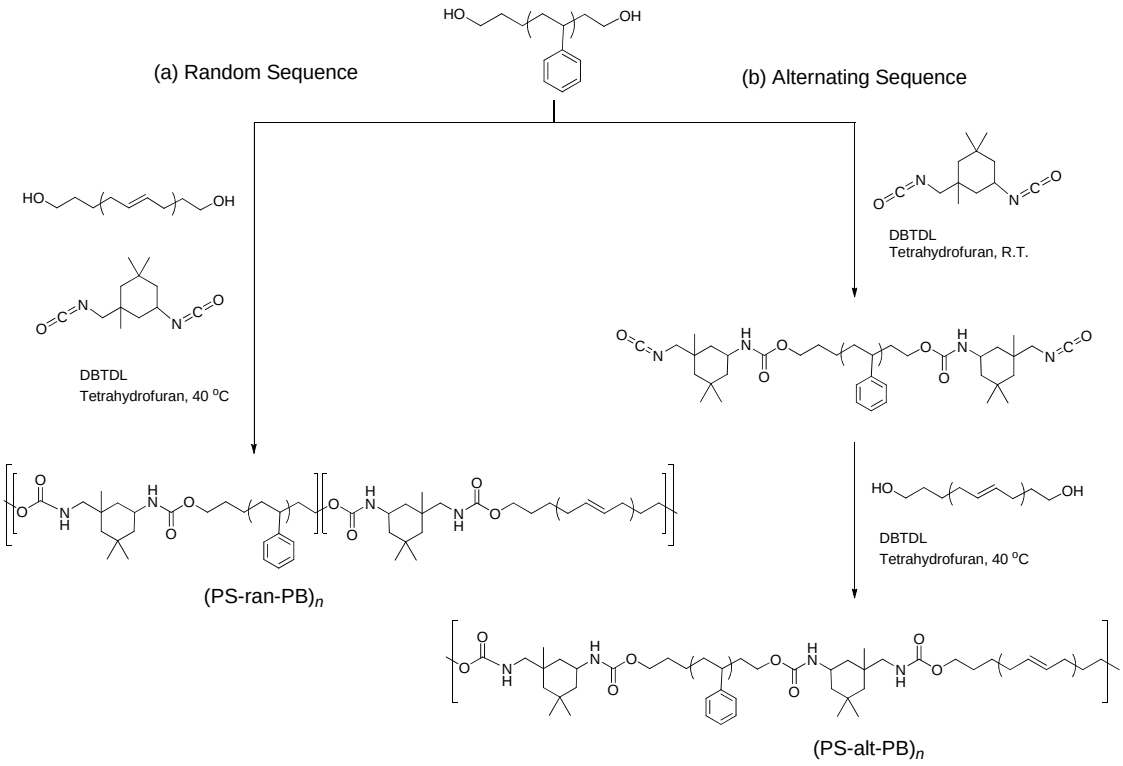

Figure 4.2 Schematic representation of the synthesis of (a) $(PS\text{-}ran\text{-}PB)_n$ and (b) $(PS\text{-}alt\text{-}PB)_n$ multiblock copolymers.

4.2.3 Synthesis of Alternating (PS-alt-PB)$_n$ Multiblock Copolymers

Alternating (PS-alt-PB)$_n$ multiblock copolymers were prepared in two steps as illustrated in Figure 4.2(b).

Synthesis of α,ω-Diisocyanato Polystyrene (OCN-PS-NCO)

α,ω-Diisocyanato polystyrene homopolymers (OCN-PS-NCO) were prepared by end-capping HO-PS-OH with diisocyanate. IPDI, DBTDL (1 wt % relative to polymer), and THF were added to the reactor under an argon atmosphere. HO-PS-OH homopolymer was dissolved in THF and added dropwise to the stirred solution followed by stirred for an additional 30 h. Three different procedures were examined in order to optimize the yield of *α,ω*-end-capped polymer while avoiding step-growth polymerization: addition of a stoichiometric amount of IPDI (2 equiv of NCO to 1 equiv of OH) at 40 °C, a stoichiometric amount of IPDI at 5 °C, and a large excess of IPDI (100 equiv of NCO to 1 equiv of OH) at room temperature. After reaction the end-capped product was isolated by precipitation with hexane (instead of methanol in order to minimize reaction of the isocyanate groups) and then and freeze-dried from benzene.

Coupling to Form Multiblock Copolymers

Alternating multiblock copolymers were formed by mixing stoichiometric amounts of OCN-PS-NCO and HO-PB-OH followed by injection of DBTDL (1 wt % relative to polymer) and THF. The solution was stirred for 120 h at 40 °C and then precipitated in methanol. The recovered polymers were freeze-dried under vacuum from benzene until

the pressure reached a baseline level.

4.2.4 Molecular Characterization

Multiblock compositions were determined by ^{1}H nuclear magnetic resonance (NMR) spectroscopy using a Varian Inova 500 spectrometer with deuterated chloroform ($CDCl_3$, Cambridge Isotope Laboratories, Inc.) as the solvent at room temperature. Block mole fractions were calculated by integration of resonance peaks associated with the protons of the PS and PB repeat units. These mole fractions were converted to volume fractions using published homopolymer densities at 140 °C (ρ_{PS} = 0.969, $\rho_{1,4\text{-PB}}$ = 0.826, $\rho_{1,2\text{-PB}}$ = 0.889 g/cm^3).[42] The number average molecular weight (M_n), weight-average molecular weight (M_w), and molecular weight distribution (M_w/M_n) of the block copolymers were analyzed by size exclusion chromatography (SEC) performed on a Thermo Separation Products (TSP) Spectra Systems AS1000 autosampler equipped with three 5 mm Phenomenex Phenogel columns, a Waters 515 pump, and a Waters 2410 differential refractive index detector. The polymer samples were run at room temperature in THF (Sigma-Aldrich) at a flow rate of 1.0 mL/min, and the instrument was calibrated using 10 polystyrene standards (M_n = 580 to 377,400 g/mol, Polymer Laboratories). Background corrected Fourier transform infrared (FTIR) spectra were obtained using a Nicolet Magna-IR 550 spectrometer with 4 cm^{-1} resolution.

4.2.5 Differential Scanning Calorimetry (DSC)

Thermal transitions were determined using a Thermal Analysis Q1000 DSC. Samples were loaded into aluminum DSC pans, heated to 125 °C, cooled to −150 °C, and reheated to 125 °C at a rate of 10 °C/min. The glass transition temperature was determined during the second heating step.

4.2.6 Small-Angle X-ray Scattering (SAXS)

Synchrotron SAXS measurements were recorded at Argonne National Laboratory (Argonne, IL) with a beam wave length of λ = 0.729 Å and a sample-to-detector distance of 4.08 m. Thin films were cast from 5 wt % solution of the multiblock copolymer in toluene. The solvent was slowly evaporated at room temperature for about 2 weeks followed by drying under vacuum for 24 h. Samples were measured at room temperature, and the two-dimensional scattering data were reduced to the one-dimensional form of relative intensity (I in arbitrary units) versus scattering wave vector magnitude, $q = (4\pi/\lambda) \sin(\theta/2)$, where θ is the scattering angle.

4.2.7 Transmission Electron Microscopy (TEM)

TEM was carried out at the College of Science and Engineering Characterization Facility at the University of Minnesota with a Tecnai T12 electron microscope. Thin (80–100 nm thickness) sections were cut at −80 °C using a Leica UC6 microtome with cryotrim 20 and cryo 45° diamond knives (Diatome US). Cryo-microtomed sections were

stained with the vapor from a 4% aqueous solution of OsO_4 for about 20 min. This metal oxide selectively reacts with the olefinic groups of the polybutadiene and enhances contrast in the microscopic image.

4.2.8 Tensile Testing

Mechanical tests were performed using a Rheometrics Scientific MINIMAT equipped with a 200 N load cell. Specimens were molded and cut into rectangular tensile bars (9 mm long by 2 mm wide and 0.7 mm thick) and loaded with an initial gauge length of 2.5 mm and drawn until failure at a constant rate of 5 mm/min at room temperature. (Some samples were tested at 2.5 mm/min for comparison with SBS triblock data from the literature; see below.) Tensile data are presented as engineering stress ($\sigma = F/A_0$) versus nominal strain ($\varepsilon = (l - l_0)/l_0$), where F is the force, l is the gauge length of the sample, and A_0 and l_0 are the initial cross-sectional area and length of the sample. The Young's modulus (E) is determined from the slope of the linear portion of the stress–strain curve. Results reported here represent averages taken from at least five specimens for each sample.

4.3 Results and Discussion

4.3.1 Synthesis

Four α,ω-dihydroxy HO-PS-OH polymers and four α,ω-dihydroxy HO-PB-OH

polymers with different molecular weights were prepared (see Table 4.1) in order to control the volume fraction of PS and PB in the final multiblock copolymers. The SEC results showed that all eight homopolymers have a relatively narrow molecular weight distribution. The quantitative presence of two OH end groups per molecule was confirmed following reaction with trifluoroacetic anhydride (TFAA), which facilitates analysis by ^{1}H NMR. The chemical shift of the neighboring CH_2 proton is shifted up field; the α-hydroxy methylene and ω-hydroxy methylene group of HO-PS-OH are shifted from about 3.3 and 3.5 ppm to about 4.0 and 4.2 ppm while the resonance associated with the hydroxy methylene group of HO-PB-OH is shifted from about 3.6 ppm to about 4.3 ppm. Initiation of the homopolymerizations with TIPSOPrLi followed by deprotection leads to the α-functionality. The degree of functionality (F_n) can be calculated by comparing the molecular weight measured by SEC and that determined by ^{1}H NMR end-group analysis.[41] The F_n values for HO-PS-OH and HO-PB-OH are shown in Table 4.1. All of the calculated values are close to $F_n = 1$, confirming one TIPSO group at the end of the polymer chain.

Table 4.1 Molecular characterization data for HO-PS-OH and HO-PB-OH homopolymers.

Sample	M_n (g/mol)[a]	M_w/M_n[b]	F_n[c]	T_g (°C)[d]
HO-PS-OH-1	9000	1.11	1.01	70.7
HO-PS-OH-2	11700	1.08	1.10	85.0
HO-PS-OH-3	17400	1.05	1.07	101.1
HO-PS-OH-4	21400	1.06	1.04	101.2
HO-PB-OH-1	3400	1.05	0.98	−95.4
HO-PB-OH-2	4900	1.05	0.93	−95.4
HO-PB-OH-3	5600	1.06	0.94	−95.8
HO-PB-OH-4	11400	1.04	0.95	−96.5

[a] Determined by SEC calibrated with polystyrene standards. [b] Polydispersity index measured by SEC calibrated with polystyrene standards. [c] Calculated by comparing M_n values measured using SEC with polystyrene standards and ^{1}H NMR end-group analysis. [d] Obtained from DSC during the second heating step.

The α,ω-diisocyanato polystyrene (OCN-PS-NCO) compounds were synthesized by end-capping of HO-PS-OH with diisocyanate. Isophorone diisocyanate (IPDI), an asymmetric cycloaliphatic diisocyanate, contains two chemically different isocyanate groups: a primary NCO, which is bonded to a methylene group (CH_2-NCO), and a secondary NCO, which is bonded to the cyloaliphatic ring (CH-NCO). These two isocyanate group have different reactivity's toward hydroxyl groups, also dependent on the catalyst. Prior studies have shown that the primary NCO group is more reactive when

a ternary amine catalyst is employed, while the secondary NCO group outcompetes this moiety when a tin catalyst is used or in the absence of a catalyst.[33,43-45] We exploited this difference in order to enhance the end-capping reaction while suppressing step-growth polymerization.

Three different procedures were evaluated in order to maximize the end-capping efficiency and the results are shown in Figure 4.3. Initially, we used stoichiometric amounts of IPDI (2 equivalents of NCO to 1 equivalent of OH) hoping to avoid the need for an additional precipitation step to remove excess IPDI, which has the potential to destroy some portion of the reactive isocyanate end groups. The first such tests were run with HO-PS-OH-2 at 40 °C. After reacting for 30 h, the product was analyzed by SEC, revealing a yield of just 27% end-capped product; most of the polymer appears at shorter retention times in the SEC trace, i.e., higher molecular weight chain-extended polymer was formed due to polycondensation. In a second attempt, a stoichiometric amount of IPDI was reacted with HO-PS-OH-4 for 30 h at 5 °C, resulting in a much higher yield; a small shoulder in the SEC trace (OCN-PS-NCO-4a in Figure 4.3) and we estimate conversion of the diol to about 87% of the desired product. The end-capping efficiency was further improved by using a large excess amount of IPDI (100 equiv of NCO to 1 equiv of OH) and conducting the reaction at room temperature, which completely suppressed polycondensation, leading to the desired product OCN-PS-NCO-4b (see Figure 4.3). This α,ω-diisocyante end-capped polystyrene was isolated by precipitation with hexane and used to synthesize alternating multiblock copolymers (see below).

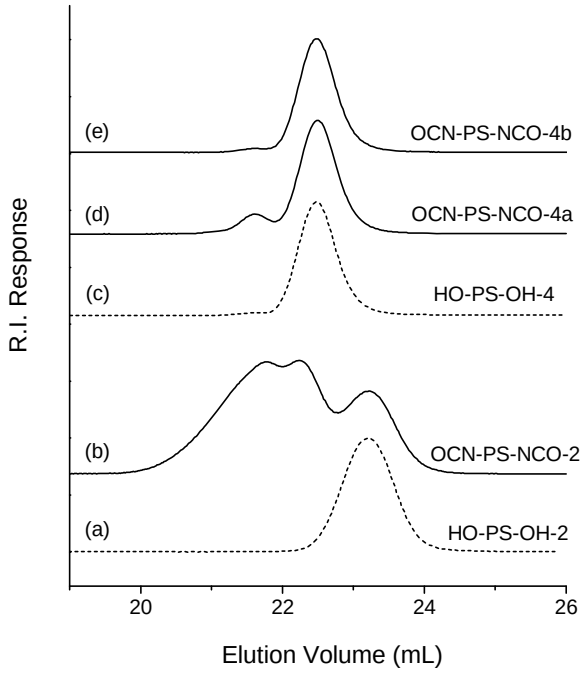

Figure 4.3 SEC traces of HO-PS-OH polymers (a and c) and following reaction with IPDI (b, d, and e). Addition of a stoichiometric amount of IPDI at 40 °C (b) and 5 °C (d) results in large and small amounts of coupled polymer, respectively. Addition of excess IPDI at room temperature (e) suppresses polycondensation leading to the desired product, OCN-PS-NCO-4b.

^{1}H NMR spectra were obtained before (HO-PS-OH-4) and after end-capping (OCN-PS-NCO-4b), and the results are shown in Figure 4.4. The NMR spectrum of HO-PS-OH-4 (Figure 4.4(a)) contains peaks assigned to the protons of the phenyl rings (6.3–7.2 ppm, δH_a and δH_b) and the α-hydroxy methylene and ω-hydroxy methylene groups (3.3 (δH_d) and 3.5 ppm (δH_c)). After end-capping, a new singlet appears at 3.0 ppm ($\delta H_{e'}$)

corresponding to the methylene protons adjacent to the primary NCO group, formed from the reaction of the secondary NCO group of IPDI with the OH group of HO-PS-OH. Absence of a peak at 2.7–2.9 ppm in Figure 4.4(b) also confirms that all the OH groups in the dihydroxy polystyrene reacted with the secondary NCO rather than the primary NCO group.[43-44] In addition, the peaks associated with the two hydroxy methylene groups (δH_c and δH_d) have disappeared, and new peaks at 3.5–4.4 ppm ($\delta H_{c'}$ and $\delta H_{d'}$) corresponding to methylene protons adjacent to the urethane (-NHCOO-) group are evident. The two different NMR chemical shifts for $H_{c'}$ and $H_{d'}$ are attributed to *cis* (Z) and *trans* (E) isomers of NCO and CH_2NCO on the cyclohexane ring of IPDI, in a 3:1 ratio, respectively.[33,44,46] As a result of these two different isomers, the $H_{c'}$ and $H_{d'}$ peaks occur over the rather broad range of 3.5–4.4 ppm.

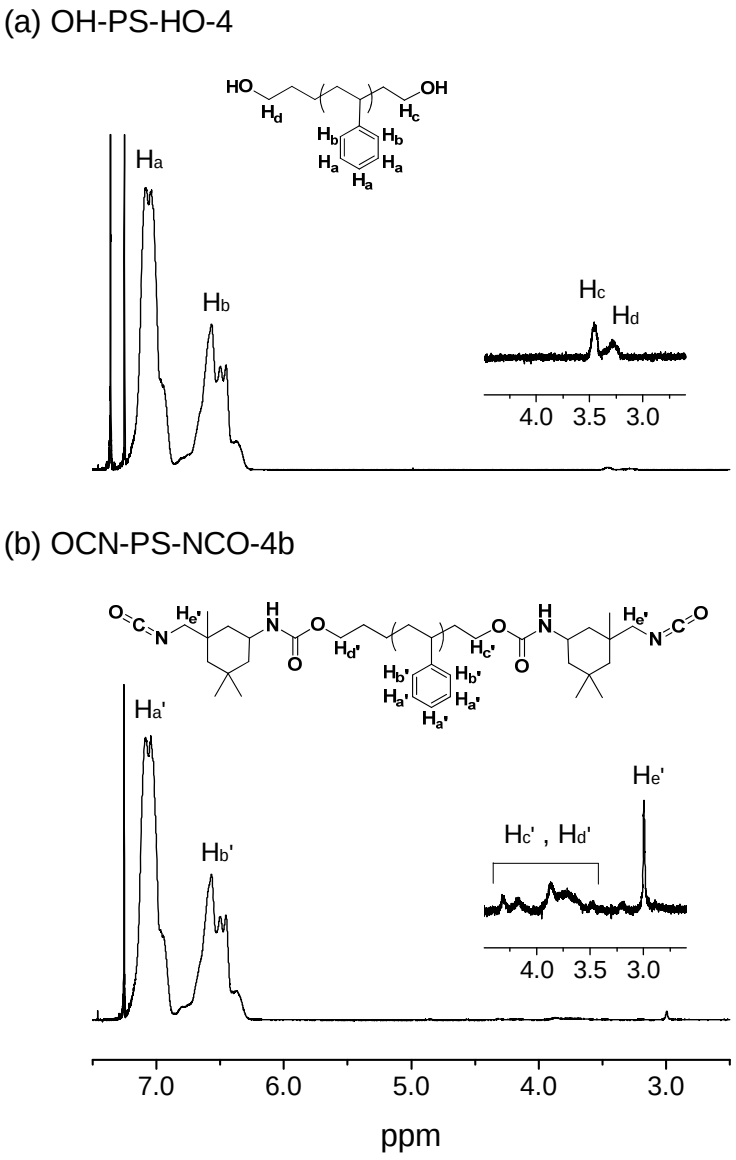

Figure 4.4 ^{1}H NMR spectra of (a) HO-PS-OH-4 and (b) OCN-PS-NCO-4b in $CDCl_3$. The insets show the 2.6–4.5 ppm region of the spectra.

FTIR spectra, shown in Figure 4.5, further support our conclusion that the end-capping procedure was performed effectively. Spectra were normalized using the C−H

stretching band at 3020 cm^{-1}, which is not influenced by the end-capping chemistry. After end-capping, OCN-PS-NCO-4b displays new (vibrational) bands at 2270 cm^{-1} (N=C=O), 1720 cm^{-1} (C=O) and 3430 cm^{-1} (N−H) relative to HO-PS-OH-4, which exhibits a spectra typical for polystyrene.[47]

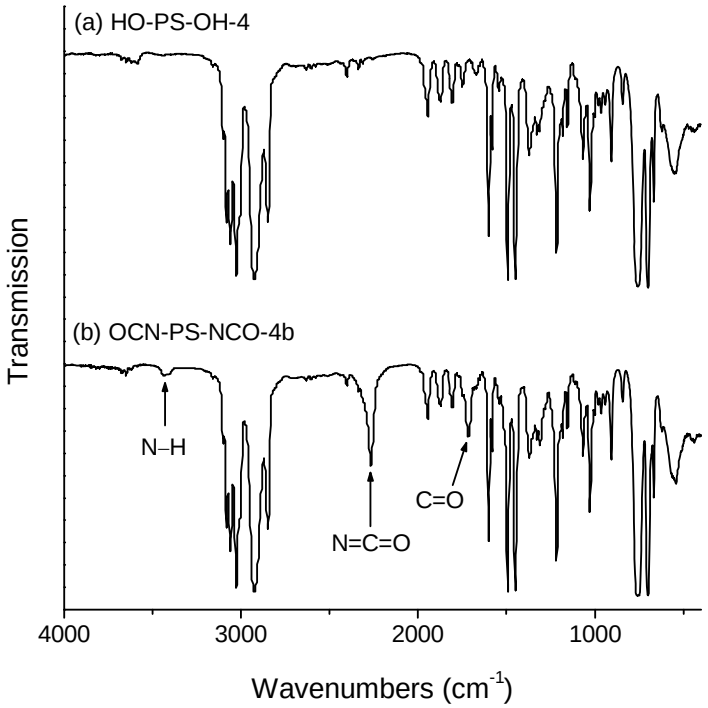

Figure 4.5 FTIR spectra of (a) HO-PS-OH-4 and (b) OCN-PS-NCO-4b.

The alternating $(PS\text{-}alt\text{-}PB)_n$ and random $(PS\text{-}ran\text{-}PB)_n$ multiblock copolymers were prepared by condensation of the terminal NCO groups and OH groups that link together PS and PB blocks through urethane (-NHCOO-) links thereby producing long multiblock polymer chains. Four $(PS\text{-}alt\text{-}PB)_n$ and five $(PS\text{-}ran\text{-}PB)_n$ multiblock materials were

produced as summarized in Table 4.2. Figure 4.6 shows representative SEC traces for PS-alt-PB-4 and PS-ran-PB-4, produced by combining HO-PS-OH-4 and HO-PB-OH-2. The chromatographic traces obtained from this homologous set of alternating and random multiblock copolymers indicate much higher molecular weights than the starting materials, approximately most probable molecular weight distributions ($M_w/M_n \cong 2$), and relatively small amounts of unreacted prepolymers (evidenced by small shoulders in the low molecular weight region of the SEC traces), consistent with the conversion of the telechelic hompolymers to multiblock copolymers.

Table 4.2 Molecular characteristics of the $(PS\text{-}PB)_n$ multiblock copolymers.

Sample	Block Sequence	Prepolymer (M_n, kg/mol)[a]		M_n (kg/mol)[a]	M_w/M_n[b]	f_{PS}[c]	$\langle n \rangle$[d]
PS-alt-PB-1	alternating	HO-PS-OH-1 (9.0)	HO-PB-OH-1 (3.4)	90	3.15	0.71	15
PS-alt-PB-2	alternating	HO-PS-OH-4 (21.4)	HO-PB-OH-4 (11.4)	110	1.94	0.60	7
PS-alt-PB-3	alternating	HO-PS-OH-4 (21.4)	HO-PB-OH-3 (5.6)	113	1.93	0.76	8
PS-alt-PB-4	alternating	HO-PS-OH-4 (21.4)	HO-PB-OH-2 (4.9)	148	1.92	0.79	11
PS-ran-PB-1	random	HO-PS-OH-1 (9.0)	HO-PB-OH-1 (3.4)	101	6.56	0.69	16
PS-ran-PB-2	random	HO-PS-OH-3 (17.4)	HO-PB-OH-3 (5.6)	285	2.00	0.73	25
PS-ran-PB-3	random	HO-PS-OH-4 (21.4)	HO-PB-OH-3 (5.6)	285	1.92	0.76	21
PS-ran-PB-4	random	HO-PS-OH-4 (21.4)	HO-PB-OH-2 (4.9)	321	1.81	0.79	24
PS-ran-PB-5	random	HO-PS-OH-4 (21.4)	HO-PB-OH-1 (3.4)	201	3.23	0.85	16

[a] Molecular weight determined by SEC calibrated with polystyrene standards. [b] Polydispersity index measured by SEC calibrated with polystyrene standards. [c] Volume fraction of PS measured by ^{1}H NMR and calculated using published bulk homopolymer densities.[42] [d] Average number of prepolymer blocks in multiblock copolymer calculated from their molecular weights.

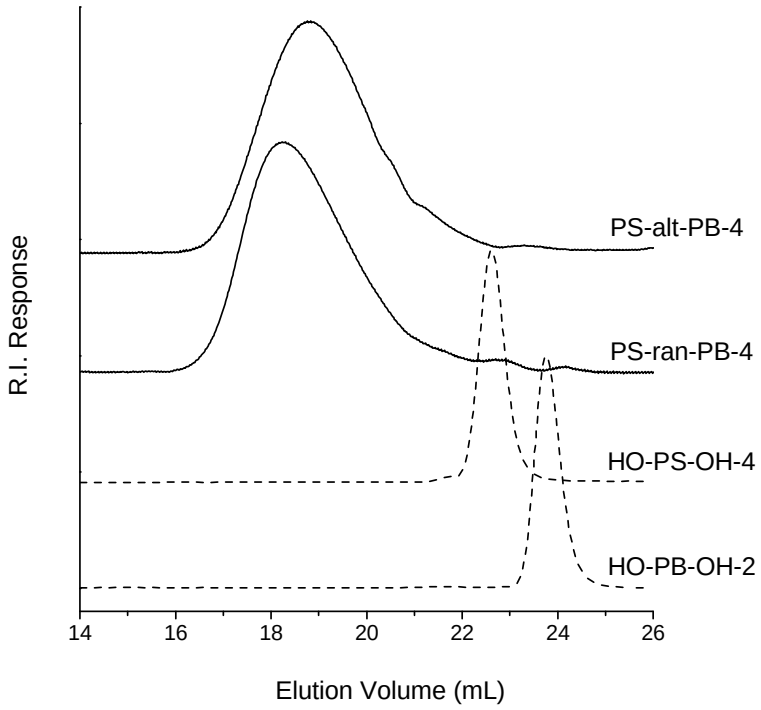

Figure 4.6 SEC traces obtained from multiblock copolymers (solid line) PS-alt-PB-4 and PS-ran-PB-4 as well as prepolymers (dashed line) HO-PS-OH-4 and HO-PB-OH-2.

Three sets of alternating and random multiblock copolymers were prepared from common sets of telechelic homopolymers having different molecular weights: PS-alt-PB-1, -3, -4 and PS-ran-PB-1, -3, -4, respectively. Even though these alternating and random block copolymers were prepared from the same PS and PB prepolymers, they produced different overall molecular weights. In all cases, the alternating sequence is lower in molecular weight than the random version, i.e., the average number of coupled

prepolymer blocks $\langle n \rangle$ is smaller. We attribute this lower coupling efficiency for the alternating compounds to spurious side reactions that may occur during the additional precipitation step (in hexane) during the preparation of the OCN-PS-NCO precursor; the isocyanate group (NCO) is very reactive.

^{1}H NMR spectra were also used to establish the composition of the multiblock copolymers. Figure 4.7 shows ^{1}H NMR spectrum of PS-alt-PB-4 multiblock copolymer. The proton peaks of phenyl rings in PS at 6.3–7.2 ppm, the proton peaks of $=CH_2$ groups in poly(1,2-butadiene) at 4.8–5.0 ppm, the proton peaks of –CH=CH– groups in poly(1,4-butadiene) and –CH= groups in poly(1,2-butadiene) at 5.3–5.5 ppm were observed. Volume fraction of PS was calculated using ^{1}H NMR spectrum and bulk homopolymer densities. NMR spectra also revealed that 1,3-butadiene was polymerized with predominantly 1,4-addition (92 mol%).

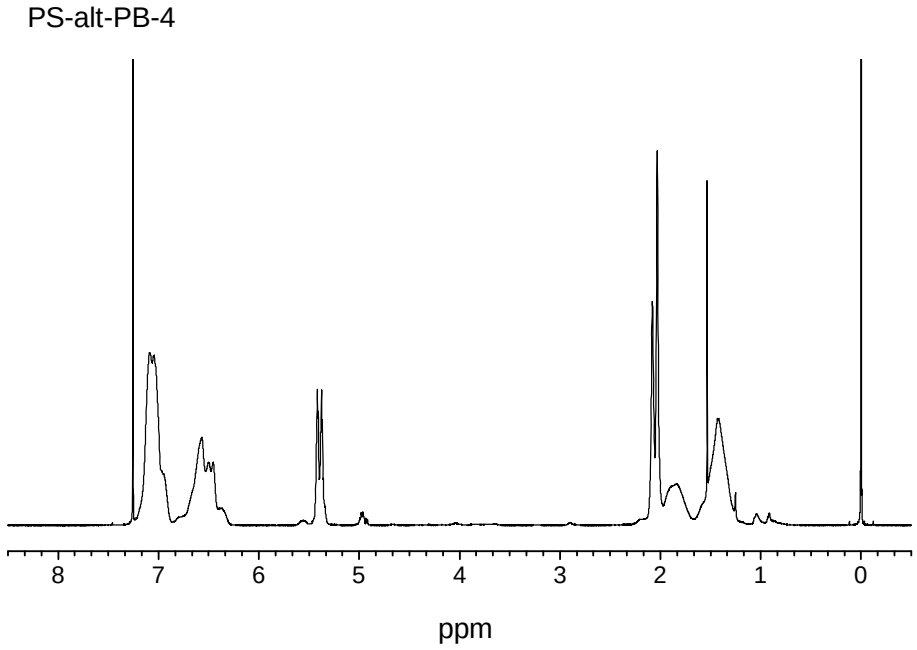

Figure 4.7 ^{1}H NMR spectrum of PS-alt-PB-4 multiblock copolymer.

4.3.2 Thermal Properties

Glass transition temperatures (T_g) were determined using DSC measurements, defined here as the mean of the onset and end-point temperatures (intersections of the tangent through the inflection of the transition with the extrapolated baselines) associated with the rise in heat capacity on heating. Representative multiblock copolymer DSC traces are shown in Figure 4.8 and the glass transition temperatures are summarized in Table 4.3; T_g values for the PS and PB prepolymers are given in Table 4.1. The PS homopolymers exhibit T_gs between 71 and 101 °C in rough agreement with the variation in molecular weight.[48-52] On the other hand, all the PB hompolymers are characterized by

T_gs ≅ −96 °C independent of molecular weight. All the multiblock copolymers samples display two T_gs, at temperatures slightly below or above T_gs for the respective homopolymer building blocks, indicative of microphase separation.[53-54] These minor shifts in T_g are attributed to some microphase mixing of the PS and PB blocks.[55-57] We have estimated the extent of such mixing using the Fox equation[58]

$$\frac{1}{T_g^{\text{PS-rich}}} = \frac{w_{PS}^{\text{PS-rich}}}{T_g^{PS}} + \frac{1 - w_{PS}^{\text{PS-rich}}}{T_g^{PB}} \tag{4.1}$$

$$\frac{1}{T_g^{\text{PB-rich}}} = \frac{1 - w_{PB}^{\text{PB-rich}}}{T_g^{PS}} + \frac{w_{PB}^{\text{PB-rich}}}{T_g^{PB}} \tag{4.2}$$

using the measured glass transition values for the block copolymers ($T_g^{\text{PS-rich}}$ and $T_g^{\text{PB-rich}}$) and prepolymers (T_g^{PS} and T_g^{PB}). Table 4.3 shows the calculated weight fractions (w) for each domain, indicating that the soft domains are ≥95 wt % rich in the PB and the hard domains ≥77 wt % rich in the PS; this asymmetry may be caused by additional segregation while cooling the specimens below T_g^{PB}. As anticipated, the greatest extent of microdomain mixing occurs with the lowest molecular weight blocks. The DSC results also reveal that the random multiblocks appear to be characterized by less microdomain mixing than the alternating multiblocks, consistent with on average larger overall block lengths due to the statistical coupling of like homopolymers.

Based on the multiblock random phase approximation theory presented by Wu et al.[15] we estimate that the ODT for PS-alt-PB-1 and PS-ran-PB-1, which contain the shortest blocks, should be close to T_g^{PS} consistent with the DSC analysis. However, dynamic mechanical spectroscopy results obtained at 110 °C evidence microphase

separated states for both materials, based on the scaling of the elastic (G') and loss (G'') moduli with frequency, $G' \sim \omega^n$ and $G'' \sim \omega^m$ with n < 1 and m < 1 in the low frequency regime. Thermal degradation of the urethane linkages prohibits determination of T_{ODT} at higher temperatures.

Table 4.3 Glass transition temperatures and calculated weight fractions of PS-rich and PB-rich microdomains.

Sample	T_g (°C)[a]		Prepolymer (T_g ,°C)[a]		$w_{PS}^{PS\text{-rich}}$ [b]	$w_{PB}^{PB\text{-rich}}$ [b]
	$T_g^{PS\text{-rich}}$	$T_g^{PB\text{-rich}}$				
PS-alt-PB-1	56.3	−73.1	HO-PS-OH-1 (70.7)	HO-PB-OH-1 (−95.4)	0.95	0.77
PS-alt-PB-2	82.9	−92.8	HO-PS-OH-4 (101.2)	HO-PB-OH-4 (−96.5)	0.95	0.96
PS-alt-PB-3	80.5	−89.1	HO-PS-OH-4 (101.2)	HO-PB-OH-3 (−95.8)	0.95	0.93
PS-alt-PB-4	81.1	−90.1	HO-PS-OH-4 (101.2)	HO-PB-OH-2 (−95.4)	0.95	0.94
PS-ran-PB-1	67.9	−80.5	HO-PS-OH-1 (70.7)	HO-PB-OH-1 (−95.4)	0.99	0.84
PS-ran-PB-2	96.0	−95.1	HO-PS-OH-3 (101.1)	HO-PB-OH-3 (−95.8)	0.99	0.99
PS-ran-PB-3	90.7	−92.7	HO-PS-OH-4 (101.2)	HO-PB-OH-3 (−95.8)	0.97	0.97
PS-ran-PB-4	89.6	−92.2	HO-PS-OH-4 (101.2)	HO-PB-OH-2 (−95.4)	0.97	0.97
PS-ran-PB-5	87.6	−83.9	HO-PS-OH-4 (101.2)	HO-PB-OH-1 (−95.4)	0.97	0.89

[a] Glass transition temperatures were obtained by DSC during the second heating step. [b] Weight fractions calculated with the Fox equation.[58]

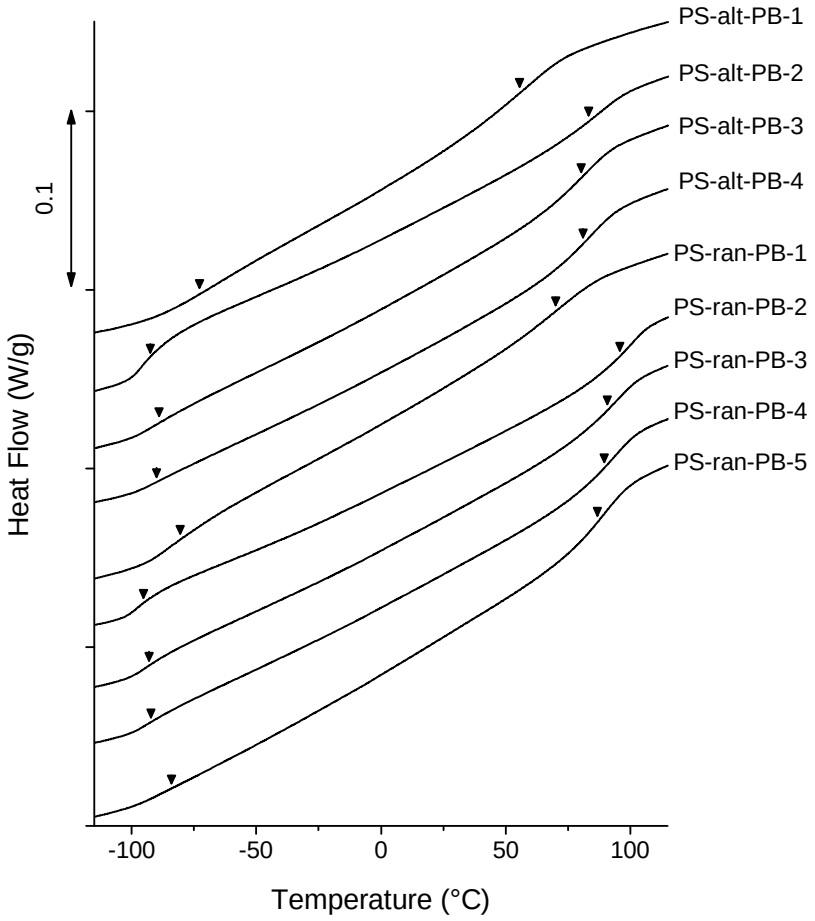

Figure 4.8 DSC traces of $(PS\text{-}PB)_n$ multiblock copolymers obtained while heating. Arrows indicate glass transition temperatures for the PS-rich and PB-rich microdomains.

4.3.3 Structural Analysis

The morphologies of the $(PS\text{-}PB)_n$ multiblock copolymers were characterized by

small-angle X-ray scattering (SAXS) and transmission electron microscopy (TEM). Thermal degradation at high temperatures (beginning in the range 80–150 °C) is an inherent characteristic of the urethane linkage: the chain cleavage process begins with disruption of the hydrogen bonds.[30,32] Due to the low thermal stability of the urethane linkage, we could not access order–disorder transition temperatures (T_{ODT}). For this reason solvent casting from toluene, a nonselective solvent, was used to produce uniform polymer specimens.

Figure 4.9 shows representative 1-dimensional synchrotron SAXS patterns obtained from the multiblock polymers at room temperature. All the multiblocks display a single broad diffraction peak, except PS-alt-PB-2, which produced a second reflection at $2q^*$, where q^* locates the position of the principal peak. The characteristic microdomain spacings, $d^* = 2\pi/q^*$, are listed in Table 4.4. These results indicate that the alternating block sequences lead to smaller d^* values (14–20 nm) than the random arrangements (22–30 nm), consistent with our previous comments regarding the average total block lengths that result from each synthetic strategy. While d^* systematically increases with the prepolymer molecular weight, this structural feature is essentially independent of the total number of prepolymer blocks in the multiblock copolymer chains, in agreement with a previous study.[15]

Table 4.4 Domain spacings of $(PS\text{-}PB)_n$ multiblock copolymers.

Sample	q^* ($Å^{-1}$)	d^* (nm)
PS-alt-PB-1	0.0442	14.2
PS-alt-PB-2	0.0309	20.3
PS-alt-PB-3	0.0360	17.5
PS-alt-PB-4	0.0382	16.4
PS-ran-PB-1	0.0281	22.4
PS-ran-PB-2	0.0209	30.1
PS-ran-PB-3	0.0212	29.6
PS-ran-PB-4	0.0225	27.9
PS-ran-PB-5	0.0234	26.9

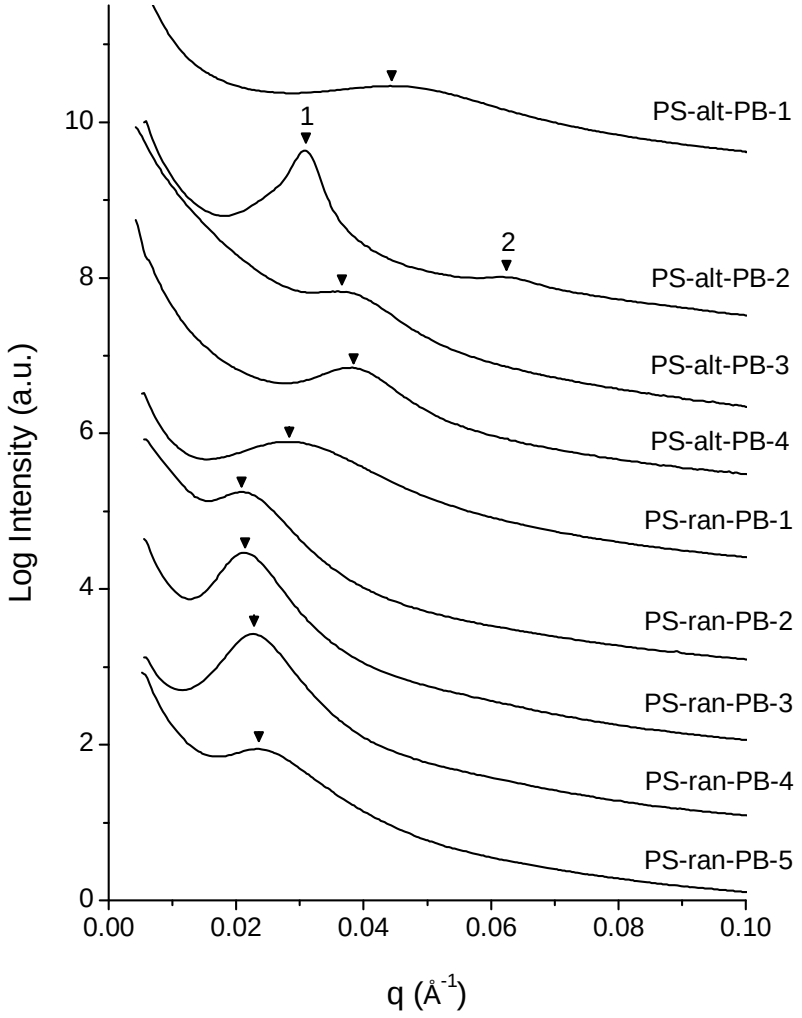

Figure 4.9 SAXS patterns obtained at room temperature for $(PS\text{-}PB)_n$ mutltiblock copolymers.

A comparison of the principal peak intensities, $I(q^*)$, for PS-alt-PB-1, -3, -4 and PS-ran-PB-1, -3, -4, respectively, reveals that the random sequences scatter more strongly than the analogous alternating sequences. PS-alt-PB-2 is an exception due to some degree

of lamellar ordering as shown below. This difference of scattering power can be accounted for based on differing degrees of microphase mixing. The overall scattering intensity depends on the variation in mean-squared electron-density, $\langle \eta^2 \rangle$, which decreases with block mixing. For any two-phase system $\langle \eta^2 \rangle$ is given by,

$$\langle \eta^2 \rangle = (\rho_1 - \rho_2)^2 \varphi_1 (1 - \varphi_1) \tag{4.3}$$

where ρ_j and φ_j are the average electron density and volume fraction of j phase (j = 1 or 2), and

$$(\rho_1 - \rho_2)^2 = (\varphi_{PS1} - \varphi_{PS2})^2 (\rho_{PS}° - \rho_{PB}°)^2 \tag{4.4}$$

in which $\rho_i°$ is the electron density of pure i polymer (i = PS or PB), and φ_{ij} is the volume fraction of i polymer in j phase.[59] Complete mixing leads to $\langle \eta^2 \rangle = 0$ while complete segregation, $(\varphi_{PS1} - \varphi_{PS2})^2 = 1$, maximizes the scattering power. Hence, the lower scattering intensity of the alternating multiblock copolymers can be attributed to a higher degree of phase mixing in each domain, in agreement with the DSC analysis (see Table 4.3).

Transmission electron microscopy (TEM) experiments further clarify the morphologies created by the multiblock molecular architectures. Representative TEM images are presented in Figure 4.10, in which the light and dark microdomains are associated with PS and PB, respectively. All but one of the materials display an irregular, disordered bicontinuous-like morphology, consistent with the single broad SAXS peaks found in Figure 4.9. Sample PS-alt-PB-2 contains an ordered lamellar morphology with d^* = 18 nm, which explains the higher-order SAXS reflection found in Figure 4.9. We

believe this result can be traced to the effects of the smallest number of regularly sequenced blocks ($\langle n \rangle = 7$, Table 4.2) amplified by the most symmetric composition (f_{PS} = 0.60 versus $0.69 \leq f_{PS} \leq 0.85$ for the other samples, Table 4.2).

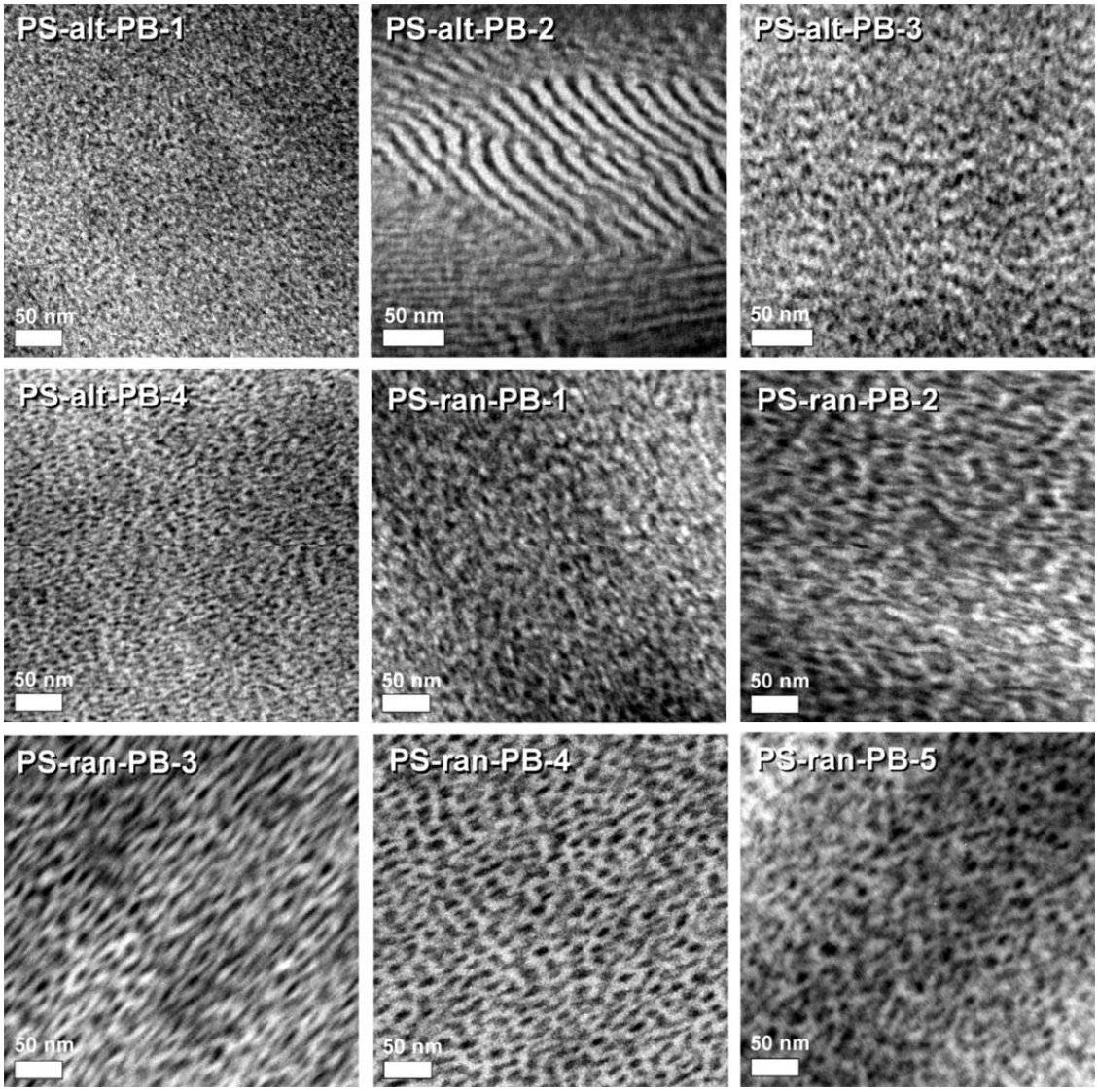

Figure 4.10 TEM images from $(PS\text{-}PB)_n$ multiblock copolymers. Each sample was stained with OsO_4. PS and PB domains appear as light and dark region, respectively. Scale bars correspond to 50 nm.

The complete absence of long-range order, which produces isotropic properties on all length scales above d^*, can be attributed to several factors. Any multiblock polymer faces both thermodynamic and kinetic barriers to self-organizing into a regular periodic structure. Theory anticipates that ordering becomes more difficult as the number of blocks in block copolymer chains increases.[60] Moreover, once local segregation occurs, rearranging the molecular configurations of chains that bridge multiple microdomains becomes asymptotically prohibitive. These tendencies will be further exacerbated by a random block sequence, which increases the average effective block length, hence the segregation strength, and broadening the distribution of block lengths, which favors disordered microstructures.[61] These arguments are consistent with the one exception found in Figure 4.9 and Figure 4.10, PS-alt-PB-2, and make contact with previous theoretical [62-64] and experimental[15] studies of exhibited periodic microstructures in multiblock copolymers.

4.3.4 Tensile Properties

The mechanical properties of the multiblock copolymers were investigated using uniaxial tensile tests. Rectangular tensile bars were drawn at a constant rate of 5 mm/min until failure at room temperature. Figure 4.11 displays representative tensile curves (selected from at least five data sets per sample) for each $(PS\text{-}PB)_n$ multiblock copolymer material, and the average results (elastic modulus E, strain at break ε_b, stress at break (tensile strength) σ_b, and yield stress σ_y) are summarized in Table 4.5. We note that the rectangular tensile specimens generally failed near the grip, hence the reported results

represent conservative estimates of ε_b and σ_b.

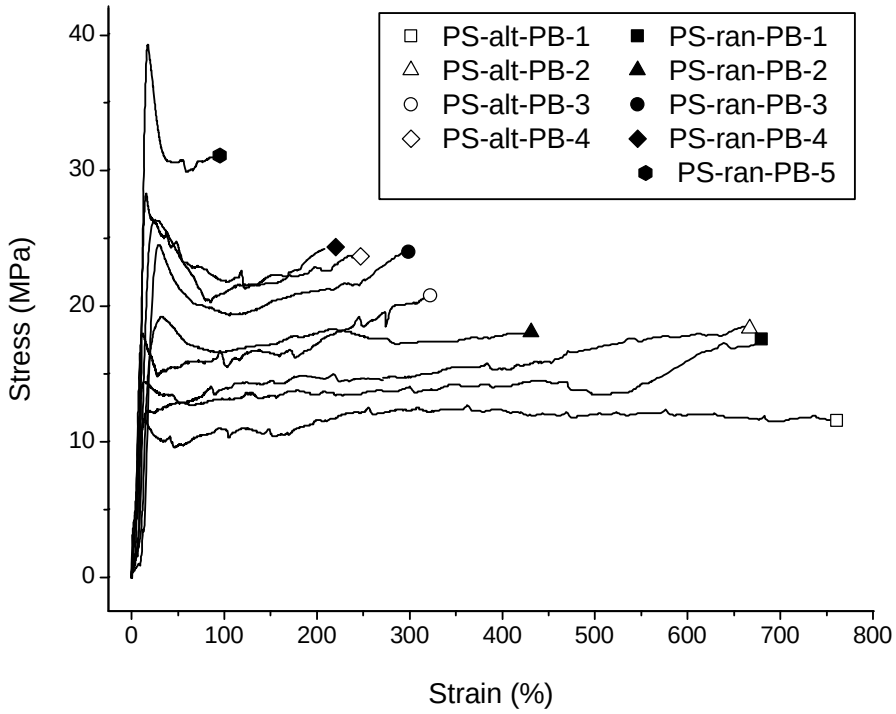

Figure 4.11 Representative engineering stress versus strain curves for the $(PS\text{-}PB)_n$ multiblock copolymers.

Table 4.5 Tensile properties of the $(PS\text{-}PB)_n$ multiblock copolymers.

Sample	E (MPa)	ε_b (%)	σ_b (MPa)	σ_y (MPa)
PS-alt-PB-1	108 ± 86	794 ± 121	13.4 ± 2.3	11.6 ± 2.0
PS-alt-PB-2	77 ± 13	683 ± 62	18.5 ± 3.0	10.7 ± 2.1
PS-alt-PB-3	293 ± 23	347 ± 40	19.7 ± 1.0	20.0 ± 2.1
PS-alt-PB-4	350 ± 51	272 ± 58	22.1 ± 0.9	26.4 ± 2.0
PS-ran-PB-1	103 ± 37	677 ± 87	16.8 ± 1.7	12.9 ± 1.1
PS-ran-PB-2	159 ± 40	431 ± 89	17.9 ± 0.6	17.6 ± 0.5
PS-ran-PB-3	224 ± 83	322 ± 84	21.7 ± 1.9	22.9 ± 1.5
PS-ran-PB-4	245 ± 78	208 ± 127	22.5 ± 2.6	26.1 ± 2.5
PS-ran-PB-5	443 ± 91	112 ± 23	28.7 ± 3.2	37.6 ± 3.8

All the $(PS\text{-}PB)_n$ multiblock copolymers exhibit yielding behavior and display varying degrees of ductility. With the exception of sample PS-alt-PB-2 (lamellar morphology), all the samples neck after yielding, followed modest strain hardening prior to rupture. Necking is generally encountered with materials that are glassy-continuous in the stretching direction.[65-67] The overall trends in the mechanical properties are correlated with the amount of glassy polystyrene, irrespective of the block sequencing (see Table 4.5). Increasing the hard block content increases E and σ_b but reduces ε_b.

The most distinctive difference with PS-alt-PB-2, which has a polygranular lamellar morphology, is no necking, evidenced by the absence of a drop in the measured stress after yielding, which we attribute to the layered (glassy/rubbery) morphology. In

fact, yielding in PS-alt-PB-2 was accompanied by crazing manifested by stress-whitening, the only multiblock sample that showed this behavior. Formation of crazes is dependent on the thickness and length of the glassy PS domains and does not occur below critical values.[68-70] We believe the bicontinuous morphology inhibits the development of crazes. Remarkably, PS-alt-PB-2 crazes and does not neck even though it contains the smallest volume fraction of PS among the multiblock samples, reinforcing the notion that the mechanical properties are governed by the bicontinuous morphology.

The results shown in Figure 4.11 and summarized in Table 4.5, in conjunction with the molecular characteristics listed in Table 4.2, demonstrate that E, σ_y, σ_b and ε_b can be broadly tuned using the multiblock strategy.

Interestingly, the $(PS\text{-}PB)_n$ multiblock copolymers are very different mechanically than the corresponding linear SBS triblock copolymers at similar molecular weight and composition. Figure 4.12 compares the stress–strain response of PS-alt-PB-3 and that reported by Adhikari and co-workers for a linear symmetric SBS triblock copolymer (LN1).[71-72] Both block copolymers have similar molecular weights and compositions (LN1: M_n = 82 000 g/mol, f_{PS} = 0.74; PS-alt-PB-3: M_n = 113 000 g/mol, f_{PS} = 0.76) and have been stretched at the same rate of 100% strain/min. These materials have very different mechanical properties. LN1 is much stiffer (E = 1810 MPa), yields at 27 MPa, and breaks at about 20% strain. PS-alt-PB-3, on the other hand, has a lower modulus (E = 279 MPa) and yield stress (σ_y = 19 MPa) and fails at ε_b = 322%. Based on the total area under the stress–stain curve, PS-alt-PB-3 is about 13.5 times tougher than LN1. These differences stem from the underlying morphologies. LN1 contains hexagonally ordered

PB cylinders dispersed in a PS matrix. The glassy continuous matrix (and discontinuous rubbery domains) fractures rather than fragmenting upon stretching without neck propagation.[73] In contrast, the glassy portions of the bicontinuous PS-alt-PB-3 material easily fragment and become dispersed in a rubbery continuous domain, resulting in a plastic-to-rubber transition, necking, and greatly enhanced toughness.[73-76] Even PS-ran-PB-5, which contains 85% by volume PS, exhibits more than 5 times the toughness of LN1 and has greater yielding and breaking stresses, although the modulus is one-quarter as large.

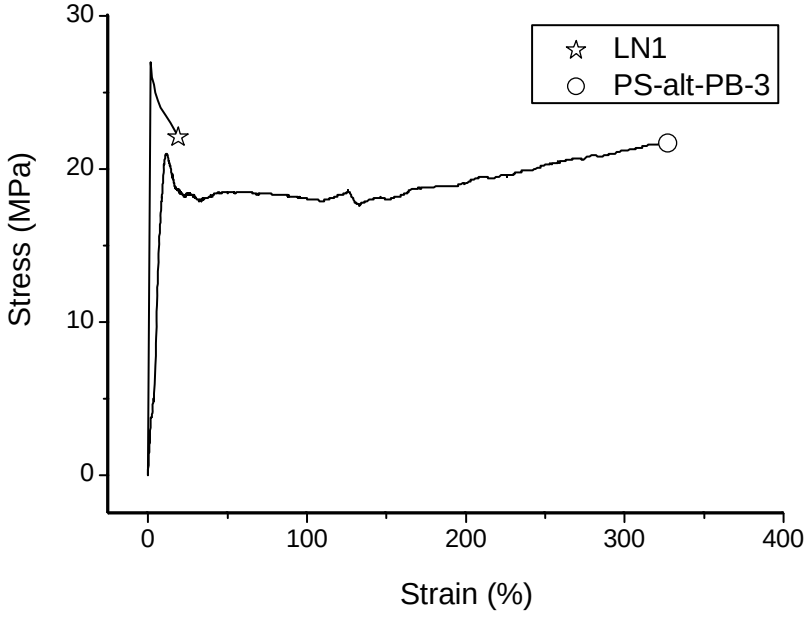

Figure 4.12 Comparison of the tensile behavior of similar composition and molecular weight SBS triblock (LN1) and $(PS\text{-}PB)_n$ multiblock (PS-alt-PB-3).

4.4 Conclusions

Poly(styrene-*b*-butadiene) $(PS\text{-}PB)_n$ multiblock copolymers were synthesized with alternating and random block sequences using a combination of living anionic polymerization and polycondensation and characterized by DSC, SAXS, TEM, and tensile testing. SAXS and TEM measurements demonstrate a random bicontinuous-like morphology over a wide range of compositions, $0.69 \leq f_{PS} \leq 0.85$, when the average number of coupled blocks $\langle n \rangle$ exceeds 7. Random versus alternating block sequencing influences the distribution of effective block lengths,[77-78] hence the average microdomain spacing and segregation strength, but does not significantly affect the overall random bicontinuous-like morphology, nor the tensile properties, which are characterized by yielding followed by necking. The modulus (E), yield stress (σ_y), and stress and strain at break (σ_b and ε_b) are each strongly influenced by the composition. These materials offer significantly greater toughness with comparable tensile strength, but lower modulus, compared to conventional SBS triblock copolymers. We believe the multiblock copolymer strategy offers a versatile approach to obtaining useful and tunable physical properties from many other combinations of α,ω-difunctional polymers, including three or more block types, through tractable condensation coupling chemistry. Multiblock polymers are particularly attractive for the development of affordable plastics and elastomers derived from sustainable sources such as sugars, cyclic esters, and cellulosic compounds,[79-83] where functional end groups are directly available along with a wealth of new block types characterized by a wide range of interaction parameters.

4.5 References

[1] Bates, F. S.; Hillmyer, M. A.; Lodge, T. P.; Bates, C. M.; Delaney, K. T.; Fredrickson, G. H. *Science* **2012,** *336*, 434-440.

[2] Russell, T. P.; Karis, T. E.; Gallot, Y.; Mayes, A. M. *Nature* **1994,** *368*, 729-731.

[3] Zhang, L.; Eisenberg, A. *Science* **1995,** *268*, 1728-1731.

[4] Jeong, B.; Bae, Y. H.; Lee, D. S.; Kim, S. W. *Nature* **1997,** *388*, 860-862.

[5] Discher, B. M.; Won, Y.-Y.; Ege, D. S.; Lee, J. C.-M.; Bates, F. S.; Discher, D. E.; Hammer, D. A. *Science* **1999,** *284*, 1143-1146.

[6] Savić, R.; Luo, L.; Eisenberg, A.; Maysinger, D. *Science* **2003,** *300*, 615-618.

[7] Dubertret, B.; Skourides, P.; Norris, D. J.; Noireaux, V.; Brivanlou, A. H.; Libchaber, A. *Science* **2002,** *298*, 1759-1762.

[8] Li, Z.; Kesselman, E.; Talmon, Y.; Hillmyer, M. A.; Lodge, T. P. *Science* **2004,** *306*, 98-101.

[9] Deplace, F.; Scholz, A. K.; Fredrickson, G. H.; Kramer, E. J.; Shin, Y.-W.; Shimizu, F.; Zuo, F.; Rong, L.; Hsiao, B. S.; Coates, G. W. *Macromolecules* **2012,** *45*, 5604-5618.

[10] Leibler, L. *Macromolecules* **1980,** *13*, 1602-1617.

[11] Mayes, A. M.; de la Cruz, M. O. *The Journal of Chemical Physics* **1989,** *91*, 7228-7235.

[12] Bates, F. S.; Fredrickson, G. H. *Annu. Rev. Phys. Chem.* **1990,** *41*, 525-557.

[13] Fredrickson, G. H.; Bates, F. S. *Annu. Rev. Mater. Sci.* **1996,** *26*, 501-550.

[14] Holden, G.; Kricheldorf, H. R.; Quirk, R. P. *Thermoplastic Elastomers*, 3rd ed.;

Hanser Gardner Publications: Cincinnati, 2004.

[15] Wu, L.; Cochran, E. W.; Lodge, T. P.; Bates, F. S. *Macromolecules* **2004,** *37*, 3360-3368.

[16] Lim, L. S.; Harada, T.; Hillmyer, M. A.; Bates, F. S. *Macromolecules* **2004,** *37*, 5847-5850.

[17] Phatak, A.; Lim, L. S.; Reaves, C. K.; Bates, F. S. *Macromolecules* **2006,** *39*, 6221-6228.

[18] Koo, C. M.; Hillmyer, M. A.; Bates, F. S. *Macromolecules* **2006,** *39*, 667-677.

[19] Arriola, D. J.; Carnahan, E. M.; Hustad, P. D.; Kuhlman, R. L.; Wenzel, T. T. *Science* **2006,** *312*, 714-719.

[20] Khariwala, D. U.; Taha, A.; Chum, S. P.; Hiltner, A.; Baer, E. *Polymer* **2008,** *49*, 1365-1375.

[21] Edson, J. B.; Wang, Z.; Kramer, E. J.; Coates, G. W. *J. Am. Chem. Soc.* **2008,** *130*, 4968-4977.

[22] Park, H. E.; Dealy, J. M.; Marchand, G. R.; Wang, J.; Li, S.; Register, R. A. *Macromolecules* **2010,** *43*, 6789-6799.

[23] Zuo, F.; Mao, Y.; Li, X.; Burger, C.; Hsiao, B. S.; Chen, H.; Marchand, G. R. *Macromolecules* **2011,** *44*, 3670-3673.

[24] Li, S.; Register, R. A.; Weinhold, J. D.; Landes, B. G. *Macromolecules* **2012,** *45*, 5773-5781.

[25] Mogi, Y.; Nomura, M.; Kotsuji, H.; Ohnishi, K.; Matsushita, Y.; Noda, I. *Macromolecules* **1994,** *27*, 6755-6760.

[26] Stadler, R.; Auschra, C.; Beckmann, J.; Krappe, U.; Voight-Martin, I.; Leibler, L. *Macromolecules* **1995,** *28*, 3080-3097.

[27] Hadjichristidis, N.; Iatrou, H.; Pitsikalis, M.; Pispas, S.; Avgeropoulos, A. *Prog. Polym. Sci.* **2005,** *30*, 725-782.

[28] Chatterjee, J.; Jain, S.; Bates, F. S. *Macromolecules* **2007,** *40*, 2882-2896.

[29] Lee, S.; Bluemle, M. J.; Bates, F. S. *Science* **2010,** *330*, 349-353.

[30] Hepburn, C. *Polyurethane Elastomers*; Applied Science: New York, 1982; p 248.

[31] Koberstein, J. T.; Galambos, A. F.; Leung, L. M. *Macromolecules* **1992,** *25*, 6195-6204.

[32] Wirpsza, Z. *Polyurethanes : chemistry, technology, and applications*; Ellis Horwood: New York, 1994.

[33] Randall, D.; Lee, S. *The polyurethanes book*; John Wiley & Sons: New York, 2002.

[34] Wu, J.; Ge, Q.; Mather, P. T. *Macromolecules* **2010,** *43*, 7637-7649.

[35] Szwarc, M. *Adv. Polym. Sci.* **1983,** *49*, 1-177.

[36] Morton, M. *Anionic Polymerization : Principles and Practice*; Academic Press New York, 1983.

[37] Hsieh, H. L.; Quirk, R. P. *Anionic Polymerization: Principles and Practical Applications*; Marcel Dekker: New York, 1996.

[38] Morton, M.; Fetters, L. J.; Inomata, J.; Rubio, D. C.; Young, R. N. *Rubber Chem. Technol.* **1976,** *49*, 303-319.

[39] Quirk, R. P.; Ma, J.-J. *J. Polym. Sci., Part A: Polym. Chem.* **1988,** *26*, 2031-2037.

[40] Hillmyer, M. A.; Bates, F. S. *Macromolecules* **1996,** *29*, 6994-7002.

[41] Meuler, A. J.; Mahanthappa, M. K.; Hillmyer, M. A.; Bates, F. S. *Macromolecules* **2007,** *40*, 760-762.

[42] Fetters, L. J.; Lohse, D. J.; Richter, D.; Witten, T. A.; Zirkel, A. *Macromolecules* **1994,** *27*, 4639-4647.

[43] Ono, H.-K.; Jones, F. N.; Pappas, S. P. *Journal of Polymer Science: Polymer Letters Edition* **1985,** *23*, 509-515.

[44] Prabhakar, A.; Chattopadhyay, D. K.; Jagadeesh, B.; Raju, K. V. S. N. *J. Polym. Sci., Part A: Polym. Chem.* **2005,** *43*, 1196-1209.

[45] Sardon, H.; Irusta, L.; Fernández-Berridi, M. J. *Prog. Org. Coat.* **2009,** *66*, 291-295.

[46] Cunliffe, A. V.; Davis, A.; Farey, M.; Wright, J. *Polymer* **1985,** *26*, 301-306.

[47] Liang, C. Y.; Krimm, S. *Journal of Polymer Science* **1958,** *27*, 241-254.

[48] Fox, J. T. G.; Flory, P. J. *J. Appl. Phys.* **1950,** *21*, 581-591.

[49] Ueberreiter, K.; Kanig, G. *Journal of Colloid Science* **1952,** *7*, 569-583.

[50] Fox, T. G.; Flory, P. J. *Journal of Polymer Science* **1954,** *14*, 315-319.

[51] Santangelo, P. G.; Roland, C. M. *Macromolecules* **1998,** *31*, 4581-4585.

[52] Hiemenz, P. C.; Lodge, T. P. *Polymer Chemistry*, 2nd ed.; Taylor & Francis Group: New York, 2007.

[53] Saam, J. C.; Fearon, F. W. G. *Product R&D* **1971,** *10*, 10-14.

[54] Dems, A.; Strobin, G. *Die Makromolekulare Chemie* **1991,** *192*, 2521-2537.

[55] Krause, S.; Lu, Z.; Iskandar, M. *Macromolecules* **1982,** *15*, 1076-1082.

[56] Granger, A. T.; Wang, B.; Krause, S.; Fetters, L. J. *Adv. Chem. Ser.* **1986**, 127-138.

[57] Granger, A. T.; Krause, S.; Fetters, L. J. *Macromolecules* **1987,** *20*, 1421-1423.

[58] Fox, T. G. *Bull. Am. Phys. Soc.* **1956,** *1*, 123.

[59] Hashimoto, T.; Tsukahara, Y.; Tachi, K.; Kawai, H. *Macromolecules* **1983,** *16*, 648-657.

[60] Krause, S. *Macromolecules* **1970,** *3*, 84-86.

[61] Fredrickson, G. H.; Milner, S. T.; Leibler, L. *Macromolecules* **1992,** *25*, 6341-6354.

[62] Benoit, H.; Hadziioannou, G. *Macromolecules* **1988,** *21*, 1449-1464.

[63] Kavassalis, T. A.; Whitmore, M. D. *Macromolecules* **1991,** *24*, 5340-5345.

[64] Zielinski, J. M.; Spontak, R. J. *Macromolecules* **1992,** *25*, 653-662.

[65] Holden, G.; Legge, N. R. In *Thermoplastic Elastomers*, 2nd ed.; Holden, G.; Legge, N. R.; Quirk, R. P.; Schroeder, H. E. Eds.; Hanser Publishers: New York, 1996; pp 48-69.

[66] Quirk, R. P.; Morton, M. In *Thermoplastic Elastomers*, 2nd ed.; Hanser Publishers: New York, 1996; pp 72-100.

[67] Dair, B. J.; Honeker, C. C.; Alward, D. B.; Avgeropoulos, A.; Hadjichristidis, N.; Fetters, L. J.; Capel, M.; Thomas, E. L. *Macromolecules* **1999,** *32*, 8145-8152.

[68] Wu, S. *J. Appl. Polym. Sci.* **1988,** *35*, 549-561.

[69] Michler, G. H.; Adhikari, R.; Lebek, W.; Goerlitz, S.; Weidisch, R.; K. Knoll *J. Appl. Polym. Sci.* **2002,** *85*, 683-700.

[70] van Melick, H. G. H.; Govaert, L. E.; Meijer, H. E. H. *Polymer* **2003,** *44*, 457-465.

[71] Adhikari, R.; Godehardt, R.; Lebek, W.; Weidisch, R.; Michler, G. H.; Knoll, K. *Journal of Macromolecular Science, Part B* **2001,** *40*, 833-847.

[72] Adhikari, R.; Michler, G. H. *Prog. Polym. Sci.* **2004,** *29*, 949-986.

[73] Sakurai, S.; Sakamoto, J.; Shibayama, M.; Nomura, S. *Macromolecules* **1993,** *26*, 3351-3356.

[74] Fujimura, M.; Hashimoto, T.; Kawai, H. *Rubber Chem. Technol.* **1978,** *51*, 215-224.

[75] Hashimoto, T.; Fujimura, M.; Saijo, K.; Kawai, H.; Diamant, J.; Shen, M. Strain-Induced Plastic-to-Rubber Transition of a SBS Block Copolymer and Its Blend with PS. In *Multiphase Polymers*, AMERICAN CHEMICAL SOCIETY: 1979; Vol. 176, pp 257-275.

[76] Kawai, H.; Hashimoto, T.; Miyoshi, K.; Uno, H.; Fujimura, M. *Journal of Macromolecular Science-Physics* **1980,** *B17*, 427-472.

[77] Meuler, A. J.; Ellison, C. J.; Qin, J.; Evans, C. M.; Hillmyer, M. A.; Bates, F. S. *J. Chem. Phys.* **2009,** *130*.

[78] Schmitt, A. L.; Mahanthappa, M. K. *Soft Matter* **2012,** *8*, 2294-2303.

[79] Biermann, U.; Friedt, W.; Lang, S.; Lühs, W.; Machmüller, G.; Metzger, J. O.; Rüsch gen. Klaas, M.; Schäfer, H. J.; Schneider, M. P. *Angew. Chem. Int. Ed.* **2000,** *39*, 2206-2224.

[80] Güner, F. S.; Yağcı, Y.; Tuncer Erciyes, A. *Prog. Polym. Sci.* **2006,** *31*, 633-670.

[81] Meier, M. A. R.; Metzger, J. O.; Schubert, U. S. *Chem. Soc. Rev.* **2007,** *36*, 1788-1802.

[82] Gandini, A. *Macromolecules* **2008,** *41*, 9491-9504.

[83] Belgacem, M. N.; Gandini, A. *Monomers, Polymers and Composites from Renewable Resources*; Elsevier: Amsterdam, 2008.

Chapter 5 Poly(lactide-*b*-butadiene) Multiblock Copolymers*

5.1 Introduction

The successful synthesis of macromolecular materials from inexpensive petroleum-based feedstock ushered in the modern age of plastics that we live in today. However, depleting fossil oil reserves, litter, and other environmental issues have aroused interest in polymers derived from non-petrochemical sources. It is obvious that sustainability in the polymer field is a necessary step, and many studies are in progress for developing plastics and elastomers from sustainable sources such as sugars, cellulosic compounds, and vegetable oils.[1-6] Polylactide (PLA), one of the most promising biopolymers, can be produced from annually renewable resources. PLA has been widely used in the biomedical, packaging, and textile industries because of its unique properties such as biodegradability and biocompatibility.[6-9] However, one drawback of PLA is the brittleness of the homopolymer, which limits its use in applications where tough

* Part of this work was carried out in collaboration with Tessie Panthani and published in 'Lee, I.; Panthani, T. R.; Bates, F. S. *Macromolecules* **2013,** *46*, 7387-7398'

mechanical behavior is required. Many strategies have been explored to extend the range of possible applications of PLA,[10] including manipulation of crystallinity,[11-12] plasticization,[13-16] blending with other polymers,[17-22] and incorporation into block copolymers.[23-24]

Modern synthetic methods allow access to numerous structures of multiblock polymers, which have attracted interest because they are expected to have distinct microstructures and exhibit different mechanical behavior compared to conventional polymers with simple architectures.[25] Numerous experimental and theoretical studies have been reported on multiblock polymers containing three or more blocks.[25-46] Recently, we synthesized poly(styrene-*b*-butadiene) multiblock copolymers using a combination of living anionic polymerization and polycondensation reaction, and found that these materials are significantly tougher than the corresponding PS-PB-PS triblock copolymers (PS and PB refer to polystyrene and polybutadiene, respectively).[47] In this report, a multiblock copolymer strategy is applied to PLA-PB block copolymers with the goal of developing mechanically improved sustainable plastics. Rubbery polybutadiene, derived from fossil based resources, is widely used to toughen brittle glassy plastics, including products such as high impact polystyrene (HIPS) and poly(acrylonitrile-butadiene-styrene) (ABS). Recent efforts to utilize biofeedstocks for polymer synthesis have led to the development of processes to obtain butadiene from bioalcohols using fermentation and catalytic reactions.[48-50] In fact, Genomatica recently announced that the successful production of biobased butadiene in pound quantities, with plans to produce this important industrial chemical on a commercial-scale. Thus, butadiene can be considered

a potential renewable monomer.[51]

This article describes the synthesis and characterization of PLA-PB multiblock copolymers, where the hard amorphous PLA blocks afford high-strength and high-modulus and the soft PB blocks introduce ductility and toughness. Here we focus on plastic materials containing greater than 50 % by volume PLA.

The PLA-PB multiblock copolymers were prepared in a two-step process; PLA-PB-PLA (LBL) triblock copolymers were first synthesized via ring-opening polymerization of D,L-lactide with dihydroxyl polybutadiene, followed by extension of the LBL triblock chains with two different chain connectors, toluene-2,4-diisocyanate (TDI) and terephthaloyl chloride (TCl). The relationship between composition, morphology, thermal behavior, and mechanical properties of these multiblock copolymers was examined and compared with those of the respective triblock copolymers.

This work was supported by the National Science Center through the Center for Sustainable Polymers at the University of Minnesota, a Center for Chemical Innovation (CHE- 1136607) and through a NSF Graduate Fellowship (Grant No 0006595 to T.R.P.). SAXS was performed at the DuPont-Northwestern-Dow Collaborative Access Team (DND-CAT) located at Sector 5 of the Advanced Photon Source (APS). DND-CAT is supported by E. I. du Pont de Nemours & Co., The Dow Chemical Company, and Northwestern University. Use of the APS, an Office of Science User Facility operated for the U.S. Department of Energy (DOE) Office of Science by Argonne National Laboratory, was supported by the U.S. DOE under Contract DE-AC02-06CH11357. Parts

of this work were carried out in the Characterization Facility, University of Minnesota, which receives partial support from the NSF through the MRSEC program. We also thank Sean Pickthorn for his help with some of the synthesis and characterization.

5.2 Experimental Section

5.2.1 Synthesis of Poly(lactide-*b*-butadiene-*b*-lactide) (LBL) Triblock Copolymers.

LBL triblock copolymers were synthesized via ring-opening polymerization using commercially available *α,ω*-dihydroxy polybutadiene (HO-PB-OH) (KRASOL® LBH-P 3000, Cray Valley USA, LLC, M_n = 3300 g/mol, $Đ$ = 1.09, 36 mol% 1,4 units, 64 mol% 1,2 units) (Figure 5.1(a)). The HO-PB-OH acted as a macroinitiator for the polymerization as well as constituted a rubbery middle block in the LBL triblock copolymers.

The HO-PB-OH was poured into a pressure vessel and dried with stirring overnight on a high vacuum line. The pressure vessel was moved to an argon glovebox and charged with D,L-lactide (Purac), tin(II) octoate ($Sn(Oct)_2$, ~ 0.1 wt% relative to D,L-lactide), and toluene (~ 30 wt% toluene solution). The reaction vessel was sealed and taken out of the glovebox, placed in a 70 °C oil bath, and stirred for 1 h. The bath temperature was then ramped up to 110 °C and the solution was stirred for 3 h. After the reaction, the solution was cooled down to room temperature and precipitated in methanol. The recovered LBL triblock copolymers were dried under vacuum until a constant

pressure was achieved.

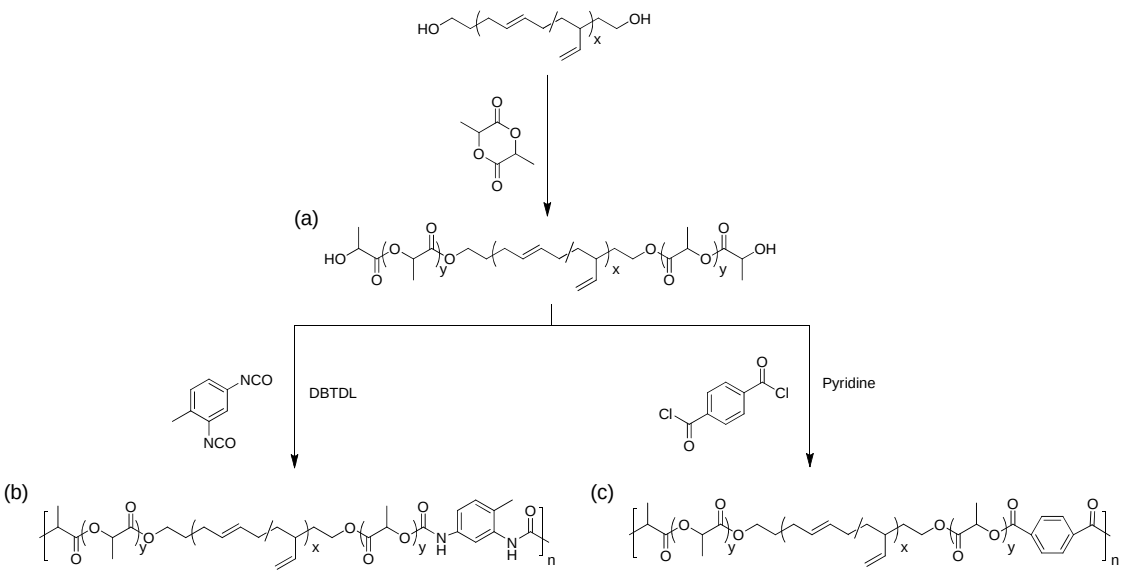

Figure 5.1 Synthetic scheme for (a) LBL triblock copolymer, (b) (LBL-OCONH-)$_n$ multiblock copolymer, and (c) (LBL-COO-)$_n$ multiblock copolymer.

5.2.2 Synthesis of PLA-PB Multiblock Copolymers

PLA-PB multiblock copolymers were synthesized by coupling previously synthesized LBL triblocks via polycondensation reactions. Two different types of multiblock copolymers were prepared with different coupling agents; a diisocyanate produced a multiblock copolymer containing urethane linkages ((LBL-OCONH-)$_n$), and a diacid chloride resulted in a similar multiblock copolymer containing ester linkages ((LBL-COO-)$_n$).

For the synthesis of (LBL-OCONH-)$_n$ multiblock copolymers (Figure 5.1(b)), the starting LBL triblock copolymers were dried overnight in the pressure vessel which was connected to a high-vacuum line. In the glovebox, a stoichiometric amount of toluene-2,4-diisocyanate (TDI, Aldrich), dibutyltin dilaurate (DBTDL, Aldrich), and toluene as a solvent were added into the same pressure vessel. After sealing and taking out of the glovebox, the vessel was set in the oil bath at 70 °C for 5 h while stirring the solution. After 5 h, the solution was cooled down to room temperature. The resulting multiblock copolymers, (LBL-OCONH-)$_n$, were recovered via precipitation with methanol followed by drying under vacuum.

(LBL-COO-)$_n$ multiblock copolymers were prepared in a similar way. The pressure vessel with dried LBL triblock copolymers was filled with a stoichiometric amount of terephthaloyl chloride (TCl, Aldrich), pyridine (Sigma-Aldrich), and toluene in the glovebox. After removing from the glovebox, the solution was stirred at 100 °C for 12 h and cooled down to room temperature. Salts formed during synthesis were isolated by filtering the polymer solution through filter paper (P5 medium porosity, Fisherbrand). Then, the final multiblock copolymers, (LBL-COO-)$_n$, were precipitated and dried as described previously.

5.2.3 Molecular Characterization

The molecular weights and block compositions of LBL triblock copolymers were determined using ^{1}H nuclear magnetic resonance (NMR) spectra. The samples were dissolved into deuterated chloroform ($CDCl_3$, Cambridge Isotope Laboratories, Inc.) and

measured with a Varian Inova 500 spectrometer at room temperature. The molecular weights and mole fractions were calculated by integration of PLA and PB proton peaks. The volume fractions were converted from mole fractions using the published homopolymer densities (ρ_{PLA} = 1.27, $\rho_{1,4\text{-PB}}$ = 0.826, $\rho_{1,2\text{-PB}}$ = 0.889 g/cm^3).[52-53] Size exclusion chromatography (SEC) was used to obtain the number-average molecular weight (M_n), weight-average molecular weight (M_w) and molecular weight distribution (M_w/M_n) of the block copolymers. SEC analyses were performed on a Thermo Separation Products (TSP) Spectra Systems AS1000 autosampler equipped with three 5 mm Phenomenex Phenogel columns, a Waters 515 pump, and a Waters 2410 differential refractive index detector. The samples were run with THF (Sigma-Aldrich) as a carrier solvent at room temperature, and calculation of molecular weight was carried out by a calibration relative to 10 polystyrene standards (580–377400 g/mol, Polymer Laboratories).

5.2.4 Differential Scanning Calorimetry (DSC)

Thermal transitions were determined using a Thermal Analysis Q1000 DSC. Samples were loaded into aluminum hermetically sealed DSC pans, heated to +125 °C, cooled to −115 °C, and reheated to +125 °C at a rate of 10 °C/min. The glass transition temperature was obtained during the second heating step

5.2.5 Dynamic Mechanical Analysis (DMA)

The order-to-disorder transition temperatures (T_{ODT}) of the triblock copolymers were determined by DMA using a Rheometrics Scientific strain-controlled ARES rheometer fitted with 25 mm parallel plates. About 1 g of sample was loaded onto the parallel plates which were heated to a temperature well above (> 30 °C) the glass transition temperature (T_g) of the polymer. All experiments were conducted at a strain of 1 %, which was determined to be in the linear viscoelastic regime for each sample. Elastic (G') and storage (G'') moduli were monitored at a constant frequency (ω = 0.1 or 1 rad/s) while heating samples at a constant rate (0.2 or 2 °C/min).

5.2.6 Small-Angle X-ray Scattering (SAXS)

Synchrotron source SAXS measurements were taken at Argonne National Laboratory (Argonne, IL) with a beam wavelength of λ = 0.793 Å and a sample-to-detector distance of 3.97 m. The collected two-dimensional scattering data were azimuthally integrated and are presented as intensity (I) vs scattering wave vector ($q = (4\pi/\lambda)\sin(\theta/2)$, where θ is the scattering angle). Samples were press-molded at 125 °C for 5–10 min and cooled down to the room temperature. Then samples were annealed at 200 °C for 3 min before taking measurements. After the molding and annealing procedure, SEC analysis was performed to prove that no appreciable degradation or cross-linking of the polymer occurred.

5.2.7 Transmission Electron Microscopy (TEM)

TEM data were obtained using a Tecnai T12 electron microscope at the College of Science and Engineering Characterization Facility at the University of Minnesota. The polymer samples were hot pressed at ~ 120 °C and cut into thin slices (80–100 nm thickness) using a Leica UC6 microtome with cryotrim 20 and cryo 45° diamond knives (Diatome US) at −80 °C. Microtomed sections were collected on copper grids and stained with the vapor from a 2 % aqueous solution of osmium tetroxide (OsO_4) for ~30 min; OsO4 reacts with the double bonds of the polybutadiene and allows enhanced contrast in the TEM images.

5.2.8 Tensile Testing

Uniaxial tensile tests were conducted with a RSA-G2 Solids Analyzer (TA Instruments). The polymer films with thickness of about 0.2 mm were prepared using a hot press at ~120 °C for 5–10 min, and dog-bone specimens for tensile test were made from the films using a punch and arbor press. Tensile specimens had the following dimensions: total length (25 mm), gauge length (6 mm), cross-section width (3.2 mm), and thickness (approximately 0.2 mm). The samples remained at room temperature for about 48 h after pressing; then the specimens were drawn until failure with a constant rate of 0.1 mm/sec. The engineering stress ($\sigma = F/A_0$) was calculated from the force (F) and the initial cross-sectional area (A_0); the nominal strain ($\varepsilon = (l - l_0)/l_0$) was determined from the change in grip-to-grip distance ($l - l_0$) and the initial gauge length (l_0). Young's modulus (E) was obtained from a slope of the linear regime of the stress-strain curve; the

area under the curve is an indication of fracture toughness, or the total energy absorbed up to failure. At least five specimens for each sample were tested and averaged for all data reported here.

5.3 Results and Discussion

5.3.1 Synthesis

The poly(lactide-*b*-butadiene-*b*-lactide) (LBL) triblock copolymers were synthesized from commercially available *α,ω*-dihydroxy polybutadiene (HO-PB-OH) via ring-opening polymerization with tin(II) octoate ($Sn(Oct)_2$) catalyst. The $Sn(Oct)_2$ is a widely used commercial catalyst for the ring-opening polymerization of lactides and lactones, which provides high reaction rates and conversion.[54-58] Another advantage of this catalyst is that it is soluble in many organic solvents and monomers. Five LBL triblock copolymers having fixed PB block length and different volume fractions of PLA (f_{PLA} = 0.5–0.9) were prepared using HO-PB-OH as a macroinitiator. These triblock copolymers were characterized by size exclusion chromatograph (SEC) for dispersity ($Đ = M_w/M_n$) and ^{1}H nuclear magnetic resonance (NMR) to determine the composition f_{PLA} and M_n (based on the M_n for HO-PB-OH and f_{PLA} along with end-group analysis). The molecular characteristics of LBL triblock copolymer are summarized in Table 5.1.

Table 5.1 Molecular characteristics LBL triblock copolymers and PLA-PB multiblock copolymers.

Triblock copolymers	M_n [a] (g/mol)	$M_{n,SEC}$ [b] (g/mol)	M_w/M_n [c]	f_{PLA} [d]	Conversion (%) [e]	$T_g^{PB\text{-}domain}$ (°C) [f]	$T_g^{PLA\text{-}domain}$ (°C) [f]
LBL50	8300	11600	1.13	0.5	> 99	−37.2	30.7
LBL60	10600	148900	1.17	0.6	99	−36.2	41.1
LBL70	15100	21200	1.10	0.7	> 99	−42.7	40.3
LBL80	22300	21400	1.38	0.8	96	−41.2	46.5
LBL90	45100	41900	1.60	0.9	94	−41.5	44.7

Multiblock copolymers	M_n [g] (g/mol)	$M_{n,SEC}$ [b] (g/mol)	M_w/M_n [c]	f_{PLA} [d]	$\langle n' \rangle$ [h]	$T_g^{PB\text{-}domain}$ (°C) [f]	$T_g^{PLA\text{-}domain}$ (°C) [f]
(LBL60-OCONH-)$_n$	41300	57000	2.49	0.6	3.9	−36.6	46.2
(LBL60-COO-)$_n$	46600	65500	2.42	0.6	4.4	−36.0	44.2
(LBL70-OCONH-)$_n$	45300	64300	2.06	0.7	3.0	−39.2	48.3
(LBL70-COO-)$_n$	55900	78200	2.11	0.7	3.7	−38.9	47.2
(LBL80-OCONH-)$_n$	46800	45600	1.77	0.8	2.1	−40.5	49.1
(LBL80-COO-)$_n$	40100	39000	1.68	0.8	1.8	−39.0	49.7
(LBL90-OCONH-)$_n$	76700	69500	1.85	0.9	1.7	−40.4	50.7
(LBL90-COO-)$_n$	85700	79500	2.06	0.9	1.9	−40.8	50.2

[a] Molecular weight calculated from ^{1}H NMR analysis. [b] Molecular weight determined by SEC calibrated with polystyrene standards. [c] Dispersity ($Đ$) measured by SEC. [d] Volume fraction of PLA measured by ^{1}H NMR and calculated using published bulk homopolymer densities.[52-53] [e] Conversion of lactide monomer after ring-opening polymerization. [f] Glass transition temperature obtained from DSC during second heating. [g] M_n values for the multiblock copolymers were obtained by multiplying the absolute (^{1}H NMR based) triblock number average molecular weights by $\langle n' \rangle$. [h] Average number of triblock copolymers in the multiblock copolymers was calculated based on SEC-measured molecular weights.

When comparing SEC traces of HO-PB-OH (before polymerization) and LBL triblock copolymers (after polymerization), triblock copolymers showed higher molecular weights with the higher content of PLA and reasonably narrow molecular weight distributions (Figure 5.2), indicating effective addition of PLA end blocks to HO-PB-OH macroinitiator via ring-opening polymerization. In the LBL90, the triblock copolymer with the highest molecular weight, a slight broadening of dispersity is observed; this may be the result of transesterification reaction between $Sn(Oct)_2$ and any hydroxyl groups present.[54]

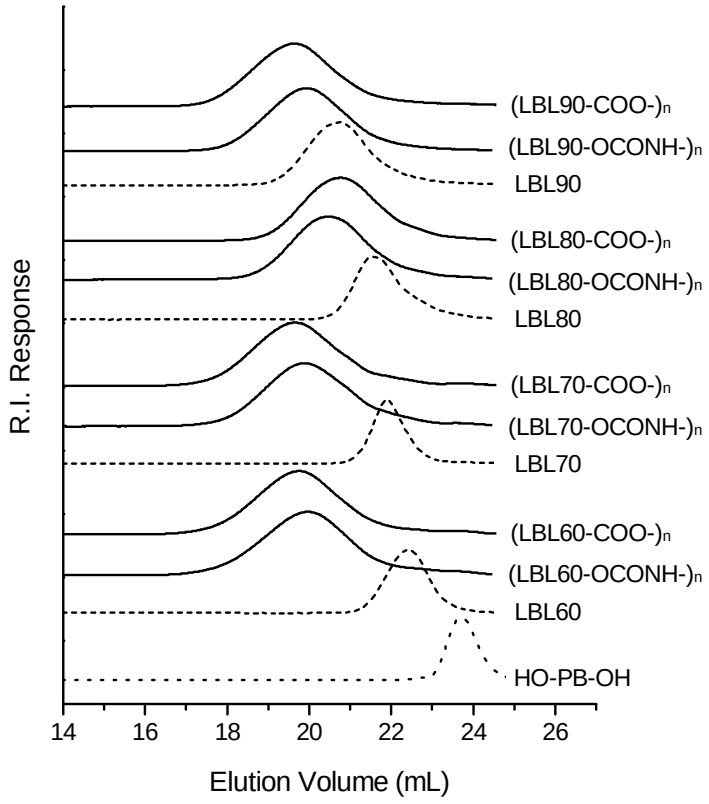

Figure 5.2 SEC traces of synthesized $(LBL\text{-}OCONH\text{-})_n$ and $(LBL\text{-}COO\text{-})_n$ multiblock copolymer series as well as starting LBL triblock copolymers and HO-PB-OH.

The number-average molecular weights and chemical structures of LBL triblock copolymers were characterized with ^{1}H NMR spectroscopy. The ^{1}H NMR spectrum of LBL60 (Figure 5.3(a)) showed the peaks attributed to the methine protons in the repeating units of PLA at 5.16 ppm (δH_a). For 1,2-PB and 1,4-PB, the peak occurring at 5.35 ppm (δH_d) was reasonably assigned to the =CH– protons of 1,4-PB, and the proton peaks of =CH– and $=CH_2$ in 1,2-PB were observed at around 5.55 ppm (δH_c) and 4.95 ppm (δH_e), respectively. Moreover, the peak of methine proton linked with the terminal hydroxyl group of LBL chain was found at 4.36 ppm ($\delta H_{a'}$). The molecular weight and block mole fractions of LBL block copolymers were calculated by integration of peaks assigned to protons in PLA and PB repeat units. These mole fractions were converted to volume fractions using the published homopolymer densities (ρ_{PLA} = 1.27, $\rho_{1,4\text{-PB}}$ = 0.826, $\rho_{1,2\text{-PB}}$ = 0.889 g/cm^3).[52-53] In order to verify the existence of terminal hydroxyl groups, ^{1}H NMR analysis with trifluoroacetic anhydride (TFAA , Sigma-Aldrich) was performed. The TFAA reacts with the hydroxyl group and changes it into a trifluoroacetate group. The terminal hydroxyl groups were confirmed by methine proton peak (4.36 ppm, $\delta H_{a'}$) shifting to higher frequency as a result of this reaction (see Figure 5.4).

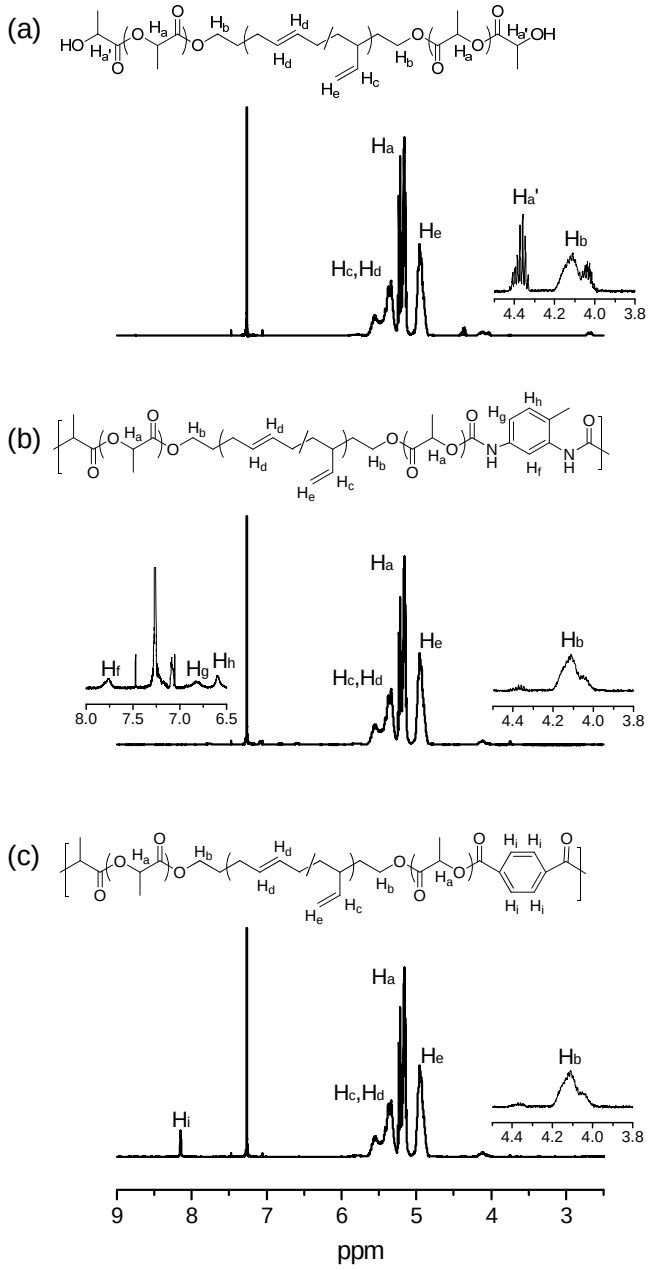

Figure 5.3 ^{1}H NMR spectra of (a) LBL60, (b) (LBL60-OCONH-)$_n$, and (c) (LBL60-COO-)$_n$ in $CDCl_3$. The insert shows the 3.8–4.5 ppm and 6.5–8.0 ppm region of spectrum. The signals between 7 and 7.5 ppm are associated with residual protons in the deuterated chloroform ($CDCl_3$).

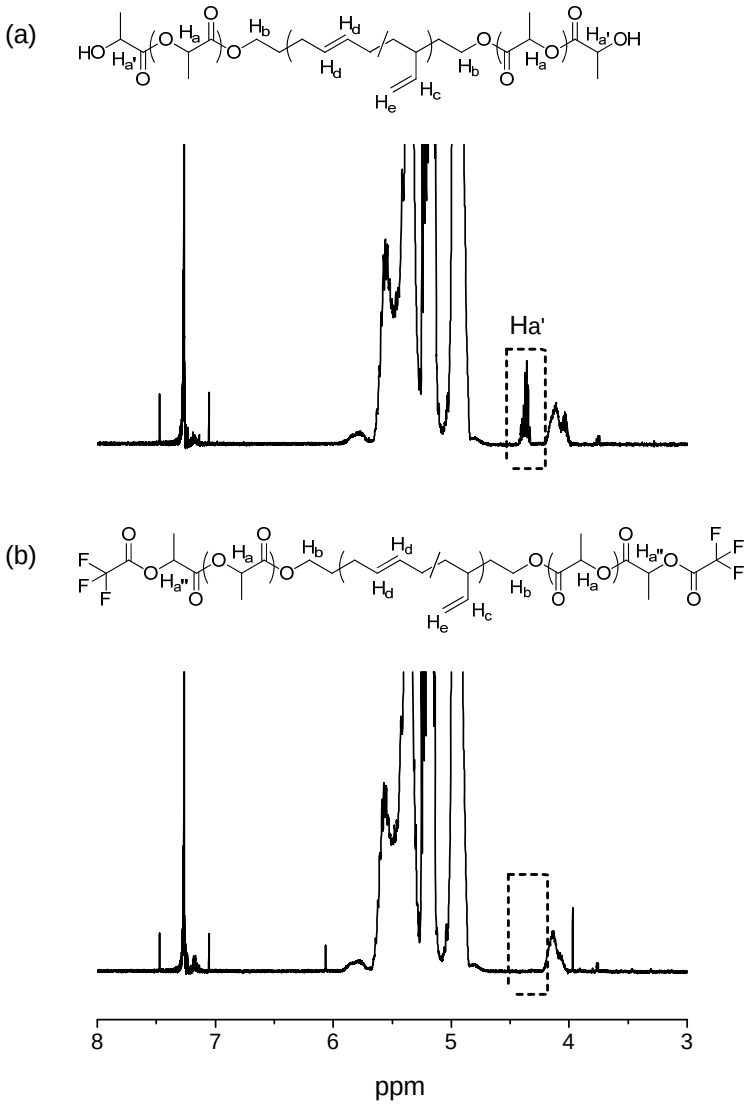

Figure 5.4 ^{1}H NMR spectra of LBL60 (a) before and (b) after the reaction with trifluoroacetic anhydride (TFAA). The modification using TFAA moves the peak of methine proton next to the terminal hydroxyl group ($\delta H_{a'}$) from 4.36 ppm to higher frequency. The shifted methine proton peak ($\delta H_{a''}$) overlaps with the proton peaks of PLA and PB repeat units (4.95–5.55 ppm).

The PLA-PB multiblock copolymers were prepared by coupling the presynthesized LBL triblock copolymers, which have dihydroxyl end group functionality. Two different coupling agents were used as connectors to synthesize two different types of multiblock chains; the coupling reaction with 2,4-diisocyanate (TDI) formed a PLA-PB multiblock copolymer containing urethane linkages, (LBL-OCONH-)$_n$, and the reaction with terephthaloyl chloride (TCl) resulted in a multiblock copolymer containing ester linkages, (LBL-COO-)$_n$. Eight PLA-PB multiblock copolymers were synthesized from four premade LBL triblock copolymers using TDI and TCl, and their molecular characteristics were summarized in Table 5.1. Figure 5.2 shows the SEC traces for synthesized PLA-PB multiblock copolymers as well as their starting LBL triblock copolymers. Both (LBL-OCONH-)$_n$ and (LBL-COO-)$_n$ multiblock copolymers exhibited higher molecular weight compared to LBL triblock copolymers with a most probable molecular weight distribution, which supports that two different coupling reactions worked well for the multiblock copolymer synthesis. In addition, the average number of triblock copolymers in the multiblock chains, $\langle n' \rangle$, was calculated based on the ratio of SEC (calibrated with polystyrene standards) determined M_n values for the multiblocks and LBL triblock copolymers. The M_n values for the multiblock copolymers listed in Table 5.1 were obtained by multiplying the absolute (^{1}H NMR based) triblock number average molecular weights by $\langle n' \rangle$.

The NMR spectra of (LBL60-OCONH-)$_n$ and (LBL60-COO-)$_n$ are shown in Figure 5.3, parts (b) and (c), respectively. Similar to the LBL triblock copolymers, the peaks belonging to protons in PLA and PB repeat units were observed at 5.16 (δH_a), 5.55 (δH_c),

5.35 (δH_d), and 4.95 ppm (δH_e) for both of two different types of multiblock copolymers. In the spectra of multiblock copolymers, the peak of the methine proton ($\delta H_{a'}$) on the lactide chain ends disappeared after the coupling reaction, which supports that the hydroxyl groups reacted with isocyanate (–NCO) or acyl chloride (–COCl) groups of the coupling agents. Two different coupling reactions were also supported by new proton peaks in NMR spectra from their connector molecules; aromatic ring protons of TDI were present at 7.75 (δH_f), 6.80 (δH_g), and 6.60 ppm (δH_h) in the (LBL60-OCONH-)$_n$, and protons on aromatic ring of TCl occurs at 8.15 ppm (δH_i) in the (LBL60-COO-)$_n$ spectrum.

5.3.2 PLA-PB χ Parameter (Order-Disorder Transition Temperature)

The order-disorder transition temperature (T_{ODT}) of the LBL triblock copolymers were determined using dynamic mechanical spectroscopy (DMS) analysis. The dynamic elastic moduli (G') were measured at a constant frequency (ω = 0.1 or 1 rad/s) while heating samples at a constant rate (0.2 or 2 °C/min). Shown in Figure 5.5, T_{ODT} values were taken from the temperature where a sharp drop in G' occurred. The measured T_{ODT} values of two different molecular weight triblock copolymers with 50 vol % PLA content were used to find χ parameter for the PLA-PB system; LBL50-2 (M_n = 5700 g/mol, f_{PLA} = 0.5) and LBL50 (M_n = 8300 g/mol, f_{PLA} = 0.5). Random phase approximation (RPA) calculation for symmetric ABA triblock copolymers gives $(\chi N)_{ODT}$ = 17.996,[34,59] where N is the overall degree of polymerization. For polymers without specific interactions, it is common to express the temperature dependence of χ parameter with

$$\chi(T) = a/T + b \tag{5.1}$$

where a is an excess enthalpic coefficient and b is an excess entropic coefficient.[60] The degree of polymerization, N, is calculated from a reference volume of 118 Å^3 and room temperature densities of the homopolymers.[52-53] From the measured order-disorder transition temperatures, 76 °C for LBL50-2 and 145 °C for LBL50, χ parameter for PLA-PB ($\chi_{PLA\text{-}PB}$) system is described by

$$\chi_{PLA\text{-}PB} = 161.6/T - 0.223 \tag{5.2}$$

For comparison, we have found the temperature dependence of χ in the literature for several other block copolymer systems and calculated the χ values at 100 °C. In cases where a different reference volume was used, χ was recalculated using a reference volume of 118 Å^3. The estimated χ values were $\chi_{PLA\text{-}PB} = 0.210$, $\chi_{PLA\text{-}PS} = 0.096$,[61] $\chi_{PLA\text{-}PMCL} = 0.064$,[62] $\chi_{PLA\text{-}PEP} = 0.375$,[63] $\chi_{PLA\text{-}PDMS} = 1.17$,[64] $\chi_{PS\text{-}PB} = 0.090$,[65] and $\chi_{PS\text{-}PI} = 0.046$.[66] (PS, PMCL, PEP, PDMS, and PI refer to polystyrene, poly(6-methyl-ε-caprolactone), poly(ethylene-*alt*-propylene), poly(dimethylsiloxane), and polyisoprene, respectively).

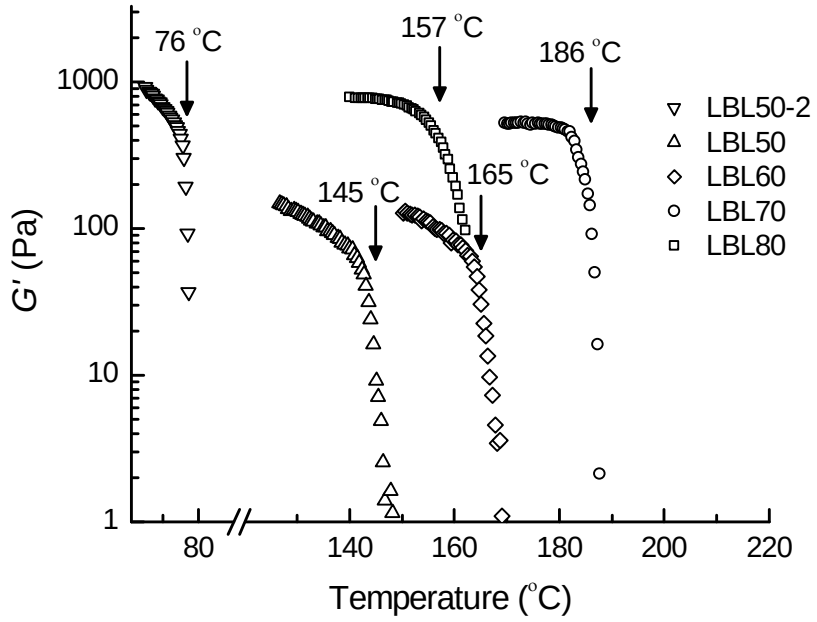

Figure 5.5 Isochoronal temperature ramp data on heating for LBL triblock copolymers: LBL50-2 (▽), LBL50 (△), LBL60 (◇), LBL70 (○), and LBL80 (□). The arrows indicate T_{ODT} values.

5.3.3 Thermal Analysis

Thermal properties of LBL triblock, $(LBL\text{-}OCONH\text{-})_n$ and $(LBL\text{-}COO\text{-})_n$ multiblock copolymers were characterized by DSC. The glass transition temperature (T_g) was determined by the midpoint of intersections defined by the tangent through the inflection and extrapolated baselines above and below glass transition. Figure 5.6 shows DSC heating curves of block copolymer samples studied in this research. All triblock and multiblock copolymer samples showed two different T_gs, which indicates microphase

separation in the condensed PB and PLA phases. The measured T_gs of PB and PLA domains ($T_g^{\text{PB-domain}}$ and $T_g^{\text{PLA-domain}}$) are shown in Table 5.1. In DSC curves, the samples with the larger volume fraction of PLA exhibited small but detectable inflections for the glass transition of PB microphases around −40 °C, which is attributed to the relatively small amount of PB microdomains.

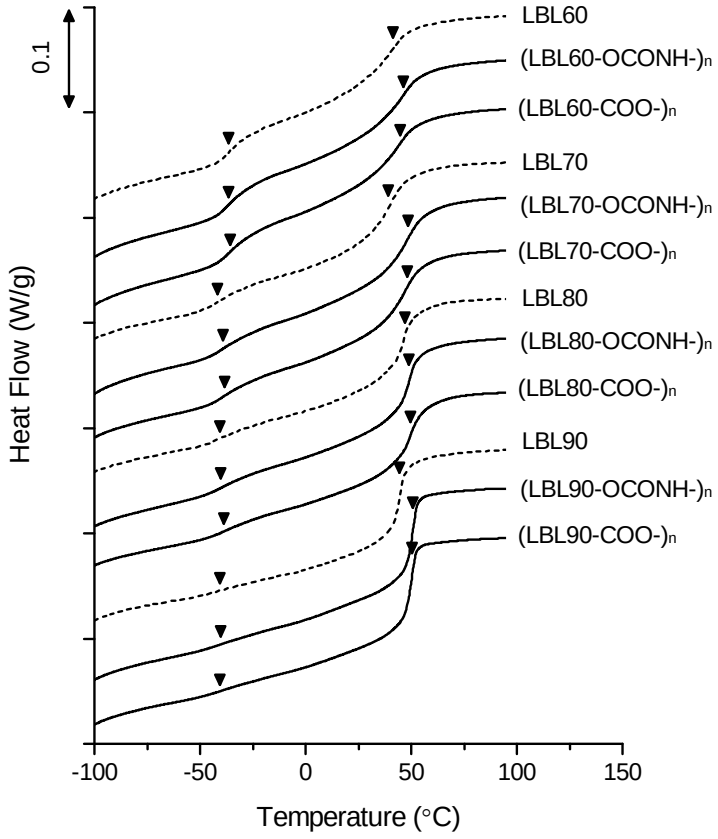

Figure 5.6 DSC heating curves of LBL triblock, (LBL-OCONH-)$_n$ and (LBL-COO-)$_n$ multiblock copolymers. Arrows indicates T_gs of PB and PLA domains ($T_g^{\text{PB-domain}}$ and $T_g^{\text{PLA-domain}}$).

Figure 5.7 shows glass transition temperatures of PB and PLA microphases in multiblock copolymers ($T_g^{PB\text{-}domain}$ and $T_g^{PLA\text{-}domain}$). T_g of PLA homopolymer as a function of molecular weight (dashed line) and T_g of PB homopolymer (HO-PB-OH, dotted line) are also added for comparison. The number-average molecular weight dependence of T_g for PLA homopolymers was calculated using Flory–Fox equation:[67]

$$T_g = T_g^{\infty} - K/M_n \quad (5.3)$$

Here T_g^{∞} is the T_g at infinite molecular weight and K is a constant representing the excess free volume of the end-groups of the polymer chains. T_g of PLA homopolymer in Figure 5.7 was generated from Flory–Fox parameters reported by Jamshidi et al.[68] (T_g^{∞} = 57 °C and $K = 7.4 \times 10^4$) and T_g of PB homopolymer, α,ω-dihydroxy polybutadiene (HO-PB-OH, KRASOL LBH-P 3000), was measured by DSC. When comparing T_gs of (LBL-OCONH-)$_n$ and (LBL-COO-)$_n$ multiblock copolymers, the different chain connectors (urethane and ester linkages) did not seem to affect the T_gs of PLA and PB microphases. The PLA-PB multiblock copolymers showed well-separated phases attributed to the strong segregation strength for PLA-PB system with a large χ parameter. In PB microdomains of multiblock copolymers, deviations of $T_g^{PB\text{-}domain}$ from the T_g of comparable PB homopolymer were observed; the deviation of T_g for PB microphase is indicative of the presence of partially mixed phases. As the PLA molecular weight decreases, more PLA chain segments can mix into PB microphase, which resulted in an increase of T_g deviation. Similar phase mixing effects have been reported in different block copolymer systems.[69-72] Interestingly, T_g of the PLA microphase followed the opposite trend; $T_g^{PLA\text{-}domain}$ deviation from homopolymer PLA increased with increasing

the molecular weight of PLA block. The larger T_g deviation with the higher molecular weight might come from some correlation of the $T_g^{PLA\text{-}domain}$ with dispersity ($Đ$).[73] From SEC results, the prepolymers having a high content of PLA (LBL80 and LBL90) showed a higher $Đ$ compared to other prepolymers, and the multiblock copolymers prepared from high-dispersity triblocks exhibited large T_g deviations. This suggests that the rubbery PB chain segments may prefer to mix into the more disperse PLA microphases or that the true number-average molecular weight values of PLA block are lower than those we calculated.

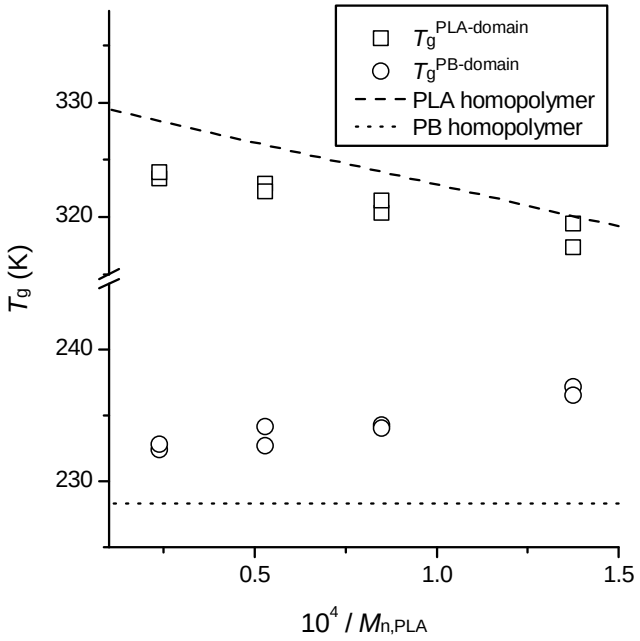

Figure 5.7 PLA block molecular weight effect on the glass transition temperatures of PB and PLA microphases in multiblock copolymers ($T_g^{PB\text{-}domain}$ and $T_g^{PLA\text{-}domain}$). The dashed line is T_g of PLA homopolymer calculated from Flory–Fox equation,[68] and the dotted line is T_g of PB homopolymer (HO-PB-OH) measured by DSC.

5.3.4 Morphological Characeristics

The microstructures of LBL triblock and PLA-PB multiblock copolymers were examined by small angle X-ray scattering (SAXS) and transmission electron microscopy (TEM). The synchrotron source SAXS patterns at room temperature for triblock and multiblock copolymers are illustrated in Figure 5.8. The plot is presented as the log-scaled scattered intensity with respect to the scattering vector $q = 4\pi/\lambda(\sin\theta/2)$, where λ is the wavelength of incident radiation and θ is the scattering angle. All polymer samples exhibited a sharp first-order scattering vector (q^*) at low scattering angle, which indicates microphase separation occurs. The morphologies of block copolymers were determined by comparing the scattering peaks with the allowed reflections for a space group using the ratio of q/q^*. The triblock and multiblock copolymers containing 60 vol% of PLA, LBL60, (LBL60-OCONH-)$_n$, and (LBL60-COO-)$_n$, showed SAXS patterns containing higher order reflections at integral multiples of the principal reflection (q^*), which indicate a lamellar (LAM) microstructure. Representative TEM images (LBL60 and (LBL60-OCONH-)$_n$) shown in Figure 5.9 (upper two panels) confirm this phase assignment. The block copolymer samples with increased PLA content ($f_{PLA} \approx 0.7$ and 0.8), LBL70, (LBL70-OCONH-)$_n$, (LBL70-COO-)$_n$, LBL80, (LBL80-OCONH-)$_n$, and (LBL80-COO-)$_n$, exhibited a sequence of Bragg reflections ($q/q^* = \sqrt{1}, \sqrt{3}, \sqrt{4}, \sqrt{7}$) consistent with hexagonal symmetry. Microscopy images obtained from these specimens reveal a morphology comprised of PB cylinders embedded in a PLA matrix denoted HEX; four representative micrographs (LBL70, (LBL70-OCONH-)$_n$, LBL80, and (LBL80-OCONH-)$_n$) are presented in Figure 5.9 (middle panels). Increasing the PLA content to

90 vol% leads to broadening of the principal (q^*) diffraction peaks and loss of distinct higher order reflections, although the SAXS patterns shown in Figure 5.8 clearly indicate a state of microphase separation. The associated TEM images (lower two panels in Figure 5.9) suggest that these scattering patterns reflect a liquid-like arrangement of spherical PB microdomains within a PLA matrix.

We have corroborated the interpretation of liquid-like packing based on the TEM results for the f_{PLA} = 0.9 specimens by modeling the SAXS data using a spherical form factor (PB cores) with a Gaussian distribution and the Percus–Yevick model[74-76] to account for interparticle interference. The scattering intensity, $I(q)$, of an ensemble of disordered spheres can be described by the following equation,[77]

$$I(q) = KnP(q)S(q) \tag{5.4}$$

where K is a constant that accounts for scattering contrast (here the difference in electron density between PB and PLA) and n is the number density of scattering particles. $P(q)$ is the form factor for a sphere of radius R,

$$P(q) = \int_0^\infty \frac{1}{\sigma_R\sqrt{2\pi}} \exp\left(\frac{-\left(R-\overline{R}\right)^2}{2{\sigma_R}^2}\right) \times \left(\frac{4\pi}{3}R^3\right)^2 \left[\frac{3}{\left(qR\right)^3}\left(\sin\left(qR\right) - qR\cos\left(qR\right)\right)\right]^2 dR \tag{5.5}$$

weighted by a Gaussian distribution about the average sphere size $\overline{R}$ with a standard deviation of σ_R to account for dispersity. S(q) is the interference factor, described for a random arrangement of spheres by following expression:[75,78-81]

$$S(q) = \frac{1}{1 + 24\eta\left(G\left(A\right)/A\right)} \tag{5.6}$$

Here, $A = 2qR_{HS}$ (R_{HS} refer to hard-sphere interaction radius) and η is the hard-sphere

volume fraction. G is a trigonometric function of A and η

$$G(A) = \frac{\alpha}{A^2}(\sin A - A\cos A) + \frac{\beta}{A^3}\left(2A\sin A + (2 - A^2)\cos A - 2\right) + \frac{\gamma}{A^5}\left(-A^4\cos A + 4\left[(3A^2 - 6)\cos A + (A^3 - 6A)\sin A + 6\right]\right) \tag{5.7}$$

where

$$\alpha = (1+2\eta)^2/(1-\eta)^4$$

$$\beta = -6\eta(1+\eta/2)^2/(1-\eta)^4 \tag{5.8}$$

$$\gamma = (\eta/2)(1+2\eta)^2/(1-\eta)^4$$

Equations 5.4–5.8 have been fit to the f_{PLA} = 0.9 SAXS data as illustrated for the scattering patterns of LBL90, (LBL90-OCONH)$_n$, and (LBL90-COO-)$_n$ in Figure 5.10; the best fit to the LBL90 scattering data was obtained with R = 5.7 nm, σ_R = 0.79 nm, R_{HS} = 9.1 nm, and η = 0.41. The best fit to (LBL90-OCONH-)$_n$ data occurs for R = 5.6 nm, σ_R = 0.81 nm, R_{HS} = 9.3 nm, and η = 0.41, whereas to (LBL90-COO-)$_n$ data, R = 5.6 nm, σ_R = 0.87 nm, R_{HS} = 9.0 nm, and η = 0.36. The Percus–Yevick model quantitatively accounts for all the features in the f_{PLA} = 0.9 SAXS results reinforcing our interpretation of the TEM micrographs.

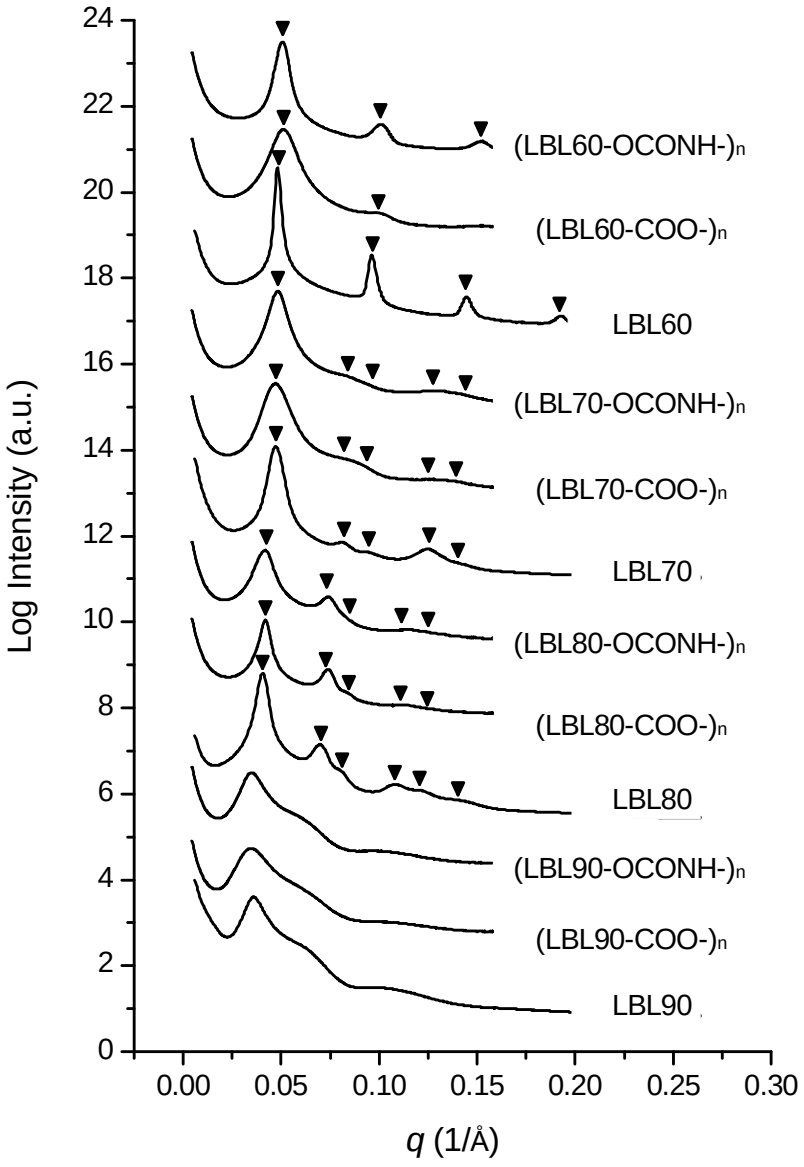

Figure 5.8 SAXS patterns for LBL triblock and PLA-PB multiblock copolymers obtained at room temperature. Data sets are shifted vertically for clarity.

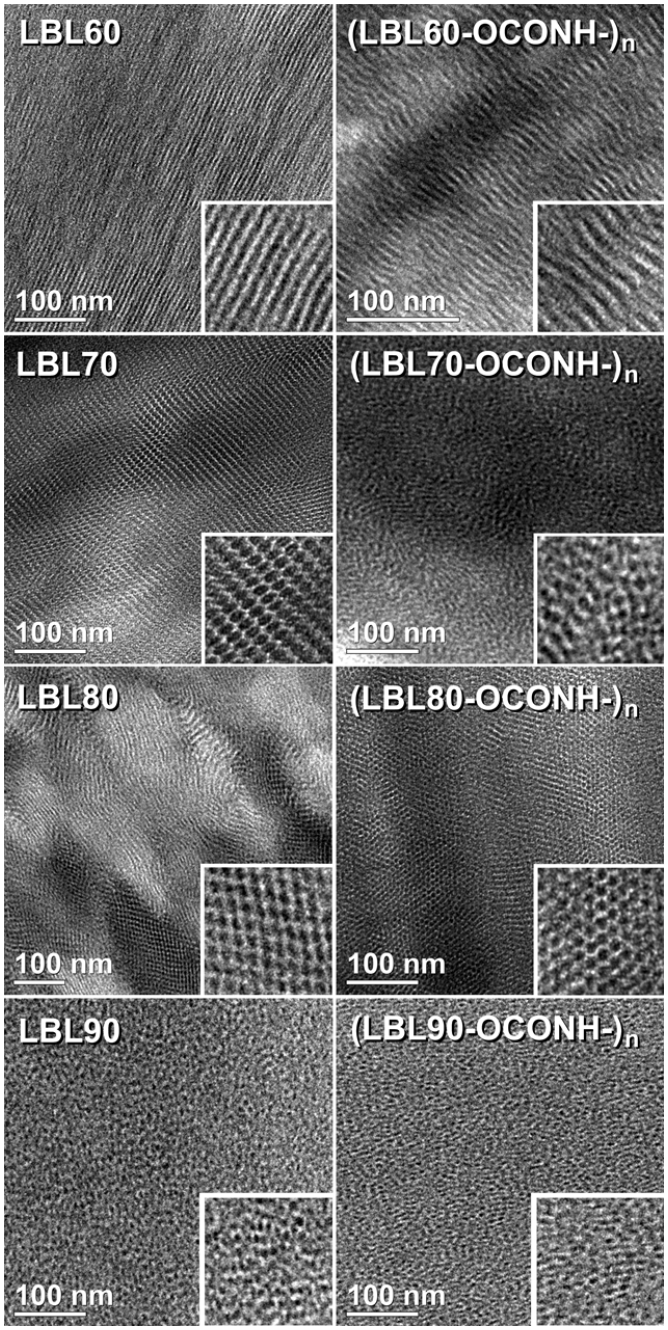

Figure 5.9 TEM images from LBL triblock and (LBL-OCONH-)$_n$ multiblock copolymers. Samples were stained with OsO_4 to enhance the contrast. The light and dark microdomains are associated with PLA and PB domains, respectively. Scale bars correspond to 100 nm and inserts are high-magnification images.

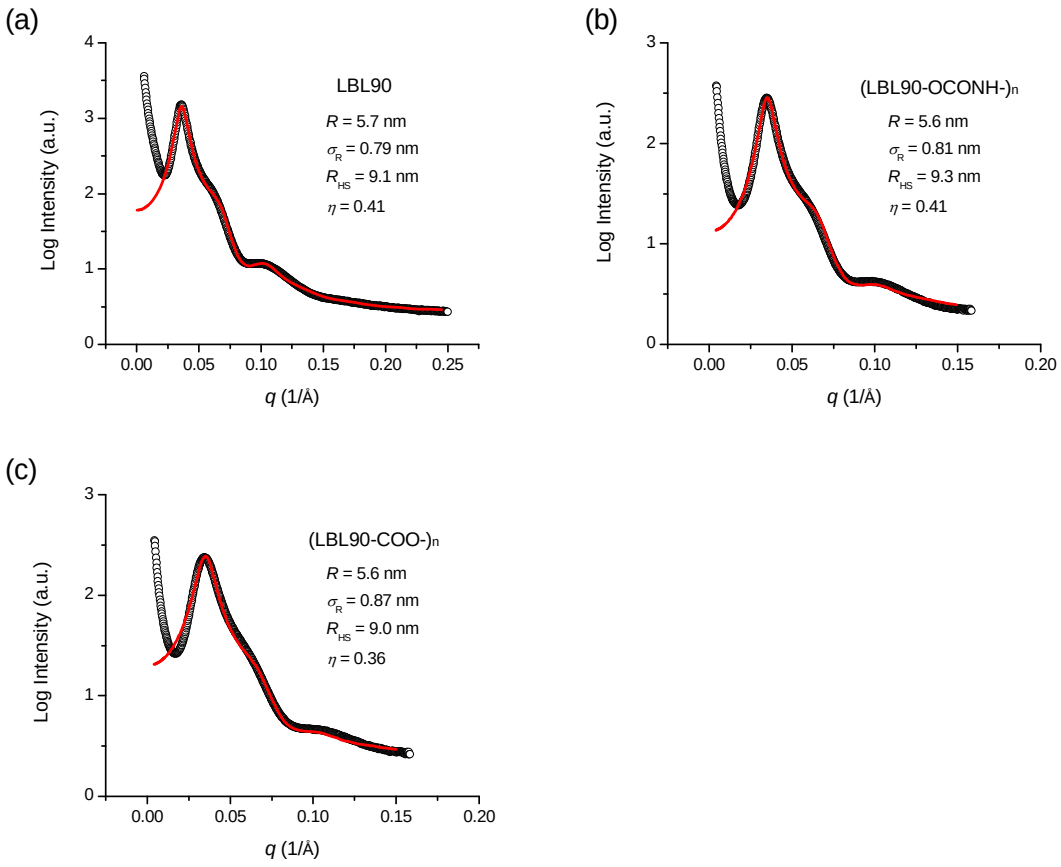

Figure 5.10 Actual experimental scattering data (○) and Percus–Yevick hard-sphere model (solid line) for (a) LBL90, (b) (LBL90-OCONH-)$_n$, and (c) (LBL90-COO-)$_n$. The best fit to the LBL90 scattering data was obtained with R = 5.7 nm, σ_R = 0.79 nm, R_{HS} = 9.1 nm, and η = 0.41. The best fit to (LBL90-OCONH-)$_n$ data occurs for R = 5.6 nm, σ_R = 0.81 nm, R_{HS} = 9.3 nm, and η = 0.41, whereas to (LBL90-COO-)$_n$ data, R = 5.6 nm, σ_R = 0.87 nm, R_{HS} = 9.0 nm, and η = 0.36.

The principal domain spacings ($D = 2\pi/q^*$) of the triblock and multiblock copolymers are tabulated in Table 5.2. Since all the block copolymers have been prepared with the same PB blocks, the *D*-spacing increases with increasing PLA molecular weight. Within 5% the domain sizes of the multiblock copolymers (D_{multi}) and those of the LBL triblock prepolymers (D_{tri}) are equal and the triblock precursor and coupled multiblock products have the same phase morphology. To understand why coupling the triblock copolymers does not affect the phase behavior of the multiblock copolymers, we can consider ordered ABA triblock copolymer (degree of polymerization $2N$) and the homologous AB diblock copolymer (degree of polymerization N). For any ordered block copolymer, the polymer chains tend to stretch in order to reduce the interfacial area while maintaining constant density. Theory and experiments have shown that breaking a ABA triblock at the center of the B block has a very small impact on the free energy of the polymer melts. Helfand and Wasserman, and others theoretically predicted similar domain sizes for homologous ABA triblock and AB diblock copolymer melts at strong segregations.[82-83] Matsushita et al. have experimentally reported that the domain spacings of PSP triblock copolymers are almost identical to those of SP diblock copolymers obtained by breaking the S block at the center[84-85] (P and S refer to poly(2-vinylpyridine) and polystyrene). Similar arguments can be applied to the PLA-PB multiblock copolymers reported here. Four different lamellae-forming LBL triblock copolymers (f_{PLA} = 0.4–0.6) were synthesized and characterized to investigate total degree of polymerization (N) dependence of microdomain size. The results are summarized in Table 5.3 and Figure 5.11. A plot of the *D*-spacings against the overall degree of

polymerization, N, for lamellae-forming LBL triblock copolymers, demonstrates that the lamella period scales as $D \sim N^{2/3}$ (see Figure 5.11). This indicates that the block copolymer samples in this report are reasonably modeled by strong segregation theory.[86-90] In the well segregated block copolymer system, connecting the LBL triblock copolymers has a limited effect on phase behavior of the consequent PLA-PB multiblock copolymers due to the same argument of domain spacing of AB and ABA block copolymers; this explains the nearly identical phase behavior between PLA-PB multiblock copolymers and the homologous LBL triblock polymers. Moreover, the SAXS and TEM results demonstrate that the type of chain connector does not affect the D-spacing or microstructure.

Table 5.2 Characterized morphologies and principal domain spacings of LBL triblock copolymers and PLA-PB multiblock copolymers

Sample	q^* ($Å^{-1}$)	D (nm)	Morphology
Triblock copolymers			
LBL60	0.0482	13.0	LAM
LBL70	0.0472	13.3	HEX
LBL80	0.0406	15.5	HEX
LBL90	0.0362	17.4	S
Multiblock copolymers			
$(LBL60\text{-}OCONH\text{-})_n$	0.0507	12.4	LAM
$(LBL60\text{-}COO\text{-})_n$	0.0512	12.3	LAM
$(LBL70\text{-}OCONH\text{-})_n$	0.0483	13.0	HEX
$(LBL70\text{-}COO\text{-})_n$	0.0471	13.3	HEX
$(LBL80\text{-}OCONH\text{-})_n$	0.0418	15.0	HEX
$(LBL80\text{-}COO\text{-})_n$	0.0418	15.0	HEX
$(LBL90\text{-}OCONH\text{-})_n$	0.0349	18.0	S
$(LBL90\text{-}COO\text{-})_n$	0.0346	18.1	S

Table 5.3 Characterization results for lamellae-forming LBL triblock copolymers

Sample	M_n (g/mol) [a]	M_w/M_n [b]	f_{PLA} [c]	N [d]	D (nm) [e]	Morphology
LBL40	6600	1.09	0.40	90.8	9.9	LAM
LBL50	8300	1.13	0.50	109.8	11.5	LAM
LBL55	9200	1.15	0.55	119.8	12.3	LAM
LBL60	10600	1.17	0.60	135.1	13.0	LAM

[a] Molecular weight calculated from ^{1}H NMR analysis. [b] Dispersity ($Đ$) measured by SEC. [c] Volume fraction of PLA measured by ^{1}H NMR and calculated using published bulk homopolymer densities. [d] Overall degree of polymerization based on a reference volume of 118 Å^3. [e] Principal domain spacing ($D = 2\pi/q^*$) calculated from room temperature SAXS principal scattering peak, q^*.

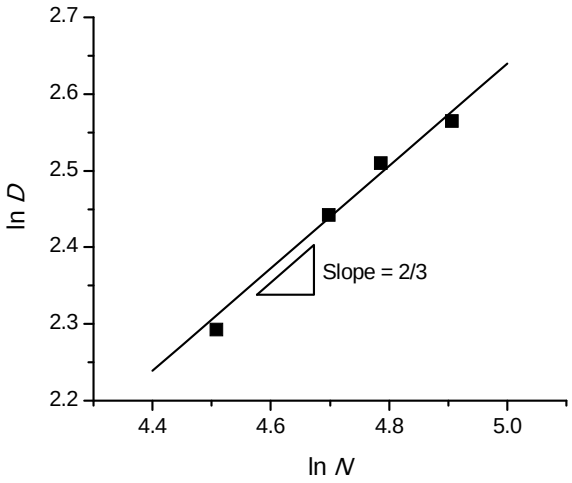

Figure 5.11 Measured domain spacing, D, as a function of the total degree of polymerization, N. The D values fall on a straight line which slope is ca. 2/3, indicating the lamella period scales as $D \sim N^{2/3}$.

5.3.5 Mechanical Properties

Mechanical properties of LBL triblock and PLA-PB multiblock copolymers were evaluated using uniaxial tensile tests. Dog-bone specimens were drawn at room temperature until failure with a constant rate of 0.1 mm/sec. For stress-strain plots, representative curves of triblock and multiblock copolymers were chosen from at least five data sets per sample and are displayed in Figure 5.12. Average values of the elastic modulus E, strain at break ε_b, stress at break (tensile strength) σ_b, yield stress σ_y, and toughness (area under the stress-strain curve) are summarized in Figure 5.13 and Table 5.4. All LBL triblock copolymers (LBL60, 70, 80, and 90) showed brittle fracture. Even though increasing the molecular weight of the PLA-block enhanced E and σ_b (see Table 3), all LBL triblock copolymers exhibit relatively poor mechanical toughness due to low values of ε_b (2–23%).

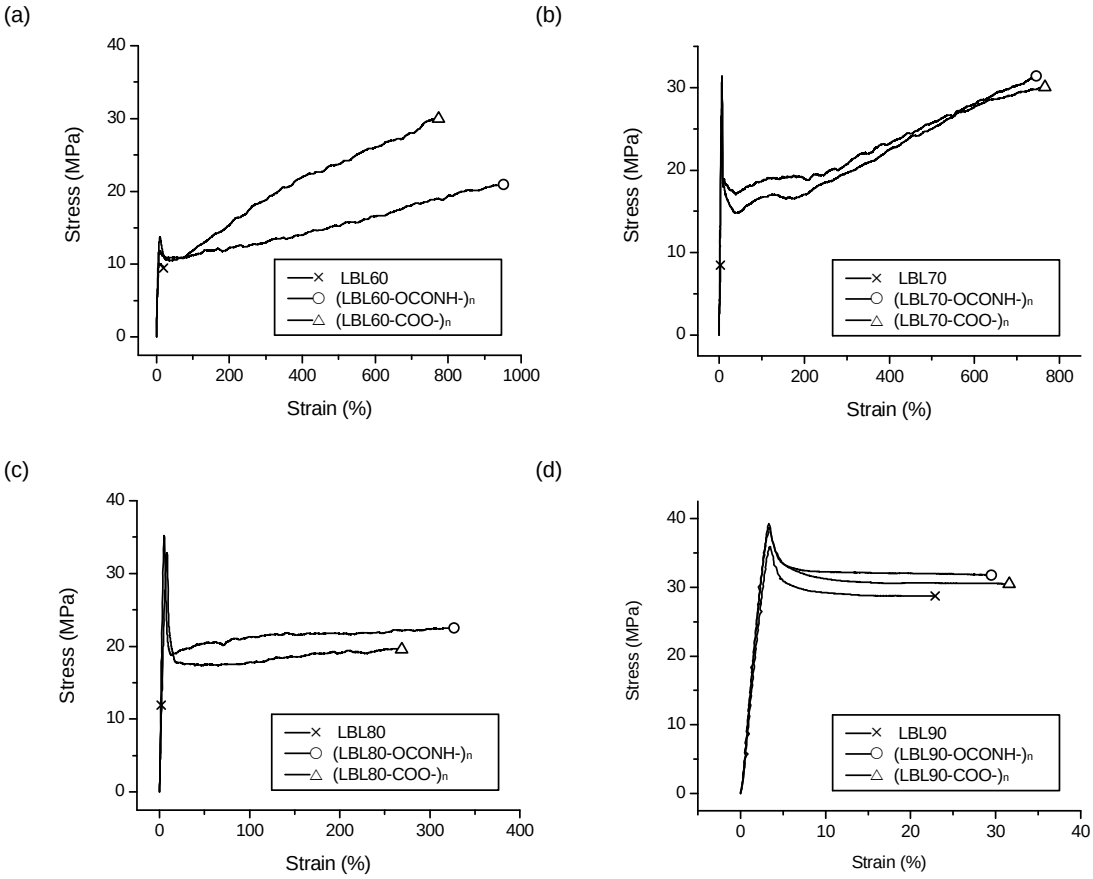

Figure 5.12 Representative stress versus strain curves for the LBL triblock, (LBL-OCONH-)$_n$ and (LBL-COO-)$_n$ multiblock copolymers.

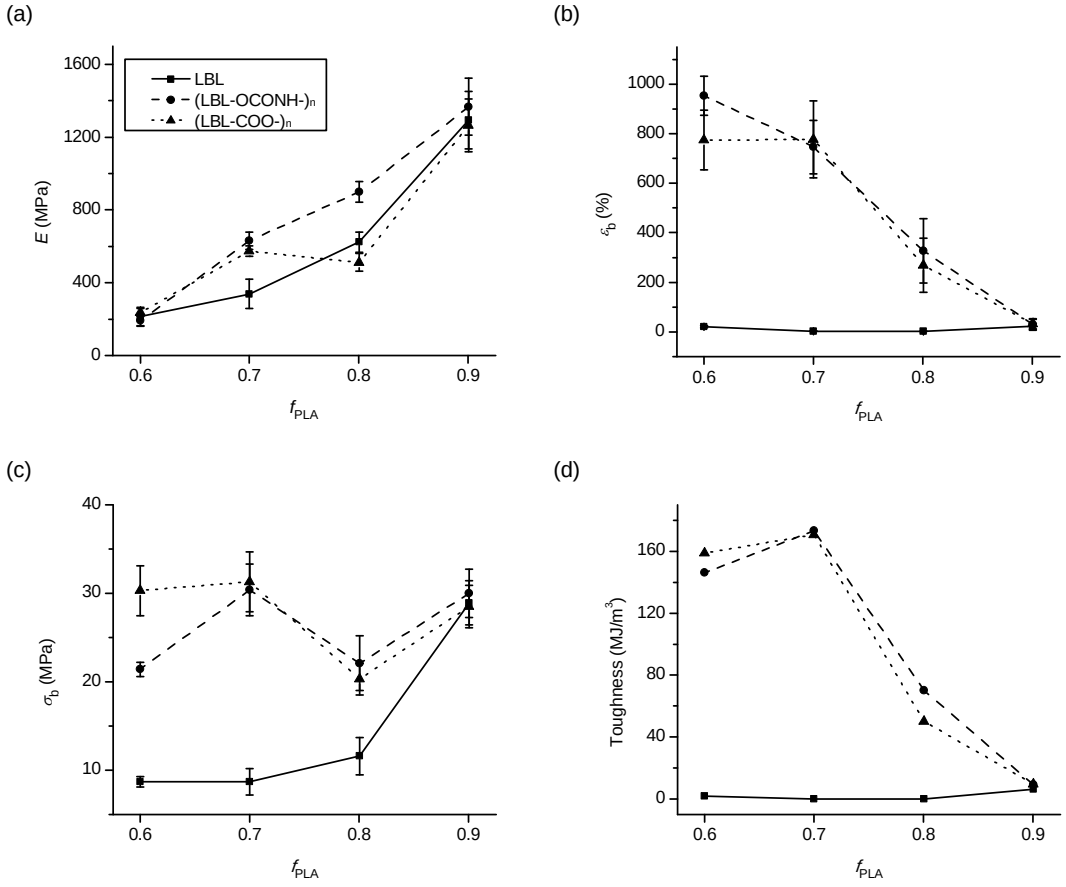

Figure 5.13 Mechanical properties of LBL triblock, (LBL-OCONH-)$_n$ and (LBL-COO-)$_n$ multiblock copolymers: (a) elastic modulus; (b) strain at break; (c) stress at break (tensile strength); (d) toughness.

Table 5.4 Tensile properties of LBL triblock, (LBL-OCONH-)$_n$ and (LBL-COO-)$_n$ multiblock copolymers

Sample	E (MPa)	ε_b (%)	σ_b (MPa)	σ_y (MPa)	Toughness (MJ/m^3)
LBL60	214 ± 50	20.8 ± 5.0	8.7 ± 0.6	10.2 ± 1.5	1.72
(LBL60-OCONH-)$_n$	192 ± 31	953 ± 79	21.4 ± 0.8	11.4 ± 1.3	146.18
(LBL60-COO-)$_n$	238 ± 22	774 ± 121	30.3 ± 2.8	13.3 ± 0.8	158.65
LBL70	338 ± 80	3.1 ± 0.7	8.7 ± 1.5	-	0.15
(LBL70-OCONH-)$_n$	631 ± 48	746 ± 108	30.4 ± 2.9	30.5 ± 1.2	173.81
(LBL70-COO-)$_n$	574 ± 28	766 ± 155	31.3 ± 3.4	27.3 ± 2.0	170.66
LBL80	624 ± 55	2.0 ± 0.4	11.6 ± 2.1	-	0.12
(LBL80-OCONH-)$_n$	899 ± 57	327 ± 130	22.1 ± 3.1	35.0 ± 1.1	70.22
(LBL80-COO-)$_n$	512 ± 49	269 ± 109	20.3 ± 1.8	32.6 ± 2.6	49.95
LBL90	1294 ± 157	22.9 ± 12.4	28.9 ± 2.5	36.0 ± 3.1	6.37
(LBL90-OCONH-)$_n$	1366 ± 156	29 ± 22	30.0 ± 2.7	37.2 ± 3.7	9.17
(LBL90-COO-)$_n$	1266 ± 145	32 ± 21	28.5 ± 2.4	35.9 ± 3.1	9.51

In sharp contrast, the PLA-PB multiblock copolymers containing 60, 70, and 80 vol% PLA, prepared by coupling with TDI and TCl, exhibited remarkably improved mechanical behavior irrespective of the types of coupling agent. The stress-strain curves obtained from these multiblock copolymers display ductile rather than brittle behavior, with modest, in most cases improved, variation in the stiffness reflected in E. Both ε_b and

σ_b are dramatically influenced by multiblock formation, resulting in much higher toughness compared to the starting triblock copolymers; calculated areas under the stress-strain curves give about 90, 1150, and 500-fold increases in toughness for the multiblock copolymers with PLA contents of 60, 70, and 80 vol%, respectively (see Table 5.4).

The superior mechanical behavior of the multiblocks can be attributed to their alternating structure composed of a large number of hard glassy PLA and soft rubbery PB blocks. The multiblock copolymers microphase-separate into two domains, with the hard block domains acting as physical cross-links and providing enhanced modulus, and the soft domains imparting facile elastic elongation to the polymer.[91-92] Previous research has indicated that increasing the number of blocks affords enhanced mechanical properties when comparing AB diblock, ABA triblock, and ABABA pentablock copolymers.[93-95] Koo et al. demonstrated the same tendency in $(AB)_n$ multiblock copolymer system containing semicrystalline and rubbery blocks, with n = 2, 4, 6, 8, 10, and 12.[36] The change in mechanical behavior by varying the number of blocks can be described by the occurrence of bridging and looping chain conformations.[93,96] Normally, AB diblock copolymers display brittle fracture due to the lack of molecular connectivity, i.e., no bridging or looping chains between domains. ABA triblocks can show ductile behavior when the middle block connects glassy end blocks (e.g., SIS triblocks), thus effectively "stitching" together neighboring domains. Further enhancement of strength and toughness is realized with ABABA pentablock copolymers such as CECEC (C represents poly(cyclohexylethylene) and E poly(ethylene)) due to the incorporation of bridging central glassy C blocks, which thwart crack propagation in the brittle glassy domains.[93]

Similarly, in our multiblock copolymer system, increasing the number of blocks diminishes the fraction of dangling chain-ends occupying each microdomain, with a concomitant increase in the fraction of midblocks that serve to bind the microdomains together. In addition, multiblock copolymer chains are able to bridge multiple domains; this multidomain bridging results in a strong physical cross-linking of the material and, hence, improvement of mechanical properties.[97] Therefore, the superior mechanical behavior of PLA-PB multiblocks is likely due to an increase in bridged midblocks and overall domain connectivity making it possible to sustain the applied stress to much higher strain levels before failure (here we note that $\langle n' \rangle$ = 2, approximately the smallest extent of coupling indicated in Table 5.1, corresponds to a LBLBL pentablock copolymer).

The comparison of stress-strain curves of (LBL60-OCONH-)$_n$ and (LBL60-COO-)$_n$ revealed the effect of connector type on the mechanical properties. In tensile test, these two polymers showed comparable toughness values, but (LBL60-OCONH-)$_n$ prepared using TDI exhibited a somewhat lower modulus and tensile strength compared to (LBL60-COO-)$_n$ synthesized with TCl. This difference might come from the methyl substituent on the TDI connector. It is recognized that methyl substituents on the chain extender can result in a drop in modulus and tensile strength in certain polyurethanes.[91] Interestingly, this effect was found only in the multiblocks with 60% PLA. With the 70, 80, and 90% PLA multiblock copolymers, there was no noticeable discrepancy in mechanical properties between (LBL-OCONH-)$_n$ and (LBL-COO-)$_n$.

The multiblock copolymers containing 70% PLA showed evidence of strain-

hardening, which can be described as a plastic-to-rubber transition.[98-100] We suspect that the fragmented glassy PLA microdomains function as physical cross-links in a rubbery phase thus reinforcing the mechanical behavior. Even though the 80% PLA multiblocks have the same cylindrical morphology as the 70% PLA multiblock copolymers, these samples displayed lower tensile strength and elongation at break and no plastic-to-rubber transition. This material has greater PLA content and likely is not able to disperse fragmented glassy domains leading to micronecking that results in sample failure at lower strains.

Unlike the other multiblock copolymer samples, the mechanical properties of $(LBL90\text{-}OCONH\text{-})_n$ and $(LBL90\text{-}COO\text{-})_n$ are nearly identical to those of the starting triblock, LBL90. We believe this dramatic transition is directly related to the change in morphology, from a 1-dimensional rubbery cylinder of PB embedded in a glassy PLA matrix to spheres of PB. For rubber-toughened glassy polymers, cavitation of rubber particles followed by plastic deformation of the matrix is normally thought to be the main toughening mechanism. However, this toughening effect requires a sufficient size and loading of dispersed rubber particles.[101-104] In this research, multiblock copolymers containing 90% PLA have a small core sphere radius of around 5.6 nm (from SAXS data) and the PB blocks contained in these domains are virtually unentangled. This would imply that the rubbery PB micelles would be rather fragile and unable to sustain significant local stress leading to disruption and macroscopic brittle failure upon loading. Curiously, the loss of enhanced toughness also is accompanied by complete loss of long-range order, although there is no obvious reason for why these two features would be

correlated. We attribute the liquid-like arrangement of PB spheres to proximity to the order-disorder transition. Theory[105-106] and experiments[107-110] indicate that the transition from order to disorder in sphere forming asymmetric block polymers results in a disordered micellar morphology very much like what we document by SAXS and TEM.

5.3.6 Comparison with PS-PB Multiblock Polymers

In a recent publication we described the synthesis, morphological characterization, and physical properties of glassy continuous poly(styrene-*b*-butadiene) (PS-PB) multiblock copolymers ($0.6 \leq f_{PS} \leq 0.85$). While the synthetic strategies (anionic polymerization and condensation coupling) for producing PS-PB multiblocks mirror the procedures reported here, the resulting materials generally displayed a disordered bicontinuous-like morphology,[47] in striking contrast to the well-ordered structural features that characterize the poly(lactide-*b*-butadiene) (PLA-PB) multiblock copolymers. We believe this important qualitative difference results from the average number of blocks that make up each set of specimens. Here we note that the definition of $\langle n' \rangle$ is different in the previous report. PS-PB multiblocks were produced by coupling α,ω-dihydroxyl PS and PB homopolymers where $\langle n \rangle_{\text{PS-PB}}$ refers to the total number of blocks in each molecule. The present study deals with coupled PLA-PB-PLA triblocks, in which the average total number of blocks, $\langle n \rangle$, is given by $\langle n \rangle_{\text{PLA-PB}} = 2\langle n' \rangle + 1$, based on the $\langle n' \rangle$ values listed in Table 5.1. Bicontinuous morphologies where obtained with $8 \leq \langle n \rangle_{\text{PS-PB}} \leq 25$ (average value = 17) whereas well-ordered phases characterize $5 \leq \langle n \rangle_{\text{PLA-PB}}$

≤ 9 (average value =7.3 excluding the f_{PLA} = 0.9 specimens). These trends are remarkably consistent with the conclusions drawn by Koo et al.[36] based on their comprehensive investigation of PE-PEP multiblocks, where a distinct transition from ordered lamellae to a disordered bicontinuous morphology was shown to occur at $\langle n \rangle_{PE\text{-}PEP} \approx 9$. Clearly, $\langle n \rangle$ is an important design parameter in developing mechanically robust sustainable multiblock polymers.

The multiblock strategy results in a dramatic enhancement of the ultimate mechanical properties (ε_b and σ_b) in both PS-PB and PLA-PB with relatively minor impact on the yield stress (σ_y), independent of the average number of blocks for $\langle n \rangle \geq 5$. However, the modulus (E) of the well-ordered PLA-PB materials appears to be significantly higher than the corresponding (i.e., comparable glass content) microphase separated but disordered PS-PB multiblocks. For example, E ($f_{PS} \approx 0.8$) ≅ 300 MPa[47] whereas E ($f_{PLA} = 0.8$) ≅ 500-900 MPa (Table 5.4). On the basis of this comparison we conclude that tuning the average number of blocks with approximately $5 \leq \langle n \rangle \leq 10$ versus $\langle n \rangle > 10$ provides a useful level of independent control over the linear elastic modulus (high versus low, respectively) without compromising the outstanding gains in toughness.

5.4 Conclusion

We have applied a multiblock copolymer strategy to a PLA-PB system to produce

tough sustainable plastics which can be used in an extended range of applications compared to PLA homopolymer. The PLA-PB multiblock copolymers were synthesized using the two-stage procedure: (i) LBL triblock copolymers were prepared using ring-opening polymerization of D,L-lactide, and (ii) synthesized LBL triblock copolymers were connected with two types of chain extenders, toluene-2,4-diisocyanate (TDI) and terephthaloyl chloride (TCl). This multiblock method allowed us to access the desired morphologies by controlling the volume fraction of PLA between f_{PLA} = 0.6 and 0.9. Molecular characterization revealed this two-step synthesis successfully yielded the desired multiblock copolymer products. All triblock and multiblock copolymers exhibited microphase-separated morphologies with varying volume fraction of PLA in general agreement with established theory and experiments. SAXS and TEM results found that the triblock and corresponding multiblock copolymers have nearly identical microphase behavior. Lamellae (f_{PLA} = 0.6) and hexagonally packed cylinder (f_{PLA} = 0.7 and 0.8) forming multiblocks displayed vastly superior mechanical behavior relative to the precursor triblock compounds, which we attribute to the formation of bridged PLA midblocks. However, the disordered sphere forming (f_{PLA} = 0.9) samples were virtually unaffected by chain coupling, i.e., the triblock and multiblock materials were equally brittle. This work demonstrates a practical approach to producing mechanically superior plastics from renewable resources. Recent progress toward developing biobased diisocyantes using environmentally friendly chemistry[111-113] promises to make this approach fully sustainable.

5.5 References

[1] Biermann, U.; Friedt, W.; Lang, S.; Lühs, W.; Machmüller, G.; Metzger, J. O.; Rüsch gen. Klaas, M.; Schäfer, H. J.; Schneider, M. P. *Angew. Chem. Int. Ed.* **2000,** *39*, 2206-2224.

[2] Güner, F. S.; Yağcı, Y.; Tuncer Erciyes, A. *Prog. Polym. Sci.* **2006,** *31*, 633-670.

[3] Meier, M. A. R.; Metzger, J. O.; Schubert, U. S. *Chem. Soc. Rev.* **2007,** *36*, 1788-1802.

[4] Gandini, A. *Macromolecules* **2008,** *41*, 9491-9504.

[5] Rose, M.; Palkovits, R. *Macromol. Rapid Commun.* **2011,** *32*, 1299-1311.

[6] Belgacem, M. N.; Gandini, A. *Monomers, Polymers and Composites from Renewable Resources*; Elsevier: Amsterdam, 2008.

[7] Garlotta, D. *J. Polym. Environ.* **2001,** *9*, 63-84.

[8] Vink, E. T. H.; Rábago, K. R.; Glassner, D. A.; Springs, B.; O'Connor, R. P.; Kolstad, J.; Gruber, P. R. *Macromolecular Bioscience* **2004,** *4*, 551-564.

[9] Auras, R.; Harte, B.; Selke, S. *Macromolecular Bioscience* **2004,** *4*, 835-864.

[10] Anderson, K. S.; Schreck, K. M.; Hillmyer, M. A. *Polymer Reviews* **2008,** *48*, 85-108.

[11] Perego, G.; Cella, G. D.; Bastioli, C. *J. Appl. Polym. Sci.* **1996,** *59*, 37-43.

[12] Bigg, D. M. *Adv. Polym. Tech.* **2005,** *24*, 69-82.

[13] Labrecque, L. V.; Kumar, R. A.; Davé, V.; Gross, R. A.; McCarthy, S. P. *J. Appl. Polym. Sci.* **1997,** *66*, 1507-1513.

[14] Jacobsen, S.; Fritz, H. G. *Polymer Engineering & Science* **1999,** *39*, 1303-1310.

[15] Baiardo, M.; Frisoni, G.; Scandola, M.; Rimelen, M.; Lips, D.; Ruffieux, K.; Wintermantel, E. *J. Appl. Polym. Sci.* **2003,** *90*, 1731-1738.

[16] Kulinski, Z.; Piorkowska, E. *Polymer* **2005,** *46*, 10290-10300.

[17] Wang, L.; Ma, W.; Gross, R. A.; McCarthy, S. P. *Polym. Degrad. Stab.* **1998,** *59*, 161-168.

[18] Broz, M. E.; VanderHart, D. L.; Washburn, N. R. *Biomaterials* **2003,** *24*, 4181-4190.

[19] Jiang, L.; Wolcott, M. P.; Zhang, J. *Biomacromolecules* **2005,** *7*, 199-207.

[20] Hashima, K.; Nishitsuji, S.; Inoue, T. *Polymer* **2010,** *51*, 3934-3939.

[21] Feng, F.; Ye, L. *J. Appl. Polym. Sci.* **2011,** *119*, 2778-2783.

[22] Kowalczyk, M.; Piorkowska, E. *J. Appl. Polym. Sci.* **2012,** *124*, 4579-4589.

[23] Zhu, K. J.; Xiangzhou, L.; Shilin, Y. *J. Appl. Polym. Sci.* **1990,** *39*, 1-9.

[24] Frick, E. M.; Zalusky, A. S.; Hillmyer, M. A. *Biomacromolecules* **2003,** *4*, 216-223.

[25] Bates, F. S.; Hillmyer, M. A.; Lodge, T. P.; Bates, C. M.; Delaney, K. T.; Fredrickson, G. H. *Science* **2012,** *336*, 434-440.

[26] Seymour, R. W.; Cooper, S. L. *Macromolecules* **1973,** *6*, 48-53.

[27] Benoit, H.; Hadziioannou, G. *Macromolecules* **1988,** *21*, 1449-1464.

[28] Kavassalis, T. A.; Whitmore, M. D. *Macromolecules* **1991,** *24*, 5340-5345.

[29] Zielinski, J. M.; Spontak, R. J. *Macromolecules* **1992,** *25*, 653-662.

[30] Ryan, A. J.; Macosko, C. W.; Bras, W. *Macromolecules* **1992,** *25*, 6277-6283.

[31] Velankar, S.; Cooper, S. L. *Macromolecules* **1998,** *31*, 9181-9192.

[32] Velankar, S.; Cooper, S. L. *Macromolecules* **2000,** *33*, 382-394.

[33] Li, W.; Ryan, A. J.; Meier, I. K. *Macromolecules* **2002,** *35*, 5034-5042.

[34] Wu, L.; Cochran, E. W.; Lodge, T. P.; Bates, F. S. *Macromolecules* **2004,** *37*, 3360-3368.

[35] Arriola, D. J.; Carnahan, E. M.; Hustad, P. D.; Kuhlman, R. L.; Wenzel, T. T. *Science* **2006,** *312*, 714-719.

[36] Koo, C. M.; Hillmyer, M. A.; Bates, F. S. *Macromolecules* **2006,** *39*, 667-677.

[37] Masuda, J.; Takano, A.; Suzuki, J.; Nagata, Y.; Noro, A.; Hayashida, K.; Matsushita, Y. *Macromolecules* **2007,** *40*, 4023-4027.

[38] Watanabe, H.; Matsumiya, Y.; Sawada, T.; Iwamoto, T. *Macromolecules* **2007,** *40*, 6885-6897.

[39] Carme Coll Ferrer, M.; Babb, D.; Ryan, A. J. *Polymer* **2008,** *49*, 3279-3287.

[40] Hong, L.; Zhu, F.; Li, J.; Ngai, T.; Xie, Z.; Wu, C. *Macromolecules* **2008,** *41*, 2219-2227.

[41] Fleury, G.; Bates, F. S. *Macromolecules* **2009,** *42*, 3598-3610.

[42] Park, H. E.; Dealy, J. M.; Marchand, G. R.; Wang, J.; Li, S.; Register, R. A. *Macromolecules* **2010,** *43*, 6789-6799.

[43] Touris, A.; Hadjichristidis, N. *Macromolecules* **2011,** *44*, 1969-1976.

[44] Li, S.; Register, R. A.; Weinhold, J. D.; Landes, B. G. *Macromolecules* **2012,** *45*, 5773-5781.

[45] Chaffin, K. A.; Buckalew, A. J.; Schley, J. L.; Chen, X.; Jolly, M.; Alkatout, J. A.; Miller, J. P.; Untereker, D. F.; Hillmyer, M. A.; Bates, F. S. *Macromolecules* **2012,** *45*, 9110-9120.

[46] Matsumiya, Y.; Watanabe, H.; Takano, A.; Takahashi, Y. *Macromolecules* **2013,** *46*,

2681-2695.

[47] Lee, I.; Bates, F. S. *Macromolecules* **2013,** *46*, 4529-4539.

[48] Christensen, C. H.; Rass-Hansen, J.; Marsden, C. C.; Taarning, E.; Egeblad, K. *ChemSusChem* **2008,** *1*, 283-289.

[49] Vispute, T. P.; Zhang, H.; Sanna, A.; Xiao, R.; Huber, G. W. *Science* **2010,** *330*, 1222-1227.

[50] Mathers, R. T. *J. Polym. Sci., Part A: Polym. Chem.* **2012,** *50*, 1-15.

[51] de Jong, E.; Higson, A.; Walsh, P.; Wellisch, M. *Biofuels, Bioproducts and Biorefining* **2012,** *6*, 606-624.

[52] Fetters, L. J.; Lohse, D. J.; Richter, D.; Witten, T. A.; Zirkel, A. *Macromolecules* **1994,** *27*, 4639-4647.

[53] Siemann, U. *Eur. Polym. J.* **1992,** *28*, 293-297.

[54] Leenslag, J. W.; Pennings, A. J. *Die Makromolekulare Chemie* **1987,** *188*, 1809-1814.

[55] Kricheldorf, H. R.; Kreiser-Saunders, I.; Boettcher, C. *Polymer* **1995,** *36*, 1253-1259.

[56] Kowalski, A.; Duda, A.; Penczek, S. *Macromol. Rapid Commun.* **1998,** *19*, 567-572.

[57] Kricheldorf, H. R.; Kreiser-Saunders, I.; Stricker, A. *Macromolecules* **2000,** *33*, 702-709.

[58] Kowalski, A.; Duda, A.; Penczek, S. *Macromolecules* **2000,** *33*, 7359-7370.

[59] Leibler, L. *Macromolecules* **1980,** *13*, 1602-1617.

[60] Hiemenz, P. C.; Lodge, T. P. *Polymer Chemistry*, 2nd ed.; Taylor & Francis Group: New York, 2007.

[61] Zalusky, A. S.; Olayo-Valles, R.; Wolf, J. H.; Hillmyer, M. A. *J. Am. Chem. Soc.* **2002,** *124*, 12761-12773.

[62] Martello, M. T.; Hillmyer, M. A. *Macromolecules* **2011,** *44*, 8537-8545.

[63] Schmidt, S. C.; Hillmyer, M. A. *J. Polym. Sci., Part B: Polym. Phys.* **2002,** *40*, 2364-2376.

[64] Rodwogin, M. D.; Spanjers, C. S.; Leighton, C.; Hillmyer, M. A. *ACS Nano* **2010,** *4*, 725-732.

[65] Papadakis, C. M.; Brown, W.; Johnsen, R. M.; Posselt, D.; Almdal, K. *The Journal of Chemical Physics* **1996,** *104*, 1611-1625.

[66] Ren, Y.; Lodge, T. P.; Hillmyer, M. A. *Macromolecules* **2000,** *33*, 866-876.

[67] Fox, J. T. G.; Flory, P. J. *J. Appl. Phys.* **1950,** *21*, 581-591.

[68] Jamshidi, K.; Hyon, S. H.; Ikada, Y. *Polymer* **1988,** *29*, 2229-2234.

[69] Granger, A. T.; Wang, B.; Krause, S.; Fetters, L. J. *Adv. Chem. Ser.* **1986**, 127-138.

[70] Granger, A. T.; Krause, S.; Fetters, L. J. *Macromolecules* **1987,** *20*, 1421-1423.

[71] Hashimoto, T.; Tsukahara, Y.; Tachi, K.; Kawai, H. *Macromolecules* **1983,** *16*, 648-657.

[72] Lu, Z. H.; Krause, S. *Macromolecules* **1982,** *15*, 112-114.

[73] Krause, S.; Lu, Z.; Iskandar, M. *Macromolecules* **1982,** *15*, 1076-1082.

[74] Kinning, D. J.; Thomas, E. L. *Macromolecules* **1984,** *17*, 1712-1718.

[75] Percus, J. K.; Yevick, G. J. *Physical Review* **1958,** *110*, 1-13.

[76] Dean, J. M.; Lipic, P. M.; Grubbs, R. B.; Cook, R. F.; Bates, F. S. *J. Polym. Sci., Part B: Polym. Phys.* **2001,** *39*, 2996-3010.

[77] Guinier, A.; Fournet, G. *Small-angle scattering of X-rays*; Wiley: New York, 1955.

[78] Wertheim, M. S. *Phys. Rev. Lett.* **1963,** *10*, 321-323.

[79] Thiele, E. *The Journal of Chemical Physics* **1963,** *39*, 474-479.

[80] Ashcroft, N. W.; Lekner, J. *Physical Review* **1966,** *145*, 83-90.

[81] Kaler, E. W.; Bennett, K. E.; Davis, H. T.; Scriven, L. E. *The Journal of Chemical Physics* **1983,** *79*, 5673-5684.

[82] Matsen, M. W.; Thompson, R. B. *The Journal of Chemical Physics* **1999,** *111*, 7139-7146.

[83] Helfand, E.; Wasserman, Z. R. *Macromolecules* **1976,** *9*, 879-888.

[84] Matsushita, Y.; Mori, K.; Saguchi, R.; Nakao, Y.; Noda, I.; Nagasawa, M. *Macromolecules* **1990,** *23*, 4313-4316.

[85] Matsushita, Y.; Nomura, M.; Watanabe, J.; Mogi, Y.; Noda, I.; Imai, M. *Macromolecules* **1995,** *28*, 6007-6013.

[86] Hashimoto, T.; Shibayama, M.; Kawai, H. *Macromolecules* **1980,** *13*, 1237-1247.

[87] Hashimoto, T. *Macromolecules* **1982,** *15*, 1548-1553.

[88] Hashimoto, T.; Shibayama, M.; Kawai, H. *Macromolecules* **1983,** *16*, 1093-1101.

[89] Semenov, A. N. *Sov. Phys. JETP* **1985,** *61*, 733-742.

[90] Matsen, M. W.; Bates, F. S. *Macromolecules* **1996,** *29*, 1091-1098.

[91] Hepburn, C. *Polyurethane Elastomers*; Applied Science: New York, 1982; p 248.

[92] Prisacariu, C. *Polyurethane Elastomers: From Morphology to Mechanical Aspects*; Springer: Berlin, Heidelberg, 2011.

[93] Hermel, T. J.; Hahn, S. F.; Chaffin, K. A.; Gerberich, W. W.; Bates, F. S.

Macromolecules **2003,** *36*, 2190-2193.

[94] Lim, L. S.; Harada, T.; Hillmyer, M. A.; Bates, F. S. *Macromolecules* **2004,** *37*, 5847-5850.

[95] Phatak, A.; Lim, L. S.; Reaves, C. K.; Bates, F. S. *Macromolecules* **2006,** *39*, 6221-6228.

[96] Mori, Y.; Lim, L. S.; Bates, F. S. *Macromolecules* **2003,** *36*, 9879-9888.

[97] Rasmussen, K. Ø.; Kober, E. M.; Lookman, T.; Saxena, A. *J. Polym. Sci., Part B: Polym. Phys.* **2003,** *41*, 104-111.

[98] Fujimura, M.; Hashimoto, T.; Kawai, H. *Rubber Chem. Technol.* **1978,** *51*, 215-224.

[99] Hashimoto, T.; Fujimura, M.; Saijo, K.; Kawai, H.; Diamant, J.; Shen, M. Strain-Induced Plastic-to-Rubber Transition of a SBS Block Copolymer and Its Blend with PS. In *Multiphase Polymers*, AMERICAN CHEMICAL SOCIETY: 1979; Vol. 176, pp 257-275.

[100] Kawai, H.; Hashimoto, T.; Miyoshi, K.; Uno, H.; Fujimura, M. *Journal of Macromolecular Science* **1980,** *B17*, 427-472.

[101] Bucknall, C. B. Rubber toughening. In *The Physics of Glassy Polymers* 2nd ed.; Haward, R. N.; Young, R. J. Eds.; Chapman & Hall: London, 1997.

[102] Kim, D. S.; Cho, K.; Kim, J. K.; Park, C. E. *Polymer Engineering & Science* **1996,** *36*, 755-768.

[103] Liang, J. Z.; Li, R. K. Y. *J. Appl. Polym. Sci.* **2000,** *77*, 409-417.

[104] Smit, R. J. M.; Brekelmans, W. A. M.; Meijer, H. E. H. *Journal of Materials Science* **2000,** *35*, 2869-2879.

[105] Dormidontova, E. E.; Lodge, T. P. *Macromolecules* **2001,** *34*, 9143-9155.

[106] Wang, J.; Wang, Z.-G.; Yang, Y. *Macromolecules* **2005,** *38*, 1979-1988.

[107] Schwab, M.; Stühn, B. *Phys. Rev. Lett.* **1996,** *76*, 924-927.

[108] Sakamoto, N.; Hashimoto, T. *Macromolecules* **1998,** *31*, 8493-8502.

[109] Kim, J. K.; Lee, H. H.; Sakurai, S.; Aida, S.; Masamoto, J.; Nomura, S.; Kitagawa, Y.; Suda, Y. *Macromolecules* **1999,** *32*, 6707-6717.

[110] Wang, X.; Dormidontova, E. E.; Lodge, T. P. *Macromolecules* **2002,** *35*, 9687-9697.

[111] Hojabri, L.; Kong, X.; Narine, S. S. *Biomacromolecules* **2009,** *10*, 884-891.

[112] Hojabri, L.; Kong, X.; Narine, S. S. *J. Polym. Sci., Part A: Polym. Chem.* **2010,** *48*, 3302-3310.

[113] Palaskar, D. V.; Boyer, A. l.; Cloutet, E.; Alfos, C.; Cramail, H. *Biomacromolecules* **2010,** *11*, 1202-1211.

Chapter 6 Concluding Remarks

6.1 Summary

This research has focused on the structural and mechanical behavior of multiblock copolymers. The most previous studies in the block copolymer field have dealt with the simplest molecular architectures. These simple structures have widely investigated, which results in a comprehensive understanding about their phase behavior and physical properties.[1-6] However, much less research has been conducted on multiblock copolymers with a larger number of blocks. Increasing the number of blocks in the block copolymer system would affect the chain configurations and thermodynamics of microphase equilibrium. Hence, multiblock copolymers containing a large number of blocks are expected to have unique microstructures and show different mechanical behavior compared to the conventional diblock and triblock copolymers. To examine the phase behavior and mechanical properties of multiblock copolymers, we have investigated CECECECEC nonablock, PS-PB multiblock, and PLA-PB multiblock copolymers, where C, E, PS, PB, and PLA denote poly(cyclohexylethylene), polyethylene, polystyrene, polybutadiene, and polylactide, respectively. The desired block copolymer

materials were prepared using a combination of different synthesis techniques and characterized with SEC, NMR, DSC, SAXS, DMS, TEM, and tensile testing. Some background information about the structural and mechanical properties of block copolymers is summarized in Chapter 1 in order to help understand this study. Various experimental techniques used in this study are described in Chapter 2.

Chapter 3 presented CECECECEC nonablock copolymer materials with a large center C block (f_5 = 0.4–0.7). The well-defined CECECECEC block copolymers were synthesized using a combination of anionic polymerization and catalytic hydrogenation. The microstructures of the multiblock copolymers varied with the PE block size. The CECECECEC samples having very small PE blocks exhibited disordered homogeneous phase with the low % crystallinity. Increasing the size of the PE blocks caused the microphase separation between the C domain of the large center block and the mixed phase of the outer CECE blocks; the ordered microstructures were controlled by the volume fraction of the center C block (f_5). With further increase of PE block size, PE chains could be large enough to have the secondary phase separation in the outer CECE blocks. Consequently, the CECECECEC sample containing the largest PE blocks was expected to have a layer-in-layer morphology, which only displayed ductile and tough mechanical behavior. The research about multiblock copolymer continued to a block copolymer system with a larger number of blocks. In an effort to overcome the limitation of sequential anionic polymerization on making a long multiblock copolymer chain, a combination of anionic polymerization and polycondensation was applied. Polycondensation of end-functionalized polymers could enhance the benefits from

anionic polymerization. In Chapter 4, PS-PB multiblock copolymers with alternating and random block sequences were synthesized by living anionic polymerization using a protected initiator (TIPSOPrLi) followed by polycondensation with isophorone diisocyanate (IPDI). PS-PB multiblock copolymers with $\langle n \rangle > 7$ displayed disordered bicontinuous-like morphology irrespective of the compositions and block sequences, where $\langle n \rangle$ refers to the total number of blocks in each molecule. The PS-PB multiblock copolymers exhibited ductile behavior and varying degree of ductility with the glassy PS content. Interestingly, these PS-PB multiblock materials showed significantly greater toughness compared to the conventional SBS triblock copolymers. The multiblock strategy allowed the enhanced mechanical properties in the block copolymer system. Then, we applied a similar multiblock method to sustainable block copolymer system which has the increasing interest because of depleting reserve of fossil fuel and other environmental issues such as global warming. Chapter 5 described the sustainable multiblock copolymers consisting of PLA and PB. PLA-PB multiblock copolymers were synthesized in a two-step procedure: PLA-PB-PLA (LBL) triblock copolymers were prepared using ring-opening polymerization of D,L-lactide, followed by chain extension of LBL triblock polymers with toluene-2,4-diisocyanate (TDI) and terephthaloyl chloride (TCl). Structural analysis revealed that LBL triblock and PLA-PB multiblock copolymers have ordered microstructures of lamellae (f_{PLA} = 0.6) and hexagonally packed cylinder (f_{PLA} = 0.7 and 0.8) in contrast with the PS-PB multiblocks which showed disordered morphologies. The microphase behavior of multiblocks and corresponding triblocks was nearly identical, while the multiblock copolymers exhibited greatly superior mechanical

behavior compared to the precursor triblock copolymers. However, the multiblock copolymers with a spherical morphology (f_{PLA} = 0.9) lost this toughening effect. Comparison of microstructures for PS-PB and PLA-PB multiblocks also concluded that the average total number of blocks $\langle n \rangle$ is an important design parameter in developing distinctive morphology and mechanical properties of multiblock copolymers. These findings demonstrate that a multiblock copolymer strategy allows a versatile pathway to create a novel material having suitable and tunable microstructures and physical properties.

6.2 Reference

[1] Leibler, L. *Macromolecules* **1980,** *13*, 1602-1617.

[2] Mayes, A. M.; de la Cruz, M. O. *The Journal of Chemical Physics* **1989,** *91*, 7228-7235.

[3] Bates, F. S.; Fredrickson, G. H. *Annu. Rev. Phys. Chem.* **1990,** *41*, 525-557.

[4] Fredrickson, G. H.; Bates, F. S. *Annu. Rev. Mater. Sci.* **1996,** *26*, 501-550.

[5] Bates, F. S.; Fredrickson, G. H. *Physics Today* **1999,** *52*, 32.

[6] Holden, G.; Kricheldorf, H. R.; Quirk, R. P. *Thermoplastic Elastomers*, 3rd ed.; Hanser Gardner Publications: Cincinnati, 2004.

Bibliography

Adhikari, R.; Godehardt, R.; Lebek, W.; Weidisch, R.; Michler, G. H.; Knoll, K. *Journal of Macromolecular Science, Part B* **2001,** *40*, 833-847.

Adhikari, R.; Michler, G. H. *Prog. Polym. Sci.* **2004,** *29*, 949-986.

Anderson, K. S.; Lim, S. H.; Hillmyer, M. A. *J. Appl. Polym. Sci.* **2003,** *89*, 3757-3768.

Anderson, K. S.; Schreck, K. M.; Hillmyer, M. A. *Polymer Reviews* **2008,** *48*, 85-108.

Anzaldi, S.; Bonifaci, L.; Malaguti, E.; Vighi, M.; Ravanetti, G. P. *J. Mater. Sci. Lett.* **1994,** *13*, 1555-1557.

Arriola, D. J.; Carnahan, E. M.; Hustad, P. D.; Kuhlman, R. L.; Wenzel, T. T. *Science* **2006,** *312*, 714-719.

Ashcroft, N. W.; Lekner, J. *Physical Review* **1966,** *145*, 83-90.

Auras, R.; Harte, B.; Selke, S. *Macromolecular Bioscience* **2004,** *4*, 835-864.

Avérous, L.; Pollet, E. *Environmental Silicate Nano-biocomposites*; Springer: 2012.

Baiardo, M.; Frisoni, G.; Scandola, M.; Rimelen, M.; Lips, D.; Ruffieux, K.; Wintermantel, E. *J. Appl. Polym. Sci.* **2003,** *90*, 1731-1738.

Bates, F. S.; Fredrickson, G. H. *Annu. Rev. Phys. Chem.* **1990,** *41*, 525-557.

Bates, F. S.; Fredrickson, G. H. *Physics Today* **1999,** *52*, 32.

Bates, F. S.; Fredrickson, G. H.; Hucul, D.; Stephen F. Hahn *AlChE J.* **2001,** *47*, 762-765.

Bates, F. S.; Hillmyer, M. A.; Lodge, T. P.; Bates, C. M.; Delaney, K. T.; Fredrickson, G. H. *Science* **2012,** *336*, 434-440.

Belgacem, M. N.; Gandini, A. *Monomers, Polymers and Composites from Renewable*

Resources; Elsevier: Amsterdam, 2008.

Benninga, H. *A history of lactic acid making*; Kluwer Academic Publishing: Boston, London, Dordrecht, 1990.

Benoit, H.; Hadziioannou, G. *Macromolecules* **1988,** *21*, 1449-1464.

Berthelot, M. P. E. *Bull. Soc. Chim.* **1869,** *11*, 278.

Biermann, U.; Friedt, W.; Lang, S.; Lühs, W.; Machmüller, G.; Metzger, J. O.; Rüsch gen. Klaas, M.; Schäfer, H. J.; Schneider, M. P. *Angew. Chem. Int. Ed.* **2000,** *39*, 2206-2224.

Bigg, D. M. *Adv. Polym. Tech.* **2005,** *24*, 69-82.

Bourissou, D.; Moebs-Sanchez, S.; Martín-Vaca, B. *Comptes Rendus Chimie* **2007,** *10*, 775-794.

Bowden, P. B.; Young, R. J. *Journal of Materials Science* **1974,** *9*, 2034-2051.

Brandrup, J.; Immergut, E. H. *Polymer Handbook*, 3rd ed.; John Wiley & Sons: New York, 1989.

Broz, M. E.; VanderHart, D. L.; Washburn, N. R. *Biomaterials* **2003,** *24*, 4181-4190.

Brunelle, D. J. *Ring-opening polymerization: Mechanisms, catalysis, structure, utility*; Hanser Publisher: Munich, 1993.

Bucknall, C. B. Rubber toughening. In *The Physics of Glassy Polymers* 2nd ed.; Haward, R. N.; Young, R. J. Eds.; Chapman & Hall: London, 1997.

Carme Coll Ferrer, M.; Babb, D.; Ryan, A. J. *Polymer* **2008,** *49*, 3279-3287.

Chaffin, K. A.; Buckalew, A. J.; Schley, J. L.; Chen, X.; Jolly, M.; Alkatout, J. A.; Miller, J. P.; Untereker, D. F.; Hillmyer, M. A.; Bates, F. S. *Macromolecules* **2012,** *45*, 9110-

9120.

Chatterjee, J.; Jain, S.; Bates, F. S. *Macromolecules* **2007,** *40*, 2882-2896.

Cheng, M.; Attygalle, A. B.; Lobkovsky, E. B.; Coates, G. W. *J. Am. Chem. Soc.* **1999,** *121*, 11583-11584.

Chiefari, J.; Chong, Y. K.; Ercole, F.; Krstina, J.; Jeffery, J.; Le, T. P. T.; Mayadunne, R. T. A.; Meijs, G. F.; Moad, C. L.; Moad, G.; Rizzardo, E.; Thang, S. H. *Macromolecules* **1998,** *31*, 5559-5562.

Christensen, C. H.; Rass-Hansen, J.; Marsden, C. C.; Taarning, E.; Egeblad, K. *ChemSusChem* **2008,** *1*, 283-289.

Cigna, G.; Matarrese, S.; Biglione, G. F. *J. Appl. Polym. Sci.* **1976,** *20*, 2285-2295.

Cochran, E. W.; Bates, F. S. *Macromolecules* **2002,** *35*, 7368-7374.

Cochran, E. W.; Bates, F. S. *Phys. Rev. Lett.* **2004,** *93*, 087802.

Cochran, E. W.; Garcia-Cervera, C. J.; Fredrickson, G. H. *Macromolecules* **2006,** *39*, 2449-2451.

Cochran, E. W.; Morse, D. C.; Bates, F. S. *Macromolecules* **2003,** *36*, 782-792.

Cohen, Y.; Albalak, R. J.; Dair, B. J.; Capel, M. S.; Thomas, E. L. *Macromolecules* **2000,** *33*, 6502-6516.

Cunliffe, A. V.; Davis, A.; Farey, M.; Wright, J. *Polymer* **1985,** *26*, 301-306.

Dair, B. J.; Honeker, C. C.; Alward, D. B.; Avgeropoulos, A.; Hadjichristidis, N.; Fetters, L. J.; Capel, M.; Thomas, E. L. *Macromolecules* **1999,** *32*, 8145-8152.

Datta, R.; Tsai, S.-P.; Bonsignore, P.; Moon, S.-H.; Frank, J. R. *FEMS Microbiology Reviews* **1995,** *16*, 221-231.

David, H.; Patrick, G.; Jim, L.; Jed, R. Polylactic Acid Technology. In *Natural Fibers, Biopolymers, and Biocomposites*, CRC Press: 2005.

de Gennes, P. G. *Scaling concepts in polymer physics*; Cornell University Press: Ithaca, 1979.

de Jong, E.; Higson, A.; Walsh, P.; Wellisch, M. *Biofuels, Bioproducts and Biorefining* **2012,** *6*, 606-624.

Dean, J. M.; Lipic, P. M.; Grubbs, R. B.; Cook, R. F.; Bates, F. S. *J. Polym. Sci., Part B: Polym. Phys.* **2001,** *39*, 2996-3010.

Dems, A.; Strobin, G. *Die Makromolekulare Chemie* **1991,** *192*, 2521-2537.

Deplace, F.; Scholz, A. K.; Fredrickson, G. H.; Kramer, E. J.; Shin, Y.-W.; Shimizu, F.; Zuo, F.; Rong, L.; Hsiao, B. S.; Coates, G. W. *Macromolecules* **2012,** *45*, 5604-5618.

Discher, B. M.; Won, Y.-Y.; Ege, D. S.; Lee, J. C.-M.; Bates, F. S.; Discher, D. E.; Hammer, D. A. *Science* **1999,** *284*, 1143-1146.

Dormidontova, E. E.; Lodge, T. P. *Macromolecules* **2001,** *34*, 9143-9155.

Drolet, F.; Fredrickson, G. H. *Macromolecules* **2001,** *34*, 5317-5324.

Dubertret, B.; Skourides, P.; Norris, D. J.; Noireaux, V.; Brivanlou, A. H.; Libchaber, A. *Science* **2002,** *298*, 1759-1762.

Dubois, P.; Coulembier, O.; Raquez, J.-M. *Handbook of Ring-Opening Polymerization*; Wiley-VCH Verlag GmbH & Co. KGaA: Weinheim, 2009.

Edson, J. B.; Wang, Z.; Kramer, E. J.; Coates, G. W. *J. Am. Chem. Soc.* **2008,** *130*, 4968-4977.

Elias, H. G.; Etter, O. J. *J. Macromol. Sci.* **1967,** *A1-5*, 943.

Feng, F.; Ye, L. *J. Appl. Polym. Sci.* **2011,** *119*, 2778-2783.

Ferry, J. D. *Viscoelastic properties of polymers*, 3rd ed.; Wiley: New York, 1980.

Fetters, L. J.; Lohse, D. J.; Richter, D.; Witten, T. A.; Zirkel, A. *Macromolecules* **1994,** *27*, 4639-4647.

Fetters, L. J.; Morton, M. *Macromolecules* **1969,** *2*, 453-458.

Fleury, G.; Bates, F. S. *Macromolecules* **2009,** *42*, 1691-1694

Fleury, G.; Bates, F. S. *Macromolecules* **2009,** *42*, 3598-3610.

Fox, J. T. G.; Flory, P. J. *J. Appl. Phys.* **1950,** *21*, 581-591.

Fox, T. G. *Bull. Am. Phys. Soc.* **1956,** *1*, 123.

Fox, T. G.; Flory, P. J. *Journal of Polymer Science* **1954,** *14*, 315-319.

Fredrickson, G. H.; Bates, F. S. *Annu. Rev. Mater. Sci.* **1996,** *26*, 501-550.

Fredrickson, G. H.; Helfand, E. *The Journal of Chemical Physics* **1987,** *87*, 697-705.

Fredrickson, G. H.; Milner, S. T.; Leibler, L. *Macromolecules* **1992,** *25*, 6341-6354.

Frick, E. M.; Zalusky, A. S.; Hillmyer, M. A. *Biomacromolecules* **2003,** *4*, 216-223.

Fujimura, M.; Hashimoto, T.; Kawai, H. *Rubber Chem. Technol.* **1978,** *51*, 215-224.

Galeski, A. *Prog. Polym. Sci.* **2003,** *28*, 1643-1699.

Gandini, A. *Macromolecules* **2008,** *41*, 9491-9504.

Garlotta, D. *J. Polym. Environ.* **2001,** *9*, 63-84.

Gehlsen, M. D. *Catalytic Hydrogenation of Polymers: Synthesis and Characterization of Model Polyolefins*. Ph.D. Dissertation, University of Minnesota, 1993.

Gehlsen, M. D.; Bates, F. S. *Macromolecules* **1993,** *26*, 4122-4127.

Gehlsen, M. D.; Weimann, P. A.; Bates, F. S.; Harville, S.; Mays, J. W.; Wignall, G. D. *J.*

Polym. Sci., Part B: Polym. Phys. **1995,** *33*, 1527-1536.

Georges, M. K.; Veregin, R. P. N.; Kazmaier, P. M.; Hamer, G. K. *Macromolecules* **1993,** *26*, 2987-2988.

Granger, A. T.; Krause, S.; Fetters, L. J. *Macromolecules* **1987,** *20*, 1421-1423.

Granger, A. T.; Wang, B.; Krause, S.; Fetters, L. J. *Adv. Chem. Ser.* **1986**, 127-138.

Guinier, A. *X-ray diffraction: in crystals, imperfect crystals, and amorphous bodies*; Dover Publications: 1994.

Guinier, A.; Fournet, G. *Small-angle scattering of X-rays*; Wiley: New York, 1955.

Güner, F. S.; Yağcı, Y.; Tuncer Erciyes, A. *Prog. Polym. Sci.* **2006,** *31*, 633-670.

Hadjichristidis, N.; Iatrou, H.; Pitsikalis, M.; Pispas, S.; Avgeropoulos, A. *Prog. Polym. Sci.* **2005,** *30*, 725-782.

Hadjichristidis, N.; Pispas, S.; Floudas, G. *Block Copolymers: Synthetic Strategies, Physical Properties, and Applications.*; Wiley-Intescience: Hoboken, 2003.

Hahn, T. *International Tables of Crystallography*, 4 ed.; Kluwer: London 1995; Vol. A.

Hajduk, D. A.; Harper, P. E.; Gruner, S. M.; Honeker, C. C.; Kim, G.; Thomas, E. L.; Fetters, L. J. *Macromolecules* **1994,** *27*, 4063-4075.

Hajduk, D. A.; Takenouchi, H.; Hillmyer, M. A.; Bates, F. S.; Vigild, M. E.; Almdal, K. *Macromolecules* **1997,** *30*, 3788-3795.

Hashima, K.; Nishitsuji, S.; Inoue, T. *Polymer* **2010,** *51*, 3934-3939.

Hashimoto, T. *Macromolecules* **1982,** *15*, 1548-1553.

Hashimoto, T.; Fujimura, M.; Saijo, K.; Kawai, H.; Diamant, J.; Shen, M. Strain-Induced Plastic-to-Rubber Transition of a SBS Block Copolymer and Its Blend with PS. In

Multiphase Polymers, AMERICAN CHEMICAL SOCIETY: 1979; Vol. 176, pp 257-275.

Hashimoto, T.; Shibayama, M.; Kawai, H. *Macromolecules* **1980,** *13*, 1237-1247.

Hashimoto, T.; Shibayama, M.; Kawai, H. *Macromolecules* **1983,** *16*, 1093-1101.

Hashimoto, T.; Tsukahara, Y.; Tachi, K.; Kawai, H. *Macromolecules* **1983,** *16*, 648-657.

Helfand, E. *Macromolecules* **1975,** *8*, 552-556.

Helfand, E.; Wasserman, Z. *Macromolecules* **1980,** *13*, 994-998.

Helfand, E.; Wasserman, Z. R. *Macromolecules* **1976,** *9*, 879-888.

Helfand, E.; Wasserman, Z. R. *Macromolecules* **1978,** *11*, 960-966.

Hepburn, C. *Polyurethane Elastomers*; Applied Science: New York, 1982; p 248.

Hermel, T. J. *Effects of Chain architecture on the Mechanical Response of Glassy/Semicrystalline Block Copolymers: CEC versus CECEC Lamellae*. Ph.D. Dissertation, University of Minnesota, 2003.

Hermel, T. J.; Hahn, S. F.; Chaffin, K. A.; Gerberich, W. W.; Bates, F. S. *Macromolecules* **2003,** *36*, 2190-2193.

Hermel, T. J.; Wu, L.; Hahn, S. F.; Lodge, T. P.; Bates, F. S. *Macromolecules* **2002,** *35*, 4685-4689.

Hiemenz, P. C.; Lodge, T. P. *Polymer Chemistry*, 2nd ed.; Taylor & Francis Group: New York, 2007.

Hillmyer, M. A.; Bates, F. S. *Macromolecules* **1996,** *29*, 6994-7002.

Hojabri, L.; Kong, X.; Narine, S. S. *Biomacromolecules* **2009,** *10*, 884-891.

Hojabri, L.; Kong, X.; Narine, S. S. *J. Polym. Sci., Part A: Polym. Chem.* **2010,** *48*, 3302-

3310.

Holden, G.; Bishop, E. T.; Legge, N. R. *Journal of Polymer Science Part C: Polymer Symposia* **1969,** *26*, 37-57.

Holden, G.; Kricheldorf, H. R.; Quirk, R. P. *Thermoplastic Elastomers*, 3rd ed.; Hanser Gardner Publications: Cincinnati, 2004.

Holden, G.; Legge, N. R. In *Thermoplastic Elastomers*, 2nd ed.; Holden, G.; Legge, N. R.; Quirk, R. P.; Schroeder, H. E. Eds.; Hanser Publishers: New York, 1996; pp 48-69.

Holden, G.; Legge, N. R.; Quirk, R. P.; Schroeder, H. E. *Thermoplastic Elastomers*, 2nd ed.; Hanser Publishers: New York, 1996.

Holden, G.; Milkovich, R. Rubberlike block copolymers. 627652, 1963.

Hong, L.; Zhu, F.; Li, J.; Ngai, T.; Xie, Z.; Wu, C. *Macromolecules* **2008,** *41*, 2219-2227.

Hormnirun, P.; Marshall, E. L.; Gibson, V. C.; White, A. J. P.; Williams, D. J. *J. Am. Chem. Soc.* **2004,** *126*, 2688-2689.

Hosoda, S.; Nomura, H.; Gotoh, Y.; Kihara, H. *Polymer* **1990,** *31*, 1999-2005.

Hsieh, H. L.; Quirk, R. P. *Anionic Polymerization: Principles and Practical Applications*; Marcel Dekker: New York, 1996.

Hucul, D. A.; Hahn, S. F. *Adv. Mater.* **2000,** *12*, 1855-1858.

Iatrou, H.; Hadjichristidis, N. *Macromolecules* **1992,** *25*, 4649-4651.

Inata, H.; Matsumura, S. *J. Appl. Polym. Sci.* **1985,** *30*, 3325-3337.

Jacobsen, S.; Fritz, H. G. *Polymer Engineering & Science* **1999,** *39*, 1303-1310.

Jamshidi, K.; Hyon, S. H.; Ikada, Y. *Polymer* **1988,** *29*, 2229-2234.

Jeong, B.; Bae, Y. H.; Lee, D. S.; Kim, S. W. *Nature* **1997,** *388*, 860-862.

Jiang, L.; Wolcott, M. P.; Zhang, J. *Biomacromolecules* **2005,** *7*, 199-207.

Jones, R. V.; Moberly, C. W.; Reynolds, W. B. *Industrial & Engineering Chemistry* **1953,** *45*, 1117-1122.

Kaler, E. W.; Bennett, K. E.; Davis, H. T.; Scriven, L. E. *The Journal of Chemical Physics* **1983,** *79*, 5673-5684.

Kamigaito, M.; Ando, T.; Sawamoto, M. *Chem. Rev.* **2001,** *101*, 3689-3746.

Kavassalis, T. A.; Whitmore, M. D. *Macromolecules* **1991,** *24*, 5340-5345.

Kawai, H.; Hashimoto, T.; Miyoshi, K.; Uno, H.; Fujimura, M. *Journal of Macromolecular Science-Physics* **1980,** *B17*, 427-472.

Kawai, H.; Hashimoto, T.; Miyoshi, K.; Uno, H.; Fujimura, M. *Journal of Macromolecular Science* **1980,** *B17*, 427-472.

Khandpur, A. K.; Foerster, S.; Bates, F. S.; Hamley, I. W.; Ryan, A. J.; Bras, W.; Almdal, K.; Mortensen, K. *Macromolecules* **1995,** *28*, 8796-8806.

Khanna, V.; Ruokolainen, J.; Kramer, E. J.; Hahn, S. F. *Macromolecules* **2006,** *39*, 4480-4492.

Khariwala, D. U.; Taha, A.; Chum, S. P.; Hiltner, A.; Baer, E. *Polymer* **2008,** *49*, 1365-1375.

Kim, D. S.; Cho, K.; Kim, J. K.; Park, C. E. *Polymer Engineering & Science* **1996,** *36*, 755-768.

Kim, J. K.; Lee, H. H.; Sakurai, S.; Aida, S.; Masamoto, J.; Nomura, S.; Kitagawa, Y.; Suda, Y. *Macromolecules* **1999,** *32*, 6707-6717.

Kinning, D. J.; Thomas, E. L. *Macromolecules* **1984,** *17*, 1712-1718.

Koberstein, J. T.; Galambos, A. F.; Leung, L. M. *Macromolecules* **1992,** *25*, 6195-6204.

Koo, C. M.; Hillmyer, M. A.; Bates, F. S. *Macromolecules* **2006,** *39*, 667-677.

Kossuth, M. B.; Morse, D. C.; Bates, F. S. *J. Rheol.* **1999,** *43*, 167-196.

Kowalczyk, M.; Piorkowska, E. *J. Appl. Polym. Sci.* **2012,** *124*, 4579-4589.

Kowalski, A.; Duda, A.; Penczek, S. *Macromol. Rapid Commun.* **1998,** *19*, 567-572.

Kowalski, A.; Duda, A.; Penczek, S. *Macromolecules* **2000,** *33*, 7359-7370.

Krause, S. *Macromolecules* **1970,** *3*, 84-86.

Krause, S.; Iskandar, M.; Iqbal, M. *Macromolecules* **1982,** *15*, 105-111.

Krause, S.; Lu, Z.; Iskandar, M. *Macromolecules* **1982,** *15*, 1076-1082.

Kricheldorf, H. R.; Kreiser-Saunders, I.; Boettcher, C. *Polymer* **1995,** *36*, 1253-1259.

Kricheldorf, H. R.; Kreiser-Saunders, I.; Stricker, A. *Macromolecules* **2000,** *33*, 702-709.

Kricheldorf, H. R.; Kreiser, I. *Die Makromolekulare Chemie* **1987,** *188*, 1861-1873.

Kricheldorf, H. R.; Sumbél, M. *Eur. Polym. J.* **1989,** *25*, 585-591.

Kulinski, Z.; Piorkowska, E. *Polymer* **2005,** *46*, 10290-10300.

Labrecque, L. V.; Kumar, R. A.; Davé, V.; Gross, R. A.; McCarthy, S. P. *J. Appl. Polym. Sci.* **1997,** *66*, 1507-1513.

Leary, D. F.; Williams, M. C. *Journal of polymer Science Part B: Polymer Letters* **1970,** *8*, 335-340.

Lee, I.; Bates, F. S. *Macromolecules* **2013,** *46*, 4529-4539.

Lee, S.; Bluemle, M. J.; Bates, F. S. *Science* **2010,** *330*, 349-353.

Leenslag, J. W.; Pennings, A. J. *Die Makromolekulare Chemie* **1987,** *188*, 1809-1814.

Leibler, L. *Macromolecules* **1980,** *13*, 1602-1617.

Li, S.; Register, R. A.; Weinhold, J. D.; Landes, B. G. *Macromolecules* **2012,** *45*, 5773-5781.

Li, W.; Ryan, A. J.; Meier, I. K. *Macromolecules* **2002,** *35*, 5034-5042.

Li, Z.; Kesselman, E.; Talmon, Y.; Hillmyer, M. A.; Lodge, T. P. *Science* **2004,** *306*, 98-101.

Liang, C. Y.; Krimm, S. *Journal of Polymer Science* **1958,** *27*, 241-254.

Liang, J. Z.; Li, R. K. Y. *J. Appl. Polym. Sci.* **2000,** *77*, 409-417.

Lim, L. S. *Effects fo Glassy, Rubbery, and Semicrystalline Blocks on the Mechanical Response of Polyolefin Block Copolymers*. Ph.D. Dissertation, University of Minnesota, 2005.

Lim, L. S.; Harada, T.; Hillmyer, M. A.; Bates, F. S. *Macromolecules* **2004,** *37*, 5847-5850.

Lligadas, G.; Ronda, J. C.; Galià, M.; Cádiz, V. *Biomacromolecules* **2010,** *11*, 2825-2835.

Lu, Z. H.; Krause, S. *Macromolecules* **1982,** *15*, 112-114.

Ma, H.; Spaniol, T. P.; Okuda, J. *Angew. Chem. Int. Ed.* **2006,** *45*, 7818-7821.

Mahanthappa, M. K.; Hillmyer, M. A.; Bates, F. S. *Macromolecules* **2008,** *41*, 1341-1351.

Mahanthappa, M. K.; Lim, L. S.; Hillmyer, M. A.; Bates, F. S. *Macromolecules* **2007,** *40*, 1585-1593.

Mandelkern, L.; Smith, F. L.; Failla, M.; Kennedy, M. A.; Peacock, A. J. *Journal of Polymer Science Part B-Polymer Physics* **1993,** *31*, 491-493.

Mark, J. E.; Erman, B.; Eirich, F. R. *Science and technology of rubber*; Academic Press: Burlington, 2011.

Martello, M. T.; Hillmyer, M. A. *Macromolecules* **2011,** *44*, 8537-8545.

Masuda, J.; Takano, A.; Nagata, Y.; Noro, A.; Matsushita, Y. *Phys. Rev. Lett.* **2006,** *97*, 098301-4.

Masuda, J.; Takano, A.; Suzuki, J.; Nagata, Y.; Noro, A.; Hayashida, K.; Matsushita, Y. *Macromolecules* **2007,** *40*, 4023-4027.

Mateva, R.; Filyanova, R.; Velichkova, R.; Gancheva, V. *J. Polym. Sci., Part A: Polym. Chem.* **2003,** *41*, 487-496.

Mathers, R. T. *J. Polym. Sci., Part A: Polym. Chem.* **2012,** *50*, 1-15.

Matsen, M. W.; Bates, F. S. *Macromolecules* **1996,** *29*, 1091-1098.

Matsen, M. W.; Bates, F. S. *The Journal of Chemical Physics* **1997,** *106*, 2436-2448.

Matsen, M. W.; Bates, F. S. *J. Polym. Sci., Part B: Polym. Phys.* **1997,** *35*, 945-952.

Matsen, M. W.; Schick, M. *Macromolecules* **1994,** *27*, 7157-7163.

Matsen, M. W.; Thompson, R. B. *The Journal of Chemical Physics* **1999,** *111*, 7139-7146.

Matsumiya, Y.; Watanabe, H.; Takano, A.; Takahashi, Y. *Macromolecules* **2013,** *46*, 2681-2695.

Matsuo, M.; Ueno, T.; Horino, H.; Chujyo, S.; Asai, H. *Polymer* **1968,** *9*, 425-436.

Matsushita, Y. *Polym. J.* **2008,** *40*, 177-183.

Matsushita, Y.; Mori, K.; Saguchi, R.; Nakao, Y.; Noda, I.; Nagasawa, M. *Macromolecules* **1990,** *23*, 4313-4316.

Matsushita, Y.; Nomura, M.; Watanabe, J.; Mogi, Y.; Noda, I.; Imai, M. *Macromolecules* **1995,** *28*, 6007-6013.

Matsushita, Y.; Suzuki, J.; Seki, M. *Physica B: Condensed Matter* **1998,** *248*, 238-242.

Mayes, A. M.; de la Cruz, M. O. *The Journal of Chemical Physics* **1989,** *91*, 7228-7235.

Mayes, A. M.; de la Cruz, M. O. *The Journal of Chemical Physics* **1991,** *95*, 4670-4677.

McCormick, H. W.; Brower, F. M.; Kin, L. *Journal of Polymer Science* **1959,** *39*, 87-100.

McGrath, J. E. *Ring-Opening Polymerization: Kinetics, Mechanisms, and Synthesis*; American Chemical Society: Washington, D.C., 1985.

Meier, D. J. *J. Polym. Sci., Part B: Polym. Phys.* **1996,** *34*, 1821-1838.

Meier, M. A. R.; Metzger, J. O.; Schubert, U. S. *Chem. Soc. Rev.* **2007,** *36*, 1788-1802.

Meuler, A. J.; Ellison, C. J.; Qin, J.; Evans, C. M.; Hillmyer, M. A.; Bates, F. S. *J. Chem. Phys.* **2009,** *130*.

Meuler, A. J.; Fleury, G.; Hillmyer, M. A.; Bates, F. S. *Macromolecules* **2008,** *41*, 5809-5817.

Meuler, A. J.; Mahanthappa, M. K.; Hillmyer, M. A.; Bates, F. S. *Macromolecules* **2007,** *40*, 760-762.

Michler, G. H.; Adhikari, R.; Lebek, W.; Goerlitz, S.; Weidisch, R.; K. Knoll *J. Appl. Polym. Sci.* **2002,** *85*, 683-700.

Milner, S. T.; Witten, T. A.; Cates, M. E. *EPL (Europhysics Letters)* **1988,** *5*, 413-418.

Milner, S. T.; Witten, T. A.; Cates, M. E. *Macromolecules* **1988,** *21*, 2610-2619.

Miyamoto, T.; Kodama, K.; Shibayama, K. *Journal of Polymer Science Part A-2: Polymer Physics* **1970,** *8*, 2095-2103.

Moad, G.; Rizzardo, E.; Thang, S. H. *Aust. J. Chem.* **2005,** *58*, 379-410.

Mogi, Y.; Nomura, M.; Kotsuji, H.; Ohnishi, K.; Matsushita, Y.; Noda, I.

Macromolecules **1994,** *27*, 6755-6760.

Mori, Y.; Lim, L. S.; Bates, F. S. *Macromolecules* **2003,** *36*, 9879-9888.

Morton, M. *Anionic Polymerization : Principles and Practice*; Academic Press New York, 1983.

Morton, M.; Fetters, L. J.; Inomata, J.; Rubio, D. C.; Young, R. N. *Rubber Chem. Technol.* **1976,** *49*, 303-319.

Nagata, Y.; Masuda, J.; Noro, A.; Cho, D.; Takano, A.; Matsushita, Y. *Macromolecules* **2005,** *38*, 10220-10225.

O'Keefe, B. J.; Hillmyer, M. A.; Tolman, W. B. *J. Chem. Soc., Dalton Trans.* **2001**, 2215-2224.

Odian, G. *Principles of Polymerization*, 4th ed.; Wiley-Intescience: Hoboken, 2004.

Ono, H.-K.; Jones, F. N.; Pappas, S. P. *Journal of Polymer Science: Polymer Letters Edition* **1985,** *23*, 509-515.

Ovitt, T. M.; Coates, G. W. *J. Am. Chem. Soc.* **1999,** *121*, 4072-4073.

Pakula, T.; Saijo, K.; Kawai, H.; Hashimoto, T. *Macromolecules* **1985,** *18*, 1294-1302.

Palaskar, D. V.; Boyer, A. l.; Cloutet, E.; Alfos, C.; Cramail, H. *Biomacromolecules* **2010,** *11*, 1202-1211.

Pan, J.; Chen, M.; Warner, W.; He, M.; Dalton, L.; Hogen-Esch, T. E. *Macromolecules* **2000,** *33*, 4673-4681.

Pang, Y. Y.; Dong, X.; Liu, K. P.; Han, C. C.; Chen, E. Q.; Wang, D. J. *Polymer* **2008,** *49*, 4259-4270.

Pangborn, A. B.; Giardello, M. A.; Grubbs, R. H.; Rosen, R. K.; Timmers, F. J.

Organometallics **1996,** *15*, 1518-1520.

Papadakis, C. M.; Brown, W.; Johnsen, R. M.; Posselt, D.; Almdal, K. *The Journal of Chemical Physics* **1996,** *104*, 1611-1625.

Park, H. E.; Dealy, J. M.; Marchand, G. R.; Wang, J.; Li, S.; Register, R. A. *Macromolecules* **2010,** *43*, 6789-6799.

Penczek, S.; Cypryk, M.; Duda, A.; Kubisa, P.; Słomkowski, S. *Prog. Polym. Sci.* **2007,** *32*, 247-282.

Penczek, S.; Kubisa, P.; Matyjaszewski, K. *Cationic ring-opening polymerization of heterocyclic monomers*; Springer-Verlag: New York, 1980.

Percus, J. K.; Yevick, G. J. *Physical Review* **1958,** *110*, 1-13.

Perego, G.; Cella, G. D.; Bastioli, C. *J. Appl. Polym. Sci.* **1996,** *59*, 37-43.

Phatak, A.; Lim, L. S.; Reaves, C. K.; Bates, F. S. *Macromolecules* **2006,** *39*, 6221-6228.

Pope, D. P.; Keller, A. *Journal of Polymer Science: Polymer Physics Edition* **1975,** *13*, 533-566.

Prabhakar, A.; Chattopadhyay, D. K.; Jagadeesh, B.; Raju, K. V. S. N. *J. Polym. Sci., Part A: Polym. Chem.* **2005,** *43*, 1196-1209.

Prisacariu, C. *Polyurethane Elastomers: From Morphology to Mechanical Aspects*; Springer: Berlin, Heidelberg, 2011.

Qi, S.; Wang, Z.-G. *Physical Review E* **1997,** *55*, 1682.

Qiao, L.; Leibig, C.; Hahn, S. F.; Winey, K. I. *Industrial & Engineering Chemistry Research* **2006,** *45*, 5598-5602.

Qin, J.; Bates, F. S.; Morse, D. C. *Macromolecules* **2010,** *43*, 5128-5136.

Quirk, R. P.; Ma, J.-J. *J. Polym. Sci., Part A: Polym. Chem.* **1988,** *26*, 2031-2037.

Quirk, R. P.; Morton, M. In *Thermoplastic Elastomers*, 2nd ed.; Hanser Publishers: New York, 1996; pp 72-100.

Randall, D.; Lee, S. *The polyurethanes book*; John Wiley & Sons: New York, 2002.

Rangarajan, P.; Register, R. A.; Fetters, L. J. *Macromolecules* **1993,** *26*, 4640-4645.

Rasmussen, K. Ø.; Kober, E. M.; Lookman, T.; Saxena, A. *J. Polym. Sci., Part B: Polym. Phys.* **2003,** *41*, 104-111.

Ren, Y.; Lodge, T. P.; Hillmyer, M. A. *Macromolecules* **2000,** *33*, 866-876.

Rodwogin, M. D.; Spanjers, C. S.; Leighton, C.; Hillmyer, M. A. *ACS Nano* **2010,** *4*, 725-732.

Rose, M.; Palkovits, R. *Macromol. Rapid Commun.* **2011,** *32*, 1299-1311.

Ruokolainen, J.; Fredrickson, G. H.; Kramer, E. J.; Ryu, C. Y.; Hahn, S. F.; Magonov, S. N. *Macromolecules* **2002,** *35*, 9391-9402.

Russell, T. P.; Karis, T. E.; Gallot, Y.; Mayes, A. M. *Nature* **1994,** *368*, 729-731.

Ruzette, A.-V.; Leibler, L. *Nat Mater* **2005,** *4*, 19-31.

Ryan, A. J.; Macosko, C. W.; Bras, W. *Macromolecules* **1992,** *25*, 6277-6283.

Ryu, C. Y.; Ruokolainen, J.; Fredrickson, G. H.; Kramer, E. J.; Hahn, S. F. *Macromolecules* **2002,** *35*, 2157-2166.

Saam, J. C.; Fearon, F. W. G. *Product R&D* **1971,** *10*, 10-14.

Saegusa, T.; Goethals, E. *Ring-Opening Polymerization*; American Chemical Society: Washington, D.C., 1977.

Sakamoto, N.; Hashimoto, T. *Macromolecules* **1998,** *31*, 8493-8502.

Sakurai, S.; Sakamoto, J.; Shibayama, M.; Nomura, S. *Macromolecules* **1993,** *26*, 3351-3356.

Santangelo, P. G.; Roland, C. M. *Macromolecules* **1998,** *31*, 4581-4585.

Sardon, H.; Irusta, L.; Fernández-Berridi, M. J. *Prog. Org. Coat.* **2009,** *66*, 291-295.

Savić, R.; Luo, L.; Eisenberg, A.; Maysinger, D. *Science* **2003,** *300*, 615-618.

Schlick, S.; Levy, M. *The Journal of Physical Chemistry* **1960,** *64*, 883-886.

Schmidt, S. C.; Hillmyer, M. A. *J. Polym. Sci., Part B: Polym. Phys.* **2002,** *40*, 2364-2376.

Schmitt, A. L.; Mahanthappa, M. K. *Soft Matter* **2012,** *8*, 2294-2303.

Schulz, M. F.; Bates, F. S.; Almdal, K.; Mortensen, K. *Phys. Rev. Lett.* **1994,** *73*, 86.

Schwab, M.; Stühn, B. *Phys. Rev. Lett.* **1996,** *76*, 924-927.

Semenov, A. N. *Sov. Phys. JETP* **1985,** *61*, 733-742.

Semenov, A. N. *Soviet Physics JETP* **1985,** *61*, 733-742.

Seymour, R. W.; Cooper, S. L. *Macromolecules* **1973,** *6*, 48-53.

Siemann, U. *Eur. Polym. J.* **1992,** *28*, 293-297.

Smit, R. J. M.; Brekelmans, W. A. M.; Meijer, H. E. H. *Journal of Materials Science* **2000,** *35*, 2869-2879.

Spassky, N.; Wisniewski, M.; Pluta, C.; Le Borgne, A. *Macromol. Chem. Phys.* **1996,** *197*, 2627-2637.

Stadler, R.; Auschra, C.; Beckmann, J.; Krappe, U.; Voight-Martin, I.; Leibler, L. *Macromolecules* **1995,** *28*, 3080-3097.

Stevels, W. M.; Ankoné, M. J. K.; Dijkstra, P. J.; Feijen, J. *Macromolecules* **1996,** *29*,

3332-3333.

Szwarc, M. *Nature* **1956,** *178*, 1168-1169.

Szwarc, M. *Adv. Polym. Sci.* **1983,** *49*, 1-177.

Szwarc, M.; Levy, M.; Milkovich, R. *J. Am. Chem. Soc.* **1956,** *78*, 2656-2657.

Thiele, E. *The Journal of Chemical Physics* **1963,** *39*, 474-479.

Touris, A.; Hadjichristidis, N. *Macromolecules* **2011,** *44*, 1969-1976.

Ueberreiter, K.; Kanig, G. *Journal of Colloid Science* **1952,** *7*, 569-583.

van Melick, H. G. H.; Govaert, L. E.; Meijer, H. E. H. *Polymer* **2003,** *44*, 457-465.

Velankar, S.; Cooper, S. L. *Macromolecules* **1998,** *31*, 9181-9192.

Velankar, S.; Cooper, S. L. *Macromolecules* **2000,** *33*, 382-394.

Vigild, M. E.; Almdal, K.; Mortensen, K.; Hamley, I. W.; Fairclough, J. P. A.; Ryan, A. J. *Macromolecules* **1998,** *31*, 5702-5716.

Vigild, M. E.; Chu, C.; Sugiyama, M.; Chaffin, K. A.; Bates, F. S. *Macromolecules* **2001,** *34*, 951-964.

Vink, E. T. H.; Rábago, K. R.; Glassner, D. A.; Springs, B.; O'Connor, R. P.; Kolstad, J.; Gruber, P. R. *Macromolecular Bioscience* **2004,** *4*, 551-564.

Vispute, T. P.; Zhang, H.; Sanna, A.; Xiao, R.; Huber, G. W. *Science* **2010,** *330*, 1222-1227.

Wang, J.; Wang, Z.-G.; Yang, Y. *Macromolecules* **2005,** *38*, 1979-1988.

Wang, L.; Ma, W.; Gross, R. A.; McCarthy, S. P. *Polym. Degrad. Stab.* **1998,** *59*, 161-168.

Wang, X.; Dormidontova, E. E.; Lodge, T. P. *Macromolecules* **2002,** *35*, 9687-9697.

Ward, I. M.; Sweeney, J. *An introduction to The Mechanical Properties of Solid Polymers*, 2nd ed.; Wiley: New York, 1983.

Watanabe, H.; Matsumiya, Y.; Sawada, T.; Iwamoto, T. *Macromolecules* **2007,** *40*, 6885-6897.

Watkins, D. M.; Fox, M. A. *Macromolecules* **1995,** *28*, 4939-4950.

Weimann, P. A.; Hajduk, D. A.; Chu, C.; Chaffin, K. A.; Brodil, J. C.; F. S. Bates *J. Polym. Sci., Part B: Polym. Phys.* **1999,** *37*, 2053-2068.

Wertheim, M. S. *Phys. Rev. Lett.* **1963,** *10*, 321-323.

Williams, C. K.; Breyfogle, L. E.; Choi, S. K.; Nam, W.; Young, V. G.; Hillmyer, M. A.; Tolman, W. B. *J. Am. Chem. Soc.* **2003,** *125*, 11350-11359.

Williams, C. K.; Hillmyer, M. A. *Polymer Reviews* **2008,** *48*, 1-10.

Williams, D. B.; Carter, C. B. *Transmission Electron Microscopy: A Textbook for Materials Science*, 2nd ed.; Springer: New York, 2009.

Wilson, A. J. C. *International Tables for Crystallography: Mathematical, physical, and chemical tables*; Published for the International Union of Crystallography by Kluwer Academic Publishers: 1992; Vol. 3.

Wirpsza, Z. *Polyurethanes : chemistry, technology, and applications*; Ellis Horwood: New York, 1994.

Wu, J.; Ge, Q.; Mather, P. T. *Macromolecules* **2010,** *43*, 7637-7649.

Wu, L.; Cochran, E. W.; Lodge, T. P.; Bates, F. S. *Macromolecules* **2004,** *37*, 3360-3368.

Wu, L.; Lodge, T. P.; Bates, F. S. *J. Rheol.* **2005,** *49*, 1231-1252.

Wu, L.; Lodge, T. P.; Bates, F. S. *Macromolecules* **2006,** *39*, 294-299.

Wu, S. *J. Appl. Polym. Sci.* **1988,** *35*, 549-561.

Yamaoka, I.; Kimura, M. *Polymer* **1993,** *34*, 4399-4409.

Yang, A. C. M.; Kramer, E. J.; Kuo, C. C.; Phoenix, S. L. *Macromolecules* **1986,** *19*, 2010-2019.

Zalusky, A. S.; Olayo-Valles, R.; Wolf, J. H.; Hillmyer, M. A. *J. Am. Chem. Soc.* **2002,** *124*, 12761-12773.

Zhang, L.; Eisenberg, A. *Science* **1995,** *268*, 1728-1731.

Zheng, W.; Wang, Z.-G. *Macromolecules* **1995,** *28*, 7215-7223.

Zhu, K. J.; Xiangzhou, L.; Shilin, Y. *J. Appl. Polym. Sci.* **1990,** *39*, 1-9.

Zielinski, J. M.; Spontak, R. J. *Macromolecules* **1992,** *25*, 653-662.

Zuo, F.; Mao, Y.; Li, X.; Burger, C.; Hsiao, B. S.; Chen, H.; Marchand, G. R. *Macromolecules* **2011,** *44*, 3670-3673.